APPLICATION OF PHYSIOLOGICALLY-BASED PHARMACOKINETIC MODELING TO CHARACTERIZE CYP3A-MEDIATED DRUG-DRUG INTERACTIONS IN THE PEDIATRIC POPULATION

Sara N. Salerno

A dissertation submitted to the faculty at the University of North Carolina at Chapel Hill in partial fulfillment of the requirements for the degree of Doctor of Philosophy in the Department of Pharmaceutical Sciences in the UNC Eshelman School of Pharmacy.

Chapel Hill
2020

Approved by:

Daniel Gonzalez

Dhiren R. Thakker

Kevin M. Watt

Julie B. Dumond

Richard A. Graham

ABSTRACT

Sara N. Salerno: Application of Physiologically-Based Pharmacokinetic Modeling to Characterize CYP3A-Mediated Drug-Drug Interactions in the Pediatric Population (Under the direction of Daniel Gonzalez)

Children are at risk for experiencing life-threatening drug-drug interactions (DDIs) because they often receive multiple medications throughout hospitalization. Although DDIs frequently occur in pediatric patients, dedicated DDI studies are rarely conducted in infants and children for ethical and practical reasons. Therefore, we typically rely on adult DDI studies although changes in metabolic pathways during development may lead to differences in DDI potential between adults and children. For example, cytochrome P450 (CYP) 3A7 is the predominant CYP3A isoform expressed in neonates and it has lower catalytic activity compared to CYP3A4, the predominant CYP3A isoform expressed in adults. Physiologically-based pharmacokinetic (PBPK) modeling can potentially overcome these challenges by predicting pediatric DDI potential when pediatric data are sparse or unavailable. In this dissertation we leveraged PBPK modeling to develop a systematic approach to provide dosing recommendations in pediatric patients experiencing CYP3A mediated DDIs spanning a variety of interaction mechanisms across the pediatric age continuum. First, we evaluated the DDI between the reversible CYP3A inhibitor, fluconazole, and the CYP3A substrate, sildenafil, administered to neonates for the co-treatment of invasive candidiasis and pulmonary hypertension. This study highlighted the feasibility of leveraging PBPK modeling to predict DDIs in infants and the need to include CYP3A7 parameters in neonates. Second, we evaluated the complex DDI between

lopinavir/ritonavir (LPV/RTV) plus rifampicin involving mixed CYP3A time-dependent and competitive inhibition plus induction in pediatric patients co-infected with human immunodeficiency virus (HIV) and tuberculosis (TB). Despite the complexity of this interaction, we were able to capture the observed magnitude of the DDI in pediatric patients receiving boosted LPV/RTV plus rifampicin. Finally, this systematic approach was applied to predict DDI potential and to optimize dosing in pediatric patients receiving a novel antibiotic and time-dependent inhibitor (solithromycin) in combination with the CYP3A substrate, midazolam, and the strong CYP3A inhibitor, ketoconazole. In this study, minor age-related differences in inhibitor concentration resulted in slight differences in the magnitude of the DDI between pediatric patients ≥ 2 months of age and adults. This systematic approach can be applied to other clinically relevant metabolic and transporter mediated DDIs when pediatric DDI data are sparse or unavailable.

ACKNOWLEDGEMENT

Thanks to my dissertation committee and the faculty and students within the Division of Pharmacotherapy and Experimental Therapeutics at the UNC Eshelman School of Pharmacy.

PREFACE

Information from previously published work has been included in this dissertation.

Chapter 1: A shortened version of the introduction chapter was published as part of the commentary by Salerno SN, Burckart GJ, Huang SM, and Gonzalez D. Pediatric Drug-Drug Interaction Studies: Barriers and Opportunities. *Clin Pharmacol Ther.* 2018; 105(5):1067-1070.

Chapter 2: This work has been published as an original publication by Salerno SN, Edginton A, Gerhart JG, Laughon MM, Ambalavan N, Sokol GM, Hornik CD, Steward D, Mills M, Martz K, and Gonzalez D; on behalf of the Best Pharmaceuticals for Children Act-Pediatric Trials Network Steering committee. Physiologically-based phamracokinetic modeling characterizes the CYP3A-mediated drug-drug interaction between fluconazole and sildenafil in infants. *Clin Pharmacol Ther.* 2020. July 21. Online ahead of print.

Chapter 3: Part of this work has been published as an original publication by Salerno SN, Edginton A, Cohen-Wolkowiez M, Hornik CP, Watt KM, Jamieson BD, and Gonzalez D. Development of an Adult Physiologically Based Pharmacokinetic Model of Solithromycin in Plasma and Epithelial Lining Fluid. *CPT Pharmacometrics Syst. Pharmacol.* 2017; 6: 814-822.

TABLE OF CONTENTS

LIST OF TABLES

LIST OF FIGURES

LIST OF ABBREVIATIONS

AADAC	Human arylacetamide deacetylase
AAG	Alpha-1-acid glycoprotein
ADH	Alcohol dehydrogenase
AFE	Average fold error
AOX	Alternative oxidase
AUC	Area under the curve
AUC_{0-12}	Area under the plasma concentration versus time curve from 0 to 12 hours
AUC_{0-24}	Area under the plasma concentration versus time curve from 0 to 24 hours
$AUC_{0-24,ss}$	Steady-state area under the plasma concentration versus time curve from 0 to 24 hours
AUC_{0-8}	Area under plasma concentration time curve from 0 to 8 hours
AUC_{0-last}	Area under the plasma concentration versus time curve from 0 until the last observed value
$AUC_{0-\tau,ss}$	Area under the plasma concentration versus time curve during the dosing interval at steady-state
$AUC_{0-\infty}$	Area under the plasma concentration versus time curve extrapolated to infinity
AUC_{ss}	Area under the plasma concentration versus time curve at steady-state
AUC_{τ}	Area under the plasma concentration versus time curve during the dosing interval
CABP	Community acquired bacterial pneumonia
CES	Carboxylesterase
CI	Confidence interval
CL	Clearance
CL_{int}	Intrinsic clearance
C_{max}	Maximal concentration

$C_{max,ss}$	Maximal concentration at steady-state
$C_{min,ss}$	Minimal concentration at steady-state
CV	Coefficient of variation
CYP	Cytochrome
CYP2C9	Cytochrome P450 Family 2 Subfamily C Member 9
CYP2D6	Cytochrome P450 Family 2 Subfamily D Member 6
CYP3A4	Cytochrome P450 Family 3 Subfamily A Member 4
CYP3A5	Cytochrome P450 Family 3 Subfamily A Member 5
CYP3A7	Cytochrome P450 Family 3 Subfamily A Member 7
CYP450	Cytochrome P450
DDI	Drug-drug interaction
DMS	N-desmethylsildenafil
EC_{50}	Concentration of half-maximal induction
E_{max}	Maximal induction
FDA	U.S. Food and Drug Administration
FMO	Flavin-binding monooxygenase family protein
F_u	Unbound fraction in plasma
GA	Gestational age
GST	Glutathione S-transferase
GSTP	Glutathione S-tranferase pi
EHR	Electronic Health Record
HIV	Human immunodeficiency virus
HPLC/MS/MS	High performance liquid chromatography with tandem mass spectrometry
IQR	Inter-quartile range
IV	Intravenous

K_{cat}	Apparent catalytic rate constant
K_I	Concentration of half-maximal inhibition
K_{inact}	Maximal rate of inactivation
$K_{inact,half}$	Concentration of half-maximal inactivation
K_M	Concentration of half-maximal metabolism or transport
K_{obs}	Pseudo first-order rate constant of inactivation
Log P	Logarithmic of octanol-water partition coefficient
LPV	Lopinavir
N/A	Not applicable
NADPH	Dihydronicotinamide-adenine dinucleotide phosphate
NNRTI	Non-nucleoside transcriptase inhibitor
NRTI	Nucleotide transcriptase inhibitor
OATP	Organic anion transporting polypeptide
OATP1B1	Organic anion transporting polypeptide 1B1
OH	Hydroxy
PAH	Pulmonary arterial hypertension
PBPK	Physiologically- based pharmacokinetic modeling
PD	Pharmacodynamic
PHIS	Pediatric health information system database
PHX	Epoxide hydrolase
PK	Pharmacokinetic
pKa	Negative log of the acid dissociation constant
PMA	Post-menstrual age
PNA	Post-natal age
PO	Oral

PopPK	Population pharmacokinetic
PXR	Pregnane X receptor
RT-PCR	Reverse transcriptase polymerase chain reaction
RTV	Ritonavir
S_{50}	Substrate concentration at half-maximal activity using sigmoidal relationships (Hill equation)
SD	Standard deviation
SULT	Sulfotransferase
TB	Tuberculosis
TDI	Time-dependent inhibition
TDM	Therapeutic Drug Monitoring
T_{max}	Time to maximal concentration
UGT	UDP glucuronosyltransferase
UGT1A1	UDP glucuronosyltransferase family 1 member A1
UGT1A4	UDP-glucuronosyltransferase family 1 member A4
UGT2B7	Uridine 5'-disphospho-glucuronosyltransferase family 2 member B7
V	Volume of distribution
V_{max}	Maximal rate of metabolism or transport
V_{ss}	Volume of distribution at steady-state
WHO	World Health Organization

CHAPTER 1 : PEDIATRIC DRUG-DRUG INTERACTION STUDIES: BARRIERS AND OPPORTUNITIES[1]

1.1 Introduction

Drug-drug interactions (DDIs) can lead to therapeutic failure and life-threatening adverse events. Hospitalized children are at particularly high risk for experiencing DDIs because they often receive multiple medications throughout hospitalization. Although regulatory agencies require an evaluation of DDI potential in adults during drug development, such studies are rarely performed in the pediatric population for ethical and practical reasons. Therefore, when pediatric patients receive unavoidable drug combinations that may result in adverse outcomes, recommendations for clinical management are typically based upon evidence from adult DDI studies. However, changes in metabolic pathways during growth and development may lead to significant differences in DDI potential between adults and children. For example, cytochrome P450 (CYP) 3A7 is the predominant CYP3A isoform expressed in neonates and it has lower catalytic activity compared to CYP3A4, the predominant CYP3A isoform expressed in adults.[1–4]

Physiologically based pharmacokinetic (PBPK) modeling integrates physiological and drug specific properties to simulate drug exposure. PBPK modeling is an attractive approach to evaluated pediatric DDI potential because it can account for developmental changes in enzymes and transporters, it can predict complex and dynamic DDIs, and models can be evaluated using

[1]This chapter previously appeared as an article in the Journal of *Clin Pharmacol Ther.* The original citation is as follows: Salerno SN, Burckart GJ, Huang SM, and Gonzalez D. Pediatric Drug-Drug Interaction Studies: Barriers and Opportunities. *Clin Pharmacol Ther.* 2018; 105(5):1067-1070.

sparse or limited pediatric datasets.[5] Although PBPK modeling is widely used to predict DDI potential in adults, there is only one published example where PBPK modeling has been applied to evaluate pediatric DDIs and it focused on children ≥ 6 years of age and assumed DDI potential was the same in adults as children.[6] The overarching goal of this research is to develop a systematic approach leveraging PBPK modeling to provide therapeutic recommendations for pediatric patients at risk for experiencing CYP3A mediated DDIs. In order to develop this framework, I first develop and evaluate PBPK models using probe drug combinations with pediatric DDI data available including: sildenafil plus fluconazole and lopinavir and ritonavir (LPV/RTV) plus rifampicin. Next, I predict DDI potential and determine optimal dosing for a CYP3A substrate and time-dependent inhibitor, solithromycin, with extremely limited pediatric DDI data available. This approach can be used to evaluate other types of metabolic and transporter mediated pediatric DDIs. This research will revolutionize our current understanding of pediatric DDIs by predicting DDI potential and informing therapeutic recommendations when pediatric clinical DDI data is not available.

1.2 Background on Drug-Drug Interactions (DDIs)

DDIs occur when one drug changes the activity of another drug, which can lead to life-threatening adverse events or therapeutic failure. DDIs can broadly be categorized as pharmaceutical incompatibility, pharmacokinetic (PK), or pharmacodynamic (PD) interactions (Figure 1.1). DDIs arising from pharmaceutical incompatibility occur when drugs with incompatible physio-chemical properties are combined, such as acids and bases and positively and negatively charged species. One example is the DDI between heparin (negatively charged) with protamine (positively charged) leading to drug inactivation of both compounds.[7] With PK mediated DDIs, one drug changes the concentration of another drug leading to 'supra-

therapeutic' (increased) or 'sub-therapeutic' (decreased) drug concentrations. 'Supra-therapeutic' concentrations can lead to adverse events, while 'sub-therapeutic' concentrations can result in therapeutic failure. The drug that causes changes in concentrations of another drug is called the 'perpetrator,' while the drug whose concentration changes is called the 'victim' or 'substrate' drug. Finally, PD mediated interactions occur when a drug changes the effects of another drug without altering drug concentrations. Synergistic PD mediated DDIs occur when a drug extends the dose-response curve of another drug to the left indicating that equal effects are produced by decreasing drug concentrations; while antagonistic DDIs occur when a drug shifts the dose-response curve of another drug to the right indicating that higher concentrations are needed in order to achieve equal drug effects.[7-8]

PK mediated DDIs can be due to changes in the rate and/or extent of absorption (e.g., alterations in drug solubility due to pH changes, changes in gastric emptying, or alterations in first-pass metabolism), distribution (e.g., displacement from protein binding sites), metabolism (e.g., inhibition or induction of the cytochrome P450 system (CYP)), transport (e.g., inhibition of transport into hepatocytes through organic anion transporting polypeptide [OATP] 1B1, 1B3, 2B1), or excretion (e.g., alterations in renal or biliary excretion). Metabolic DDIs can further be categorized based on whether the mechanism involves induction or inhibition of a drug metabolizing enzyme. Enzyme induction is the process where a drug enhances the metabolism of another drug, typically through upregulation of nuclear receptors such as pregnane X receptor, constitutive androstane receptor, and aryl hydrocarbon receptor, which increases expression of the drug metabolizing enzyme. In contrast, enzyme inhibition is the process by which a drug inhibits the metabolism of another drug. Inhibition can be classified as competitive, noncompetitive, uncompetitive, or time-dependent inhibition (TDI) based on the biochemical

mechanism. Competitive inhibitors bind to the same site on the enzyme as the substrate, and the interaction can be overcome by adding high substrate concentrations. Uncompetitive inhibitors bind to the enzyme-substrate complex rather than to the free enzyme. With noncompetitive inhibition, the inhibitor can bind to both the free enzyme (competitive) as well as the enzyme-substrate complex (uncompetitive). Time-dependent inhibitors exhibit increased potency of inhibition when pre-incubated with the enzyme prior to addition of substrate. Time-dependent inhibition (TDI) can result from irreversible covalent binding of the drug to the enzyme, quasi-irreversible noncovalent tight binding of an intermediate to the enzyme, or reversible inhibition from a metabolite produced during the enzymatic reaction. Mechanism-based inactivation is a type of TDI in which the enzyme reacts with the substrate to form a chemically reactive metabolite that inactivates the enzyme.[7–10] Mechanism-based inhibitors can lead to permanent inactivation of the target enzyme that is only restored by enzyme re-synthesis resulting in slow-onset and long-lasting clinical effects.

Since DDIs can lead to therapeutic failure and life-threatening adverse events, it is critical to evaluate DDI potential for new molecular entities during drug development. The U.S. Food and Drug Administration (FDA) has described the recommended *in-vitro* studies to determine DDI potential during drug development. For metabolism mediated DDIs, an investigation should be performed to determine the metabolizing enzymes involved in drug disposition as well as whether the investigational drug is an inhibitor or inducer of key metabolizing enzymes (CYP1A2, CYP2B6, CYP2C8, CYP2C9, CYP2D6, and CYP3A4/5) (Figure 1.2).[11] Reaction phenotyping experiments should be performed to determine the specific metabolizing enzymes that are involved in the metabolism of an investigational drug using (1) chemicals, drugs, or antibodies as specific enzyme inhibitors with pooled human liver microsomes and (2) individual

human recombinant CYP enzymes. Additional studies should also be performed to determine whether the investigational drug is an enzyme inhibitor or inducer using human liver microsomes, microsomes obtained from recombinant CYP-expression systems, or hepatocytes.[11] Results from these assays can determine if the sponsor should conduct an *in-vivo* clinical DDI study in adults or perform modeling and simulation to evaluate adult DDI potential.

The FDA has also issued a draft guidance on the study design, data analysis, and clinical implications on conducting clinical DDI studies.[12] Clinical DDI studies should be performed before the drug is administered to patients who are likely to take concomitant medications that can interact with the investigational drug. These clinical DDI studies compare substrate concentrations in the absence and presence of strong index perpetrator drugs, which predictably inhibit or induce drug metabolizing enzymes or transporters in a known manner. If a drug is anticipated to be an inducer or inhibitor of drug metabolizing enzymes, then studies should also be performed in the absence and presence of sensitive index substrates, defined as drugs known to be susceptible to metabolism by drug metabolizing enzymes. Typically, clinical DDI studies are performed in healthy adult volunteers using a randomized, two-way crossover design to reduce inter-subject variability. An intensive PK sampling strategy followed by non-compartmental analysis is generally performed to determine PK endpoints such as area under the plasma concentration versus time curve from zero to infinity ($AUC_{0-\infty}$) for single dose studies, area under the plasma concentration versus time curve from zero to tau (AUC_{τ}) for multiple dose studies, maximal plasma concentration (C_{max}), and the time to C_{max} (T_{max}). The FDA has recommended that PK results be reported as the geometric mean ratio of the observed PK parameter with and without the perpetrator drug along with the associated 90% confidence interval. No-effect boundaries are used to determine whether the interaction is significant, and

can be determined based on (1) the concentration-response relationship of the drug or (2) if the 90% confidence intervals for systemic exposure ratios (C_{max}, AUC) fall entirely within the equivalence range of 80% to 125%. If clinically significant DDIs are anticipated based on these results, then clinical management can include contraindicating the drug combination, temporarily discontinuing one of the interacting drugs, modifying dosages of the new drug or concomitant drug, staggering drug administration, or monitoring patients receiving the drug combination for safety and efficacy.

1.3 Pediatric Patients Are at Risk for Experiencing DDIs

Children are at risk for experiencing DDIs because they receive multiple medications throughout hospitalization. A retrospective cohort study using the Pediatric Health Information System database (PHIS) reported that out of 54,549 admissions to the pediatric intensive care unit, children were exposed on average, to 10 distinct medications daily and to 20 medications cumulatively during hospitalization.[13] The most common medications in this study included acetaminophen, fentanyl, midazolam, ranitidine, heparin, morphine, potassium chloride, furosemide, lidocaine, and epinephrine.[13] In another retrospective cohort study using the PHIS, approximately half of hospitalized children were associated with a potential DDI based upon 498,956 pediatric hospitalizations within 42 United States children's hospitals.[14] Additionally, 5%, 41%, 28%, and 11% of these potential DDIs were considered "contraindicated," "major," "moderate," and "minor" based on the Micromedex® DRUG-REAX® classification system.[14] The most common therapeutic categories implicated in these potential DDIs included: opioids (25%), antiinfective agents (17%), neurologic agents (15%), gastrointestinal agents (13%), and cardiovascular agents (13%). While actual adverse events could not be determined in this population given limitations with the database, the most common adverse events associated with

these potential DDIs are additive respiratory depression (21%), bleeding risk (5%), QT interval prolongation (4%), reduced iron absorption/availability (4%), central nervous system depression (4%), hyperkalemia (3%), and altered diuretic effectiveness (3%).[14] These studies affirm the need to determine DDI potential along with clinical management strategies to minimize risks associated with DDIs in the pediatric population.[14]

1.4 Ethical and Practical Challenges with Conducting Pediatric DDI Studies

Dedicated DDI studies are rarely performed in the pediatric population for a variety of ethical and practical reasons. As a vulnerable population, it is unethical to expose pediatric patients to a DDI that may result in therapeutic failure or adverse events. Per 21 CFR 50 subpart D regarding clinical investigations in pediatric subjects that are associated with a more than minimal risk, children cannot be enrolled in clinical trials unless there is an anticipated benefit for the research subjects.[15] Consequently, a DDI assessment would have to be conducted in pediatric patients requiring the drug combination as part of routine therapy. There are also numerous practical challenges associated with conducting pediatric trials. There are fewer children than adults in general, leading to a small population of children with the disease or condition that are eligible for study inclusion. Consent rates are typically low for pediatric trials because of parental concerns enrolling their children into research studies, which is influenced by socioeconomic status, race, recruitment strategy, perceived risks, as well as the age and health status of the child.[16,17] Furthermore, there are logistical concerns with conducting pediatric DDI PK studies including: limited blood volume available in infants and young children for PK sampling, difficulty obtaining blood samples from infants, and the need for multiple clinical trial sites to complete enrollment.[18]

1.5 Age Related Changes in DDI Potential

Since prospective DDI studies are rarely performed in the pediatric population for the aforementioned reasons, recommendations from adult DDI studies are often extrapolated to pediatric patients to guide clinical management of potentially interacting drug combinations. However, extrapolating adult DDI data to pediatric patients can under or over predict the magnitude of DDIs. In a systematic literature review, fold interactions were compared between 31 pediatric studies and 33 adult studies for 24 drug pairs using clearance, steady state plasma concentrations, or AUC.[19] Fold interactions were higher (>1.25-fold) or lower (<0.8-fold) in pediatric patients compared to adults for 15 and 8, respectively, out of these 33 cases.[19] By example, digoxin plus amiodarone and lamotrigine plus valproate resulted in a 2.18-fold higher and 0.58-fold lower exposure, respectively, in pediatrics compared to adults.[19] Furthermore, a PBPK model demonstrated that the magnitude of metabolic DDIs depended on the ontogeny profiles of the relevant drug metabolizing enzymes as well as the fractional elimination pathway of the drug being inhibited.[20] For example, for a theoretical drug with a fraction metabolized of 0.5 for both CYP2D6 and CYP3A4 at birth, co-administration of ketoconazole (3 mg/kg) resulted in a 1.9-fold, 3.1-fold, and 4.7-fold difference in inhibited versus uninhibited AUC for newborns, 1-year olds, and adults, respectively.[20] These results highlight that there may be different risks associated with DDIs in pediatric patients at various ages compared to adults.

1.6 Clinically Relevant CYP3A Substrates in the Pediatric Population

The CYP3A subfamily has been reported to metabolize approximately 30% to 60% of clinically used drugs in adults.[3,21] Based on the top ten medications administered to hospitalized pediatric patients from the largest clinical and operational comparative data warehouses in the nation (Premier Perspective database) as of 2008, 30% of these top ten medications were

metabolized primarily or partially by CYP3A (lidocaine, fentanyl, and ondansetron).[22] The top ten medications differed slightly by pediatric sub-age groups. The top ten medications that were CYP3A substrates included lidocaine and fentanyl for children under 2 years of age; ondansetron, prednisolone, fentanyl, methylprednisolone, and midazolam for children between 2 and 4 years of age; ondansetron, fentanyl, midazolam, and lidocaine for children between 5 and 11 years of age; and ondansetron, fentanyl, and midazolam for children between 12 and 17 years of age.[22] Another study reported the top 100 medications commonly administered to neonates using a database containing information on infants discharged from 305 neonatal intensive care unit from 2005–2010 managed by the Pediatrix Medical Group.[23] Using drug specific information reported in Epocrates® and DrugBank® for these top 100 medications, 50% of the drugs metabolized by phase 1 metabolism in the liver were CYP3A substrates including: fentanyl, midazolam, indomethacin, hydrocortisone, erythromycin, dexamethasone, clindamycin, lansoprazole, fluticasone, budesonide, omeprazole, methadone, prednisone, beclomethasone, diazepam, and sildenafil.[23–25] Since hospitalized children are frequently prescribed drugs metabolized by CYP3A, managing CYP3A mediated DDIs can improve medication use in this vulnerable group.

1.7 Age Dependent Changes in Expression and Catalytic Activity of CYP3A

The first two years of life are a time of rapid growth and development. In particular, the maturation of drug-metabolizing enzymes contribute significantly to age-related changes in non-renal drug clearance (CL). Hines et al. have postulated that there are three major classes describing the developmental trajectories of hepatic drug metabolizing enzymes (Table 1.1).[26] Class 1 enzymes, such as CYP3A7, are highly expressed in the fetus during the first trimester of life with levels either remaining elevated or decreasing throughout gestation. Expression of class

2 enzymes, such as CYP3A5 and CYP2C19, remain relatively constant throughout gestation and into adulthood. The majority of enzymes fall into Class 3, in which expression is low during gestation with levels increasing significantly upon maturation.[26] CYP3A4 is an example of a class 3 enzyme with levels reaching full capacity around 2 to 3 years of life. A developmental switch has been used to describe maturation of the CYP3A subfamily where CYP3A7 expression dominates in the fetus and neonate while CYP3A4 expression dominates in the adult.[1] For example, the mean expression of CYP3A7 decreases from 142.2 pmol/mg during the neonatal period (first 30 days after birth) to 4 pmol/mg in adults, while the mean expression of CYP3A4 increases from 5 pmol/mg during the neonatal period to 98 pmol/mg in adults.[1,27,28] These expression differences can lead to profound changes in drug metabolism for CYP3A substrates between adults and young children.

Although there is an overlap in sequence homology and substrate specificity, catalytic activity can also differ among the CYP3A subfamily. A study comparing the metabolic capacity for CYP3A using 10 different CYP3A substrates reported an equal or reduced metabolic capability for CYP3A5 compared to CYP3A4, and a significantly lower catalytic activity for CYP3A7 compared to CYP3A4.[3] The *in-vitro* clearance values measured using low substrate concentrations were higher for CYP3A4 compared to CYP3A5 and CYP3A7 for all of these 10 substrates evaluated: midazolam, testosterone, alprazolam, estradiol, triazolam, nifedipine, diltiazem, BFC, tamoxifen, and clarithromycin (Table 1.2).[3] Similarly, another study comparing the *in-vitro* biotransformation of midazolam, triazolam, testosterone, and nifedipine using recombinant CYP3A4 and CYP3A5 reported lower intrinsic clearance values for CYP3A5 compared to CYP3A4.[29] Additionally, the inhibitory potency of fluconazole and ketoconazole were approximately 9-fold lower and 4 to 19-fold lower, respectively, for CYP3A5 relative to

CYP3A4.[29,30] Finally, TDI kinetic parameters were either lower or TDI was not observed at all for CYP3A5 compared to CYP3A4 for 10 out of 12 CYP3A4 time-dependent inhibitors evaluated.[4] Although limited inhibition data are available for CYP3A7, these studies indicate that CYP3A5 and CYP3A7 have lower catalytic and inhibitory potency compared to CYP3A4. These differences in catalytic activity along with the ontogeny profiles of CYP3A can lead to profound differences in CYP3A mediated DDI potential between adults and pediatric patients.

1.8 Additional Factors Leading to Age Related Changes in DDI Potential

There are additional variables besides ontogeny of drug metabolizing enzymes that can influence DDI potential in pediatric patients relative to adults. Other developmental changes may need to be considered, including changes in intragastric pH, gastric emptying, intestinal motility, protein binding, and transporter ontogeny. Differences in diet, drug combinations, formulations, and dosing may also play an important role in dictating pediatric DDI potential. Additionally, the exposure-response relationship may differ between adults and pediatric patients because of altered expression and function of proteins mediating drug effect. In fact, the majority of potential DDIs identified retrospectively in hospitalized pediatric patients were associated with PD interactions such as additive respiratory depression and gastrointestinal toxicity.[14] Moreover, age-related changes in disease progression and safety can occur due to organ development and altered tissue distribution.[19]

1.9 Potential Opportunities for Evaluating DDIs in Pediatric Patients

Since pediatric DDIs can be life threatening, a plan for assessing the interaction potential should be part of every pediatric drug development program. Unfortunately, DDI studies are rarely performed so there is a paucity of information available regarding pediatric DDIs, particularly in infants and young children. Therefore, we need to develop novel strategies that

can overcome the myriad of barriers that make an evaluation of DDIs potential in pediatric patients challenging. Some potential opportunities for evaluating PK/PD mediated DDIs throughout pediatric drug development and clinical use include leveraging modeling and simulation approaches and "real-world" data as well as innovative clinical trial design strategies such as adaptive trials (Figure 1.3).

1.9.1 Modeling and Simulation May Predict and Evaluate Pediatric DDIs

In 2012, the Advisory Committee for Pharmaceutical Science and Clinical Pharmacology of the FDA Center for Drug Evaluation and Research agreed that modeling and simulation should be considered in all pediatric drug development programs.[31] Modeling and simulation approaches, such as population based pharmacokinetics (PopPK) and PBPK, can be used to evaluate pediatric DDIs during pediatric drug development. PopPK modeling combined with sparse sampling is widely used to characterize drug disposition in neonates and children.[32,33] Implementing allometric scaling for size in addition to a sigmoidal function accounting for organ maturation may be able to distinguish age and size effects on clearance from other patient specific factors including DDIs.[34] If a concomitant drug is identified as a significant predictor of variability in a PK parameter, simulations can be performed to optimize dosing for children receiving the drug combination. PBPK modeling, which integrates physiological information along with drug-specific properties to predict drug-disposition throughout the body, can facilitate the evaluation of potential pediatric DDIs. A major advantage is that PBPK modeling can predict *a priori* exposure and can be extrapolated to different populations and pediatric age groups. However, there are some gaps in knowledge regarding age related changes in drug absorption, distribution, excretion, and ontogeny of metabolizing enzymes and transporters, which still require further exploration. Additional opportunities exist for leveraging PBPK modeling to

account for age related changes and to predict pediatric DDI potential during drug development (Figure 1.4).

1.9.2 Adaptive Trials May Mitigate the Risks Associated with Performing Prospective Pediatric DDI Studies

The risks associated with prospectively evaluating pediatric DDIs may be mitigated using adaptive trials, in which modifications to the trial or statistical procedure are modified at pre-specified times without diminishing the validity of the study. One study in healthy adults used an adaptive 2-cohort strategy to mitigate tolerability concerns associated with evaluating the DDI potential between GSK239512 and the strong CYP P450 3A inhibitor ketoconazole.[35] PBPK modeling predicted a 4-fold increase in GSK239512 exposure after coadministration with ketoconazole, which informed the dose selected for subjects in cohort 1.[35] The safety and pharmacokinetic data from cohort 1 justified providing a higher dose of GSK239512 for subjects in cohort 2 receiving the drug combination.[35] A similar approach can be applied for pediatric patients where dose adjustments are first based upon scaling an adult PBPK model to pediatric populations, followed by prospectively evaluating the drug combination in pediatric patients with safety monitored throughout the trial at pre-specified times (Figure 1.4).

1.9.3 Opportunistic Clinical Data May Facilitate Pediatric DDI Evaluation

Some of the challenges associated with evaluating pediatric DDIs as postmarketing requirements or for marketed drugs may be overcome by leveraging opportunistic data, which are data collected in pediatric patients receiving medications per standard of care. Drug concentration measurements from remaining blood samples collected at times of routine laboratory draws can be used for PopPK and PBPK model development and evaluation.[33,36–38] Opportunistic clinical data that are documented in the patient chart, such as vital signs (e.g., heart

rate, blood pressure), laboratory values (e.g., serum creatinine, liver transaminases) and clinical symptoms (e.g., sedation, pain), can be used for PD assessment. Consent rates are likely higher because of the minimal risk that these studies pose to pediatric patients. However, limitations with opportunistic data include the random nature of sample collection and measurement of drug responses, as well as the fact that many confounding variables may affect the interpretation of the patient data (e.g., organ dysfunction, other concomitant medications, and comorbidities). As a result, use of opportunistic data would likely require collecting data from a sufficiently large sample size while also controlling for confounding factors.

1.9.4 Leveraging Electronic Health Record (EHR) Data for Pediatric DDI Evaluation Can Overcome Ethical Barriers

Although several retrospective cohort studies have reported potential DDIs in children, limitations in the EHR database precluded determination of clinical outcomes associated with these potential DDIs.[14] Consequently, opportunities exist to relate potential DDIs in children with clinical outcomes using EHR data. In addition, pharmacokinetic DDIs could be prospectively assessed for drugs undergoing therapeutic drug monitoring (TDM), such as gentamicin, vancomycin, phenobarbital, carbamazepine, phenytoin, tacrolimus, cyclosporine, and caffeine. Recently, a pediatric PopPK model was developed for posaconazole utilizing TDM data and was able to detect a 42% reduction in bioavailability in the presence of proton pump inhibitors.[39] Additionally, PD analyses utilizing clinical or laboratory adverse events can be performed with or without PK data to assess pediatric DDIs. Controlling for confounding variables will likely be required given the retrospective study design and complexity of the patient population. Additional limitations include suboptimal PK sampling times (e.g., only troughs or peaks may be measured) plus laboratory or adverse events are restricted to those that

are measured and recorded in the EHR. However, advantages of this approach are that institutional review boards generally consider these studies to be exempt or have expedited approval, and information from a large pediatric population can be evaluated.

1.10 PBPK Modeling Can Facilitate DDI Assessment in the Pediatric Population

PBPK modeling is particularly advantageous for characterizing pediatric DDI potential because PBPK models can (1) be extrapolated to special populations, (2) account for developmental changes such as the ontogeny of drug metabolizing enzymes and transporters, and (3) characterize complex and dynamic DDIs in which drug concentrations change as a function of time (such as TDI and induction). For example, an adult PBPK model incorporating *in-vitro* and clinical DDI data can be used to predict pediatric DDI potential, pediatric PBPK models can be evaluated using opportunistic PK data in children receiving the drug combination per standard of care, and the final model can be used to make appropriate therapeutic recommendations in children receiving the drug combination. In addition, results from PBPK modeling can be used to inform prospective DDI studies in children. PBPK modeling is therefore a powerful tool that can potentially overcome the need to conduct pediatric DDI studies.

PBPK models are frequently used during drug development to predict DDI potential in adults and to guide clinical study planning. In fact, 66% of the 180 PBPK submissions to the FDA Office of Clinical Pharmacology between 2008 and 2015 were used for DDI prediction.[40] The FDA has provided a general framework for utilizing PBPK modeling to explore DDI potential between a substrate and an interacting drug.[11] Before utilizing PBPK modeling to predict untested DDI scenarios and to make dose recommendations, the FDA recommends first verifying model predictions using clinical DDI data between the investigational drug and strong index enzyme inhibitors and inducers.[11,41] Although PBPK models are widely used during drug

development for providing therapeutic management in adults experiencing DDIs, this strategy has infrequently been applied to the pediatric population.

There has only been one example to date where dose recommendations were developed and approved for US labeling in children and adolescents based on an adult PBPK model: guanfacine, a CYP3A substrate, in the presence of CYP3A inhibitors and inducers.[6] In this example, an adult PBPK model was developed using phase 1 healthy adult DDI data for guanfacine given in the presence of the strong index CYP3A inhibitor (ketoconazole) and inducer (rifampicin). Next, simulated exposure in adults was predicted for the moderate CYP3A inhibitors (fluconazole and erythromycin) and inducer (efavirenz). These adult PBPK model predictions were used to provide dosing recommendations in pediatric patients from 6 to 17 years of age receiving guanfacine in combination with strong and moderate CYP3A inhibitors and inducers. A major assumption of this study was that DDI potential would be the same in children as adults since most developmental processes are complete by six years of age (e.g. hepatic blood flow, CYP3A4 activity, and renal function) and the PK profile for guanfacine was similar between pediatric patients and adults when appropriately scaled by weight.[6] Limitations with this approach include the fact that pediatric clinical data were not used for model development or evaluation, ontogeny and catalytic activity was not considered for CYP3A5 and CYP3A7, and the assumption that DDI potential is the same in pediatric patients as adults may not be true particularly for infants and younger children**.**

To overcome some of these limitations, we have developed a systematic approach using PBPK modeling to characterize CYP3A mediated DDI potential and provide therapeutic recommendations for children of all ages receiving CYP3A substrates in combination with CYP3A perpetrators. This approach includes pediatric clinical data for PBPK model

development and evaluation, will be applicable for all pediatric populations from preterm infants to adolescents, will include ontogeny and catalytic activity information for the CYP3A subfamily (CYP3A4, CYP3A5, and CYP3A7), and will include complex interaction scenarios such as induction plus competitive and time-dependent inhibition.

1.11 Project Rationale and Specific Aims

The objective of this dissertation is to develop a systematic approach leveraging PBPK modeling that can provide dosing recommendations in pediatric patients experiencing CYP3A mediated DDIs (Figure 1.5). We develop a systematic approach to characterize CYP3A mediated DDIs in infants and children using PBPK that is broadly applicable for a variety of interaction mechanisms causing DDIs. We selected probe DDIs that encompassed many of these interaction mechanisms such as TDI, competitive inhibition, noncompetitive inhibition, and induction. We also focused on DDIs that were clinically relevant and that had sufficient clinical data available for model evaluation: sildenafil plus fluconazole and lopinavir and ritonavir (LPV/RTV) plus rifampicin. The competitive CYP3A inhibitor, fluconazole, and the CYP3A substrate sildenafil are commonly administered to neonates in the neonatal intensive care unit. LPV/RTV is one of the preferred agents for HIV treatment in treatment naïve infants and children from two weeks post-natal age to three years of age.[42] RTV undergoes mixed competitive plus TDI as well as induction of CYP3A, and is administered with LPV as a boosting agent to improve its bioavailability. LPV/RTV is used in combination with the CYP3A inducer, rifampicin, in HIV infected children co-infected with tuberculosis. This systematic approach will next be applied to predict DDI potential and optimal dosing for a novel drug (solithromycin) lacking DDI data in children.

1.11.1 Specific Aim 1

Apply PBPK modeling to characterize competitive inhibition between the CYP3A inhibitor fluconazole and the CYP3A substrate sildenafil in preterm and term infants.

Hypothesis: Sildenafil clearance will be 47% lower in infants receiving fluconazole with sildenafil compared to infants receiving sildenafil alone.

Sub-aim 1.1: Determine the inhibition constant (K_I) for fluconazole for CYP3A4,5,7 using recombinant enzymes.

Sub-aim 1.2: Develop an adult and pediatric PBPK model for the CYP3A substrates sildenafil, which incorporates competitive inhibition for fluconazole.

Sub-aim 1.3: Perform simulations to assess optimal dosing of sildenafil when administered with fluconazole in preterm and term infants.

1.11.2 Specific Aim 2

Apply PBPK modeling to characterize competitive and time-dependent inhibition plus induction of CYP3A between LPV/RTV and the CYP3A inducer rifampicin in infants and children.

Hypothesis: Rifampicin will increase the clearance of lopinavir and ritonavir by 58% and 34%, respectively in adults and 48% and 22%, respectively, in children.

Sub-aim 2.1: Develop and evaluate an adult PBPK for LPV/RTV plus rifampicin that accounts for mixed competitive and TDI and induction of CYP3A.

Sub-aim 2.2: Scale the LPV/RTV plus rifampicin adult model to pediatrics and evaluate using pediatric data available in pediatric patients from 2 weeks to 17 years of age.

Sub-aim 2.3: Perform dosing simulations for LPV/RTV when used in combination with the CYP3A inducer rifampicin in infants and children.

1.11.3 Specific Aim 3

Apply this systematic approach to characterize competitive and TDI plus induction of CYP3A in infants and children receiving solithromycin.

Hypothesis: When co-administered with solithromycin, strong CYP3A inhibitors will result in a ≥ 80% decrease, in solithromycin AUC in adult and pediatric patients.

Sub-aim 3.1: Characterize the in-vitro enzymatic activity (K_m, V_{max}) and TDI parameters (K_{inact}, K_I) of CYP3A4, 5, 7 for solithromycin using recombinant enzyme systems.

Sub-aim 3.2: Develop adult and pediatric PBPK models for solithromycin incorporating time-dependent autoinhibition.

Sub-aim 3.3: Determine optimal dosing for pediatric patients receiving solithromycin in combination with the CYP3A substrate, midazolam, and the CYP3A strong inhibitor, ketoconazole.

1.12 Tables

Table 1.1: Classes of human hepatic drug metabolizing enzyme developmental trajectories[26]

Class 1	Class 2	Class 3
ADH1A	CYP2C19	ADH1B
CYP3A7	CYP2B6	ADH1C
FMO1	CYP3A5	AOX1
GSTP	GSTA1	CES1
SULT1E1	GSTA2	CES2
SULT1A3	SULT1A1	CYP2C9
		CYP2D6
		CYP2E1
		CYP3A4
		EPHX1
		EPHX2
		FMO3
		GSTM1
		GSTZ1
		SULT2A1
		UGT1A1
		UGT1A6
		UGT2B7

*Permission was obtained from the International Journal of Pharmaceutics for re-use of this figure.

Abbreviations: ADH: alcohol dehydrogenase; CYP: cytochrome P450; FMO: Flavin-binding monooxygenase family protein; GSTP: glutathione S-tranferase pi; GST: glutathione S-transferase; SULT: sulfotransferase; GST: glutathione S-transferase; AOX: alternative oxidase; CES: carboxylesterase; EPHX: epoxide hydrolase; UGT: UDP glucuronosyltransferase

Table 1.2: In-vitro clearance at low substrate concentrations of substrate by CYP3A4, CYP3A5, and CYP3A7[3]

Metabolite	CYP3A4	CYP3A5	CYP3A7
	mL/min/nmol P450		
1-OH-Midazolam	3.34	3.31	0.02
4-OH-Midazolam	0.99	0.15	0.04
1-OH-Alprazolam	0.05	0.03	0.003
4-OH-Alprazolam	1.1	0.34	0.02
1-OH-Triazolam	0.54	0.14	0.004
4-OH-Triazolam	0.3	0.05	0.061
N-Desmethyl diltiazem	0.69	0.2	0.18
6-OH-Testosterone	2.34	0.06	0.02
N-Desmethyl clarithromycin	51.2	4.3	5.06
14-OH-Clarithromycin	7.03	0.23	0.53
2-OH-Estradiol	0.44	0.01	0.005
4-OH-Estradiol	0.1	0.006	0.0002
Oxidized-nifedipine	5	0.24	0.08
7-Hydroxy-4-trifluoromethyl coumarin	0.02	0.0004	0.0006
N-Desmethyl tamoxifen	0.28	0.13	0.045

Abbreviations: CYP: cytochrome P450; OH: hydroxy

1.13 Figures

Figure 1.1: Major categories of drug-drug interactions (DDIs)

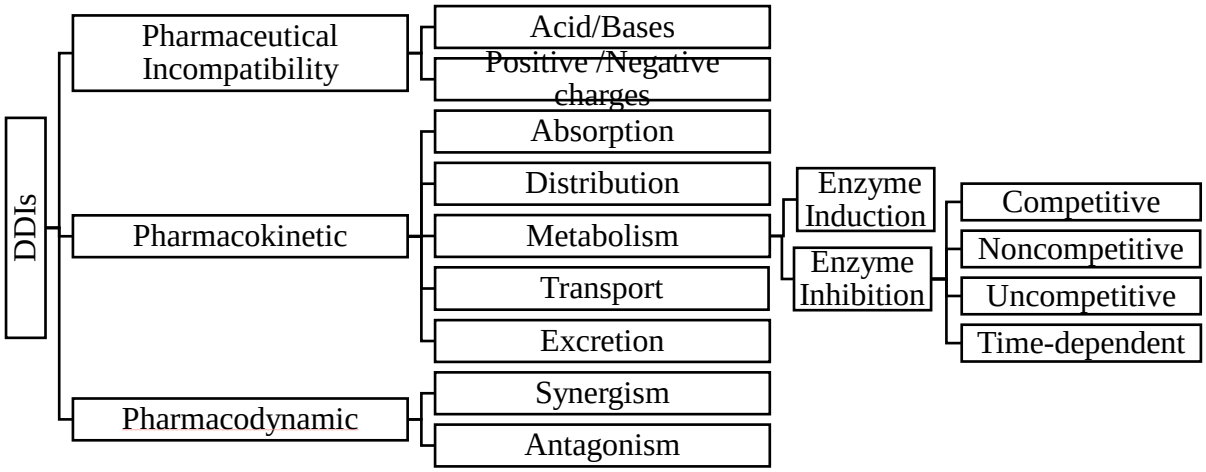

Drug-drug interactions (DDIs) can broadly be categorized as pharmaceutical incompatibility or pharmacokinetic (PK) or pharmacodynamic (PD) interactions. DDIs arising from pharmaceutical incompatibility occur when drugs with incompatible physiochemical properties are combined, such as acids and bases and positively and negatively charged species. PK DDIs occur when a drug changes the concentration of another drug at the level of absorption, distribution, metabolism, transport, or excretion. PD mediated interactions occur when a drug increases (synergism) or decreases (antagonism) the effects of another drug without altering drug concentrations. Metabolic DDIs can be classified as enzyme induction, where a drug enhances the metabolism of another drug, or enzyme inhibition, where a drug inhibits the metabolism of another drug. Enzyme inhibition can further be classified as competitive, noncompetitive, uncompetitive, and time-dependent inhibition (TDI) based on the biochemical mechanism.

Figure 1.2: U.S. Food and Drug Administration (FDA) recommended *in vitro* studies to evaluate metabolism mediated drug-drug interactions (DDIs) and determine if clinical studies are recommended[11]

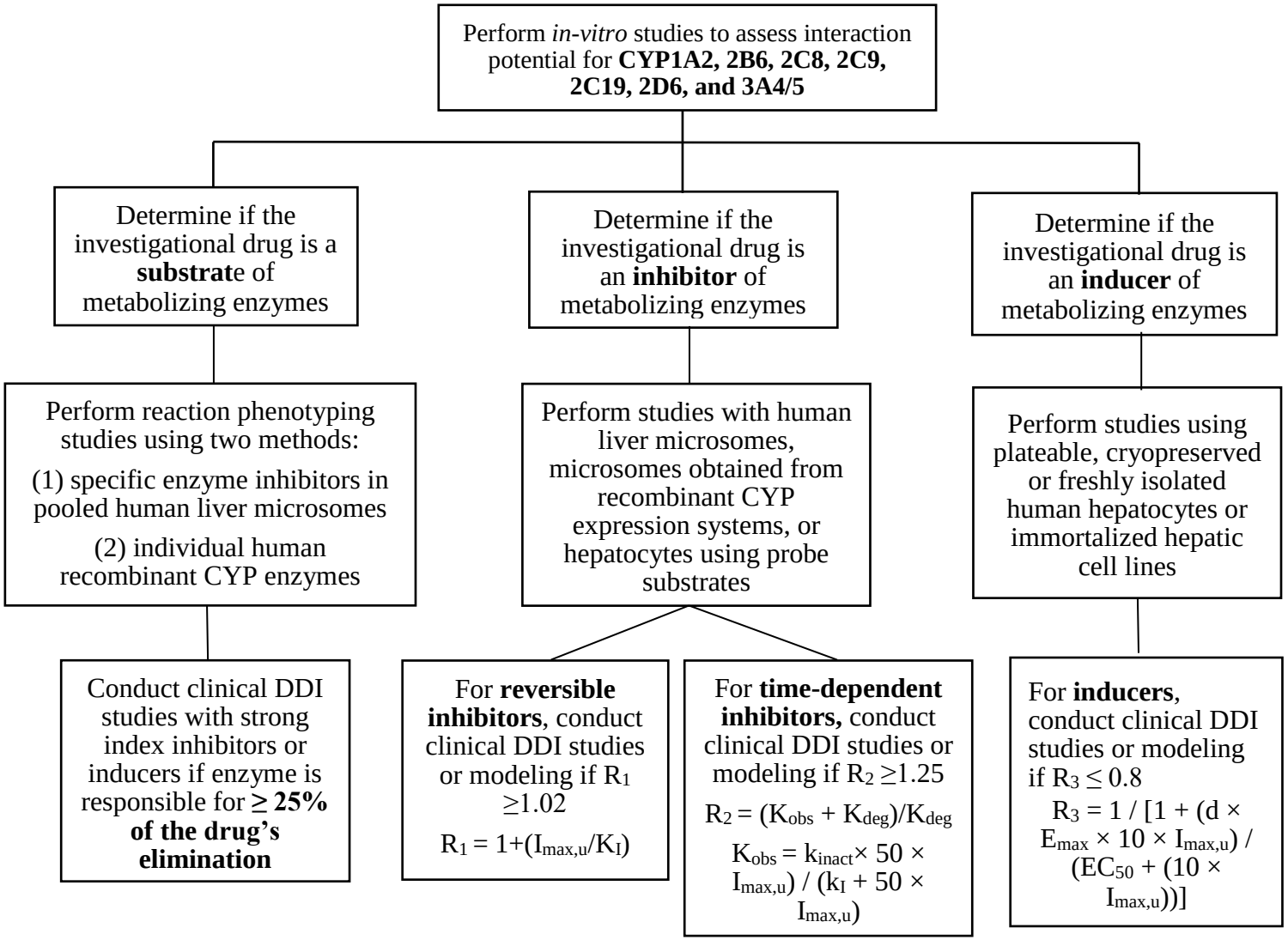

Abbreviations: CYP: cytochrome; R_1: predicted ratio of victim drug's area under the plasma concentration versus time curve (AUC) in the presence and absence of an inhibitor; $I_{max,u}$: maximal unbound plasma concentration of the interacting drug; K_I: unbound inhibition constant determined *in-vitro*; R_2: predicted ratio of victim drug's AUC in the presence and absence of an inhibitor for models of time-dependent inhibition; k_{obs}: observed (apparent first order) inactivation rate constant of the affected enzyme; k_{deg}: apparent first-order degradation rate constant of the affected enzyme; k_I: inhibitor concentration causing half-maximal inactivation; k_{inact}: maximal inactivation rate constant; R_3: predicted ratio of the victim drug's AUC in the presence and absence of an inducer for basic models of enzyme induction; d: scaling factor and is assumed to be 1 unless supported by prior experience with the system used; E_{max}: maximum induction effect determined in vitro; $I_{max,u}$: maximal unbound plasma concentration of the interacting drug; EC_{50} is the concentration causing half-maximal effect determined in vitro.

Figure 1.3: Approaches to evaluate pediatric pharmacokinetic (PK) drug-drug interactions (DDIs) throughout pediatric drug development and post-marketing.[a]

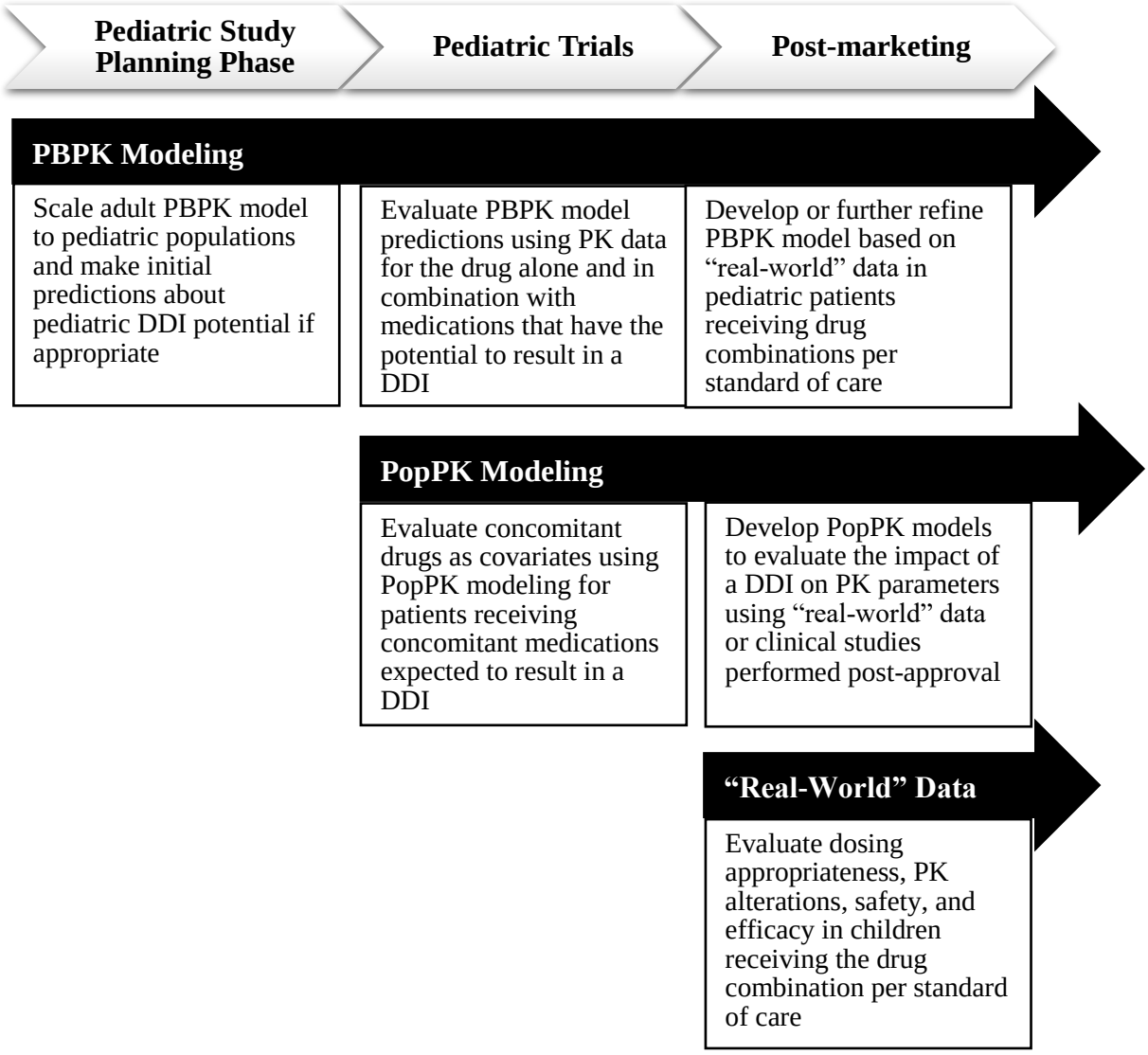

[a]Figure reprinted with approval from: Salerno SN, Burckart GJ, Huang SM, and Gonzalez D. Pediatric Drug-Drug Interaction Studies: Barriers and Opportunities. *Clin Pharmacol Ther*. 2018; 105(5):1067-1070. Prior to pediatric drug approval, physiologically-based pharmacokinetic (PBPK) modeling and simulation can investigate pediatric drug-drug interaction (DDI) potential and inform dose adjustments that can be evaluated through prospective pediatric trials. PBPK models can also be developed or further refined using "real-

world" pediatric DDI data for marketed drugs. Once pediatric pharmacokinetic (PK) and coadministered drug data are available, population based pharmacokinetic (PopPK) models can be developed and concomitant drugs can be evaluated as predictors of inter-individual variability in pharmacokinetic (PK) parameters. Dosing simulations can then be performed based on the final PopPK model to optimize dosing for children receiving the drug combination of interest. After drug approval, studies leveraging "real-world" data can be performed to evaluate dosing appropriateness, PK alterations, safety, and efficacy in children receiving the drug combination of interest per standard of care.

Figure 1.4: Application of physiologically-based pharmacokinetic (PBPK) modeling and simulation to predict drug-drug interaction (DDI) potential in pediatric patients[a]

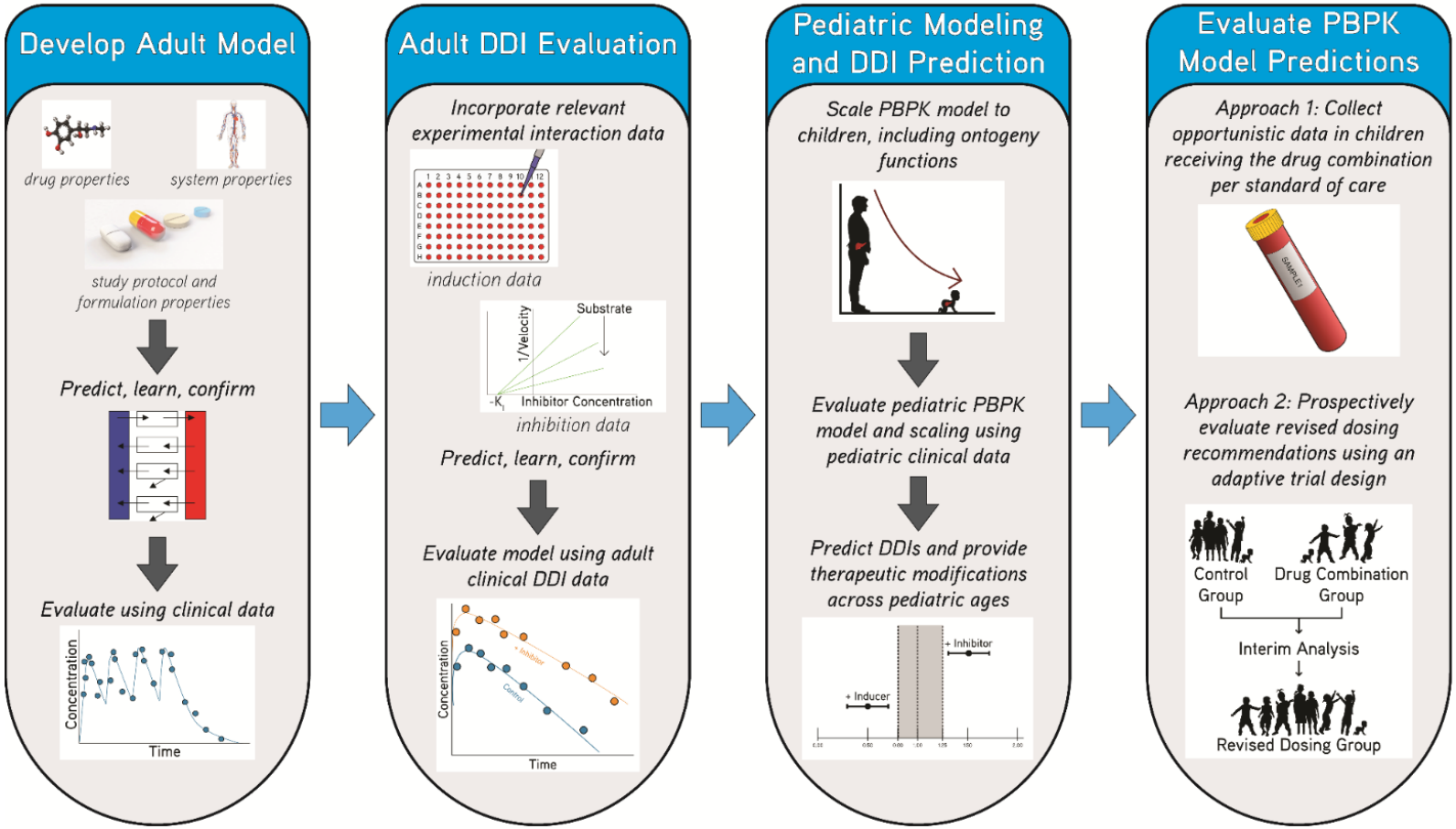

[a]Figure reprinted with approval from: Salerno SN, Burckart GJ, Huang SM, and Gonzalez D. Pediatric Drug-Drug Interaction Studies: Barriers and Opportunities. *Clin Pharmacol Ther*. 2018; 105(5):1067-1070. Adult physiologically-based pharmacokinetic (PBPK) models can be developed incorporating drug-specific, system-specific, and study protocol and formulation properties, and then evaluated and further refined using adult clinical data. Next, drug-drug interaction (DDI) potential can be evaluated by incorporating *in-vitro* induction or inhibition parameters and then further refined using adult DDI data. Adult PBPK models can be scaled to pediatric patients including anthropomorphic and ontogeny functions, and then model performance and scaling can be evaluated using available pediatric data. Next, DDIs can be simulated in pediatric patients in order to provide therapeutic recommendations across pediatric ages likely to receive the drug. Finally, dosing recommendations can be evaluated using opportunistic pharmacokinetic data or using prospectively captured data from an adaptive trial. During adaptive trials, efficacy and safety of the dosages and drug combinations can be monitored in pediatric patients throughout the trial at pre-specified times and the dosing regimen can be modified according to these interim study results.

Figure 1.5: Dissertation research overview

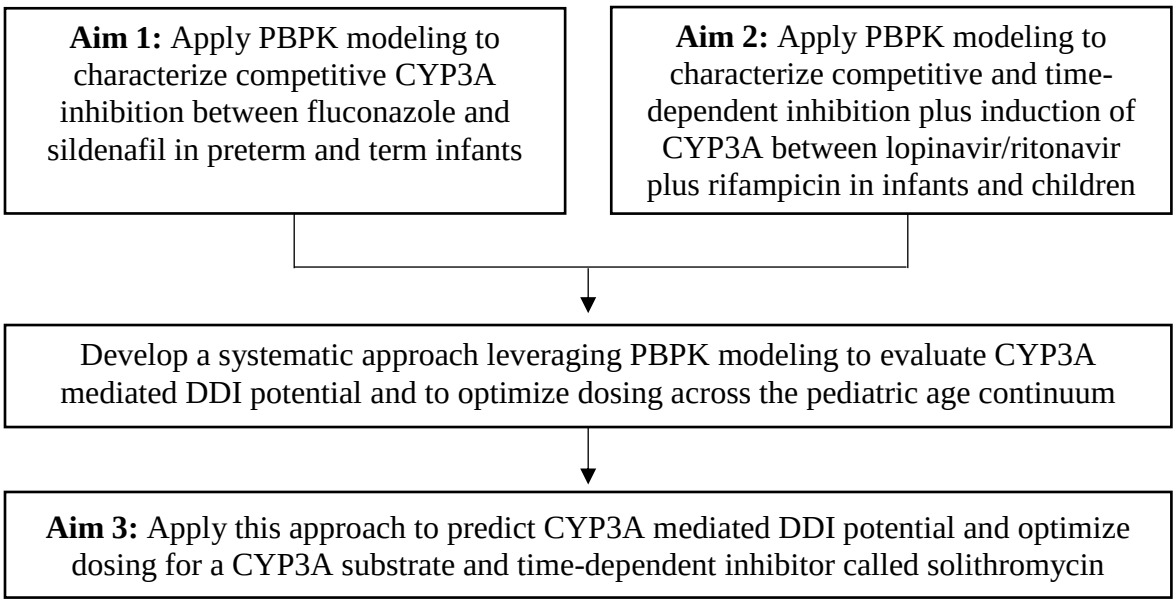

REFERENCES

1. Hines, R. N. Ontogeny of human hepatic cytochromes P450. *J. Biochem. Mol. Toxicol.* **21**, 169–75 (2007).

2. Stevens, J. C. *et al.* Developmental expression of the major human hepatic CYP3A enzymes. *J. Pharmacol. Exp. Ther.* **307**, 573–582 (2003).

3. Williams, J. A. *et al.* Comparative metabolic capabilities of CYP3A4, CYP3A5, and CYP3A7. *Drug Metab. Dispos.* **30**, 883–91 (2002).

4. Soars, M. G., Grime, K. & Riley, R. J. Comparative analysis of substrate and inhibitor interactions with CYP3A4 and CYP3A5. *Xenobiotica* **36**, 287–299 (2006).

5. Salerno, S. N., Burckart, G. J., Huang, S.-M. & Gonzalez, D. Pediatric drug-drug interaction studies: Barriers and opportunities. *Clin. Pharmacol. Ther.* (2018).

6. Li, A., Yeo, K., Welty, D. & Rong, H. Development of guanfacine extended-release dosing strategies in children and adolescents with ADHD using a physiologically based pharmacokinetic model to predict drug–drug interactions with moderate CYP3A4 inhibitors or inducers. *Pediatr. Drugs* **20**, 181–194 (2018).

7. Freedman, M. D. Drug Interactions: Classification and systematic approach. *Am. J. Ther.* **2**, 433–443 (1995).

8. Hermann, R., Derendorf, H., Richter, O. von & Rostami-Hodjegan, A. Core entrustable professional activities in clinical pharmacology: Pearls for clinical practice: Drug-drug and food-drug interactions. *J. Clin. Pharmacol.* **58**, 704–716 (2018).

9. Grimm, S. W. *et al.* The conduct of in vitro studies to address time-dependent inhibition of drug-metabolizing enzymes: A perspective of the pharmaceutical research and manufacturers of America. *Drug Metab. Dispos.* **37**, 1355–1370 (2009).

10. Ramsay, R. R. & Tipton, K. F. Assessment of enzyme inhibition: A review with examples from the development of monoamine oxidase and cholinesterase inhibitory drugs. *Molecules* **22**, 1192 (2017).

11. Food and Drug Administration. In vitro metabolism- and transporter-mediated drug-drug interaction studies guidance for industry (2017). <http://www.raps.org/Regulatory-Focus/News/2017/10/25/28747/FDA-Offers-Two-Draft-Guidances-on-Drug-Drug-Interactions/> Accessed May 04, 2019.

12. Food and Drug Administration, Center for Drug Evaluation and Research. Clinical drug interaction studies — Study design, data analysis, and clinical implications guidance for industry clinical drug interaction studies — Study design, data analysis, and clinical implications guidance for industry. (2017) <https://www.fda.gov/downloads/drugs/guidances/ucm292362.pdf> Accessed May 04, 2019.

13. Dai, D., Feinstein, J. A., Morrison, W., Zuppa, A. F. & Feudtner, C. Epidemiology of polypharmacy and potential drug–drug interactions among pediatric patients in ICUs of U.S. children's hospitals. *Pediatr. Crit. Care Med.* **17**, e218–e228 (2016).

14. Feinstein, J., Dai, D., Zhong, W., Freedman, J. & Feudtner, C. Potential drug−drug interactions in infant, child, and adolescent patients in children's hospitals. *Pediatrics* **135**, 3–12 (2015).

15. *Protection of Human Subjects. Additional Safeguards for Children in Clinical Investigations.* 21 C.F.R. § 50.52 (2017).

16. Greenberg, R. G. *et al.* Parents' perceived obstacles to pediatric clinical trial participation: Findings from the clinical trials transformation initiative. *Contemp. Clin. trials Commun.* **9**, 33–39 (2018).

17. Laughon, M. M. *et al.* Innovative clinical trial design for pediatric therapeutics. *Expert Rev. Clin. Pharmacol.* **4**, 643–52 (2011).

18. Autmizguine, J. *et al.* Pharmacokinetic studies in infants using minimal-risk study designs. *Curr. Clin. Pharmacol.* **9**, 350–8 (2014).

19. Salem, F., Rostami-Hodjegan, A. & Johnson, T. N. Do children have the same vulnerability to metabolic drug-drug interactions as adults? A critical analysis of theliterature. *J. Clin. Pharmacol.* **53**, 559–566 (2013).

20. Salem, F., Johnson, T. N., Barter, Z. E., Leeder, J. S. & Rostami-Hodjegan, A. Age related changes in fractional elimination pathways for drugs: Assessing the impact of variable ontogeny on metabolic drug-drug interactions. *J. Clin. Pharmacol.* **53**, 857–865 (2013).

21. Zanger, U. M. & Schwab, M. Cytochrome P450 enzymes in drug metabolism: Regulation of gene expression, enzyme activities, and impact of genetic variation. *Pharmacol. Ther.* **138**, 103–141 (2013).

22. Lasky, T., Ernst, F. R., Greenspan, J., Wang, S. & Gonzalez, L. Estimating pediatric inpatient medication use in the United States. *Pharmacoepidemiol. Drug Saf.* **20**, 76–82 (2011).

23. Hsieh, E. M. *et al.* Medication use in the neonatal intensive care unit. *Am. J. Perinatol.* **31**, 811–21 (2014).

24. DrugBank, DrugBank *version 5.1.2* (2019) <https://www.drugbank.ca> Accessed 04 May, 2019.

25. Triumeq Pharmacology. Epocrates Online. (2019) <https://online.epocrates.com/drugs/695907/Triumeq/Pharmacology> Accessed May 04, 2019.

26. Hines, R. N. Developmental expression of drug metabolizing enzymes: Impact on disposition in neonates and young children. *Int. J. Pharm.* **452**, 3–7 (2013).

27. Sim, S. C., Edwards, R. J., Boobis, A. R. & Ingelman-Sundberg, M. CYP3A7 protein expression is high in a fraction of adult human livers and partially associated with the CYP3A7*1C allele. *Pharmacogenet. Genomics* **15**, 625–631 (2005).

28. Rodrigues, A. D. Integrated cytochrome P450 reaction phenotyping. Attempting to bridge the gap between cDNA-expressed cytochrome P450 and native human liver microsomes. *Biochem. Pharmacol.* **57**, 465–480 (1999).

29. Patki, K. C., Moltke, L. L. Von & Greenblatt, D. J. In vitro metabolism of midazolam, triazolam, nifedipine, and testosterone by human liver microsomes and recombinant cytochromes P450: role of CYP3A4 and CYP3A5. *Drug Metab. Dispos.* **31**, 938–944 (2003).

30. Gibbs, M. A., Thummel, K. E., Shen, D. D. & Kunze, K. L. Inhibition of cytochrome P-450 3A (CYP3A) in human intestinal and liver microsomes: Comparison of K1 values and impact of CYP3A5 expression. *Drug Metab. Dispos.* **27**, 180–187 (1999).

31. Food and Drug Administration Center for Drug Evaluation and Research Summary Minutes of the Advisory Committee for Pharmaceutical Science and Clinical Pharmacology. (2019) <https://wayback.archive-it.org/7993/20170404154933/https:/www.fda.gov/downloads/AdvisoryCommittees/CommitteesMeetingMaterials/Drugs/AdvisoryCommitteeforPharmaceuticalScienceandClinicalPharmacology/UCM306989.pdf> Accessed May 04, 2019.

32. Standing, J. F. *et al.* Dosing of ceftriaxone and metronidazole for children with severe acute malnutrition. *Clin. Pharmacol. Ther.* **104**(6): 1165-1174 (2018).

33. Tremoulet, A. *et al.* Characterization of the population pharmacokinetics of ampicillin in neonates using an opportunistic study design. *Antimicrob. Agents Chemother.* **58**, 3013–20 (2014).

34. Germovsek, E., Barker, C. I. S., Sharland, M. & Standing, J. F. Pharmacokinetic–pharmacodynamic modeling in pediatric drug development, and the importance of standardized scaling of clearance. *Clin. Pharmacokinet.* **58**(1)39-52 (2018).

35. Xu, J. *et al.* An adaptive design to investigate the effect of ketoconazole on pharmacokinetics of GSK239512 in healthy male volunteers. *J. Clin. Pharmacol.* **55**, 505–511 (2015).

36. Hornik, C. P. *et al.* Development of a pediatric physiologically-based pharmacokinetic model of clindamycin using opportunistic pharmacokinetic data. *Clin. Pharmacokinet.* **56**(11):1343-1353 (2017).

37. Thakkar, N. *et al.* An opportunistic study evaluating pharmacokinetics of sildenafil for the treatment of pulmonary hypertension in infants. *J. Perinatol.* **36**(9): 744-747 (2016).

38. Leroux, S. *et al.* Pharmacokinetic studies in neonates: The utility of an opportunistic sampling design. *Clin. Pharmacokinet.* **54**, 1273–1285 (2015).

39. Boonsathorn, S. *et al.* Clinical pharmacokinetics and dose recommendations for posaconazole in infants and children. *Clin. Pharmacokinet.* **58**:53-61(2019).

40. Mehrotra, N. *et al.* Role of quantitative clinical pharmacology in pediatric approval and labeling. *Drug Metab. Dispos.* **44**, 924–933 (2016).

41. Wagner, C. *et al.* Application of physiologically based pharmacokinetic (PBPK) modeling to support dose selection: Report of an FDA public workshop on PBPK. *CPT Pharmacometrics Syst. Pharmacol.* **4**, 226–230 (2015).

42. Guidelines for the Use of Antiretroviral Agents in Pediatric HIV Infection Guidelines for the Use of Antiretroviral Agents in Pediatric HIV Infection How to Cite the Pediatric Guidelines: Panel on Antiretroviral Therapy and Medical Management of HIV-Infec. *AIDSinfo.* (2019) <https://aidsinfo.nih.gov/guidelines> Accessed May 04, 2018.

CHAPTER 2 : PHYSIOLOGICALLY-BASED PHARMACOKINETIC MODELING CHARACTERIZES THE CYP3A-MEDIATED DRUG-DRUG INTERACTION BETWEEN FLUCONAZOLE AND SILDENAFIL IN INFANTS[1]

2.1 Introduction

If an investigational drug is suspected to interact with concomitant medications, drug-drug interaction (DDI) studies are performed in healthy adult volunteers during drug development and are communicated in the product label.[1] For ethical reasons, pediatric DDI studies are rarely conducted unless children receive the drugs per standard of care. There are also logistic challenges for conducting pediatric DDI studies, such as low enrollment and smaller blood volume, particularly in neonates, available for pharmacokinetic (PK) sampling. Consequently, therapeutic management of pediatric DDIs is based on adult DDI studies although developmental differences in activity of drug metabolizing enzymes may lead to age-related differences in DDI potential. Within the CYP3A (cytochrome P450 3A) subfamily, CYP3A7 is highly expressed in fetal tissue and neonates and typically has reduced metabolic capacity for drugs compared to CYP3A4, which is primarily expressed in adults.[2–7]

Physiologically-based pharmacokinetic (PBPK) modeling can predict pediatric DDIs by incorporating drug and system properties, in vitro data, and maturation of drug metabolizing

[1]This chapter previously appeared as an article in the *Clin Pharmacol Ther*. The original citation is as follows: Salerno, SN, et al. Physiologically-Based Pharmacokinetic Modeling Characterizes the CYP3A-Mediated Drug-Drug Interaction between Fluconazole and Sildenafil in Infants. *Clin Pharmacol Ther.* July 21, 2020. Online ahead of print.

enzymes. PBPK modeling has been applied to characterize CYP3A-mediated DDIs in children >2 years of age.[8,9] Using the CYP3A-mediated DDI between sildenafil with fluconazole, we leveraged PBPK modeling and sildenafil PK data collected in preterm infants with and without fluconazole to characterize CYP3A DDIs in adults and infants. Sildenafil is a phosphodiesterase type 5 inhibitor used off-label in infants for pulmonary hypertension.[10] Hospitalized preterm infants receiving sildenafil are at risk for fungal infection, thus may also be prescribed the moderate CYP3A inhibitor, fluconazole, for the prophylaxis and treatment of invasive candidiasis.[11]

Sildenafil is metabolized primarily by CYP3A, with minor contribution by CYP2C9, into 16 metabolites.[12–14] Sildenafil has 96% plasma protein binding, preferentially towards alpha-1-acid glycoprotein (AAG), that is concentration independent from 0.1 to 10 µg/mL (0.21 to 21 µmol/L).[15,16] The active metabolite, N-desmethylsildenafil (DMS), has half the phosphodiesterase type 5 inhibitory activity as sildenafil.[13,17] One study determined that the *in vitro* formation kinetic intrinsic clearance (CL_{int}) (µL/min/pmol CYP3A) for DMS was similar for CYP3A4 (0.733) and CYP3A5 (0.788), but significantly lower for CYP3A7 (0.079).[18] Based on a study in 36 term neonates receiving intravenous (IV) sildenafil for persistent pulmonary hypertension of the newborn or hypoxemia, sildenafil clearance (CL) increased 3-fold in the first week of life from 0.84 L/h on day 1 to 2.58 L/h at 7 days of age.[19] This is likely due to the developmental switch from CYP3A7 to CYP3A4 expression shortly after birth.

A population pharmacokinetic (PopPK) model developed in 11 infants (2–121 days) receiving sildenafil for pulmonary hypertension, of which 3 also received fluconazole, reported that fluconazole decreased sildenafil clearance by 47%.[20] Similarly, another PopPK study based on 34 preterm infants receiving sildenafil, with 4 also receiving fluconazole, reported a 59%

decrease in sildenafil CL by fluconazole.[21] One study reported that the fluconazole inhibitory constant was 9-fold higher for CYP3A5 than CYP3A4 (84.6 ± 12.9 µM versus 9.21 ± 0.51 µM), however data are not available for CYP3A7.[5] Therefore, the goals of this study were : 1) to develop an adult PBPK model for sildenafil and DMS; 2) to determine and incorporate CYP3A4, CYP3A5, and CYP3A7 inhibitory constants (K_I) for fluconazole; 3) to evaluate CYP3A DDI potential for sildenafil and DMS in adults; 4) to scale and evaluate the DDI between sildenafil with fluconazole in infants; and 5) to optimize dosing for infants receiving sildenafil with fluconazole.

2.2 Materials and Methods

2.2.1 Adult PBPK Model Development

A whole-body adult PBPK model was developed for sildenafil and DMS in PK-Sim® as part of the open source Open Systems Pharmacology Suite version 8.0 (www.open-systems-pharmacology.org) incorporating CYP3A.[22] We compared model simulations with and without CYP2C9-mediated metabolism incorporated into the model because it has been postulated to play a minor role in formation of DMS. Adult PK data were digitized from the literature for model development and evaluation (Table 2.1). A 36-year-old European male with a weight of 73.8 kg and a height of 175.5 cm was used for model development. The relative organ contributions for CYP enzymes were taken from the built-in database query using array levels.[23] The reference concentration refers to the highest organ expression per age (whereby the ontogeny factor is 1). The default reference concentration in PK-Sim® was 4.32, 0.04, and 3.84 µmoL/L liver tissue for CYP3A4, CYP3A5, and CYP2C9, respectively.[24] CYP3A4 concentrations in pediatrics are calculated as a fraction of 4.32 µmol/L using the CYP3A4 ontogeny function. Since CYP3A7 is greatest at birth, we calculated the liver reference

concentration for CYP3A7 in preterm infants as follow: 4 µmol/L for a preterm infant: 158 pmol/mg microsomal protein x 26 mg microsomal protein/g liver x 1 g/mL x 1000 mL/L x $1*10^{-6}$ µmol/pmol.[2,25,26] Adult CYP3A7 liver concentrations are therefore calculated as a fraction of 4 µmol/L using the CYP3A7 ontogeny function.

Sildenafil and DMS were co-modeled using CYP3A4, CYP3A5, CYP3A7, and CYP2C9 formation kinetics from the literature for DMS.[12,18,27] Parameter optimization was performed for sildenafil and DMS lipophilicity using the digitized IV adult data incorporating the Monte Carlo algorithm.[28] The organ-to-plasma partition coefficients were calculated using the Rodgers and Rowland method.[29] Since kinetics for formation of the remaining CYP3A catalyzed sildenafil metabolites are unknown, the sildenafil CYP3A maximal velocity (V_{max}) for the remainder of sildenafil metabolites was optimized using the Monte Carlo algorithm (fixing the concentration of half-maximal velocity (K_M) to 15 uM[18,27]). The relative contribution by CYP3A4/5/7 to formation of the remainder of sildenafil metabolites was calculated assuming the same proportion of intrinsic clearance (CL_{int}) activity as for formation of DMS.[18] In brief, the optimized V_{max} for CYP3A4 (10 pmol/min/pmol CYP3A4) was multiplied by the ratio of CL_{int} of CYP3A5 to CYP3A4 (1.08) or CYP3A7 to CYP3A4 (0.108) to obtain the V_{max} for CYP3A5 (10.8 pmol/min/pmol CYP3A5) and CYP3A7 (1.08 pmol/min/pmol CYP3A7), respectively.[18] The final V_{max} for CYP3A4 was calculated by subtracting the V_{max} multiplied by reference concentration for CYP3A5 and CYP3A7 from the optimized value for CYP3A4, and then dividing by the reference concentration for CYP3A4. The equation is as follows: (10 pmol/min/pmol CYP3A4 x 4.32 µmol/L of CYP3A4 in the liver) minus (1.08 x 10 pmol/min/pmol CYP3A5 x 0.04 µmol/L of CYP3A5 in the liver) minus (0.108 x 10 pmol/min/pmol CYP3A7 x 4 µmol/L of CYP3A7 in the liver x the ontogeny factor (0.02) in

adults, which is equal to 42.68. Next, 42.68 is divided by 4.32 µmol/L CYP3A4 liver to obtain the final CYP3A4 V_{max} (9.9 pmol/min/pmol CYP3A4). The Michaelis-Menten constant (K_M) was fixed to 15 uM for CYP3A4/5/7 while V_{max} was optimized. Sildenafil CYP3A7 V_{max} was optimized using the preterm infant PK data since CYP3A7 is minimally expressed in adults. After sildenafil clearance was optimized, CYP3A4 and CYP3A7 CL_{int} for DMS were manually optimized using adult and preterm infant data, respectively.

2.2.2 Adult PBPK Model Evaluation

One hundred virtual male adults from 18–58 years of age (healthy male population) or 100 adult patients (50% male) from 46–76 years of age (pulmonary arterial hypertension population) were created based on reported demographics. Population simulations were performed, and the ratio for the mean simulated and observed area under the concentration versus time curve (AUC) from 0 until the last observed value ($AUC_{0\text{-}last}$) or from 0 to infinity ($AUC_{0\text{-}\infty}$), as reported, was compared for each dosing regimen. The mean CL and volume of distribution at steady-state (V_{ss}) was also compared between simulations and observations.

2.2.3 6β-Hydroxytestosterone Assay

A Thermo TSQ Quantum Ultra triple-quadrupole mass spectrometer and an Agilent Poroshell (Santa Clara, California, USA) 120 EC-C18 2.7 µm column (2.1 x 50 mm) were used. A gradient with 0.1% formic acid and acetonitrile delivered at 350 µL/min was used as the mobile phase. Calibration standard concentrations (0.05, 0.1, 0.5, 1, 5, 10, 50, and 100 µM 6β-hydroxytestosterone plus 0.5 µM for 4-androsten-19-1al 3,17-dione) were used for method validation. The mobile phase consisted of water with 0.1% formic acid and acetonitrile delivered at 350 µL/min with the following gradient: 85% water plus 15% acetonitrile between 0 to 0.3 minutes, 70% water plus 30% acetonitrile between 0.3 to 4 minutes, 50% water and acetonitrile

between 4 to 5 minutes, and then 85% acetonitrile plus 15% water between 4 to 6 minutes. A positive mode electrospray ionization was used. 6β hydroxytestosterone and 4-androsten-19-1al 3,17-dione eluted at 2.8 and 3.2 minutes. The ionization source parameters are spray voltage, 3000 V; vaporizer temperature, 300°C; sheath gas flow, 35 (arbitrary units); auxiliary gas flow, 20 (arbitrary units); capillary temperature, 285°C. The precursor to product ions monitored with corresponding collision energies were 303.1 to 267.1 at 15V, 285.1 at 15V, 303.1 at 10V; and 305.1 to 269.1 at 15V, 287.1 at 15V, and 305.1 at 10V.

2.2.4 Linearity Experiments for Fluconazole Inhibition

Initial experiments were performed to determine the linear stage of 6β hydroxytestosterone formation. Incubations (1 mL) with testosterone (15 µM, 250 µM) were performed with cDNA expressed cytochrome P450 (CYP) 3A4 (20 pmol/mL), CYP3A5 (20 pmol/mL) or CYP3A7 (40 pmol/mL) in buffer containing 100 mM potassium phosphate, pH 7.4. The reactions were pre-incubated at 37°C for 5 minutes, and then the reaction was initiated with dihydronicotinamide-adenine dinucleotide phosphate (NADPH) (1 mM final). The reactions were incubated at 37°C for 0, 2, 5, 10, 15, 20, 30, 60, 90, 120 minutes. Finally, 50 uL aliquots were added to 150 µL of ice cold acetonitrile containing 0.5 µM 4-androsten-19-1al 3,17-dione, centrifuged at 3700 x g for 15 minutes, and then analyzed by high performance liquid chromatography with tandem mass spectrometry (HPLC/MS/MS).

2.2.5 Fluconazole Inhibition Kinetics

NADPH, acetonitrile, fluconazole, and testosterone was purchased from Sigma-Aldrich (St. Louis, MO, USA). Human CYP3A4, CYP3A5, and CYP3A7 + reductase + b5 and 0.5 M phosphate buffer, pH 7.4, were purchased from Corning Life Sciences (Corning, NY, USA). All experiments were performed in triplicate. To determine fluconazole inhibition, a 4 x 7 matrix of

testosterone (15, 50, 150, 250 µM) and fluconazole concentrations (0, 15, 50, 100, 200, 300, 400 µM) were evaluated. The reaction volume was 100 µL and contained 20 pmol/mL of CYP3A4/5 or 40 pmol/mL of CYP3A7 in 100 mM potassium phosphate buffer at pH 7.4. The reaction was pre-incubated at 37°C for 5 minutes and then initiated with NADPH (1 mM final). After 5 minutes (CYP3A4/5) or 30 minutes (CYP3A7) of incubation at 37°C, 50 µL was removed and added to 150 µL of ice cold acetonitrile containing 0.5 µM 4-androsten-19-1al 3,17-dione, centrifuged at 3700 x g for 15 minutes, and then analyzed by HPLC/MS/MS.

Model discrimination was made by visual inspection of Lineweaver-Burk plots, as well as by comparing reversible unweighted nonlinear regression fits. The mechanism of reversible fluconazole inhibition was determined in GraphPad Prism 8.0® by comparing Akaike information criterion for competitive, uncompetitive, noncompetitive, and mixed inhibition models as described below. V_{max} is the maximum enzyme velocity without inhibitor (I), expressed in the same units as the velocity (Y). K_I is the inhibition constant, expressed in the same units as I. K_M is s the Michaelis-Menten constant, expressed in the same units as the substrate concentration (X).[30]

Mixed model enzyme inhibition:

Equation 1: Apparent V_{max} ($V_{max,App}$)=V_{max}/(1+I/(Alpha*K_I)

Equation 2: Apparent K_M ($K_{M,App}$)=K_M*(1+I/K_I)/(1+I/(Alpha*K_I))

Equation 3: Y=$V_{max,App}$*X/($K_{M,App}$ + X)

Competitive enzyme inhibition:

Equation 4: Observed K_M ($K_{M,Obs}$)=K_M*(1+[I]/K_I)

Equation 5: Y=V_{max}*X/($K_{M,Obs}$+X)

Noncompetitive enzyme inhibition:

Equation 6: Inhibitor V_{max} ($V_{max,inh}$) =V_{max}/(1+I/K_I)

Equation 7: Y=$V_{max,inh}$*X/(K_M+X)

Uncompetitive enzyme inhibition:

Equation 8: $V_{max,App}$=V_{max}/(1+I/AlphaK_I)

Equation 9: $K_{M,App}$=K_M/(1+I/AlphaK_I)

Equation 10: Y=$V_{max,App}$*X/($K_{M,App}$+X)

AlphaK_I is the inhibition constant, expressed in the same units as inhibitor (I), which is the product of K_I (which is very high, because uncompetitive inhibitors do not bind to the enzyme) and Alpha (which is very low). It is not possible to fit Alpha and K_I separately, but only to determine their product. Alpha determines mechanism. Its value determines the degree to which the binding of inhibitor changes the affinity of the enzyme for substrate. Its value is always greater than zero. When Alpha=1, the inhibitor has equal affinity for the enzyme and the enzyme-substrate complex and is also noncompetitive inhibition. When Alpha is greater than one, the inhibitor preferentially binds to the free enzyme. When Alpha is very large, binding is almost entirely to the free enzyme, and the mixed-model approaches competitive inhibition. When Alpha is less than one, the inhibitor preferentially binds to the enzyme-substrate complex. When Alpha is very small (but greater than zero), the inhibitor binds almost entirely to the enzyme-substrate complex and approaches uncompetitive inhibition.

2.2.6 Adult Ritonavir PBPK Model

PK data from 63 HIV-infected adults (155 samples) receiving 200, 300, 400, 500 mg oral of ritonavir on day 1 and twice a day for 14 days on days 3-17 were digitized from the literature and used for model development and evaluation.[31] The average and range of age, weight, and height were 29 (21-42) years, 67.8 (51-92) kg, and 175.2 (162-190) cm, respectively. Based on

the mean patient demographics from this study, a virtual European male subject (29 years of age, weight of 67.8 kg, and height of 175.2 cm) was used for model development and evaluation.[31] Protein expression for CYP3A4, CYP3A5, CYP2D6, and P-glycoprotein was integrated from the built-in database query using array levels.[23] Standard meals (1000 kcal; 0.59 L; 0.60 meal fraction solid) were administered with each dose per study administration. Transcellular intestinal permeability and lipophilicity were manually optimized and then parameter optimization was performed to optimize P-glycoprotein V_{max}. Population simulations for 100 male subjects were performed based on the patient demographics with age, weight, height, and AAG concentration ranging from 21 to 42 years, 51 to 92 kg, 162 to 190 cm, and 0.53 to 1.7 g/L.[31]

2.2.7 Adult ritonavir plus midazolam DDI simulations

The adult PBPK model for midazolam was based on drug properties (Table 2.2) and was evaluated using IV and oral data digitized from the literature (Table 2.1). Studies in human liver microsomes indicate the midazolam is primarily metabolized by CYP3A4.[32,33] Lipophilicity and transcellular intestinal permeability were optimized using the digitized adult IV and oral data with the Monte Carlo algorithm. Partition coefficients were calculated using the Rodgers and Rowland method and cellular permeability was calculated using the PK-Sim® Standard method. Population simulations based on 100 virtual subjects (white American population from 18 to 46 years of age) receiving a 2 mg IV infusion over 30 minutes and 15 mg orally midazolam were performed and compared with observed data provided in Table 2.1 (Figure 2.1). We simulated the interaction between midazolam plus ritonavir in 100 virtual white American male subjects from 21-50 years of age and 52 to 97 kg of weight and then compared with observed data in healthy adults receiving 3 mg oral midazolam plus three oral doses of 100 mg ritonavir or

placebo over 24 hours.[34] The simulated versus observed average midazolam plus ritonavir/midazolam ratios were 31.4 versus 28.4 for $AUC_{0-\infty}$ and 9.47 versus 4.47 for C_{max}, respectively.

2.2.9 Adult Erythromycin Plus Midazolam DDI Simulations

CYP3A time-dependent inhibition for erythromycin was evaluated by comparing the simulated and observed changes in midazolam based on a double-blind, randomized, crossover study in 12 healthy volunteers receiving 500 mg erythromycin three times a day orally for a week in combination with placebo, IV (0.05 mg/kg) midazolam or oral (15 mg) midazolam.[41] The simulated versus observed mean fold-change for oral midazolam plus erythromycin relative to midazolam alone was 2.6 versus 2.7 for C_{max} and was 4.26 versus 4.42 for $AUC_{0-\infty}$, respectively. The simulated versus observed mean reduction in clearance for IV midazolam plus erythromycin relative to midazolam plus placebo was 47% versus 54%.[41]

2.2.10 Adult DDI Evaluation for Sildenafil Plus Ritonavir and Erythromycin

In order to ensure that CYP3A CL for DMS and sildenafil was accurately parameterized, sildenafil (100 mg oral tablet given on day 1 and day 8) was co-modeled with the CYP3A inhibitor ritonavir administered at 300, 400, 500 mg orally twice daily on day 2, 3, and 4–8, respectively. The area under the concentration versus time curve from 0 to tau (AUC_{τ}), $AUC_{0-\infty}$, maximal concentration (C_{max}), and the fold increase in AUC and C_{max} with and without ritonavir were compared between the observed and simulated data.[42] We also evaluated the DDI between sildenafil plus erythromycin based on a study in 26 male volunteers (18-45 years of age) receiving 100 mg sildenafil on days 1 and 6 along with 500 mg oral erythromycin or placebo twice daily on days 2-6.[43] Finally, the DDI between sildenafil with fluconazole was simulated in healthy adults receiving sildenafil 10 mg IV three times daily plus fluconazole 800 mg IV

followed by 400 mg IV daily using a published fluconazole PBPK model.[44] The DDI between sildenafil with fluconazole was simulated in adults, although adult DDI data were not available for model evaluation.

2.2.11 Pediatric PBPK Model Development

2.2.11a Preterm Infant Population

Physiological parameters regarding body weight, height, organ volumes and blood flow rates, as well as tissue composition (water, protein, and lipids) have already been integrated into PK-Sim®. In brief, developmental changes in organ blood flow rates were the same as neonates, which assumed adult proportions to the contribution towards cardiac output for all organs except those with published data (brain, kidney, muscle, and skin). Exsanguinated organ weight measurements were available for brain, lung, heart, liver, spleen, pancreas, and kidney; while weight-age relationships were determined for skin and stomach using surface area and thickness. The proportion of organ blood content was assumed to be the same as in adults.[45]

2.2.11b Sildenafil PBPK Model Development and Evaluation

PK data for sildenafil and DMS were available from 9 preterm infants (<32 weeks gestational age [GA] and between 3–42 days post-natal age [PNA]) receiving a single dose of sildenafil (0.125 or 0.25 mg/kg IV) per standard of care as part of the Phase 1, multi-center, open label Pediatric Trials Network study (ClinicalTrials.gov Identifier: NCT01670136) (Table 2.1).[21] Samples were collected, when possible, within 15 minutes, 1–2 hours, 3–4 hours, 7–8 hours, 12–14 hours, 24–30 hours, and 48–56 hours post the 90-minute infusion and 30-minute flush time. PK data were dose-normalized to 0.25 mg/kg sildenafil IV. The 4 preterm infants receiving sildenafil with fluconazole were administered sildenafil via the IV route.

The healthy male virtual subject was scaled to a male virtual preterm infant based on mean observed demographics (22 days PNA, 25 weeks GA, and 849 g weight). CL was scaled using PK-Sim® ontogeny functions in equations 11-17.[47] Protein binding to AAG was scaled using a Hill-function-like increase and decrease during the maturation and aging phases, respectively.[48] Clearance was scaled using the PK-Sim® default sigmoidal Hill equations where A is the relative activity at PMA in weeks, $A_{0.5}$ is the PMA in weeks at 50% activity compared to an adult, and n is the Hill coefficient (Equation 11).[47] In the case of proteins showing decreased expression with increasing age, an inverse fit function with an offset activity in adults was used (Equation 12). Variability in the ontogeny was also introduced by simulating a virtual population with 10,000 individuals and then fitting the geometric mean and geometric standard deviation around all of the fitted parameters.[47]

The ontogeny function for CYP3A4 (equation 13) was derived using the following literature data: mRNA expression data and testosterone and dehydoepiandrosterone hydroxylation activity obtained from human livers in fetuses 14-40 weeks, children 1 day to 9 years, and adult donors for transplantation[49]; formation of amprenavir metabolites in human liver microsomes obtained from a fetus, neonate at 1 day, neonate at 2 days, infant at 1 month, infant at 3 months, and an adult[50]; and CYP3A4 expression levels in 77 fetal and pediatric liver microsome samples from 217 to 287 estimated gestational age and 3 to 6 months postnatal age.[2] CYP3A5 has an ontogeny factor of 1 for all ages.[2] The ontogeny function for CYP3A7 (equation 14) was derived using the following literature data: mRNA expression data and testosterone and dehydroepiandrosterone hydroxylation activity obtained from human livers in fetuses 14-40 weeks, children 1 day to 9 years, and adult donors for transplantation[49]; and CYP3A7 expression levels in 77 fetal and pediatric liver microsome samples from 217 to 287 estimated gestational

age and 3 to 6 months postnatal age.[2] The ontogeny function for CYP2C9 (equation 15) was derived using the following literature data: protein content and diclofenac 4-hydroxylase metabolic activity in 237 pediatric liver microsomal liver samples from 8 weeks gestational age to 18 years postnatal age[51]; *in vitro* tolbutamide hydroxylation and CYP2C9 mRNA expression from human liver microsomes obtained from 53 fetuses (16 to 40 weeks) and 15 adults[52]; CYP2C9 mRNA expression as well as 4'-hyroxydiclofenac activity and protein content in liver samples obtained from 15 adults (37 to 81 years).[53]

The CL_{int} per organ (µL/min/organ) is the sum of the V_{max}/K_M of each CYP (µL/min/µmol CYP) multiplied by the reference concentration (µmol CYP/L organ), ontogeny factor, and organ volume (L). Hepatic (CL_H) and plasma CL following IV dosing (CL_{IV}) is described in Equations 16 and 17, where Q_H is liver blood flow, F_u is the fraction unbound, B/P is the blood to plasma partitioning ratio, and CL_R is renal clearance. For model evaluation, simulations in term infants were performed using a virtual population of 100 term infants (36 to 40 weeks GA, and 0 to 3 days PNA). CL and V_{ss} were compared against published values from two PopPK models developed in preterm and term infants.[19,21]

Equation 11[7]: $A = \frac{PMA^n}{A_{0.5}{}^n + PMA^n}$

Equation 12[7]: $A = 1 - \frac{PMA^n}{A_{0.5}{}^n + PMA^n}$ + offset activity in adults

Equation 13[7]: CYP3A4 ontogeny factor at PMA = $\frac{PMA^{3.331}}{73.019^{3.331} + PMA^{3.331}}$

Equation 14[7]: CYP3A7 ontogeny factor at PMA = $1 - \frac{PMA^{27.615}}{48.051^{27.615} + PMA^{27.615}} + 0.0253$

Equation 15[7]: CYP2C9 ontogeny factor at PMA = $\frac{PMA^{8.135}}{36.773^{8.135} + PMA^{8.135}}$

Equation 16: $CL_H = (Q_H * F_u * CL_{int})/(Q_H + F_u * CL_{int})$

Equation 17: $CL_{IV} = (CL_H*B/P) + CL_R$

Figures shown in full age-length and as a zoom-in version in the first period after birth can be found within the PK-Sim® Ontogeny Database Version 7.3.

2.2.12 Sensitivity Analysis

Sensitivity analyses were performed for a healthy adult, preterm infant, term infant at birth, term infant at two weeks of age, 1-month-old, 2-month-old, 3-month-old, 6-month-old, 1-year-old, 2-year-old, 5-year-old, and a 12-year-old. The virtual preterm infant received IV sildenafil whereas the other virtual subjects received sildenafil orally. In PK-Sim®, the input parameter (P_i) is varied around the value in the simulation by a small change and a new simulation is performed keeping all other input values constant. The change in the pharmacokinetic parameter estimate (ΔPK_j) was calculated as the difference between the values in the new simulation and the original simulation. The sensitivity for the PK parameter to the input parameter is calculated as the ratio of the relative change of that PK parameter ($\Delta PK_j/PK_j$) and the relative variation of the input parameter ($\Delta P_i/P_i$) with the equation: $(\Delta PK_j/\Delta P_i)*(P_i/PK_j)$. For example, an interpretation of a sensitivity value -1 or 1 indicates that a 10% increase of the parameter leads to a 10% decrease or increase of the PK parameter value, respectively. Parameters with sensitivity values < -1 or > 1 were reported for sildenafil C_{max} and $AUC_{0-\infty}$. Sensitivity values for CYP3A relative expression were compared among these age groups.

2.2.13 Pediatric DDI Dosing Evaluation and Recommendations

There were 4 preterm infants with PK data who received sildenafil with fluconazole. We co-modeled sildenafil with fluconazole in preterm infants leveraging a previously published fluconazole PBPK model in adults and infants including renal clearance and uridine 5'-disphospho-glucuronosyltransferase family 2 member B7 (UGT2B7) metabolism.[44,46] As

previously described, an adult fluconazole PBPK model was scaled to infants accounting for age dependencies in glomerular filtration and metabolism and was optimized using 760 plasma samples from 166 infants (median postmenstrual age ((PMA) range) 28 weeks (24-50)) and 27 cerebrospinal fluid samples from 22 infants (PMA age 28 weeks (24-33) (Figure 2.3). Additionally, the clearance from a simulated population of 1,000 infants was within twofold of the clearance reported within the product label for infants from 26 to 29 weeks gestational age (GA) for all ages except for infants at 26 weeks PMA).[46]

Only the indication (prophylaxis versus treatment) for fluconazole was recorded for these preterm infants. Without specific details on the exact dosing or route of fluconazole administration, we assumed fluconazole dosing based on the 2016 Infectious Diseases Society of America recommended guidelines for neonatal candidiasis: 12 mg/kg daily administered IV for treatment and 6 mg/kg administered IV every 72 hours for prophylaxis.[54] We simulated prophylaxis and treatment dosing for fluconazole in combination with sildenafil and compared with data in preterm infants receiving fluconazole for prophylaxis or treatment, respectively.

To simulate optimal dosing for this combination in neonates, we created a virtual population of 1,000 preterm and term infants (50% female) ranging from 24 to 40 weeks GA and 0–14 days PNA. Following the U.S. Food and Drug Administration (FDA) guidance, we targeted dosing that would achieve simulated geometric mean ratios of C_{max} and AUC from 0-24 hours (AUC_{0-24}) for sildenafil with fluconazole relative to sildenafil alone within the 80%–125% equivalence range. C_{max} and AUC_{0-24} included both sildenafil and DMS, taking into account differences in relative phosphodiesterase 5 inhibitory activity and free fraction (Equation 18).[1]

Equation 18: AUC_{0-24} (C_{max}) sildenafil + AUC_{0-24} (C_{max}) DMS x 0.5 x 1.25

where 0.5 and 1.25 refers to relative differences in phosphodiesterase type 5 inhibitory activity and protein binding between DMS and sildenafil, respectively.

Exposure ratios were stratified by post-menstrual age using the World Health Organization categories of preterm birth: GA <28 (extremely preterm), ≥28 to <32 (very preterm, ≥32 to <37 (moderate to late preterm), and ≥37 weeks (term). The reference dose for sildenafil was 0.25, 0.5, and 1 mg/kg IV every 8 hours (90-minute infusion). Sildenafil (0.09, 0.13, 0.18, 0.26, 0.36, and 0.52 mg/kg every 8 hours, administered by a 30- and 90-minute infusion) plus fluconazole (12 mg/kg IV daily, administered by a 60-minute infusion) were simulated and compared against reference doses of sildenafil.

2.2.14 Adult Erythromycin PBPK Model

We used an open-source erythromycin PBPK model with the respective evaluation report and complete references at: https://github.com/Open-Systems-Pharmacology/Erythromycin-Model. This model was developed based on clinical data from healthy adult subjects in the literature receiving various IV and oral formulations. The model included CYP3A4 N-demethylation and time-dependent inhibition along with total hepatic clearance to account for acid-catalyzed degradation (hydrolysis) in the stomach, biliary excretion, and CYP4F11 metabolism.[35–37] Using the IV data, the glomerular filtration rate fraction was optimized to 1.16 to reflect the fraction excreted in urine after IV administration.[38,39] IV and oral data were used to optimize the catalytic activity for organic anion transporting polypeptide 1B1 (OATP1B1), transcellular intestinal permeability, and total hepatic clearance (Table 2.2). Partition coefficients were calculated using the Rodgers and Rowland method and cellular permeability were calculated using the charge dependent Schmitt method. The erythromycin enteric-coated tablet (free base) was modeled as a suspension using a Weibull function (dissolution time of 1.75

minutes, a lag time of 54.35 min, and a dissolution shape of 1.06). The film tablet containing erythromycin stearate was modeled as a suspension using a Weibull function (dissolution time of 1.70 minutes and a dissolution shape of 1.10). Population simulations were performed based on 100 virtual subjects (white American population from 21 to 30 years of age) receiving 500 mg erythromycin stearate (Figure 2.2).[40]

2.3 Results

2.3.1 Adult PBPK Model

We developed a whole-body PBPK model for sildenafil and DMS incorporating Michaelis-Menten kinetics by CYP3A4, CYP3A5, CYP3A7 for sildenafil CL and first-order CL_{int} by CYP3A4 and CYP3A7 for elimination of the DMS metabolite (Table 2.3; Figure 2.4). The role of CYP2C9 was insignificant, for example, the $AUC_{0-\infty}$ for the 100 mg dose was 1580 versus 1581 ng*h/mL for sildenafil and was 661 versus 659 ng*h/mL for DMS with and without CYP2C9, respectively. Therefore, unless stated otherwise, all results are without CYP2C9 contribution for parsimony. The adult sildenafil PBPK model adequately captured observed data digitized from the literature (Figure 2.5-Figure 2.9; Table 2.4 and Table 2.5).

2.3.2 Fluconazole Inhibition Studies

6β-hydroxytestosterone production was linear upwards 5 minutes for CYP3A4 and CYP3A5 and 30 minutes for CYP3A7 (Figure 2.10 and Figure 2.11). Fluconazole was a mixed competitive inhibitor for CYP3A4, CYP3A5, and CYP3A7 (Figure 2.12). Alpha values greater than 1 indicate that fluconazole preferentially binds to the free enzyme (competitive inhibition). Fluconazole inhibition was higher for CYP3A4 relative to CYP3A5 and CYP3A7 (Table 2.6).

2.3.3 Adult DDI Evaluation

We evaluated DDI potential for sildenafil in combination with ritonavir and erythromycin in healthy adults. The simulated versus observed geometric mean fold changes in the AUC and C_{max} with and without ritonavir were 13- versus 11-fold and 2.4- versus 3.9-fold for sildenafil $AUC_{0-\infty}$ and C_{max}, and 2.0- versus 1.7-fold and 1.1- versus 0.5-fold for DMS AUC_{0-24} and C_{max} on day 8 (Table 2.7 and Figure 2.13).[42] The simulated versus observed mean fold changes of $AUC_{0-\infty}$ and C_{max} with and without erythromycin were 2.24- versus 2.82-fold and 1.28- versus 2.60-fold for sildenafil and 1.67- versus 1.37-fold and 0.98- versus 0.76-fold for DMS (Table 2.8).[43] There was model misspecification regarding C_{max}, but we were primarily focused on changes in CL and AUC for dosage modification of sildenafil in combination with CYP3A inhibitors.

2.3.4 Pediatric PBPK Model

The adult PBPK model was scaled to infants using CYP3A ontogeny and anthropomorphic functions. Simulated concentrations were compared to 24 and 26 plasma samples for sildenafil and DMS, respectively, from 9 preterm infants (median [range] GA of 25 [23–27] weeks and PNA of 18 [7–40] days) receiving sildenafil, 4 of which also received fluconazole (Table 2.1). The simulated mean CL and V_{ss} in the absence of fluconazole was relatively similar to published values in preterm infants receiving enteral or IV doses, and to term infants receiving a continuous infusion of sildenafil except for DMS in one subject receiving sildenafil with treatment doses of fluconazole (Table 2.5 and Figure 2.14). The discrepancy may be associated with differences in the actual dosage or timing of fluconazole co-administration in this preterm infant since this information was not recorded. Additionally, the simulated

variability in infants for CL and V_{ss} was underpredicted, which could be overcome by an additional 50% coefficient of variability on protein binding (Table 2.5).

2.3.5 Sensitivity Analysis

In order to evaluate the critical parameters influencing sildenafil C_{max} and $AUC_{0-\infty}$, a sensitivity analysis was performed from preterm infants to adults (Table 2.9 and

Table **2.10**). The most sensitive parameters for sildenafil $AUC_{0-\infty}$ included: CYP3A4 K_M/V_{max}, CYP3A4 ontogeny factor and reference concentration, fraction unbound, lipophilicity, and the plasma protein scale factor (Table 2.9). Sildenafil $AUC_{0-\infty}$ was more sensitive to the reference concentration of CYP3A7 compared to CYP3A4 in infants <2 months of age (Figure 2.15 and Table 2.9).

2.3.6 Pediatric DDI Evaluation and Dosing Recommendations

Based on simulations in virtual adults, fluconazole (800 mg IV loading dose, then 400 mg IV daily) administered with sildenafil (10 mg IV three times daily) resulted in an increase in sildenafil plus DMS (accounting for differences in activity and protein binding) AUC_{0-24} at steady-state ($AUC_{0-24,ss}$) of 2.11-fold. The adult PBPK model was scaled to infants and was compared with observations in preterm infants receiving IV sildenafil with prophylaxis and steady-state treatment doses of fluconazole including the minor role of CYP2C9 (Figure 2.14). When sildenafil (0.25 mg/kg IV three times daily) was administered with and without fluconazole (12 mg/kg IV daily), the simulated $AUC_{0-24,ss}$ fold change of sildenafil plus DMS was 2.82-fold in virtual infants (24–40 weeks GA and 0–14 days PNA). Stratifying by PMA age <36 and ≥36 weeks, the simulated $AUC_{0-24,ss}$ fold change of sildenafil plus DMS was 2.87 and 2.55 in virtual preterm and term infants, respectively (Table 2.11).

Optimal dosing simulations were performed for sildenafil with fluconazole in infants with and without CYP2C9 DMS formation and CYP2C9 inhibition and the results were nearly identical. When given in combination with treatment doses of fluconazole (12 mg/kg IV daily), reducing the sildenafil dose by 64% (administered IV over a 90-minute infusion) resulted in a geometric mean ratio of 1.01 for simulated $AUC_{0\text{-}24,ss}$ relative to virtual infants (24–42 weeks [PMA]) receiving sildenafil alone (Figure 2.16 and Table 2.12). Simulated unbound sildenafil C_{max} values, targeted to achieve 53%, 77%, and 90% phosphodiesterase type 5 activity inhibition based on a dose-ranging study of oral sildenafil in children aged 1–17 years of age with pulmonary arterial hypertension, were slightly lower for virtual infants receiving sildenafil with fluconazole compared to sildenafil alone (Figure 2.17).[55] To achieve similar C_{max} values, we reduced the sildenafil dose by 48% (administered IV over a 90-minute infusion) with 12 mg/kg fluconazole, which resulted in a geometric mean ratio for simulated C_{max} of 0.99 relative to infants receiving sildenafil alone, but overestimated simulated $AUC_{0\text{-}24,ss}$ (Figure 2.16 and Table 2.13). Additionally, reducing the sildenafil dose by 64%, but shortening the IV infusion time to 30 minutes, resulted in a geometric mean ratio for simulated C_{max} of 0.90 (Table 2.14).

2.4 Discussion

We developed an adult and pediatric PBPK model for sildenafil with fluconazole incorporating CYP3A and CYP2C9 activity and ontogeny to characterize age-related differences in CYP3A-mediated DDI potential. We first developed and evaluated a sildenafil PBPK model in adults to gain confidence in the structural model before scaling to pediatrics (Figure 2.4). We assumed that DMS CL was mediated through CYP3A based on a proteomics study suggesting that DMS undergoes modification by CYP3A to form two additional metabolites.[56] The adult sildenafil PBPK model captured the observed DDI in healthy adults receiving sildenafil in

combination with ritonavir or erythromycin.[42,43] CYP3A7 CL_{int} was optimized using preterm infant PK data because CYP3A7 expression is minimal in adults and highest in preterm infants.

The simulated sildenafil CL and V_{ss} for adults and infants were comparable and all within two-fold of observed values, except for one study in infants, which suggests reasonable agreement between our model predictions and observations (Table 2.5). This one study reported a higher V_{ss} in full-term neonates (456 L/70 kg [22.4 L]) than reported in preterm infants and adults, which the authors suggested may be due to lower protein binding of sildenafil in infants relative to adults (93.9% versus 96%).[20] It seems unlikely that term infants would have a significantly higher volume of distribution than preterm infants. In addition, the CL and V_{ss} reported in infants was much higher than the variability generated using the infant virtual population in PK-Sim® (Table 2.5). Critically ill infants receiving sildenafil with fluconazole may have higher or more variable protein binding associated with illness, stress, or inflammation. For example, AAG is an acute phase protein that has been shown to increase and fluctuate in infants and children with illness and inflammation.[57,58] To test this hypothesis, we increased the coefficient of variation on protein binding through AAG in the simulated infant population, a reasonable assumption based on the high variability of plasma AAG levels observed in infants, resulting in similar observed and simulated CL and V_{ss} variability (Table 2.5).[59] Infants with pulmonary arterial hypertension may have differences in organ function and/or blood flow relative to the virtual infant population in PK-Sim® possibly leading to higher variability.

Sensitivity analysis for sildenafil across age highlights that CYP3A7 should be included for CYP3A substrates in infants ≤2 months of age (Figure 2.15). However, we often do not have CYP3A7 *in-vitro* parameters and instead only scale using CYP3A4 activity. This assumption is

reasonable for children because CYP3A4 expression reaches full capacity by approximately 1.3 years of age, but may lead to model misspecification in neonates primarily expressing CYP3A7.[60] CYP3A7 expression decreases from 142.2 pmol/mg in neonates to 4 pmol/mg in adults.[2,3,7] CYP3A7 changes with age with mean values of 201 pmol/mg in fetal liver samples (estimated GA of 31 to 41 weeks) and 158 pmol/mg in premature birth liver samples (estimated GA <40 weeks).[2] In contrast, CYP3A4 increases from 5 pmol/mg in neonates to 98 pmol/mg in adults.[2,3,7]

Fluconazole CYP3A inhibition data were experimentally generated to characterize DDI potential between sildenafil with fluconazole in infants. Fluconazole was a mixed inhibitor of CYP3A, when tested using testosterone as the probe substrate, and was a more potent inhibitor of CYP3A4 relative to CYP3A5 and CYP3A7 (Table 2.4). When comparing the metabolic capacity for CYP3A using 10 different CYP3A substrates, one study reported an equal or reduced metabolic capability for CYP3A5 compared to CYP3A4 and a significantly lower catalytic activity for CYP3A7 compared to CYP3A4.[4] The K_I for CYP3A4 and CYP3A5 from this study differed from another study using midazolam as the CYP3A probe substrate (29.4 µM versus 9.21 µM for CYP3A4 and 182.5 µM versus 84.6 µM for CYP3A5).[5] Results can differ based on the CYP3A probe substrate used, and two distinct substrate groups have been postulated including testosterone in one group and midazolam in the other group.[61] The magnitude of the simulated DDI between sildenafil with fluconazole was slightly greater in neonates than adults (a fold change in $AUC_{0\text{-}24,SS}$ of 2.82 versus 2.11). This may be attributed to a lower catalytic activity for CYP3A7 relative to CYP3A4 particularly since the difference was greater for preterm than term infants. Additionally, neonates receive a higher fluconazole treatment dose (12 mg/kg IV daily) relative to adults (6 mg/kg IV daily) and fluconazole

inhibition is dose-dependent. Given the lack of adult DDI data available for sildenafil with fluconazole model evaluation, it is difficult to determine if this difference is significant and clinically relevant.

The pediatric sildenafil with fluconazole PBPK model was applied to provide dosing recommendations in infants and compared against pharmacodynamic and efficacy endpoints. Based on the FDA clinical drug interaction studies guidance, we targeted geometric mean ratios for C_{max} and $AUC_{0\text{-}24,ss}$ with and without fluconazole within the 0.8 to 1.25 equivalence range.[1] This approach was applied since there is no optimal dosing or exposure-response relationship established for sildenafil in infants. However, in adults with pulmonary arterial hypertension, the concentration-response relationship for pulmonary vascular resistance has a concentration of half-maximal effect of 17 ng/mL and a maximal effect of 100 ng/mL.[62] There was a dose-ranging, placebo-controlled study performed in children with pulmonary arterial hypertension from 1 to 17 years old receiving 3 sildenafil doses targeted to achieve steady-state C_{max} values of 47, 140, and 373 ng/mL corresponding with 53%, 77%, and 90% unbound inhibition of *in vitro* phosphodiesterase type 5 activity, respectively. Interestingly, in this study, the low dose (10 mg in children >20 kg) was ineffective while the high dose (20, 40, and 80 mg for children between ≥8–20, >20–45, and >45 kg, respectively) was associated with an increased risk of mortality after 2 years of treatment relative to children receiving lower doses of sildenafil.[24] Another study reported that newborns with persistent pulmonary hypertension of the newborn, who achieved an initial sildenafil concentration of 58.4 ± 44.8 ng/mL, experienced significant improvements in oxygenation after 4 hours of a continuous sildenafil infusion, whereas those with levels of 3.7 ± 4.6 ng/mL did not experience improvements in oxygenation.[63] These model simulations suggest that sildenafil dosing of 0.5 mg/kg IV every 8 hours alone and 0.18 mg/kg sildenafil IV every 8

hours when given in combination with 12 mg/kg IV daily fluconazole results in simulated C_{max} values exceeding the 77% unbound inhibition target. Additional studies are needed to further evaluate the relationship between sildenafil exposure, efficacy, and safety in premature infants.

We present a novel approach for characterizing DDIs in pediatric patients; yet there are limitations that warrant further discussion. All simulations were performed in infants receiving IV sildenafil with fluconazole since the preterm infants who received sildenafil with fluconazole received sildenafil IV. Furthermore, oral absorption in preterm infants is not enabled within the PK-Sim®/MoBi® software. Therefore, these dose recommendations may differ for infants receiving oral sildenafil with fluconazole. Another limitation is that the sildenafil with fluconazole DDI data used for model evaluation was available for preterm infant data only. However, the percentage reduction in CL in this study following IV administration was similar to another study in neonates with a median (range) PNA of 20 (2–121) days (GA not reported) who received sildenafil via nasogastric tube in combination with fluconazole (65 versus 47%).[20] The interaction with fluconazole is also dose-dependent and our simulations focused on treatment doses of fluconazole and infants in the published studies may have received prophylaxis doses.[20] Additionally, there was no available clinical DDI data in adults receiving sildenafil with fluconazole to confirm the adult DDI model predictions. Nonetheless, we were able to model the DDI between sildenafil with ritonavir and erythromycin in healthy adults (Table 2.7 and Table 2.8).

In conclusion, it is critical to incorporate CYP3A7 parameters into PBPK models to accurately predict CYP3A mediated drug distribution and DDI potential in infants ≤2 months of age. Additional PBPK models developed for other CYP3A inhibitors or inducers can be co-

modeled using this sildenafil PBPK model to guide model-informed precision dosing in infants receiving sildenafil with other interacting drugs such as erythromycin and protease inhibitors.

2.5 Tables

Table 2.1: Clinical data used for pharmacokinetic (PBPK) model development and evaluation.

Subjects	Drug	Age, Median (Range)	Dose and Administration	Reference
13	Sildenafil	healthy males, 36 (22–47) years	25 mg oral tablet single dose	[64]
6	Sildenafil	healthy males 45-58 years	25 mg IV over 25 minutes single dose	[13]
6	Sildenafil	healthy males 45-58 years	50 mg oral solution single dose	[13]
16	Sildenafil	healthy males, 27.0 (18–54) years	100 mg oral single dose	[65]
12 32	Sildenafil	healthy males 18-45 years	50 mg IV over 50 minutes and 50 mg oral capsule single dose 25, 50, 100, 200 mg oral tablets single dose	[66]
18	Sildenafil	healthy males 26.4 (20-40) years	20 mg oral tablet TID x 3 days, 80 mg oral tablet TID x 3 days	[67]
10	Sildenafil	adults with pulmonary arterial hypertension 59.5 (46-76) years	20 mg oral tablet TID x 30 days, 10 mg IV bolus	[68]
28	Sildenafil	healthy males 18-45 years	sildenafil: 100 mg oral tablet day 1 and day 7-8 ritonavir: 300, 400, 500 mg oral BID on day 2, 3, and 4-8, respectively	[42]
9	Sildenafil	25 (23-27) weeks GA; 800 (425-980) grams birth weight; and 18 (7-40) days PNA	median (min-max) dose of sildenafil: 0.247 (0.127-0.254) mg/kg IV with an infusion time of 90	[21]

			(45-93) minutes; 4 infants received fluconazole	
27	Midazolam	healthy adults 18-51 years	2.5 mg IV bolus, single	[69]
9	Midazolam	healthy adults 22-55 years	5, 15 and 30 µg/kg IV bolus, single 15, 50 and 100 µg/kg PO, single	[70]
5	Midazolam	healthy males	15 mg PO, single	[71]
18	Midazolam	healthy adults 19-46 years	7.5 mg PO, single	[72]
18	Midazolam	healthy males 27 (20-44) years	2 mg PO syrup, single	[73]
14	Midazolam	healthy adults 19-46 years	0.075 mg/kg PO, single	[74]
18	Midazolam	healthy adults 31 (21-49) years	2 mg IV, single 6 mg PO, single	[75]
27	Midazolam	healthy adults 18-55 years	2 mg IV, single	[76]
9	Midazolam	healthy adults 19-41 years	2.5 mg IV bolus, single	[69]
10	Erythromycin*	healthy adults 21-30 years	500 mg PO every 8 hours for 4 doses	[40]

Ref, reference; IV, intravenously; PO, oral; BID, twice daily; TID, three times daily; GA, gestational age; PNA, post-natal age.

*A complete list of all of the data used for erythromycin PBPK model development can be found at: https://github.com/Open-Systems-Pharmacology/Erythromycin-Model

Table 2.2: Final physiologically-based pharmacokinetic (PBPK) model parameters for ritonavir, midazolam, and erythromycin.

Parameter	Ritonavir	Source	Midazolam	Source	Erythromycin	Source
Lipophilicity	3.57	Optimized	2.76	Optimized	2.82	[77]
Molecular Weight	721 g/mol	[78]	325.77	[78]	733.9 g/mol	[78]
Fraction Unbound	0.02	[78]	0.03	[78]	0.305	[79]
Solubility	0.00126 mg/mL	[78]	0.001 mg/mL	[78]	28.1 mg/L	Optimized
pKa (Acid or Base)	2.84 (Base)	[78]	6.57 (Base)	[78]	8.9 (Base)	[77]
Transcellular Intestinal Permeability	$1.5 * 10^{-3}$ cm/min	Optimized	$1.25 * 10^{-5}$	Optimized	$3.87 * 10^{-4}$	Optimized
CYP3A4 K_M	0.068 µM	[80]	1.88 µM	[33]	70 µM	[81,82]
CYP3A4 V_{max}	1.37 pmol/min/mg	[80]	6.12 pmol/min/pmol	[33]	918.3 pmol/min/mg	[81,82]
CYP3A5 K_M	0.047 µM	[80]	N/A	N/A	N/A	N/A
CYP3A5 V_{max}	1.00 pmol/min/mg	[80]	N/A	N/A	N/A	N/A
CYP2D6 K_M	1.0 µM	[80]	N/A	N/A	N/A	N/A
CYP2D6 V_{max}	0.93 pmol/min/mg	[80]	N/A	N/A	N/A	N/A
P-glycoprotein K_M	0.13 µM	[83]	N/A	N/A	N/A	N/A
P-glycoprotein V_{max}	1.32 pmol/min/pmol	Optimized	N/A	N/A	N/A	N/A
CYP3A4 $K_{inact,half}$	0.10 µM	[84]	N/A	N/A	8.71 µM	[85–87]
CYP3A4 K_{inact}	$0.32\ min^{-1}$	[84]	N/A	N/A	0.05 1/min	[85–87]
CYP3A4 K_I	0.03 µM	[88]	N/A	N/A	N/A	N/A
CYP3A4 EC_{50}	1.0 µM	[89]	N/A	N/A	N/A	N/A
CYP3A4 E_{max}	68.5	[89]	N/A	N/A	N/A	N/A

CYP3A5 $K_{inact,half}$	0.12 µM	[84]	N/A	N/A	N/A	N/A
CYP3A5 K_{inact}	0.08 min^{-1}	[84]	N/A	N/A	N/A	N/A
CYP3A5 K_I	0.03 µM	[88]	N/A	N/A	N/A	N/A
P-glycoprotein K_I	0.2 µM	[90]	N/A	N/A	N/A	N/A
OATP1B1 K_{cat}	N/A	N/A	N/A	N/A	2.02 1/min	Optimized
Specific Hepatic Clearance	N/A	N/A	N/A	N/A	4.15 1/min	Optimized

$K_{inact,half}$, concentration of half-maximal inactivation; K_{inact}, maximal rate of inactivation; K_I, concentration of half-maximal inhibition; K_M, concentration of half-maximal metabolism or transport; V_{max}, maximal rate of metabolism or transport; pKa: negative log of the acid dissociation constant; CYP, cytochrome P450; Kcat: catalytic activity; N/A: not-applicable.

Table 2.3: Final physiologically-based pharmacokinetic (PBPK) model parameters for sildenafil.

Parameter	**Sildenafil**	**Source**	**DMS**	**Source**
Molecular weight (g/mol)	474.58	[78]	460.55	[78]
Log P	3.02	Optimized	2.29	Optimized
pKa	5.97	[78]	7.16	[78]
Water solubility (mg/mL)	3.50	[78]	0.419	[78]
Compound type	Base	[78]	Base	[78]
*f*u (predominant plasma binding protein)	0.04 (AAG)	[15,16]	0.04 (AAG)	[15,16]
Intestinal Permeability (cm/min)	8.31×10^{-6}	a	1.34×10^{-6}	a
V_{max} CYP3A4 sink (pmol/min/pmol)	10.0	Optimized		-
K_m CYP3A4/5/7 sink (μM)	15	[27]	-	-
V_{max} CYP3A5 sink (pmol/min/pmol)	10.8	Optimized	-	-
V_{max} CYP3A7 sink (pmol/min/pmol)	3.86	Optimized	-	-
V_{max} CYP3A4 DMS (pmol/min/pmol)	1.00	[27]	-	-
K_m CYP3A4 DMS (μM)	15	[27]	-	-
V_{max} CYP3A5 DMS (pmol/min/pmol)	1.38	[27]	-	-
K_m CYP3A5 DMS (μM)	14.7	[27]	-	-
V_{max} CYP3A7 DMS (pmol/min/pmol)	0.05	Optimized	-	-
K_m CYP3A7 DMS (μM)	5.71	[12]	-	-
V_{max} CYP2C9 DMS (pmol/min/mg)	78	[12]	-	-
K_m CYP2C9 DMS (μM)	27	[12]	-	-
Intrinsic Clearance (L/min)				
CYP3A7	-	-	0.09	Optimized
CYP3A4	-	-	0.32	Optimized

[a]Intestinal permeability via transcellular route is calculated as 266 * (Molecular Weight * 10^9) ^ (- 4.5) * 10^Log(Molecular Weight) * 60 *10^{-1}.

Abbreviations: AAG, alpha-1-acid glycoprotein; *f*u, unbound fraction in plasma; K_M, Michaelis-Menten constant, which describes the interaction of substrate and enzyme in the absence of inhibitor; Log P, logarithmic of octanol-water partition coefficient; pKa, negative logarithmic of the acid dissociation constant; V_{max}, maximal rate of metabolism

Table 2.4: Comparison of the observed and simulated AUC for the adult sildenafil PBPK model.

Dosing Regimen	Sildenafil AUC (ng*hr/mL) Simulated[a]	Observed[b]	Ratio	DMS AUC (ng*hr/mL) Simulated[a]	Observed[b]	Ratio	Reference for Observed Data
Single oral dose							
25 mg[c]	320	361	0.89	150	147	1.02	[66]
50 mg[c]	693	738	0.94	310	328	0.95	[66]
100 mg[c]	1580	1685	0.94	661	776	0.85	[66]
200 mg[c]	3805	3755	1.01	1450	1822	0.80	[66]
Multiple oral dose							
80 mg PO TID[d]	1209	1720	0.70	--	--	--	[67]
Single intravenous dose							
10 mg IV bolus[e]	402	330	1.22	--	--	--	[68]
25 mg/25 minute infusion IV[f]	999	971	1.03	276	147	1.88	[13]
50 mg/50 minute infusion IV[c]	2149	1291	1.66	--	--	--	[66]

[a,b]Simulated values are reported as the arithmetic mean, and observed values are reported as the geometric mean.

[c]Healthy males receiving 50 mg IV over 50 minutes and 50 mg PO capsule single dose plus 25, 50, 100, 200 mg oral tablets single dose.[66]

[d]Healthy males receiving 20 mg TID for 3 days followed by 80 mg PO tablet TID for 3 days.[67]

[e]Adults with pulmonary arterial hypertension receiving 20 mg PO tablet TID for 30 days followed by 10 mg IV bolus.[68]

[f]Healthy adult males receiving 25 mg IV over 25 minutes single dose or 50 mg PO solution single dose.[13] $AUC_{0-\infty}$ was reported for 25-200 mg single oral dose, the 25 mg/25 minute infusion IV, and the 50 mg/50 infusion IV. AUC_{τ} was reported for the 80 mg PO TID dose and 10 mg IV bolus (8 hours dosing interval).

Abbreviations: AUC, area under the plasma concentration versus time curve; $AUC_{0-\infty}$, area under the plasma concentration vs. curve from 0 to infinity; AUC_{τ}, area under the plasma concentration vs. time curve from 0 to tau; DMS, N-desmethylsildenafil; IV, intravenous; PBPK, physiologically-based pharmacokinetic; PO, taken orally; TID, three times daily

Table 2.5: Comparison of sildenafil CL and V_{ss} between simulated and observed values.

	Sildenafil CL (Liters/hour)[a]			Sildenafil Vss (Liters)[a]			
Population	**Simulated**	**Observed**	**Ratio**	**Simulated**	**Observed**	**Ratio**	**Reference**
Patients with PAH	22.3 (38.6%)	32.2 (N/A) [c]	0.69	107 (44.1%)	137 (N/A)[c]	0.78	[68]
Healthy males	26.5 (37.4%)	29.5 (31.2%)[d]	0.90	87 (51.1%)	107 (55.6%)[d]	0.81	[91]
Preterm infants	34.2 (19.6%)	27.8 (33.3%)[b,e]	1.23	157 (6.5%)	144 (98.6%)[b,e]	1.09	[21]
Preterm infants with 50% CV on F_u	34.7 (42.3%)	27.8 (33.3%)[b,e]	1.25	161 (36.7%)	144 (98.6%)[b,e]	1.12	[21]
Term infants	37.5 (20.7%)	24.7 (54.7%)[b,f]	1.52	159 (8.0%)	456 (41.1%)[b,f]	0.35	[19]
Term infants with 50% CV on F_u	34.1 (46%)	24.7 (54.7%)[b,f]	1.38	147 (43%)	456 (41.1%)[b,f]	0.32	[19]

[a]Simulated and observed values are reported as the mean (coefficient of variation, %). For observed values derived from population pharmacokinetic (PopPK) analysis, the coefficient of variation represents the inter-individual variability in the parameter.

[b]Scaled to a 70 kg weight using typical values based on population pharmacokinetic (PopPK) models.

[c]Adults with pulmonary arterial hypertension (PAH) receiving 20 mg oral tablet three times daily (TID) for 30 days followed by 10 mg intravenous (IV) bolus.[68]

[d]Based on a PopPK analysis combining oral and IV data in healthy adult patients from three different studies.[91]

[e]Based on a PopPK model developed in preterm infants receiving enteral and I.V. sildenafil.[21]

[f]Based on a PopPK model developed in term neonates receiving IV sildenafil for persistent pulmonary hypertension of the newborn or hypoxemia.[19]

Abbreviations: CL, clearance; CV, coefficient of variation; f_u, unbound fraction in plasma; PAH, pulmonary arterial hypertension; Vss, volume of distribution at steady-state; N/A: not applicable

Table 2.6: Fluconazole mixed inhibition parameters.

Enzyme	Inhibition type	K_I (µM) global[a,c]	Alpha[a,b]	K_I (µM) competitive[a,c]	K_I (µM) uncompetitive[a,c]
CYP3A4	Mixed	29.4 (20.3-43.8)	16.6 (6.1-178)	20.9 (16.8-25.9)	83.1 (67.4-102.9)
CYP3A5	Mixed	182.5 (86.7-556.4)	2.6 (0.5-13.9)	70.8 (48.5-104.3)	238.7 (183.2-318.9)
CYP3A7	Mixed	84.8 (30.5-296.8)	13.5 (1.8-∞)	45.9 (21.7-88.9)	389.0 (266.7-610.3)

[a]Value and the 90% confidence interval based on triplicate samples using recombinant enzyme expressing either cytochrome P450 3A4 (CYP3A4), CYP3A5, or CYP3A7.

[b]Alpha determines the degree to which the binding of inhibitor changes the affinity of the enzyme for substrate. When Alpha=1, the mixed-model is identical to noncompetitive inhibition. When Alpha is very large, the mixed-model becomes identical to competitive inhibition. When Alpha is very small (but greater than zero), the mixed model becomes nearly identical to an uncompetitive model.

[c]The global K_I (inhibition constant) reflects the net value for the mixed model. The K_I is also reported separately for the individual contributions from competitive and uncompetitive inhibition.

CYP, cytochrome P450; K_M, Michaelis-Menten constant, which describes the interaction of substrate and enzyme in the absence of inhibitor; V_{max}, maximum enzyme velocity without inhibitor

Table 2.7: Summary of the drug-drug interaction (DDI) between sildenafil and ritonavir in adults.

Treatment	**Sildenafil**		**N-desmethylsildenafil (DMS)**		**Ritonavir**	
	$AUC_{0-\infty}$ (ng*h/mL)	C_{max} (ng/mL)	AUC_{0-24} (ng*h/mL)	C_{max} (ng/mL)	AUC_{τ} (ng*h/mL)	C_{max} (ng/mL)
Observed data[b]						
Sildenafil	1419	321	567	132	-	-
Sildenafil + Ritonavir	13278	1063	840	55	121,865	15,441
Fold Change	11 (9, 12)[a]	3.9 (3.2, 4.9)[a]	1.7	0.5	-	-
Simulated data						
Sildenafil	1365	360	543	65	-	-
Sildenafil + Ritonavir	18351	852	1081	70	111,732	12,098
Fold Change	13 (11, 16)	2.4 (2.0, 2.7)	2.0	1.1	-	-

Data for the AUC_{0-24}, area under the concentration versus time curve from 0 to 24 hours; $AUC_{0-\infty}$: area under the concentration versus time curve from 0 to infinity; and C_{max}, maximal concentration, for sildenafil and N-desmethylsildenafil (DMS) are presented as the geometric mean. The C_{max} and AUC_{τ}, area under the curve from 0 to tau at steady-state, for ritonavir are presented as the arithmetic mean. [a]The geometric mean and associated 95% confidence interval was reported for sildenafil but not for DMS. [b]Observed data were obtained in healthy males receiving 100 mg oral sildenafil with and without ritonavir (300, 400, 500 mg oral twice daily on day 2, 3, and 4-8).[42]

Table 2.8: Summary of the drug-drug interaction (DDI) between sildenafil and erythromycin in adults.

	Sildenafil		**N-desmethylsildenafil (DMS)**	
	Observed[a]	Simulated	Observed[a]	Simulated
$AUC_{0-\infty}$ Fold Change	2.82 (2.19-3.63)	2.24 (2.19, 2.28)	1.37 (1.17-1.60)	1.67 (1.62, 1.72)
C_{max} Fold Change	2.60 (1.93-3.51)	1.28 (1.27, 1.30)	0.76 (0.55-1.05)	0.98 (0.94, 1.03)

Data for the mean (and associated 95% confidence interval) fold change for the area under the concentration versus time curve from 0 to infinity ($AUC_{0-\infty}$) and maximal concentration (C_{max}) for sildenafil and N-desmethylsildenafil (DMS) with erythromycin relative to sildenafil and DMS alone. [a]Observed data were obtained from a study in healthy male volunteers receiving erythromycin (500 mg) or placebo twice daily on days 2-6 and 100 mg oral sildenafil on days 1 and days 6.[43]

Table 2.9: Parameters with sensitivity values < -1 or > 1 for sildenafil area under the plasma concentration versus time curve from 0 to infinity ($AUC_{0-\infty}$).

Population	Parameter	Sensitivity Value
2 years	CYP3A4 (remainder) K_M	1.11
12 years	CYP3A4 (remainder) K_M	1.12
Adult	CYP3A4 (remainder) K_M	1.37
Adult	CYP3A4 (remainder) V_{max}	-1.45
12 years	CYP3A4 (remainder) V_{max}	-1.19
2 years	CYP3A4 (remainder) V_{max}	-1.17
6 months	CYP3A4 (remainder) V_{max}	-1.00
Adult	CYP3A4 Ontogeny factor	-1.60
12 years	CYP3A4 Ontogeny factor	-1.31
2 years	CYP3A4 Ontogeny factor	-1.29
6 months	CYP3A4 Ontogeny factor	-1.10
Adult	CYP3A4 Reference concentration	-1.60
12 years	CYP3A4 Reference concentration	-1.31
2 years	CYP3A4 Reference concentration	-1.29
6 months	CYP3A4 Reference concentration	-1.10
3 months	Fraction unbound	-1.01
2 years	Fraction unbound	-1.03
12 years	Fraction unbound	-1.02
6 months	Fraction unbound	-1.02
2 months	Plasma protein scale factor	-1.01
2 months	Fraction unbound	-1.00
Adult	Fraction unbound	-1.00
5 years	Lipophilicity	-3.43
Adult	Lipophilicity	3.55
2 years	Plasma protein scale factor	-1.03
12 years	Plasma protein scale factor	-1.02
6 months	Plasma protein scale factor	-1.02
3 months	Plasma protein scale factor	-1.02
Adult	Plasma protein scale factor	-1.00

CYP3A4, cytrochrome P450 3A4; K_M, Michaelis-Menten constant; V_{max}, maximal rate of metabolism.

Table 2.10: Parameters with sensitivity values < -1 or > 1 for maximal concentration (C_{max}) after single dose.

Population	Parameter	Sensitivity Value
5 years	CYP3A4 (remainder)[a] K_M	1.12
5 years	CYP3A4 (remainder)[a] V_{max}	-1.20
5 years	CYP3A4 Ontogeny factor	-1.32
5 years	CYP3A4 Reference concentration	-1.32
5 years	Fraction unbound	-1.02
Adult	Lipophilicity	1.44
2 years	Lipophilicity	-3.19
1 years	Lipophilicity	-3.20
12 years	Lipophilicity	-3.44
6 months	Lipophilicity	-3.52
1 month	Lipophilicity	-3.56
2 weeks	Lipophilicity	-3.63
2 months	Lipophilicity	-3.66
3 months	Lipophilicity	-3.76
Neonate	Lipophilicity	-3.92
Preterm infant	Lipophilicity	-4.20

[a]Remainder referring to the metabolism of sildenafil into all other metabolites besides N-desmethylsildenafil. V_{max}, maximal rate of metabolism; K_m, Michaelis-Menten constant.

Table 2.11: Comparison of the simulated drug-drug interaction (DDI) between sildenafil and treatment dosing of fluconazole between infants and adults.

Population	**Simulated Fold Change (IQR) Sildenafil + DMS $AUC_{0\text{-}24,ss}$**	**Simulated Fold Change (IQR) Sildenafil + DMS C_{max*}**	**Simulated Fold decrease (IQR) Sildenafil CL**
Adult[a]	2.11 (1.89, 2.41)	1.29 (1.24, 1.35)	53 (47, 59)%
Infant[b]	2.82 (2.60, 3.06)	1.81 (1.66, 1.97)	65 (62, 68)%
Preterm	2.87 (2.67, 3.10)	1.86 (1.74, 2.00)	66 (63, 68)%
Term	2.55 (2.30, 2.88)	1.58 (1.46, 1.76)	61 (57, 66)%

Median (interquartile range (IQR)) fold change with and without fluconazole calculated as the daily area under the concentration versus time curve at steady-state ($AUC_{0\text{-}24,ss}$) or maximal concentration (C_{max}) for sildenafil plus 0.5 x 1.25 x $AUC_{0\text{-}24,ss}$ or C_{max} of N-desmethylsildenafil (DMS). [a]One hundred virtual adults received 10 mg intravenous (IV) sildenafil every 8 hours plus a 800 mg loading dose followed by 400 mg IV daily fluconazole. [b]One thousand virtual infants (24 to 40 weeks gestational age and 1-14 days post-natal age) received 0.25 mg/kg IV every 8 hours sildenafil plus 12 mg/kg IV daily fluconazole overall and also stratified by preterm (post-menstrual age < 37 weeks) or term (post-menstrual age ≥ 37 weeks).

Table 2.12: Exposure ratios with and without fluconazole in virtual infants optimized based on daily area under the concentration versus time curve at steady-state from 0 to 24 hours ($AUC_{0\text{-}24,ss}$) without the incorporation of CYP2C9 (A) and with the incorporation of CYP2C9 (B).

A.

	0.09 mg/kg IV TID sildenafil + 12 mg/kg IV daily fluconazole vs. 0.25 mg/kg IV	**0.18 mg/kg IV TID sildenafil + 12 mg/kg IV daily fluconazole vs. 0.5 mg/kg IV**	**0.36 mg/kg IV TID sildenafil + 12 mg/kg IV daily fluconazole vs. 1 mg/kg IV**
PMA (weeks)	$AUC_{0\text{-}24,ss}$ Ratio	$AUC_{0\text{-}24,ss}$ Ratio	$AUC_{0\text{-}24,ss}$ Ratio
<28	1.06	1.06	1.06
≥ 28 to < 32	1.05	1.04	1.04
≥32 to < 37	1.03	1.03	1.02
≥ 37	0.93	0.93	0.93
Overall	1.01	1.01	1.01

B.

	0.09 mg/kg IV TID sildenafil + 12 mg/kg IV daily fluconazole vs. 0.25 mg/kg IV	**0.18 mg/kg IV TID sildenafil + 12 mg/kg IV daily fluconazole vs. 0.5 mg/kg IV**	**0.36 mg/kg IV TID sildenafil + 12 mg/kg IV daily fluconazole vs. 1 mg/kg IV**
PMA (weeks)	$AUC_{0\text{-}24,ss}$ Ratio	$AUC_{0\text{-}24,ss}$ Ratio	$AUC_{0\text{-}24,ss}$ Ratio
<28	1.06	1.06	1.06
≥ 28 to < 32	1.04	1.04	1.04
≥32 to < 37	1.03	1.03	1.02
≥ 37	0.93	0.93	0.93
Overall	1.01	1.01	1.01

Ratio calculated as the geometric mean for sildenafil plus N-desmethylsildenafil (DMS) x 0.5 x 1.25 (accounting for differences in activity and protein binding) in infants receiving sildenafil plus 12 mg/kg intravenously (IV) daily relative to infants receiving the reference dose of sildenafil without fluconazole. All sildenafil doses were IV over a 90-minute infusion given every 8 hours. Data are stratified by post-menstrual age (PMA). TID, three times daily.

Table 2.13: Exposure ratios with and without fluconazole in infants optimized based on maximal concentration (C_{max}) values without the incorporation of CYP2C9 (A) and with the incorporation of CYP2C9 (B).

A.

	0.13 mg/kg IV TID sildenafil + 12 mg/kg IV daily fluconazole vs. 0.25 mg/kg IV	**0.26 mg/kg IV TID sildenafil + 12 mg/kg IV daily fluconazole vs. 0.5 mg/kg IV**	**0.52 mg/kg IV TID sildenafil + 12 mg/kg IV daily fluconazole vs. 1 mg/kg IV**
PMA (weeks)	C_{max} Ratio	C_{max} Ratio	C_{max} Ratio
<28	1.04	1.04	1.04
≥ 28 to < 32	1.02	1.02	1.02
≥32 to < 37	1.01	1.01	1.01
≥ 37	0.91	0.91	0.90
Overall	0.99	0.99	0.99

B.

	0.13 mg/kg IV TID sildenafil + 12 mg/kg IV daily fluconazole vs. 0.25 mg/kg IV	**0.26 mg/kg IV TID sildenafil + 12 mg/kg IV daily fluconazole vs. 0.5 mg/kg IV**	**0.52 mg/kg IV TID sildenafil + 12 mg/kg IV daily fluconazole vs. 1 mg/kg IV**
PMA (weeks)	C_{max} Ratio	C_{max} Ratio	C_{max} Ratio
<28	1.04	1.04	1.04
≥ 28 to < 32	1.02	1.02	1.02
≥32 to < 37	1.02	1.01	1.02
≥ 37	0.91	0.90	0.91
Overall	0.99	0.99	0.99

Ratio calculated as the geometric mean for sildenafil plus N-desmethylsildenafil (DMS) x 0.5 x 1.25 (accounting for differences in potency and protein binding) in infants receiving sildenafil plus 12 mg/kg IV daily fluconazole relative to infants receiving the reference dose of sildenafil without fluconazole. All sildenafil doses were given intravenously (IV) over a 90 minute infusion every 8 hours. Data are stratified by post-menstrual age (PMA). TID, three times daily.

Table 2.14: Area under the concentration versus time curve at steady-state from 0 to 24 hours ($AUC_{0\text{-}24,ss}$) and maximal concentration (C_{max}) for a 64% dose reduction of intravenous (IV) sildenafil administered over 30 minutes every 8 hours (TID) plus 12 mg/kg IV daily fluconazole relative to a 90 minute IV infusion of sildenafil TID in infants without the incorporation of CYP2C9 (A) and with the incorporation of CYP2C9 (B).

A.

	0.09 mg/kg IV over 30 minutes TID + 12 mg/kg fluconazole vs. 0.25 mg/kg IV over 90 minutes TID		**0.18 mg/kg IV over 30 minutes TID + 12 mg/kg fluconazole vs. 0.5 mg/kg IV over 90 minutes TID**		**0.36 mg/kg IV over 30 minutes TID + 12 mg/kg fluconazole vs. 1 mg/kg IV over 90 minutes TID**	
PMA (weeks)	$AUC_{0\text{-}24,ss}$ Ratio	C_{max} Ratio	$AUC_{0\text{-}24,ss}$ Ratio	C_{max} Ratio	$AUC_{0\text{-}24,ss}$ Ratio	C_{max} Ratio
<28	1.07	0.92	1.07	0.92	1.07	0.92
≥ 28 to < 32	1.07	0.92	1.07	0.92	1.07	0.92
≥32 to < 37	1.05	0.92	1.05	0.92	1.05	0.91
≥ 37	0.98	0.89	0.98	0.89	0.98	0.89
Overall	1.01	0.90	1.01	0.90	1.01	0.90

B.

	0.09 mg/kg IV over 30 minutes TID + 12 mg/kg fluconazole vs. 0.25 mg/kg IV over 90 minutes TID		**0.18 mg/kg IV over 30 minutes TID + 12 mg/kg fluconazole vs. 0.5 mg/kg IV over 90 minutes TID**		**0.36 mg/kg IV over 30 minutes TID + 12 mg/kg fluconazole vs. 1 mg/kg IV over 90 minutes TID**	
PMA (weeks)	$AUC_{0\text{-}24,ss}$ Ratio	C_{max} Ratio	$AUC_{0\text{-}24,ss}$ Ratio	C_{max} Ratio	$AUC_{0\text{-}24,ss}$ Ratio	C_{max} Ratio
<28	1.06	0.91	1.06	0.91	1.06	0.91
≥ 28 to < 32	1.05	0.91	1.04	0.91	1.04	0.91
≥32 to < 37	1.03	0.91	1.03	0.91	1.03	0.91
≥ 37	0.93	0.87	0.93	0.87	0.93	0.87
Overall	1.01	0.90	1.01	0.90	1.01	0.90

Ratio calculated as the geometric mean for sildenafil plus N-desmethylsildenafil (DMS) x 0.5 x 1.25 (accounting for differences in potency and protein binding) in infants receiving sildenafil plus 12 mg/kg intravenously (IV) daily relative to infants receiving the reference dose of sildenafil without fluconazole. Data are stratified by post-menstrual age (PMA).

2.6 Figures

Figure 2.1: Population simulations for midazolam.

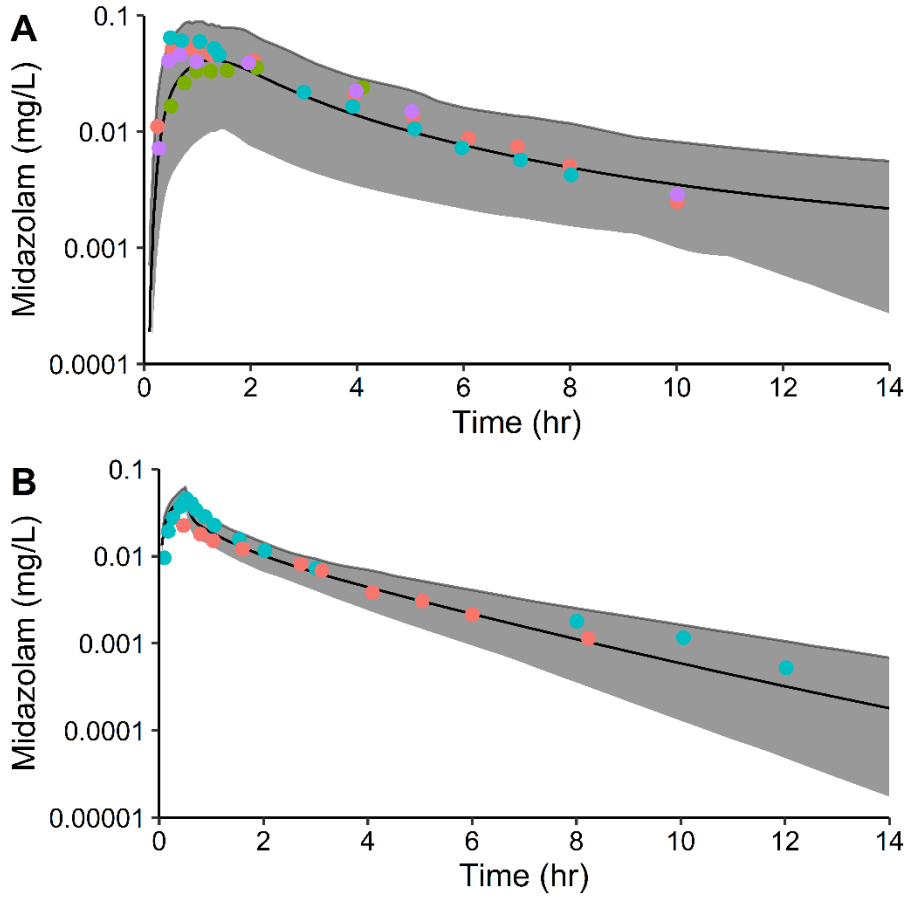

A: 15 mg oral (PO) midazolam single dose; B: 2 mg intravenous (IV) single dose. The solid grey region is the 90% prediction interval, the solid black line is the mean, and the colored dots are mean observations from clinical studies. A: observed data in healthy adults following a 15 mg PO tablet dose under fasting conditions (orange), one hour before a meal (blue), with a meal (purple), and one hour after a meal (green).[71] B: observed data from healthy adults receiving 2 mg IV midazolam over a 30 minute infusion (blue[76] and orange[75]).

Figure 2.2: Population simulations for erythromycin stearate 500 mg via oral (PO) administration every 8 hours.

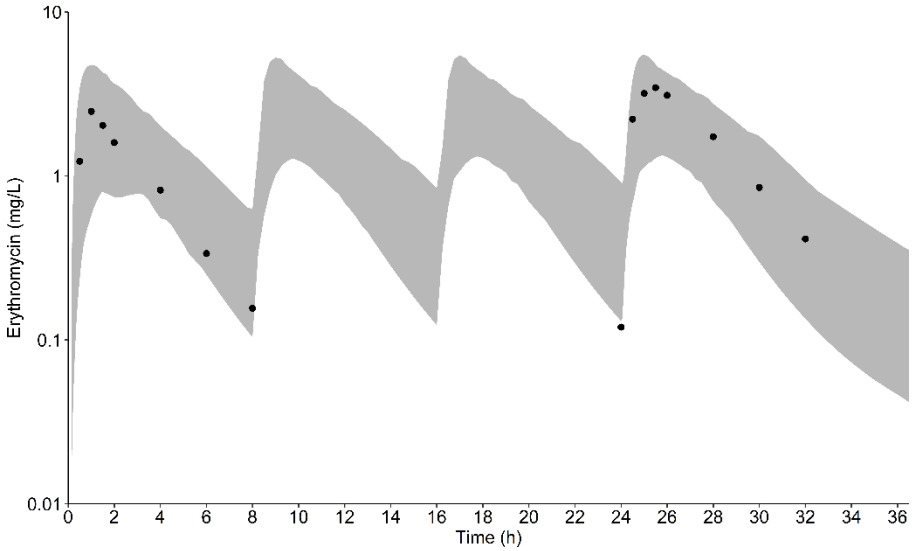

The solid grey region is the 90% prediction interval, the solid black line is the mean, and the colored dots are mean observations from the clinical study in healthy adults receiving 4 doses of 500 mg erythromycin every 8 hours.[40]

Figure 2.3: Population simulations for fluconazole in preterm infants.

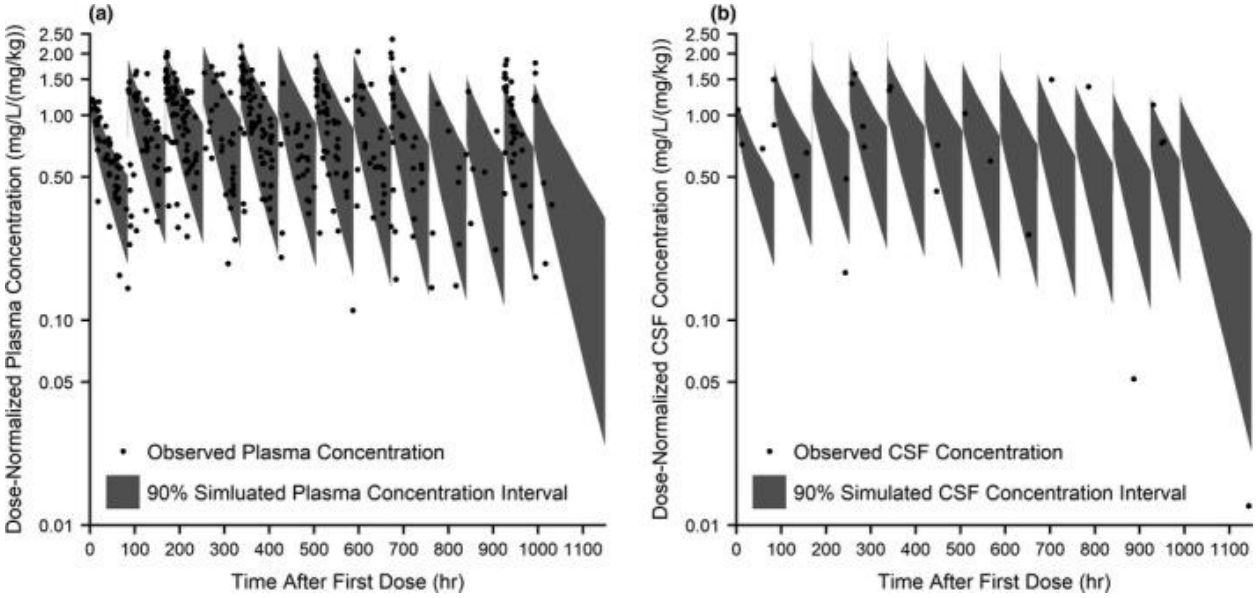

Population simulations (n = 1,000) of plasma and CSF fluconazole concentration following prophylactic dosing (6 mg/kg twice weekly) in preterm infants. Population simulations of plasma (**a**) and CSF (**b**) are shown overlaid with observed time-normalized and dose-normalized data. The shaded regions are the 5–95% range in concentration from 1,000 simulated infants reflective of the prophylaxis study demographics. CSF, cerebrospinal fluid; hr, hour.

*This figure was printed without modifications or adaptations from: Gerhart JG, Watt KM, Edginton A, Wade KC, Salerno SN, Benjamin DK, et al. Physiologically-based pharmacokinetic modeling of fluconazole using plasma and cerebrospinal fluid samples from preterm and term infants. *CPT Pharmacometrics Syst Pharmacol.* 2019;8(7):500–510.

Figure 2.4: Physiologically-based pharmacokinetic (PBPK) modeling approach to evaluate the drug-drug interaction (DDI) between sildenafil and fluconazole in infants.

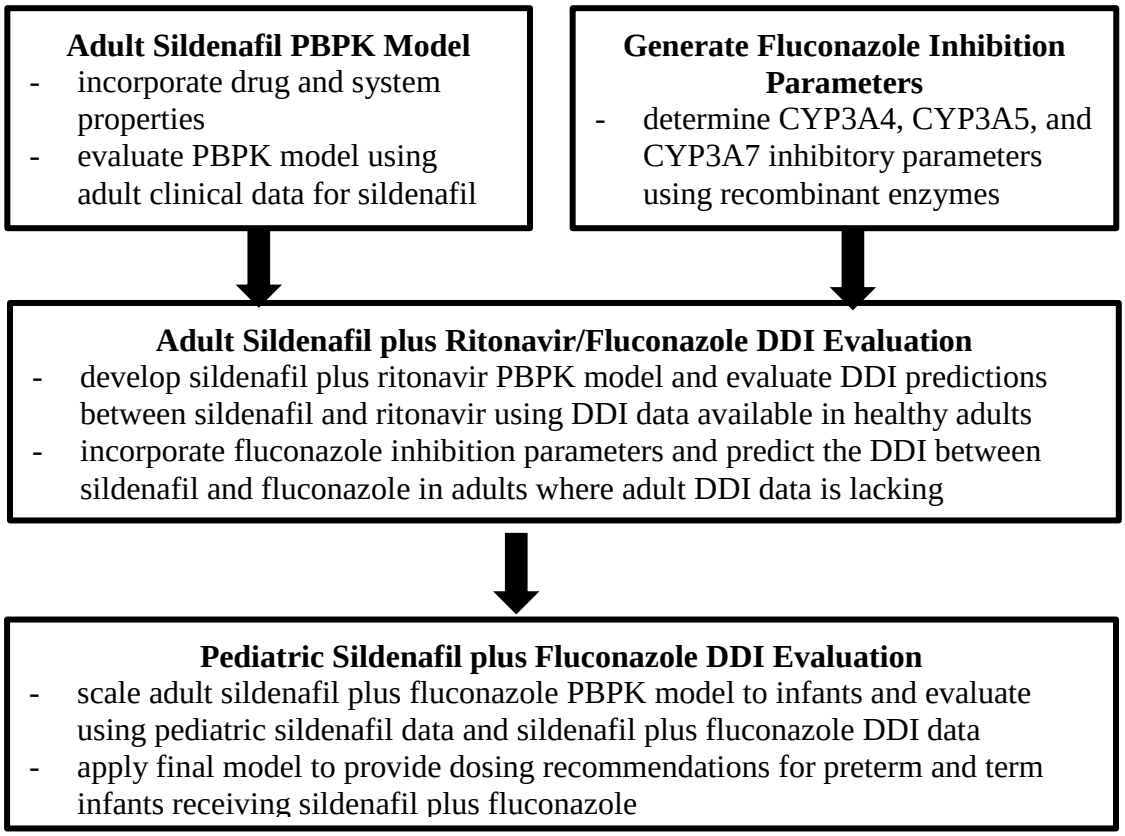

Figure 2.5: Population simulations for a single 10 mg intravenous (IV) bolus of sildenafil in patients with pulmonary arterial hypertension.

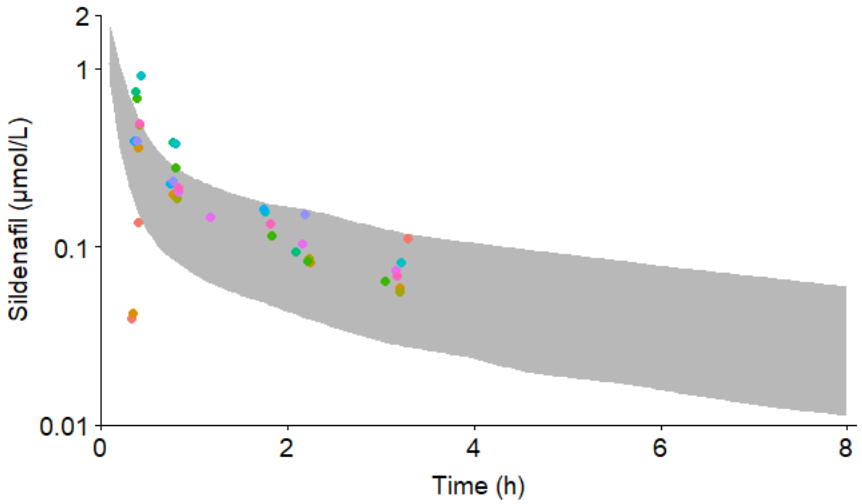

Population simulations for sildenafil in 100 virtual adults with pulmonary arterial hypertension receiving a 10 mg IV bolus. The solid grey area is the 95% prediction interval and the dots are concentrations colored per individual reported from a study in adults with pulmonary arterial hypertension whom received a 10 mg IV bolus after administration of a 20 mg oral tablet three times a day for 30 days.[68] N-desmethylsildenafil (DMS) data not measured from this study.

Figure 2.6: Population simulations of N-desmethylsildenafil (DMS) for a single 25 mg intravenous (IV) infusion of sildenafil over 25 minutes in healthy adults.

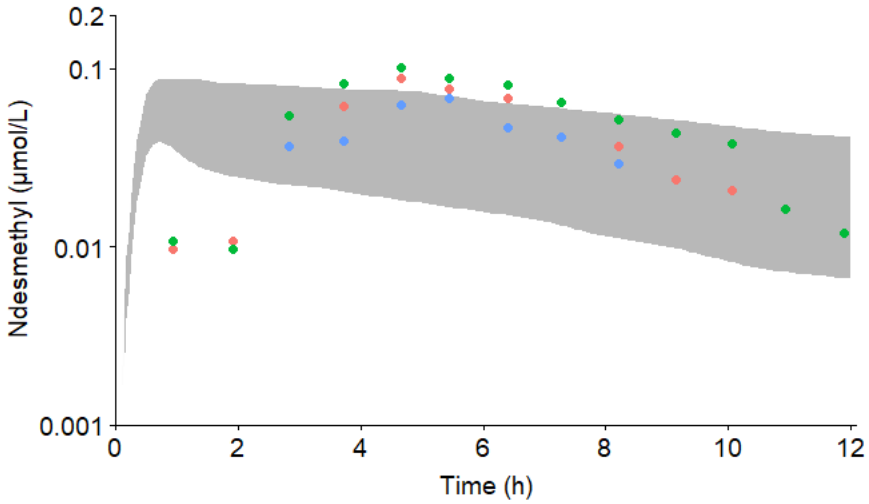

Population simulations for DMS in 100 virtual healthy adults receiving 25 mg sildenafil IV. The solid grey area is the 95% prediction interval and the dots are concentrations colored by individual in healthy males receiving 25 mg IV sildenafil over 25 minutes.[66] Sildenafil data not measured from this study.

Figure 2.7: Population simulations for a single 50 mg intravenous (IV) sildenafil infusion over 50 minutes in healthy adults.

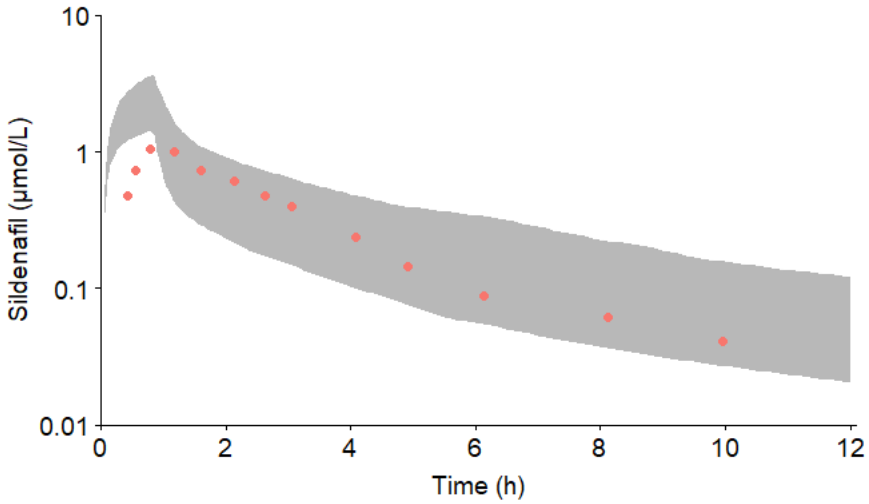

Population simulations for sildenafil in 100 virtual healthy adults receiving 50 mg IV. The solid grey area is the 95% prediction interval and the dots are mean concentrations from healthy males receiving 50 mg IV sildenafil over 50 minutes.[66] N-desmethylsildenafil (DMS) data not measured from this study.

Figure 2.8: Population simulations for sildenafil and DMS in healthy adults receiving single oral doses (25 mg, 50 mg, 100 mg, and 200 mg) of sildenafil.

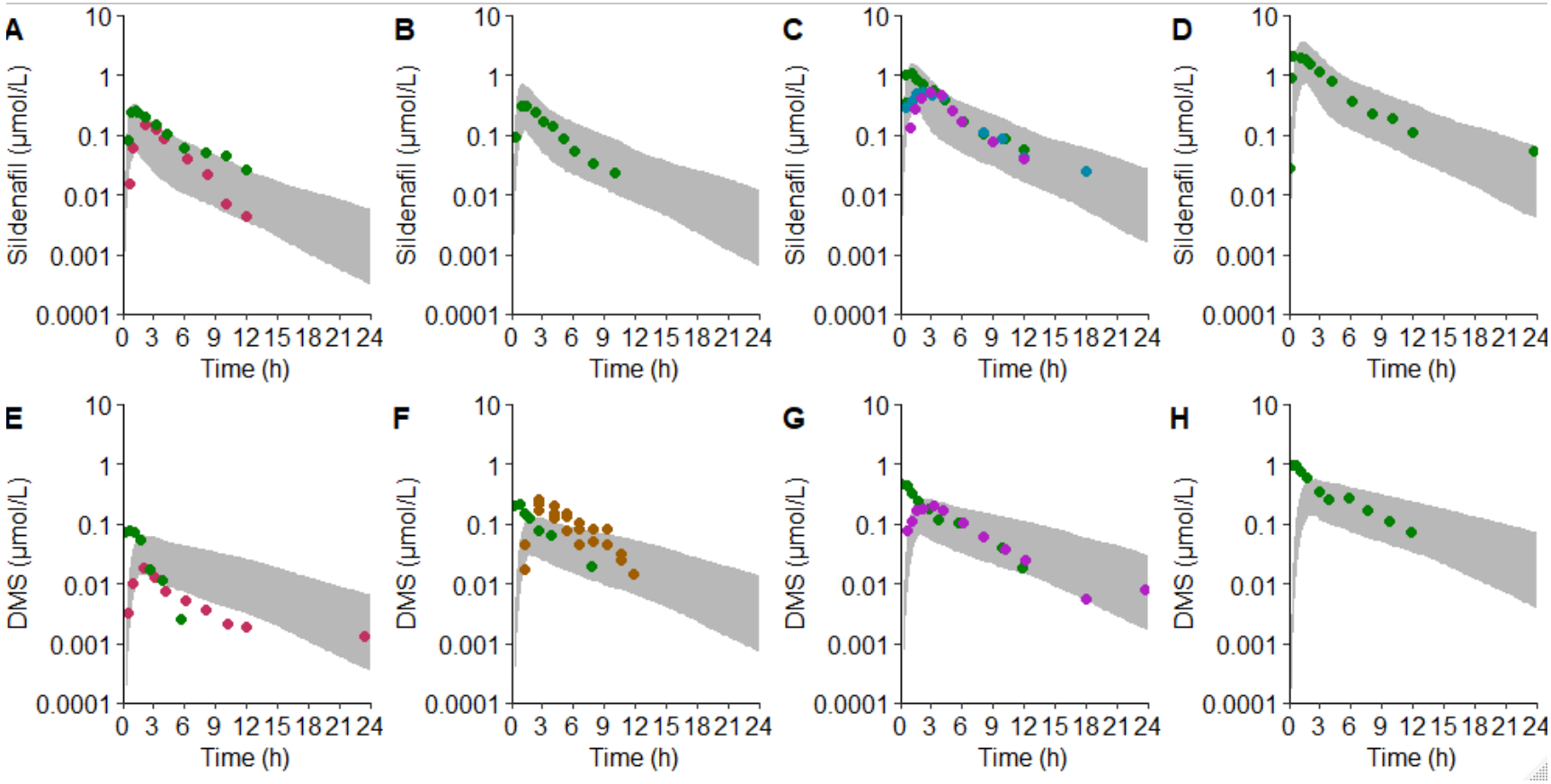

Population simulations for sildenafil (A,B,C,D) and DMS (E,F,G,H) in 100 virtual healthy adults receiving 25 mg sildenafil (A,E), 50 mg sildenafil (B,F), 100 mg sildenafil (C,G), and 200 mg sildenafil (D,H). The solid grey area is the 95% prediction interval and the dots are mean concentrations colored per study as described in Table 1.

Figure 2.9: Population simulations for the last dose of sildenafil in healthy adults receiving 20 mg intravenously (IV) every 8 hours for 3 days followed by 80 mg orally every 8 hours for 3 days.

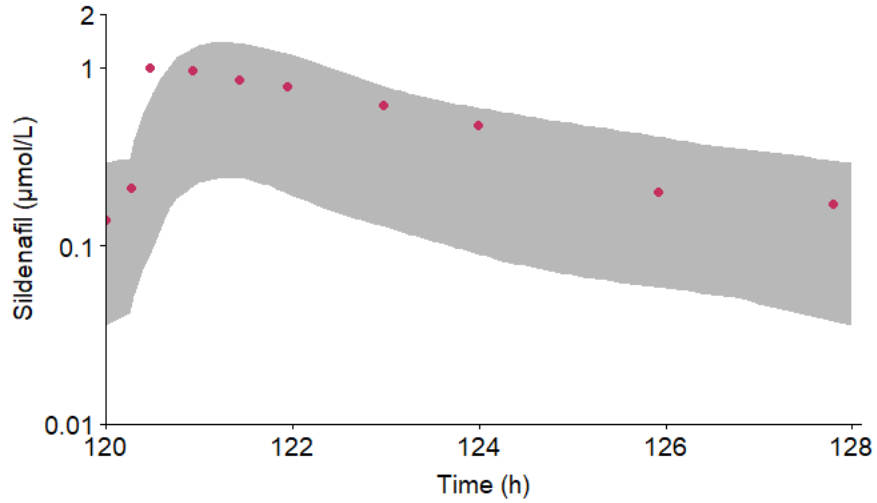

Population simulations for sildenafil in 100 virtual healthy adults receiving 20 mg IV every 8 hours for 3 days followed by 80 mg orally every 8 hours for 3 days, with concentrations plotted after the last study dose (day 6). The solid grey area is the 95% prediction interval and the dots are mean concentrations from healthy males receiving 20 mg IV sildenafil every 8 hours for 3 days followed by 80 mg orally every 8 hours for 3 days.[67] Time is measured after the first dose. N-desmethylsildenafil (DMS) data not measured from this study.

Figure 2.10: 6β-Hydroxytestosterone production as a function of time for cytochrome P450 3A4 (CYP3A4) and cytochrome P450 3A5 (CYP3A5).

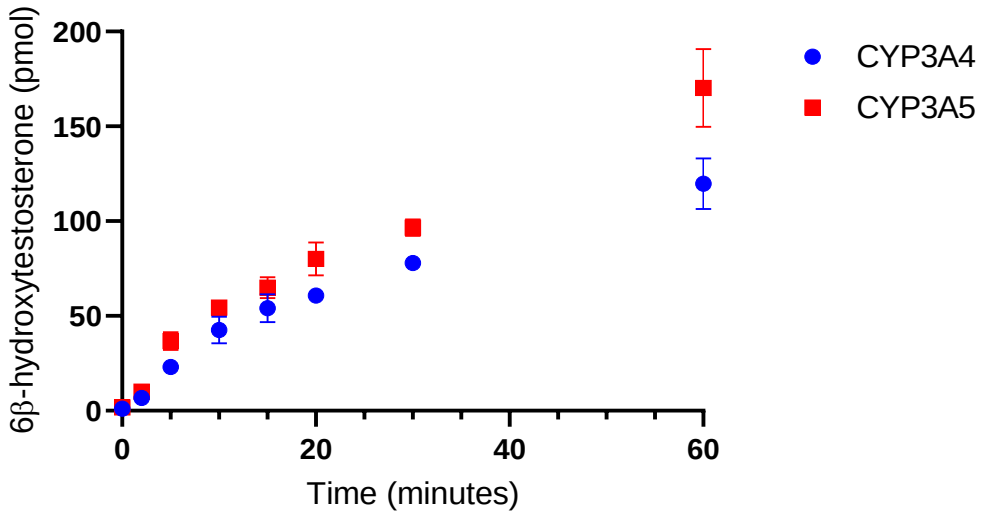

Data presented as the mean (±standard deviation) of triplicates for CYP3A4 (blue dots) and CYP3A5 (red squares).

Figure 2.11: 6β-hydroxytestosterone production as a function of time for cytochrome P450 3A7 (CYP3A7).

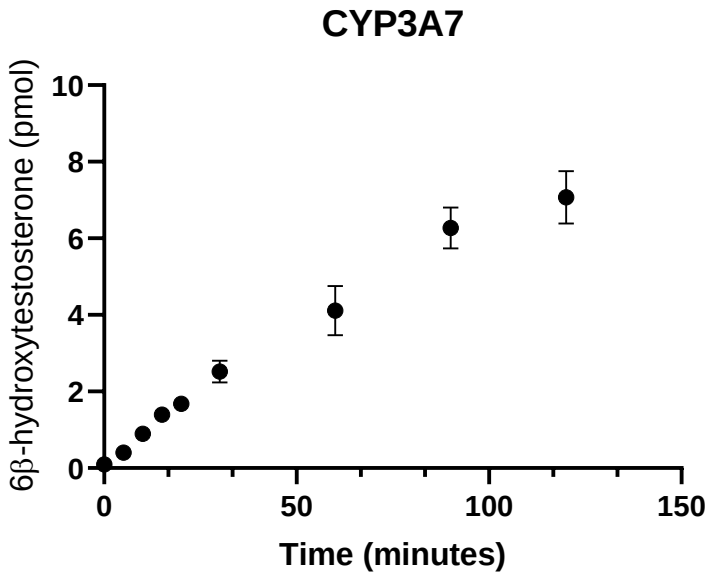

Data presented as the mean (±standard deviation) of triplicate samples.

Figure 2.12: Lineweaver-Burk plots for cytochrome P450 3A4 (CYP3A4), cytochrome P450 3A5 (CYP3A5), and cytochrome P450 3A7 (CYP3A7) fluconazole inhibition.

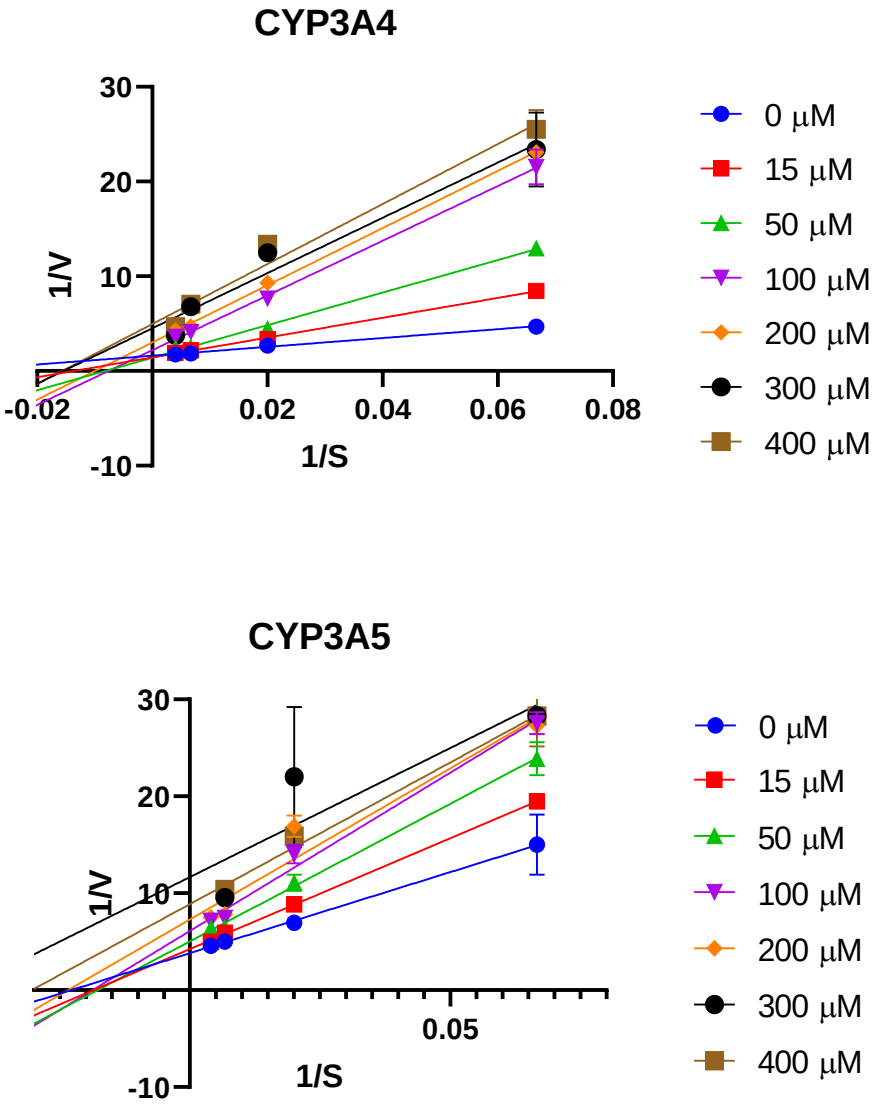

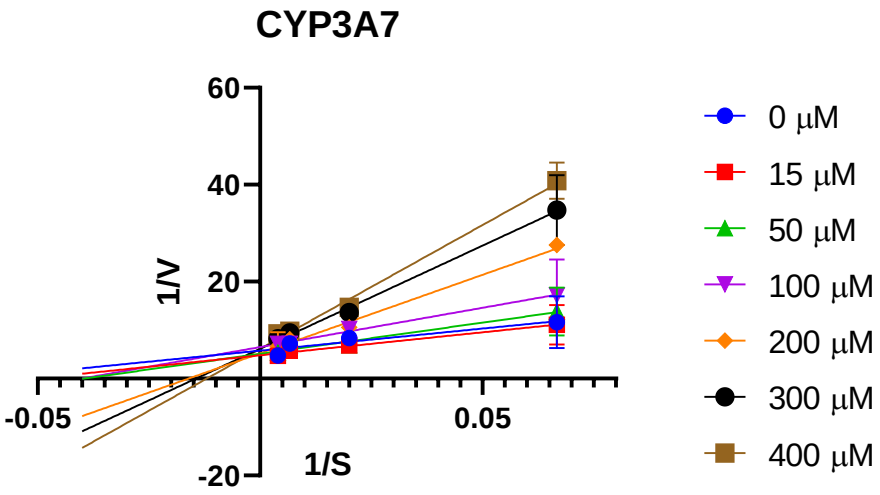

Data presented as the mean (±standard deviation) of triplicate samples. Data were linearized based on 1/V (velocity) measured as formation of 6β-hydroxytestosterone (pmol/min/pmol CYP3A) versus 1/Substrate (S) corresponding to testosterone concentrations (μM). Different concentrations of fluconazole (μM) are represented by different colors and symbols per right legend.

Figure 2.13: Population simulations for healthy adults receiving 100 mg oral sildenafil plus ritonavir (300, 400, 500 mg oral twice daily [BID] on day 2, 3, and 4-8, respectively).

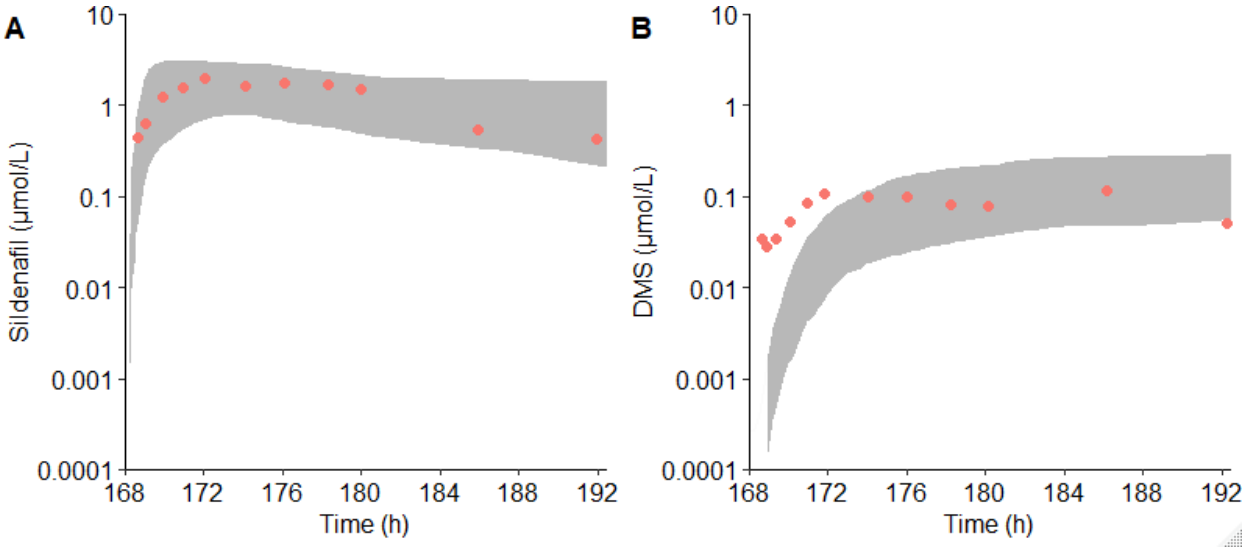

Population simulations for sildenafil (A) and N-desmethylsildenafil (DMS) (B) in 100 virtual healthy adults receiving 100 mg oral sildenafil plus ritonavir (300, 400, 500 mg oral twice daily (BID) on days 2, 3, and 4-8, respectively). The solid grey area is the 95% prediction interval and the dots are mean concentrations from healthy males receiving 100 mg sildenafil with and without ritonavir (300, 400, 500 mg oral BID on days 2, 3, and 4-8).[42]

Figure 2.14 Sildenafil and N-desmethyl sildenafil (DMS) with and without fluconazole physiologically:-based pharmacokinetic (PBPK) model population simulations in preterm infants.

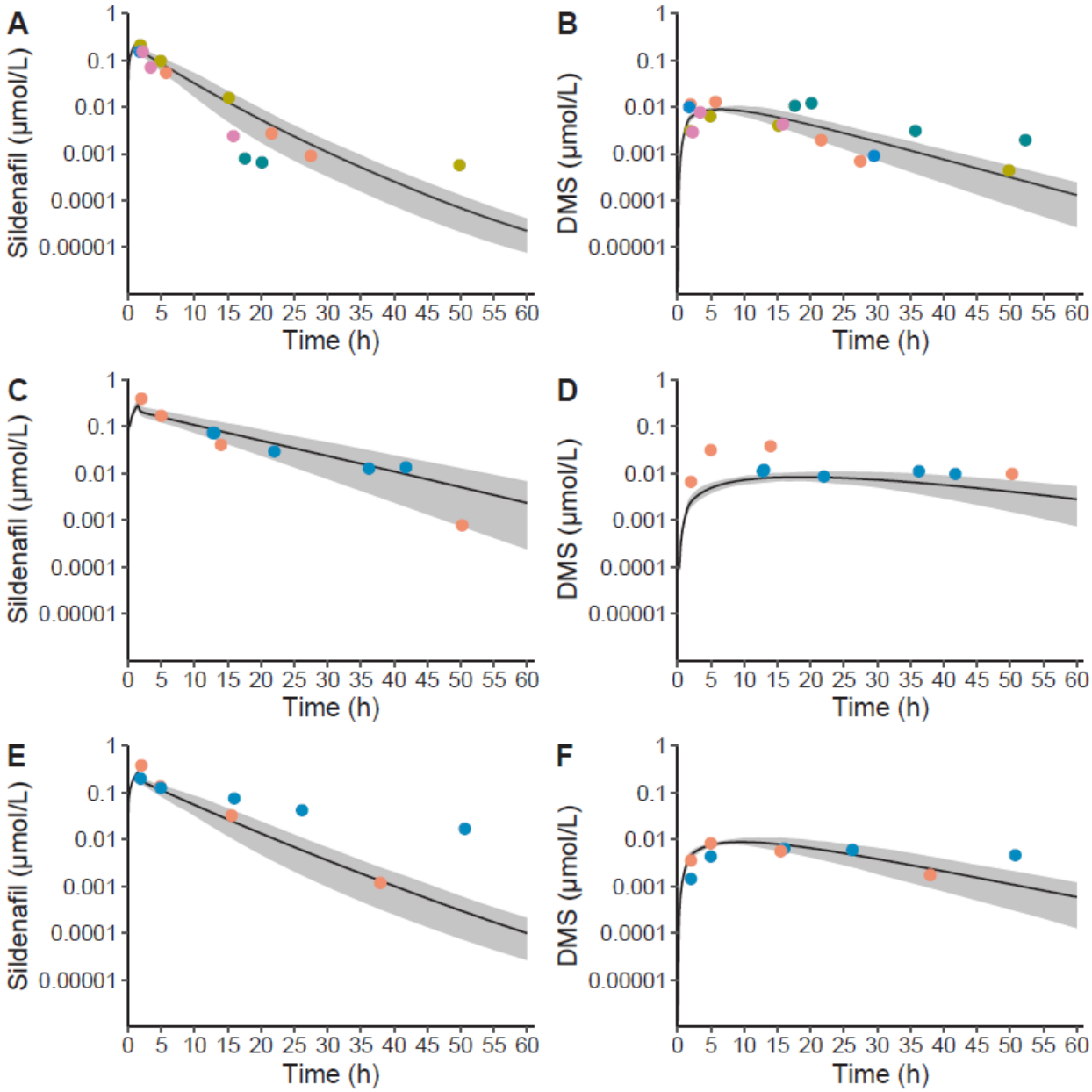

Population simulations in 100 preterm infants (33% female, 7-40 days postnatal age, 24-27 weeks gestational age, and 590-1242 grams) for sildenafil (A) and DMS (B) in infants receiving sildenafil alone, and for sildenafil (C) and DMS (D) in infants receiving sildenafil with steady-state administration of fluconazole for treatment (12 mg/kg IV daily) and for sildenafil (E) and

DMS (F) in infants receiving sildenafil with fluconazole for prophylaxis (6 mg/kg IV every 72 hours). A single dose of 0.25 mg/kg IV sildenafil with 6 mg/kg fluconazole IV in preterm infants resulted in a simulated mean fold-change of 1.08 for maximal concentration (C_{max}) and 1.40 for the area under the curve extrapolated to infinity ($AUC_{0-\infty}$) for sildenafil plus DMS accounting for different phosphodiesterase type 5 inhibitory activity and protein binding (Sildenafil + 0.5*1.25*DMS). A single dose of 0.25 mg/kg IV sildenafil with six days of fluconazole dosing of 12 mg/kg fluconazole IV in preterm infants resulted in a simulated mean fold-change of 1.13 for C_{max} and 2.59 for $AUC_{0-\infty}$ for sildenafil plus DMS. The solid grey area is the 95% prediction interval and the dots are concentrations colored by individuals. Results were obtained using the default PK-Sim® ontogeny functions for alpha-1-acid glycoprotein without additional variability introduced on the fraction unbound. Observed concentrations were dose normalized to 0.25 mg/kg. Abbreviations: DMS, N-desmethylsildenafil; h, hours

Figure 2.15: Results of a sensitivity analysis comparing the influence of cytochrome P450 3A4 (CYP3A4), cytochrome P450 3A5 (CYP3A5), and cytochrome P450 3A7 (CYP3A7) reference concentration on sildenafil $AUC_{0-\infty}$ after single oral dose for all ages, except that an intravenous dose was simulated for preterm infants, as a function of age.

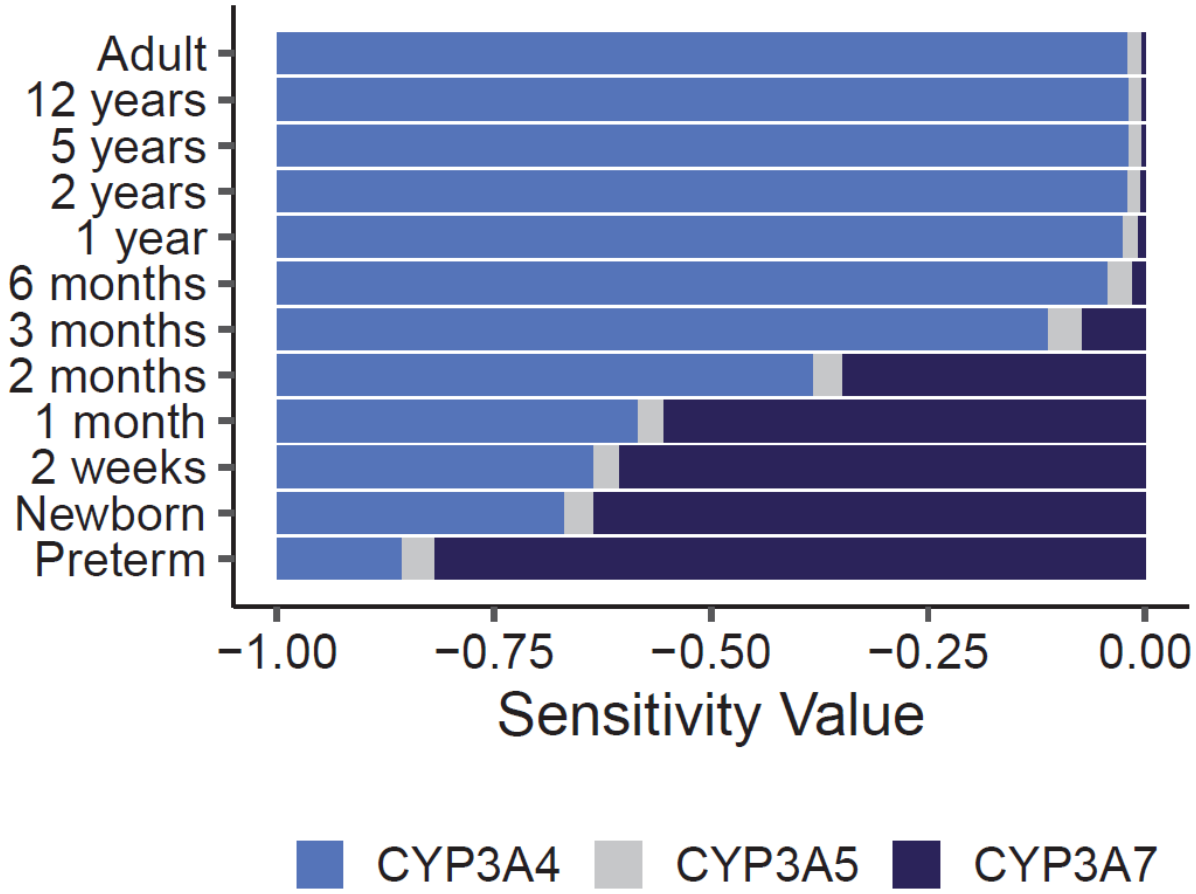

Comparison of sensitivity values for the impact of reference concentration of CYP3A4 (blue), CYP3A5 (grey), and CYP3A7 (navy) on sildenafil $AUC_{0-\infty}$ in typical subjects of various ages. A sensitivity analysis was performed for the typical healthy adult, the preterm infant (22 days PNA, 25 weeks GA, and 849 g weight), a term infant at birth (neonate), term infant at two weeks of age, 1 month, 2 months, 3 months, 6 months, 1 year, 2 years, 5 years, and 12 years. A sensitivity of -1.0 implies that a 10% increase of CYP3A reference concentration leads to a 10% decrease of $AUC_{0-\infty}$, and a sensitivity of +1 implies that a 10% increase of CYP3A reference concentration

leads to a 10% increase of $AUC_{0-\infty}$. Abbreviations: $AUC_{0-\infty}$, area under the plasma concentration versus time curve from zero to infinity; GA, gestational age; PNA, postnatal age.

Figure 2.16: Changes in daily AUC_{ss} and C_{max} in preterm and term infants receiving modified doses of IV sildenafil given TID in combination with fluconazole compared to preterm and term infants receiving sildenafil alone.

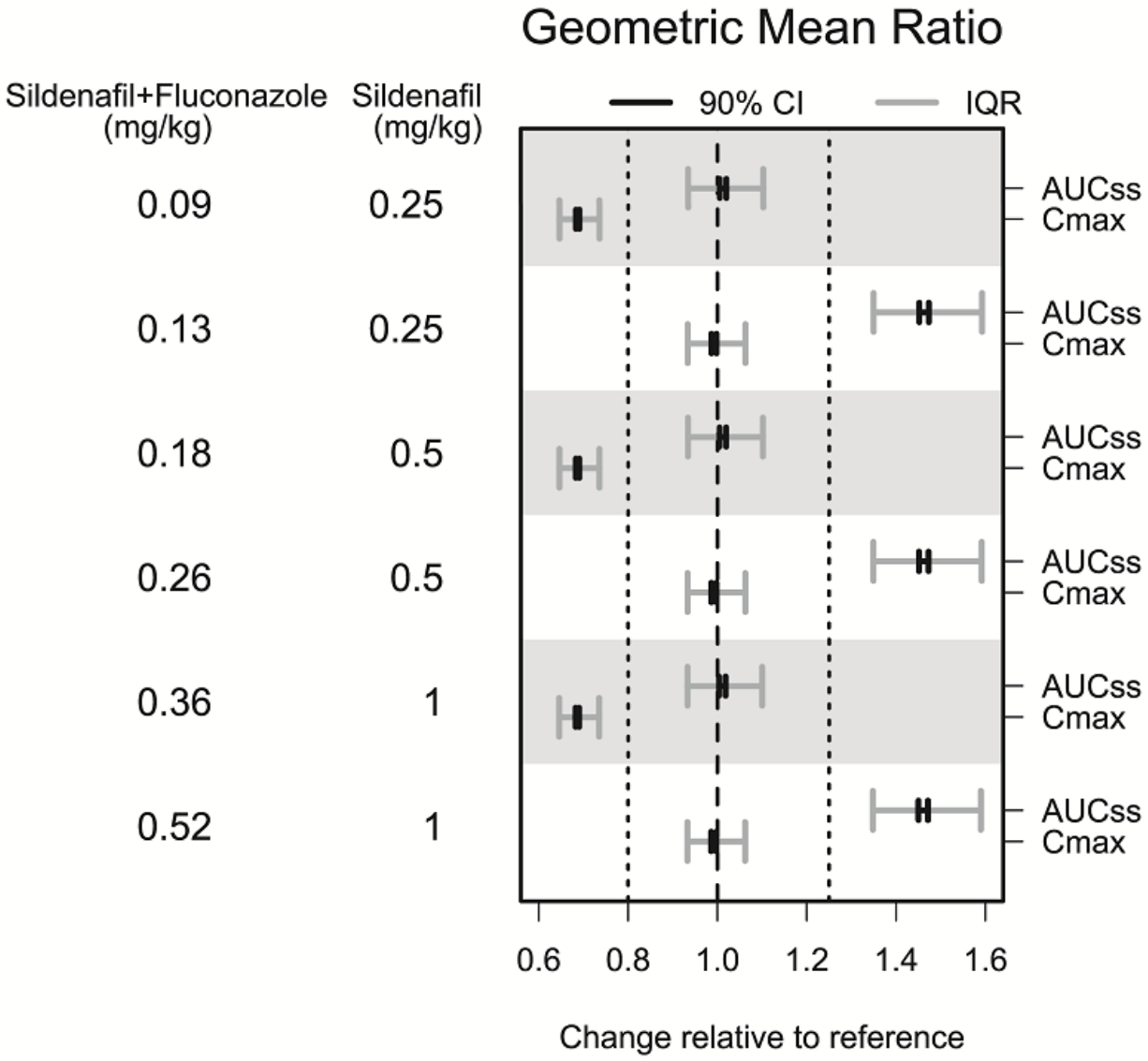

Data presented as the geometric mean and associated 90% prediction interval of the change in sildenafil plus 0.5*1.25*DMS (accounting for differences in potency and protein binding) AUC_{ss} and C_{max} in infants receiving sildenafil with fluconazole relative to infants receiving sildenafil without fluconazole. The reference sildenafil doses were 0.25 mg/kg IV, 0.5 mg/kg IV or 1 mg/kg IV, each dose administered over a 90 minute infusion every 8 hours. The fluconazole dose was 12 mg/kg daily, administered IV over a 60 minute infusion. When given in combination

with fluconazole, reducing the sildenafil dose by 64% resulted in a geometric mean ratio of 1.01 for $AUC_{ss,}$ relative to infants receiving sildenafil alone but C_{max} was under-predicted. To achieve similar C_{max} values, reducing the sildenafil dose by 48% with fluconazole resulted in a geometric mean ratio for C_{max} of 0.99 relative to infants receiving sildenafil alone, however, but AUC_{ss} was over-predicted. Abbreviations: AUC_{ss}, area under the plasma concentration versus time curve at steady-state; C_{max}, maximal concentration; DMS, N-desmethylsildenafil; IV, intravenous; TID, three times a day; IQR: inter-quartile range; CI: confidence interval.

Figure 2.17: Comparison of the steady-state maximal concentration (C_{max}) for dose adjusted sildenafil plus fluconazole relative to sildenafil alone in infants.

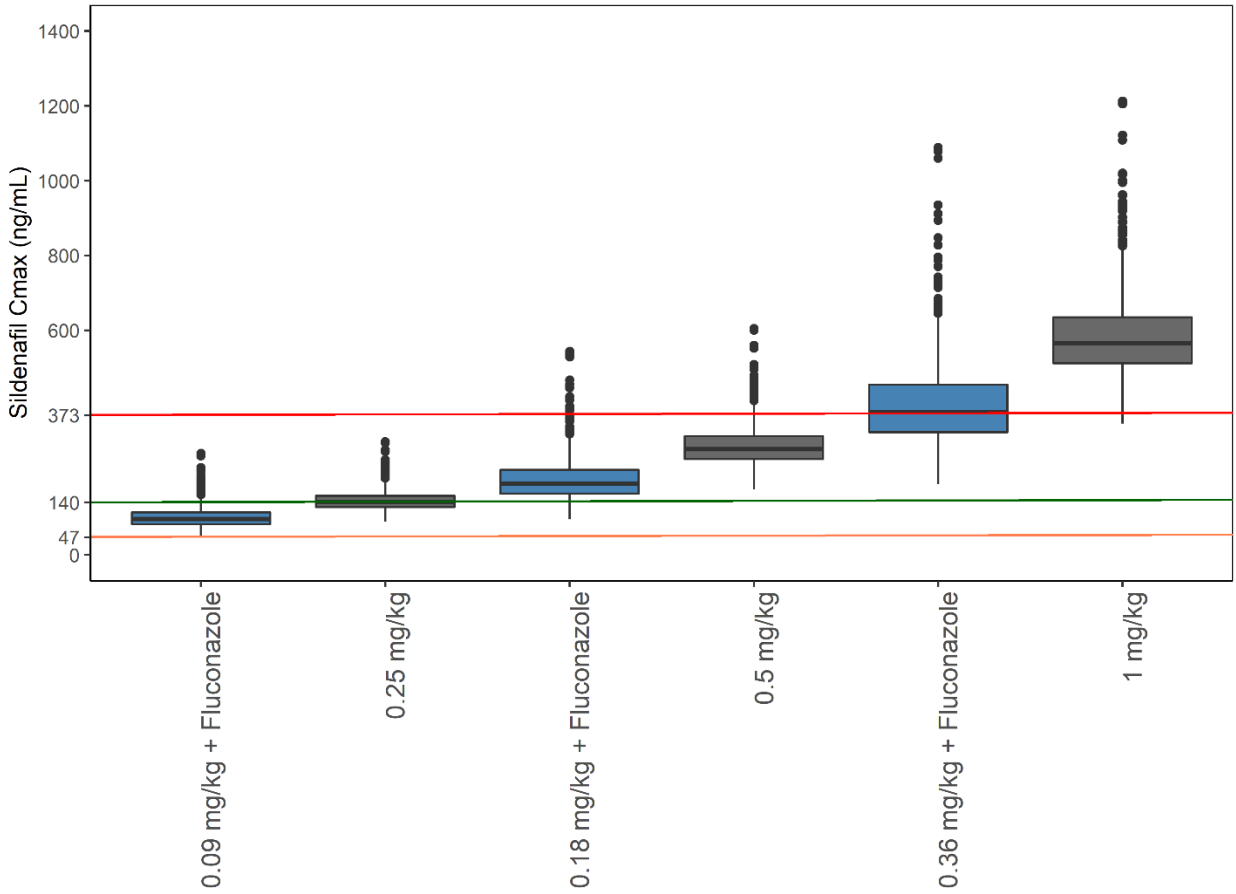

Comparison of steady-state C_{max} in infants receiving sildenafil (0.09 mg/kg, 0.18 mg/kg, and 0.36 mg/kg IV every 8 hours) plus 12 mg/kg IV daily fluconazole relative to infants receiving the reference dose of sildenafil (0.25 mg/kg, 0.5 mg/kg, and 1 mg/kg IV every 8 hours) without fluconazole. The orange, green, and red lines at 47, 140 and 373 ng/mL, respectively, correspond to 53%, 77% and 90% unbound inhibition of phosphodiesterase 5 activity *in vitro*, respectively.

REFERENCES

1. US Food and Drug Administration Center for Drug Evaluation and Research. Clinical drug interaction studies-cytochrome P450 enzyme-and transporter-mediated drug interactions. Guidance for industry <https://www.fda.gov/media/134581/download> 2020. Accessed August 5, 2020.

2. Stevens, J. C. *et al.* Developmental expression of the major human hepatic CYP3A enzymes. *J. Pharmacol. Exp. Ther.* **307**, 573–582 (2003).

3. Sim, S. C., Edwards, R. J., Boobis, A. R. & Ingelman-Sundberg, M. CYP3A7 protein expression is high in a fraction of adult human livers and partially associated with the CYP3A7*1C allele. *Pharmacogenet. Genomics* **15**, 625–631 (2005).

4. Williams, J. A. *et al.* Comparative metabolic capabilities of CYP3A4, CYP3A5, and CYP3A7. *Drug Metab. Dispos.* **30**, 883–91 (2002).

5. Gibbs, M. A., Thummel, K. E., Shen, D. D. & Kunze, K. L. Inhibition of cytochrome P-450 3A (CYP3A) in human intestinal and liver microsomes: Comparison of Ki values and impact of CYP3A5 expression. *Drug Metab. Dispos.* **27**, 180–187 (1999).

6. Soars, M. G., Grime, K. & Riley, R. J. Comparative analysis of substrate and inhibitor interactions with CYP3A4 and CYP3A5. *Xenobiotica* **36**, 287–299 (2006).

7. Hines, R. N. Ontogeny of human hepatic cytochromes P450. *J. Biochem. Mol. Toxicol.* **21**, 169–75 (2007).

8. Li, A., Yeo, K., Welty, D. & Rong, H. Development of guanfacine extended-release dosing strategies in children and adolescents with ADHD using a physiologically based pharmacokinetic model to predict drug–drug interactions with moderate CYP3A4 inhibitors or inducers. *Pediatr. Drugs* **20**, 181–194 (2018).

9. Olafuyi, O., Coleman, M. & Badhan, R. K. S. Development of a paediatric physiologically based pharmacokinetic model to assess the impact of drug-drug interactions in tuberculosis co-infected malaria subjects: A case study with artemether-lumefantrine and the CYP3A4-inducer rifampicin. *Eur. J. Pharm. Sci.* **106**, 20–33 (2017).

10. Perez, K. M. & Laughon, M. Sildenafil in term and premature infants: a systematic review. *Clin. Ther.* **37**, 2598-2607.e1 (2015).

11. Greenberg, R. G. & Benjamin, D. K. Neonatal candidiasis: diagnosis, prevention, and treatment. *J. Infect.* **69**, S19–S22 (2014).

12. Hyland, R., Roe, E. G., Jones, B. C. & Smith, D. A. Identification of the cytochrome P450 enzymes involved in the N-demethylation of sildenafil. *Br. J. Clin. Pharmacol.* **51**, 239–48 (2001).

13. Muirhead, G. J., Rance, D. J., Walker, D. K. & Wastall, P. Comparative human pharmacokinetics and metabolism of single-dose oral and intravenous sildenafil. *Br. J. Clin. Pharmacol.* **53 Suppl 1**, 13S-20S (2002).

14. Warrington, J. S., Shader, R. I., Moltke, L. L. von & Greenblatt, D. J. In vitro biotransformation of sildenafil (Viagra): identification of human cytochromes and potential drug interactions. *Drug Metab. Dispos.* **28**, 392–7 (2000).

15. Walker, D. K. Pharmacokinetics and metabolism of sildenafil in mouse, rat, rabbit, dog and man. *Xenobiotica* **29**, 297–310 (1999).

16. Haspel, H.C.et al. Binding of phosphodiesterase type 5 inhibitors sildenafil, tadalafil, and vardenafil to total human plasma proteins and human serum albumin (HSA) and 1-acid glycoprotein (AGP). In 14th North American International Society for the Study of Xenobiotics Meeting. Rio Grande, Puerto Rico <https://www.researchgate.net/publication/268138068_Binding_of_Phosphodiesterase_Type_5_Inhibitors_Sildenafil_Tadalafil_and_Vardenafil_to_Total_Human_Plasma_Proteins_and_Human_Serum_Albumin_HSA_and_1-Acid_Glycoprotein_AGP> (2006). Accessed March 20, 2020. 17. Pfizer Revatio (sildenafil) Product Insert. at <https://www.pfizermedicalinformation.com/en-us/revatio/clinical-pharmacology>

18. Takahiro, R. *et al.* Contribution of CYP3A isoforms to dealkylation of PDE5 inhibitors: a comparison between sildenafil N-demethylation and tadalafil demethylenation. *Biol. Pharm. Bull.* **38**, 58–65 (2015).

19. Mukherjee, A., Dombi, T., Wittke, B. & Lalonde, R. Population pharmacokinetics of sildenafil in term neonates: evidence of rapid maturation of metabolic clearance in the early postnatal period. *Clin. Pharmacol. Ther.* **85**, 56–63 (2009).

20. Ahsman, M. J. *et al.* Sildenafil exposure in neonates with pulmonary hypertension after administration via a nasogastric tube. *Arch. Dis. Child. - Fetal Neonatal Ed.* **95**, F109–F114 (2010).

21. Gonzalez, D. *et al.* Population pharmacokinetics of sildenafil in extremely premature infants. *Br. J. Clin. Pharmacol.* **85**, 2824–2837 (2019).

22. Lippert, J. *et al.* Open systems pharmacology community-An open access, open source, open science approach to modeling and simulation in pharmaceutical sciences. *CPT pharmacometrics Syst. Pharmacol.* **8**, 878–882 (2019).

23. Meyer, M., Schneckener, S., Ludewig, B., Kuepfer, L. & Lippert, J. Using expression data for quantification of active processes in physiologically based pharmacokinetic modeling. *Drug Metab. Dispos.* **40**, 892–901 (2012).

24. Rodrigues, A. D. Integrated cytochrome P450 reaction phenotyping. Attempting to bridge the gap between cDNA-expressed cytochrome P450 and native human liver microsomes. *Biochem. Pharmacol.* **57**, 465–480 (1999).

25. Pelkonen, O. Drug metabolism in the human fetal liver. Relationship to fetal age. *Arch. Int. Pharmacodyn. Ther.* **202**, 281–7 (1973).

26. Barter, Z. E. *et al.* Covariation of human microsomal protein per gram of liver with age: absence of influence of operator and sample storage may justify interlaboratory data pooling. *Drug Metab. Dispos.* **36**, 2405–9 (2008).

27. Ku, H.-Y. *et al.* The contributions of cytochromes P450 3A4 and 3A5 to the metabolism of the phosphodiesterase type 5 inhibitors sildenafil, udenafil, and vardenafil. *Drug Metab. Dispos.* **36**, 986–90 (2008).

28. Hindmarsh, A. C. *et al.* Open systems pharmacology suite manual, version 7.4. 329 (2018). <http://www.open-systems-pharmacology.org> Accessed March 20, 2020.

29. Rodgers, T. & Rowland, M. Physiologically based pharmacokinetic modelling 2: Predicting the tissue distribution of acids, very weak bases, neutrals and zwitterions. *J. Pharm. Sci.* **95**, 1238–1257 (2006).

30. Motulsky, H. J. *GraphPad Curve Fitting Guid.* (2020). <http://www.graphpad.com/guides/prism/7/curve-fitting/index.htm> Accessed March 20, 2020.

31. Hsu, A. *et al.* Multiple-dose pharmacokinetics of ritonavir in human immunodeficiency virus-infected subjects. *Antimicrob. Agents Chemother.* **41**, 898–905 (1997).

32. Food and Drug Administration *Midazolam Injection, USP*. **March**, (2017). <https://www.accessdata.fda.gov/drugsatfda_docs/label/2017/208878Orig1s000lbl.pdf> Accessed March 20,2020.

33. Xiao, K. *et al.* CYP3A4/5 Activity Probed with Testosterone and Midazolam: Correlation between two substrates at the microsomal and enzyme levels. *Mol. Pharm.* **16**, 382–392 (2019).

34. Greenblatt, D. J. *et al.* Inhibition of oral midazolam clearance by boosting doses of ritonavir, and by 4,4-dimethyl-benziso-(2H)-selenazine (ALT-2074), an experimental catalytic mimic of glutathione oxidase. *Br. J. Clin. Pharmacol.* **68**, 920–927 (2009).

35. Mordi, M. N., Pelta, M. D., Boote, V., Morris, G. A. & Barber, J. Acid-catalyzed degradation of clarithromycin and erythromycin B: A comparative study using NMR spectroscopy. *J. Med. Chem.* **43**, 467–474 (2000).

36. Chelvan, P., Hamilton-Miller, J. & Brumfitt, W. Biliary excretion of erythromycin after parenteral administration. *Br. J. Clin. Pharmacol.* **8**, 233–235 (1979).

37. Kalsotra, A., Turman, C. M., Kikuta, Y. & Strobel, H. W. Expression and characterization of human cytochrome P450 4F11: Putative role in the metabolism of therapeutic drugs and eicosanoids. *Toxicol. Appl. Pharmacol.* **199**, 295–304 (2004).

38. Pasic, J. *et al.* The interaction between chronic oral slow-release theophylline and single-dose intravenous erythromycin. *Xenobiotica* **17**, 493–497 (1987).

39. Austin, K., Mather, L., Philpot, C. & McDonald, P. Intersubject and dose-related variability after intravenous administration of erythromycin. *Br. J. Clin. Pharmacol.* **10**, 273–279 (1980).

40. Berend, N., Rutland, J. & Marlin, G. E. Plasma and saliva concentrations for a new formulation of erythromycin stearate. *Curr. Med. Res. Opin.* **6**, 118–123 (1979).

41. Olkkola, K. T. *et al.* A potentially hazardous interaction between erythromycin and midazolam. *Clin. Pharmacol. Ther.* **53**, 298–305 (1993).

42. Muirhead, G. J., Wulff, M. B., Fielding, A., Kleinermans, D. & Buss, N. Pharmacokinetic interactions between sildenafil and saquinavir / ritonavir. *Clin. Pharmacol.* **50**, 99–107 (2000).

43. Muirhead, G. J., Faulkner, S., Harness, J. A. & Taubel, J. The effects of steady-state erythromycin and azithromycin on the pharmacokinetics of sildenafil citrate in healthy volunteers. *Br. J. Clin. Pharmacol.* **53**, 37S-43S (2002).

44. Watt, K. M. *et al.* Physiologically based pharmacokinetic approach to determine dosing on extracorporeal life support: fluconazole in children on ECMO. *CPT pharmacometrics Syst. Pharmacol.* **7**, 629–637 (2018).

45. Claassen, K. *et al.* Development of a physiologically-based pharmacokinetic model for preterm neonates: evaluation with in vivo data. *Curr. Pharm. Des.* **21**, 5688–5698 (2015).

46. Gerhart, J. G. *et al.* Physiologically-based pharmacokinetic modeling of fluconazole using plasma and cerebrospinal fluid samples from preterm and term infants. *CPT pharmacometrics Syst. Pharmacol.* **8**, 500–510 (2019).

47. PK-Sim®. PK-Sim® Ontogeny Database. **Version 7.**, 1–47 (2017).

48. Mayer, H. *et al.* A novel approach to estimate ontogenies for PBPK applications – From literature data to simulations. *PAGE. Abstr. Annu. Meet. Popul. Approach Gr. Eur.* 27 (2018). <https://www.page-meeting.org/default.asp?abstract=8583> Accessed 20 March 2020.

49. Lacroix, D., Sonnier, M., Moncion, A., Cheron, G. & Cresteil, T. Expression of CYP3A in the human liver - Evidence that the shift between CYP3A7 and CYP3A4 occurs immediately after birth. *Eur. J. Biochem.* **247**, 625–634 (1997).

50. Tréluyer, J. M. *et al.* Oxidative metabolism of amprenavir in the human liver. Effect of the CYP3A maturation. *Drug Metab. Dispos.* **31**, 275–281 (2003).

51. Koukouritaki, S. B. *et al.* Developmental expression of human hepatic CYP2C9 and CYP2C19. *J. Pharmacol. Exp. Ther.* **308**, 965–974 (2004).

52. Treluyer, J. M., Gueret, G., Cheron, G., Sonnier, M. & Cresteil, T. Developmental expression of CYP2C and CYP2C-dependent activities in the human liver: In-vivo/in-vitro correlation and inducibility. *Pharmacogenetics* **7**, 441–452 (1997).

53. Läpple, F. *et al.* Differential expression and function of CYP2C isoforms in human intestine and liver. *Pharmacogenetics* **13**, 565–575 (2003).

54. Pappas, P. G. *et al.* Clinical practice guideline for the management of candidiasis: 2016 update by the infectious diseases society of America. *Clin. Infect. Dis.* **62**, e1–e50 (2015).

55. Barst, R. J. *et al.* A randomized, double-blind, placebo-controlled, dose-ranging study of oral sildenafil citrate in treatment-naive children with pulmonary arterial hypertension. *Circulation* **125**, 324–334 (2012).

56. Kim, J.-H. *et al.* Non-targeted metabolomics-guided sildenafil metabolism study in human liver microsomes. *J. Chromatogr. B* **1072**, 86–93 (2018).

57. Klein, M. *et al.* Predictors of inflammation in a cohort of bolivian infants and toddlers. *Am. J. Trop. Med. Hyg.* **95**, 954–963 (2016).

58. Merrill, R. *et al.* Factors associated with inflammation in preschool children and women of reproductive age: Biomarkers Reflecting Inflammation and Nutritional Determinants of Anemia (BRINDA) project. *Am. J. Clin. Nutr.* **106**, 348S-358S (2017).

59. Maharaj, A. R., Gonzalez, D., Cohen-Wolkowiez, M., Hornik, C. P. & Edginton, A. N. Improving pediatric protein binding estimates: an evaluation of α1-acid glycoprotein maturation in healthy and infected subjects. *Clin. Pharmacokinet.* **57**, 577–589 (2018).

60. Salem, F., Johnson, T. N., Abduljalil, K., Tucker, G. T. & Rostami-Hodjegan, A. A re-evaluation and validation of ontogeny functions for cytochrome P450 1A2 and 3A4 based on in vivo data. *Clin. Pharmacokinet.* **53**, 625–636 (2014).

61. Kenworthy, K. E., Bloomer, J. C., Clarke, S. E. & Houston, J. B. CYP3A4 drug interactions: correlation of 10 in vitro probe substrates. *Br. J. Clin. Pharmacol.* **48**, 716–27 (1999).

62. US Food and Drug Administration Center for Drug Evaluation and Research. Pharmacometrics Addendum to Clinical Pharmacology & Biopharmaceutics Review <https://www.accessdata.fda.gov/drugsatfda_docs/nda/2005/021845s000_Revatio_biopharmr.pdf> (2004). Accessed March 2, 2020.

63. Steinhorn, R. H. *et al.* Intravenous sildenafil in the treatment of neonates with persistent pulmonary hypertension. *J. Pediatr.* **155**, 841-847.e1 (2009).

64. Mora-Peris, B. *et al.* A Phase I study to assess the safety, tolerability and pharmacokinetic profile of boceprevir and sildenafil when dosed separately and together, in healthy male volunteers. *J. Antimicrob. Chemother.* **70**, 1812–5 (2015).

65. Sekar, V. *et al.* Effect of repeated doses of darunavir plus low-dose ritonavir on the pharmacokinetics of sildenafil in healthy male subjects: phase I randomized, open-label, two-way crossover study. *Clin. Drug Investig.* **28**, 479–85 (2008).

66. Nichols, D. J., Muirhead, G. J. & Harness, J. A. Pharmacokinetics of sildenafil after single oral doses in healthy male subjects: absolute bioavailability, food effects and dose proportionality. *Br. J. Clin. Pharmacol.* **53 Suppl 1**, 5S-12S (2002).

67. Burgess, G., Hoogkamer, H., Collings, L. & Dingemanse, J. Mutual pharmacokinetic interactions between steady-state bosentan and sildenafil. *Eur. J. Clin. Pharmacol.* **64**, 43–50 (2008).

68. Vachiery, J.-L. *et al.* Safety, tolerability and pharmacokinetics of an intravenous bolus of sildenafil in patients with pulmonary arterial hypertension. *Br. J. Clin. Pharmacol.* **71**, 289–92 (2011).

69. Veldhorst-Janssen, N. M. L. *et al.* Pharmacokinetics and Tolerability of Nasal Versus Intravenous Midazolam in Healthy Dutch Volunteers: A Single-Dose, Randomized-Sequence, Open-Label, 2-Period Crossover Pilot Study. *Clin. Ther.* **33**, 2022–2028 (2011).

70. Misaka, S. *et al.* Pharmacokinetics and pharmacodynamics of low doses of midazolam administered intravenously and orally to healthy volunteers. *Clin. Exp. Pharmacol. Physiol.* **37**, 290–295 (2010).

71. Bornemann, L. D., Crews, T., Chen, S. S., Twardak, S. & Patel, I. H. Influence of food on midazolam absorption. *J. Clin. Pharmacol.* **26**, 55–9 (1986).

72. Juif, P.-E., Boehler, M., Donazzolo, Y., Bruderer, S. & Dingemanse, J. A pharmacokinetic drug–drug interaction study between selexipag and midazolam, a CYP3A4 substrate, in healthy male subjects. *Eur. J. Clin. Pharmacol.* **73**, 1121–1128 (2017).

73. Winter, H. *et al.* Evaluation of Pharmacokinetic Interaction between PA-824 and Midazolam in Healthy Adult Subjects. *Antimicrob. Agents Chemother.* **57**, 3699–3703 (2013).

74. Ma, J. D., Nafziger, A. N., Rhodes, G., Liu, S. & Bertino, J. S. Duration of pleconaril effect on cytochrome P450 3A activity in healthy adults using the oral biomarker midazolam. *Drug Metab. Dispos.* **34**, 783–785 (2006).

75. Tsunoda, S. M., Velez, R. L., Moltke, L. L. von & Greenblatt, D. J. Differentiation of intestinal and hepatic cytochrome P450 3A activity with use of midazolam as an in vivo probe: Effect of ketoconazole. *Clin. Pharmacol. Ther.* **66**, 461–471 (1999).

76. Pentikis, H. S., Connolly, M., Trapnell, C. B., Forbes, W. P. & Bettenhausen, D. K. The effect of multiple-dose, oral rifaximin on the pharmacokinetics of intravenous and oral midazolam in healthy volunteers. *Pharmacotherapy* **27**, 1361–1369 (2007).

77. McFarland, J. W. *et al.* Quantitative structure-activity relationships among macrolide antibacterial agents: In vitro and in vivo potency against Pasteurella multocida. *J. Med. Chem.* **40**, 1340–1346 (1997).

78. DrugBank. version 5.1.2 <https://www.drugbank.ca> Accessed March 20, 2020.

79. Barre, J. *et al.* Pharmacokinetics of erythromycin in patients with severe cirrhosis. Respective influence of decreased serum binding and impaired liver metabolic capacity. *Br. J. Clin. Pharmacol.* **23**, 753–757 (1987).

80. Koudriakova, T. *et al.* Metabolism of the human immunodeficiency virus protease inhibitors indinavir and ritonavir by human intestinal microsomes and expressed Cytochrome P4503A4/3A5: Mechanism-based inactivation of cytochrome P4503A by ritonavir. *Drug Metab. Dispos.* **26**, 552–561 (1998).

81. Wang, R. W., Newton, D. J., Scheri, T. D. & Lu, A. Y. H. Human cytochrome P450 3A4-catalyzed testosterone 6β-hydroxylation and erythromycln N-demethylation: Competition during catalysis. *Drug Metab. Dispos.* **25**, 502–507 (1997).

82. Riley, R. J. & Howbrook, D. In vitro analysis of the activity of the major human hepatic CYP enzyme (CYP3A4) using [N-Methyl-14C]-erythromycin. *J. Pharmacol. Toxicol. Methods* **38**, 189–193 (1998).

83. Woodahl, E. L., Yang, Z., Bui, T., Shen, D. D. & Ho, R. J. Y. MDR1 G1199A polymorphism alters permeability of HIV protease inhibitors across P-glycoprotein-expressing epithelial cells. *AIDS* **19**, 1617–25 (2005).

84. Ernest, C. S., Hall, S. D. & Jones, D. R. Mechanism-based inactivation of CYP3A by HIV protease inhibitors. *J. Pharmacol. Exp. Ther.* **312**, 583–91 (2005).

85. Kanamitsu, S. I. *et al.* Prediction of in vivo interaction between triazolam and erythromycin based on in vitro studies using human liver microsomes and recombinant human CYP3A4. *Pharm. Res.* **17**, 419–426 (2000).

86. Obach, R. S., Walsky, R. L. & Venkatakrishnan, K. Mechanism-based inactivation of human cytochrome P450 enzymes and the prediction of drug-drug interactions. *Drug Metab. Dispos.* **35**, 246–255 (2007).

87. Watanabe, A., Nakamura, K., Okudaira, N., Okazaki, O. & Sudo, K. I. Risk assessment for drug-drug interaction caused by metabolism-based inhibition of CYP3A using automated in vitro assay systems and its application in the early drug discovery process. *Drug Metab. Dispos.* **35**, 1232–1238 (2007).

88. Granfors, M. T. *et al.* Differential Inhibition of Cytochrome P450 3A4, 3A5 and 3A7 by Five Human Immunodeficiency Virus (HIV) Protease Inhibitors in vitro. *Basic Clin. Pharmacol. Toxicol.* **98**, 79–85 (2006).

89. Fahmi, O. A. *et al.* A combined model for predicting CYP3A4 clinical net drug-drug

interaction based on CYP3A4 inhibition, inactivation, and induction determined in vitro. *Drug Metab. Dispos.* **36**, (2008).

90. Kirby, B. J. *et al.* Complex drug interactions of HIV protease inhibitors 1: Inactivation, induction, and inhibition of cytochrome P450 3A by ritonavir or nelfinavir. *Drug Metab. Dispos.* **39**, 1070–1078 (2011).

91. US Food and Drug Administration Center for Drug Evaluation and Research. Clinical pharmacology review NDA 22-473, Intravenous sildenafil<https://www.accessdata.fda.gov/drugsatfda_docs/nda/2009/022473s000_ClinPharmR.pdf> (2009). Accessed March 20, 2020.

CHAPTER 3 : PHYSIOLOGICALLY-BASED PHARMACOKINETIC MODELING CHARACTERIZES CYP3A AND P-GLYCOPROTEIN INHIBITION AND INDUCTION BETWEEN LOPINAVIR PLUS RITONAVIR WITH RIFAMPICIN IN CHILDREN

3.1 Introduction

Human immunodeficiency virus (HIV) and tuberculosis (TB) co-infection is a serious problem worldwide and is particularly problematic in sub-Saharan Africa. HIV prevalence among children with TB ranges from 10% to 60% in countries with moderate to high TB prevalence. TB is the leading cause of death among HIV-infected children resulting in 52,000 TB related deaths globally among HIV positive children in 2016.[1] Lopinavir (LPV) is a protease inhibitor that is co-administered with low-dose ritonavir (RTV) in the fixed-dose combination (Kaletra®) for enhanced bioavailability, as well as a reduction in clearance and prolonging of the half-life, through P-glycoprotein and cytochrome P450 (CYP) 3A inhibition. LPV/RTV in combination with two nucleoside reverse transcriptase inhibitors (NRTIs) is the first-line regimen of choice in treatment-naïve children from 2 weeks to <3 years of age, and it is also commonly used as second-line therapy in children failing a non-nucleoside reverse transcriptase inhibitor (NNRTI) based initial regimen.[2] Rifampicin is a key medication used for TB treatment in both adults and children. LPV/RTV with rifampicin is often unavoidable for the management of HIV/TB treatment in pediatric patients despite a clinically significant interaction.

LPV is primarily metabolized by CYP3A with 2.2% and 19.8% of drug excreted unchanged in urine and feces, respectively.[3,4] LPV is highly protein bound with a concentration dependent decrease in binding ranging from 97.4% at 100 µg/mL LPV to 99.7% at 0.1 µg/mL LPV in human plasma.[4] Although LPV binds to both human serum albumin and α1-acid-

glycoprotein (AAG), it has a higher affinity for AAG.[4,5] RTV is predominantly metabolized by CYP3A with a minor pathway through CYP2D6.[6] RTV is cleared primarily through hepatobiliary elimination with 3.5% and 33.8% of drug excreted unchanged in urine and feces, respectively.[7] The protein binding of RTV in human serum ranged from 99.3% to 99.5% at RTV concentrations ranging from 0.01 to 30 µg/ml, and both human serum albumin and AAG contribute to protein binding.[7,8] LPV and RTV are substrates, inhibitors, and inducers of P-glycoprotein.[9–12] Additionally, LPV and RTV are time-dependent inhibitors of CYP3A but RTV is a more potent time-dependent inhibitor.[13] RTV is also a mixed competitive CYP3A inhibitor, and RTV can induce CYP3A through the pregnane X receptor (PXR).[12,14]

Rifampicin can weakly inhibit but is primarily a strong inducer of CYP3A and P-glycoprotein through upregulation of the PXR receptor.[15–18] Co-administration of rifampicin 600 mg oral (PO) daily with LPV/RTV [400/100 mg PO twice daily (BID) for one week] in HIV infected adults resulted in a significant decrease in the median (interquartile range) LPV trough concentrations from 0.13 (0.10–0.18) mg/L to 0.03 (0.01–0.05) mg/L.[19] In healthy and HIV infected adults, this interaction can be overcome by super-boosting the RTV dose (LPV/RTV 400/400 mg PO BID) or doubling the dose (LPV/RTV 800/200 mg PO BID).[19–21] However in young children, doubling the dose of LPV/RTV (460/115 mg/m^2 by body-surface area PO BID) in combination with rifampicin 10 mg/kg PO once daily resulted in 60% of children [median (interquartile range) age of 1.25 (0.98-1.93) years] achieving sub-therapeutic LPV trough concentrations (<1 mg/L) compared to 8% of children [median (interquartile range) age of 1.59 (1.15-2.23) years] receiving LPV/RTV (230/57.5 mg/m^2 PO BID) without rifampicin.[22] Super-boosting LPV/RTV (230/230 mg/m^2 PO BID) was able to overcome the induction effects of

rifampicin (10 mg/kg PO daily) in children [median (interquartile range) of 16 (14-24) months], where 87% of these children achieved therapeutic LPV trough values (>1 mg/L).[23]

However, the drug-drug interaction (DDI) between LPV/RTV with the revised World Health Organization (WHO) rifampicin dosing of 15 mg/kg (ranges from 10.7 to 18.7 mg/kg based on weight and the number of tablets administered) using the fixed-dose combination (75 mg rifampicin with 50 mg isoniazid and 150 mg pyrazinamide) has not been evaluated.[24] Optimal dosing of LPV/RTV with rifampicin in pediatric patients requires further research since this interaction can result in therapeutic failure and antiretroviral drug resistance. Therefore, the study objective is to develop adult and pediatric PBPK models for LPV/RTV with rifampicin in order to optimize boosted LPV/RTV dosing in HIV/TB infected pediatric patients (between 3.0 and 24.9 kg body weight) concurrently receiving 15 mg/kg PO daily rifampicin.

3.2 Materials and Methods

3.2.1 Adult RTV PBPK Model Development

A 29 year-old European male with expressions of CYP3A4, CYP3A5, and P-glycoprotein using the Array Database was used for LPV/RTV model development and evaluation using the software PK-Sim®/MoBi® that is part of the open source Open Systems Pharmacology Suite version 9.0 (www.open-systems-pharmacology.org). We first developed and evaluated an adult PBPK model for RTV administered as a boosting agent with elvitegravir for 10 days in healthy adults, and from 200-500 mg PO every 12 hours for 2 weeks in HIV infected males (Table 3.1).[25,26] Clearance was parameterized using Michaelis-Menten kinetics for CYP3A4, CYP3A5, and CYP2D6 metabolism and P-glycoprotein transport as well as renal clearance via glomerular filtration. Interactions included time-dependent inhibition and competitive inhibition for CYP3A4 and CYP3A5, induction for CYP3A4, as well as competitive

inhibition for P-glycoprotein (Table 3.2). The aqueous solubility, transcellular intestinal permeability, and P-glycoprotein V_{max} were optimized using parameter identification with the Monte Carlo algorithm. To best characterize the maximum concentration (C_{max}) and area under the plasma concentration-time curve (AUC) data for doses ranging from 20 mg to 500 mg, one transcellular intestinal permeability value was optimized for doses <200 mg and another value was optimized for doses ≥ 200 mg (Table 3.2). Cellular permeability was calculated using the default PK-Sim® algorithm, and the tissue-to-plasma partition coefficients were calculated using the Rodgers & Rowland method.[27,28] The LPV and RTV PO formulation absorption characteristics were optimized using the Weibull formulation with a 50% dissolution time of 30 minutes, a lag-time of 30 minutes, and a dissolution shape of 0.92.

3.2.2. CYP3A Mediated DDI Potential for Ritonavir

CYP3A mediated DDI simulations between ritonavir and the probe CYP3A substrates (midazolam and sildenafil) have been evaluated extensively in a prior publication.[29] We simulated the interaction between midazolam plus ritonavir in 100 virtual white American male subjects from 21-50 years of age and 52 to 97 kg of weight, and then compared with observed data in healthy adults receiving 3 mg oral midazolam plus three oral doses of 100 mg ritonavir or placebo over 24 hours.[30] The simulated versus observed average midazolam plus ritonavir/midazolam ratio was 31.4 versus 28.4 for area under the curve from 0 to infinity ($AUC_{0-\infty}$) and was 9.47 versus 4.47 for the maximal concentration (C_{max}), respectively.[29,30]

Additionally, we simulated the interaction between sildenafil (100 mg oral tablet given on day 1 and day 8) plus ritonavir administered at 300, 400, 500 mg orally twice daily on days 2, 3, and 4–8, respectively, in 100 virtual white American male subjects from 18 to 58 years of age. The simulated versus observed geometric mean fold change (associated 95% confidence

intervals) for $AUC_{0-\infty}$ and C_{max} for sildenafil with and without ritonavir was 13-fold (11, 16) versus 11-fold (9, 12) and 2.4-fold (2.0, 2.7) versus 3.9-fold (3.2, 4.9), respectively.[29,31]

3.2.3 P-glycoprotein Mediated DDI Potential for Ritonavir

Leveraging a previously published model for digoxin, we simulated the interaction between ritonavir and the P-glycoprotein substrate, digoxin, and compared model simulations with observed DDI data reported in 12 healthy subjects receiving digoxin plus ritonavir.[32] Based on this study, we simulated 100 European adults (67% female) between 23 to 45 years of age and weighing between 49 to 87 kg, who received 0.4 mg oral digoxin before and after 14 days of ritonavir 200 mg oral twice daily.[33] The simulated versus observed geometric mean fold change (associated 90% confidence interval) for digoxin plus ritonavir relative to digoxin administered alone was 1.30-fold (1.27, 1.33) versus 1.29-fold (1.11, 1.47) for AUC from 0 to 8 hours, and was 1.33 (1.29, 1.37) versus 1.26 (0.98, 1.53) for C_{max}.

3.2.4 Adult LPV PBPK Model Development

The LPV PBPK model was developed and evaluated using LPV PK data administered concurrently with RTV in heathy adults (Table 3.1).[34–36] The model included Michaelis-Menten CYP3A4 metabolism and P-glycoprotein transport, renal clearance via glomerular filtration, and CYP3A4 and CYP3A5 time-dependent inhibition (Table 3.2). We assumed that LPV inhibition of P-glycoprotein was minimum relative to RTV. Transcellular intestinal permeability and P-glycoprotein V_{max} were optimized using parameter identification with the Monte Carlo algorithm. Cellular permeability was calculated using the default PK-Sim® algorithm, and the tissue-to-plasma partition coefficients were calculated using the Rodgers & Rowland method.[27,28]

3.2.5 Adult LPV/RTV PBPK Model Evaluation

Model evaluation for literature data was determined by comparing the ratio of simulated and observed PK parameters (C_{max}, AUC) for LPV and RTV (Table 3.1). Additionally, we used a model evaluation dataset consisting of LPV/RTV (400/100 mg) Kaletra® administered PO BID to 12 healthy adults (84 plasma samples) and 12 HIV infected adults (94 plasma samples).[37–39] Population simulations were performed based on 100 virtual white American adults (50% female) from 25 to 47 years of age. The simulated AUC within a dosing interval at steady-state ($AUC_{0\text{-}\tau,ss}$) (corresponding to 0 to 12 hours) as well as the maximum concentration at steady-state ($C_{max,ss}$) for LPV and RTV were compared to observed parameters in healthy adults as well as HIV infected subjects. Additionally, the average fold error (AFE) was calculated comparing the simulated geometric mean with observed concentration data using Equation 1. A two-fold error (0.5 to 2.0) for AFE and the simulated to observed PK parameters was considered acceptable for all adult and pediatric model evaluations.

$$AFE = 10^{(1/n)(\sum \log(simulated/observed))} \quad (1)$$

3.2.6 Adult Rifampicin PBPK Model Development and Evaluation

A previously published adult PBPK model for rifampicin by Hanke et al. was modified using PK data from 174 adults (946 plasma samples) with newly diagnosed pulmonary tuberculosis (TB) who received 450 mg (<50 kg) or 600 mg (≥50 kg) rifampicin as the fixed dose PO tablet in combination with isoniazid, ethambutol and pyrazinamide (Table 3.1).[32,40] Based on demographics of the underlying population, population simulations were performed using a Black American population of 100 virtual adults (34% female) from 18 to 63 years of age and 48 to 81 kg body weight. The average fold error was calculated based on PK data collected on day 1 and at steady-state in adults with newly diagnosed pulmonary TB in South

Africa, whom received 450 mg oral (PO) (body weight < 50 kg) or 600 mg PO rifampicin daily in combination with isoniazid, pyrazinamide, and ethambutol as the fixed-dose combination tablets.[40]

A virtual 30 year-old Black American male with an array expression of P-glycoprotein (consistent with the population used for LPV/RTV model development), and reverse transcriptase polymerase chain reaction (RT-PCR) expression of organic anion transporting polypeptide B1 (OATP1B1) and human liver arylacetamide deacetylase (AADAC) (consistent with the previously published rifampicin model) was used for model development and evaluation. The published model included metabolism and auto-induction by AADAC, transport and auto-induction by P-glycoprotein and OATP1B1, as well as renal clearance via glomerular filtration (Table 3.2). We made the following revised assumptions to this published model. First, we optimized the glomerular filtration rate to 1.80 based on observed data for the fraction of unchanged drug excreted in urine.[41] Transport and induction for OATP1B1 were based on literature data (Table 3.2).[42–44] The maximum velocity (V_{max}) for AADAC metabolism and lipophilicity were optimized, leveraging both literature data in healthy adults provided by Hanke et al. as well as leveraging the adult TB data previously described, through parameter identification using the Monte Carlo algorithm.[32,40] Transcellular intestinal permeability, oral absorption (Weibull function with a 50% dissolution time of 5 minutes, lag time of 45 minutes, and shape of 0.92), and AADAC maximum induction maximal induction (E_{max}) were manually optimized using the adult TB data.[40] Cellular permeability was calculated using the default PK-Sim® algorithm, and the organ to plasma partition coefficients were calculated using the Rodgers & Rowland method.[27,28]

Previous assumptions regarding CYP3A and P-glycoprotein inhibition and induction were based on the published adult rifampicin model and no further changes were made.[32] Rifampicin mediated CYP3A4 induction was incorporated using the weighted mean from *in vitro* CYP3A4 induction studies conducted in primary human hepatocytes with induction measured through probe substrate metabolism and corrected for binding to hepatocytes.[15,32] Simultaneous competitive inhibition of CYP3A4 by rifampicin was also integrated based on *in vitro* data obtained in human liver microsomes.[18,32] Hanke et al. evaluated these rifampicin CYP3A4 interaction parameters by comparing the simulated DDI between rifampicin and midazolam with observed data reported in adults receiving PO or intravenous midazolam plus PO rifampicin. As described in the original publication, the geometric mean fold error (range) was 1.30 (1.00 to 3.11) for the predicted to observed AUC ratio and was 1.48 (1.08 to 2.83) for the predicted to observed C_{max} ratio for data including 18 clinical studies.[32] Induction of P-glycoprotein by rifampicin was modeled assuming the same concentration of half-maximum induction (EC_{50}) as for CYP3A4 since both are mediated through pregnane X receptor.[32] The P-glycoprotein maximal induction (E_{max}) was experimentally determined in a clinical study using human duodenal biopsies.[16] Simultaneous competitive inhibition of P-glycoprotein by rifampicin was also incorporated based on a study in LLC-MDR1 polarized cell monolayers.[17,32] Hanke et al. evaluated these rifampicin parameters for P-glycoprotein by comparing the simulated DDI between rifampicin and digoxin with observed data reported in adults receiving PO or intravenous digoxin with PO rifampicin. As described in the original publication, the geometric mean fold error (range) was 1.41 (1.05 to 2.36) for the predicted to observed AUC ratio and was 1.36 (1.00 to 2.36) for the predicted to observed C_{max} ratio for data including 7 clinical studies.[32]

3.2.7 DDI Evaluation for Adults Receiving LPV/RTV Plus Rifampicin

The DDI between LPV/RTV plus rifampicin was simulated and compared with observed PK data collected in healthy adults receiving LPV/RTV in combination with rifampicin. Population simulations were performed in 100 virtual white American adults (60% female) from 22 to 70 years of age receiving standard dosing (400/100 mg LPV/RTV PO BID), double dosing (800/200 mg LPV/RTV PO BID), or boosting dosing (400/400 mg LPV/RTV PO BID) with 600 mg PO daily rifampicin. Simulated geometric mean fold ratios (90% confidence intervals) for LPV $C_{max,ss}$, $AUC_{0-\tau,ss}$, and the minimum steady-state concentration ($C_{min,ss}$) were compared with observed data in healthy and HIV infected subjects.[5,19,21]

Since experimental studies have reported that LPV/RTV can inhibit and induce OATP1B1, we performed a simulation for boosted dosing of LPV/RTV (400/400 PO BID) plus 600 mg PO daily rifampicin with OATP1B1 inhibition by LPV/RTV (a competitive inhibition constant (K_I) of 0.5 µM for LPV and 1.4 µM for RTV) and OATP1B1 induction by RTV (E_{max} of 5 fold). The simulated geometric mean for the rifampicin C_{max} and $AUC_{0-24,ss}$ with and without these OATP1B1 interaction parameters were 4.40 vs 4.47 mg/L and 32.27 vs 32.79 mg*h/L, respectively. Because of the negligible impact, all other DDI simulations between LPV/RTV plus rifampicin did not include LPV/RTV mediated induction and inhibition of OATP1B1.

3.2.8 LPV/RTV Pediatric PBPK Model Development and Evaluation

Pediatric data for LPV/RTV model development and evaluation was available from the pediatric AIDS Clinical Trials Group P1030, P1038, P1080, and P1083 studies (Table 3.1).[45] In total, there were 160 pediatric subjects (1203 LPV samples) in pediatric HIV-1 infected subjects ranging from 0.115 to <18 years of age available for model evaluation. A virtual 30 year-old white American was scaled to pediatric virtual subjects between 2 weeks and 18 years of age

based on pre-established age-dependent algorithms in PK-Sim® to generate anatomical and physiological parameters (e.g., body weight, height, organ weights), as well as to account for the maturation of CYP3A4, P-glycoprotein, and AAG. The ontogeny functions for CYP3A4 at post-menstrual age (PMA) in weeks in the liver were based upon the default ontogeny functions within PK-Sim® (Equation 2).[46] CYP3A5 has an ontogeny factor of 1 across all ages. The ontogeny function for P-glycoprotein was based upon protein expression data quantified using 69 human pediatric and 41 adult livers (Equation 3).[47] Protein binding to AAG was scaled using a Hill-function-like increase during the maturation phase and a Hill-function-like decrease during the ageing phase.[48]

$$\text{CYP3A4 ontogeny factor} = \frac{\text{PMA}^{3.331}}{73.019^{3.331}+\text{PMA}^{3.331}} \quad (2)$$

$$\text{P-glycoprotein expression (fmol/µg) at age (years)} = 0.15 + \frac{0.41 * Age^{0.78}}{2.94^{0.78} + Age^{0.78}} \quad (3)$$

Since the majority of children < 6 years of age receive Kaletra® PO solution (80 mg LPV plus 20 mg RTV per mL), a fraction of the administered dose was modified based on a bioequivalence study comparing the liquid and soft-gel capsule formulations of Kaletra®. In this clinical study, the 90% confidence intervals for C_{max} and $AUC_{0-\infty}$ for the liquid co-formulation were not bioequivalent to the co-formulated capsules. In the fasted state, LPV $AUC_{0-\infty}$ and C_{max} were approximately 22% lower, while RTV $AUC_{0-\infty}$ and C_{max} were 31% and 25% lower, respectively, for liquid relative to the soft-gel capsules. Under non-fasting conditions (a diet of 500 kcal with 25% fat content), the bioavailability of the liquid co-formulation was approximately 90% lower for liquid relative to the soft-gel capsules.[3] Consequently, liquid Kaletra® was adjusted to be a fraction of the administered dose, which was 0.8 for LPV and 0.7 for RTV in the fasting state and 0.9 for both LPV/RTV in the fed state.

For model evaluation, population simulations were performed with 100 virtual pediatric subjects simulated in each age category (0 to < 2 years, 2 to < 6 years, 6 to <12 years, and 12 to <18 years of age) and then compared with the observed data for LPV and RTV. The majority of children in the 0 to < 2 years age category were < 6 months of age, and children typically do not begin eating solid foods until at least 6 months of age. Therefore, the liquid formulation of Kaletra® in the fasted state was used for the < 2 years of age population simulation. The majority of children ≥ 6 years of age received either the soft-gel capsules or the melt-extrusion tablet so the previously described Weibull function for LPV/RTV was implemented. For the 2 to < 6 years of age population simulation, only subjects receiving the tablet formulation were included. The plasma concentration data was dose-normalized linearly to the most frequent administration per age group: 120/30, 160/40, 200/50, and 400/100 mg of LPV/RTV for the 0 to < 2 years, 2 to <6 years, 6 to <12 years, and 12 to <18 years of age groups, respectively. The AFE was calculated using the simulated geometric mean.

3.2.9 Rifampicin Pediatric PBPK Model Development and Evaluation

Data collected from 76 South African children with TB (27 were co-infected with HIV) between 2 months to 11.3 years of age receiving approximately 10 to 15 mg/kg of rifampicin in combination with isoniazid and pyrazinamide as the dispersible fixed dose combination tablets were used for model evaluation.[49] There were a total of 606 plasma samples available after excluding 23 samples below the lower limit of quantification (<0.1 mg/L or <0.25 mg/L from two different studies in children receiving 10 mg/kg rifampicin and 15 mg/kg rifampicin, respectively, with pyrazinamide and isoniazid).[50,51] Concentration data were dose normalized to a 10 mg/kg dose. A virtual 30 year-old Black American male was scaled to virtual pediatric

patients between 2 months to 12 years of age in PK-Sim® incorporating ontogeny information for albumin (equation 4) and P-glycoprotein (equation 3).

$$\text{Albumin ontogeny factor} = \frac{PMA^{3.24}}{21.533^{3.24}+PMA^{3.24}} \quad (4)$$

Ontogeny information for AADAC is lacking, so information was leveraged for a similar human esterase, the human liver serine esterase family that includes human hepatic carboxylesterase (CES) 1 and 2. The developmental expression pattern for human hepatic CES enzymes was determined by protein expression of cytosolic and microsomal samples from a bank of 165 human pediatric liver samples.[52] Microsomal CES1 activity was significantly lower between birth and 3 weeks of age than those from 3 weeks to 6 years of age with median (interquartile range) values of 6.27 (4.2-13.4) versus 16.8 (13.2-20.8) pmol/mg microsomal protein, respectively. However, microsomal CES1 activity in ages from 3 weeks to 6 years was not statistically different from ages greater than 6 years with median (interquartile range) values of 16.8 (13.2-20.8) versus 18.3 (16.7-21.1) pmol/mg microsomal protein, respectively.[52] Microsomal CES2 increased statistically with age with median (interquartile) values of 1.8 (1.6-2.5), 2.9 (2.1-3.7), and 4.2 (2.7-5.2) pmol/mg microsomal protein for the age groups of birth to 3 weeks, 3 weeks to 6 years, and greater than 6 years, respectively.[52] Therefore, we assumed that AADAC activity would be relatively similar between pediatric patients ≥ 2 months of age relative to adults, and thus ontogeny of AADAC was not included.

The ontogeny of OATP1B1 was determined based on protein expression from 71 hepatic tissue samples in fetuses (15.3-41.3 weeks gestational age (GA)), preterm newborns (24.9-36.7 weeks GA and 0.14-11.4 weeks postnatal age (PNA)), term newborns (39.7-41.3 weeks GA and 0.29-18.1 weeks PNA), pediatric patients (1.08-7.44 years), as well as adults.[53] The median (range) protein expression of OATP1B1 was 26.6 (7.1-101.7), 15.0 (7.0-46.8), 11.3 (4.9-16.5),

17.9 (8.2-23.2) and 17.7 (9.1-53.7) pmol/g liver tissue in the fetal, preterm newborn, term newborn, pediatric, and adult groups, respectively.[53] Therefore, we assumed that OATP1B1 expression would be comparable to adults for ages ≥ 2 months and thus the maturation of OATP1B1 was not included.

The transcellular intestinal permeability was manually optimized using the available pediatric rifampicin data since the bioequivalence of the pediatric formulation may differ from adults. There may be clinical factors as a multivariate analysis in 62 children with a diagnosis of TB receiving rifampicin as part of first-line therapy reported that the variability in rifampicin C_{max} was influenced by HIV infection and the site of TB infection (pulmonary versus extrapulmonary).[54] The bioavailability also differs across formulations. For example, a study comparing the PO bioavailability in 20 pediatric patients from 3 months to 2.9 years of age reported that only 50 ± 22% of a freshly prepared PO suspension was absorbed (in contrast to steady-state bioavailability of 68% in adults).[55] Furthermore, in a study of 146 TB infected children receiving anti-tubercular treatment, rifampicin exposures were 76% lower among children that received the R-Cin® suspension relative to those whom received the granulate preparation for suspension (Eremfat®).

The AFE comparing the simulated geometric mean and the observed concentration data was calculated with a two-fold error (0.5 to 2.0) considered acceptable. In addition, the mean AUC (from 0 to 5 hours, 0 to 6 hours, or 0 to 8 hours) and the C_{max} were simulated in a virtual population of 100 Black American pediatric subjects from 2 months to 4 years of age using non-compartmental analysis in Pheonix WinNonlin® version 8.3 (Certara).

3.2.10 DDI Simulations Between LPV/RTV plus Rifampicin in Pediatric Patients

We simulated standard dosing (230/57.5 mg/m^2 LPV/RTV PO BID) with and without 10 mg/kg PO daily rifampicin, as well as boosted dosing (230/230 mg/m^2) and double dosing (460/115 mg/m^2) LPV/RTV PO BID with 10 mg/kg daily PO rifampicin. The population simulations were performed in 100 virtual children between 0.5 and 4.5 years of age for two weeks using the liquid formulation of Kaletra® in the fed-state. The simulated PK parameters were compared with observed data in children.[22,23]

Dosing simulations were next performed to optimize dosing in children (2 months to 8 years of age) receiving boosted LPV/RTV with 10 mg/kg and 15 mg/kg PO daily rifampicin. We simulated 100 virtual subjects per WHO simplified weight bands (3-5.9, 6-9.9, 10-13.9, 14 to 19.9, and 20-24.9 kg), and targeted weight based dosing for boosted LPV/RTV (1:1 ratio) that would achieve ≥ 90% of virtual subjects obtaining LPV trough values > 1 mg/L.[24] The PBPK simulated results were also compared with suggested dosing obtained from a population based PK (PopPK) study developed in HIV infected children with and without TB receiving boosted LPV/RTV with and without 10 mg/kg PO daily rifampicin.[56]

3.3. Results

3.3.1 Adult LPV/RTV PBPK Model Evaluation

The RTV PBPK model was parameterized with CYP3A4, CYP3A5, and CYP2D6 metabolism; P-glycoprotein transport; glomerular filtration; CYP3A4 and CYP3A5 time-dependent and competitive inhibition; CYP3A4 induction; and P-glycoprotein competitive inhibition (Table 3.2). The LPV PBPK model was parameterized with CYP3A4 metabolism and P-glycoprotein transport, glomerular filtration, and CYP3A4 and CYP3A5 time-dependent

inhibition (Table 3.2). All of the simulated to observed $AUC_{0\text{-}\tau,ss}$, $AUC_{0\text{-}24,ss}$ and $C_{max,ss}$ mean ratios were between 0.7 and 2.0 (Table 3.3-Table 3.6 and Figure 3.1).

3.3.2 Adult Rifampicin PBPK Model Evaluation

The previously published rifampicin PBPK model was parameterized with metabolism and auto-induction by AADAC, transport and auto-induction by P-glycoprotein and OATP1B1, as well as renal clearance via glomerular filtration. We further optimized the glomerular filtration rate using literature data, and optimized the AADAC V_{max}, AADAC E_{max}, lipophilicity, and transcellular intestinal permeability (Figure 3.1). The AFE was calculated based on PK data collected on day 1 and at steady-state in adults with newly diagnosed pulmonary TB in South Africa, whom received 450 mg PO (body weight < 50 kg) or 600 mg PO rifampicin daily in combination with isoniazid, pyrazinamide, and ethambutol as the fixed-dose combination tablets.[40] The AFE was 1.05 for adults receiving 450 mg daily rifampicin and was 1.44 for adults receiving 600 mg daily rifampicin (Figure 3.2).

3.3.3 Adult LPV/RTV with Rifampicin DDI Evaluation

Standard dosing, supra-boosted dosing, and double-dosing of LPV/RTV with 600 mg PO daily rifampicin were simulated and compared with observed data. The simulated to observed geometric mean fold ratios for $C_{max,ss}$, $AUC_{0\text{-}\tau,ss}$, and $C_{min,ss}$ LPV were similar and all within 2-fold except for the the $C_{min,ss}$ at standard dosing (400/100) LPV/RTV) with 600 mg PO daily rifampicin that was ~9-fold higher (Figure 3.7).

3.3.4 Pediatric LPV/RTV PBPK Model Evaluation

Population simulations were performed for LPV/RTV and compared with observed data collected in 160 HIV-1 infected pediatric subjects (1203 LPV samples) from 0.115 to <18 years of age that received LPV/RTV.[45] The AFE ranged from 0.67 to 1.94 for LPV and 0.68 to 1.62

for RTV, and the simulated versus observed median AUC_{0-12}, C_{min}, and C_{max} were very similar (Table 3.8 and Figure 3.3-Figure 3.6).

3.3.5. Pediatric Rifampicin PBPK Model Evaluation

The model AFE ranged from 0.82 to 1.25 based on observed data in 76 South African children with TB from 2 months to 11.3 years of age receiving 10-15 mg/kg rifampicin (Figure 3.7).[49] However, there was underprediction of rifampicin at the earlier timepoints, suggesting that rate of absorption may be greater in pediatric patients. This is likely associated with differences in the formulations of the fixed-dosed combination of rifampicin between pediatric patients and adults. In addition, the mean simulated AUC and the C_{max} were similar to those reported in TB positive children although the observed data varied considerably by rifampicin dosing, age, HIV infection status, and formulation (Table 3.9).[50,51,54,57] The simulated median (inter-quartile range) steady-state oral clearance (CL/F) for virtual children between 2 to <6 years and 6 to <12 years was 7.53 (5.39, 9.75) L/h and 13.1 (9.89, 17.4) L/h, respectively, compared to 7.7 (5.2-11.4) L/h in 62 children with a median (inter-quartile range) of 5.0 years (2.8-8.9).[54]

3.3.6 Pediatric LPV/RTV with Rifampicin DDI Model Evaluation

The simulated and observed PK parameters were comparable in children between 0.5 and 4.5 years receiving the 230/57.5 mg/m^2 PO BID LPV/RTV and 230/230 mg/m^2 PO BID LPV/RTV with 10 mg/kg PO daily rifampicin regimens, however, there was considerable discrepancy for 460/115 mg/m^2 LPV/RTV PO BID with 10 mg/kg PO daily rifampicin (Table 3.8).[22,23] Based on our simulations, the double dosing was able to overcome the rifampicin inductive effects in adults and pediatric patients slightly better than boosted dosing (Figure 3.8). The simulated RTV $AUC_{0-\tau,ss}$ for the 12 hour dosing interval was significantly lower in children

compared to adults for all dosing regimens evaluated (Figure 3.8). In addition, for the standard LPV/RTV dose with rifampicin, the simulated impact of rifampicin on inducing oral clearance was slightly lower in children relative to adults (Figure 3.8).

3.3.7 Dosing Simulations to Optimize Dosing for LPV/RTV in Pediatric Patients

The simplified weight based dosing for boosted LPV/RTV in children (2 months to 8 years of age) was optimized when administered concurrently with 10 mg/kg rifampicin as well as the WHO recommended dosing of 15 mg/kg rifampicin (Table 3.10). We simulated that 14-16 mg/kg of boosted LPV/RTV (1:1 ratio administered PO BID) in combination with 10 mg/kg PO daily rifampicin resulted in 94% to 100% of simulated subjects achieving LPV $C_{min,ss}$ values > 1 mg/L (Table 3.10). Similarly, a previously published PopPK model reported that boosted LPV/RTV dosing from 12 mg/kg (14-19.9 kg) to 22 mg/kg (3-5.9 kg) resulted in ≥ 95% of subjects achieving LPV $C_{min,ss}$ values > 1 mg/L.[56] Furthermore, increasing the rifampicin dosing to 15 mg/kg PO daily with 16 mg/kg PO BID of boosted LPV/RTV resulted in 93% to 98% of simulated subjects achieving LPV $C_{min,ss}$ values > 1 mg/L (Table 3.10).

3.4 Discussion

In this study, adult and pediatric PBPK models for LPV/RTV with rifampicin were developed and evaluated in order to optimize dosing for LPV/RTV with rifampicin in pediatric patients co-infected with HIV and TB. Adult simulations for LPV/RTV with rifampicin were performed using a published rifampicin model (with some revised model assumptions), and then simulations were compared with observed data reported in healthy and HIV/ TB co-infected adults.[32] The LPV/RTV and rifampicin PBPK models were scaled to pediatric patients and evaluated using pediatric PK data. Next, the LPV/RTV with rifampicin DDI was simulated and compared with PK parameters reported in pediatric patients with HIV and TB receiving double

or boosted doses of LPV/RTV with rifampicin. Finally, dosing recommendations of boosted LPV/RTV (1:1 ratio) were simulated in pediatric patients from 2 months to 8 years of age using the WHO revised dosing of rifampicin (15 mg/kg) stratified by WHO simplified weight bands.[24]

The RTV PBPK model leveraged literature data and then the solubility, lipophilicity, transcellular intestinal permeability, and P-glycoprotein V_{max} were optimized (Table 3.1). RTV is essentially insoluble in water but the soft-gel capsule and the melt-extrusion tablet formulations of Kaletra® have higher RTV solubility.[58] Since the solubility of RTV is unknown in these formulations, the aqueous solubility of RTV was optimized. The transcellular intestinal permeability was also optimized using a higher value in simulations with doses ≥ 200 mg. Another published PBPK model developed for RTV also optimized the fraction absorbed from 0.08 to 1.00 for doses ranging from 20 mg to 200 mg.[59] This suggests that there may be some model misspecification regarding CYP3A4 and/or P-glycoprotein intestinal inhibition in the model, however, RTV is typically administered at doses under 200 mg in adults and children. However, the RTV-mediated DDI potentials for CYP3A4/5 and P-glycoprotein were evaluated based on comparing simulations with clinical DDI data for RTV plus midazolam and sildenafil (CYP3A probes) and digoxin (P-glycoprotein probe).

The interaction potential of RTV is highly complex, as it can both induce and inhibit hepatic and intestinal CYP3A4 as well as P-glycoprotein. Studies using midazolam as the probe CYP3A4 substrate reported that chronic dosing of RTV (400 mg PO BID) decreased intestinal and hepatic CYP3A activity by 78% and 90%, respectively.[60] Another study using fexofenadine as the P-glycoprotein probe substrate reported that RTV inhibited P-glycoprotein with an increase in the AUC of fexofenadine of 2.8-fold after 600 mg PO on day 1 and 1.4-fold after 400 mg PO BID for 2 weeks.[61] RTV has been reported to induce P-glycoprotein 2- to 9-fold;

however, P-glycoprotein induction was not included in the model because there is uncertainty in the induction parameters and net P-glycoprotein inhibition is observed clinically.[61]

The LPV PBPK model was developed and evaluated as the LPV/RTV co-formulation since clinical data for LPV alone is limited due to its poor bioavailability (Table 3.1 and Table 3.2). RTV significantly increases LPV bioavailability, presumably through P-glycoprotein and CYP3A inhibition. LPV-mediated P-glycoprotein inhibition was not included in the model although both induction and inhibition of P-glycoprotein have been reported experimentally for LPV.[10] In healthy human volunteers, co-administration of a single 400 mg dose of LPV with 50 mg RTV enhanced the $AUC_{0-\infty}$ of LPV in plasma by 77-fold relative to dosing of LPV alone.[8] Additionally, LPV doses up to 600 mg did not affect the PK profile of 50 mg or 100 mg RTV after multiple dosing of LPV/RTV.[3] This suggests that P-glycoprotein and/or CYP3A inhibition by LPV is negligible relative to RTV when administered concurrently.

A previously developed adult PBPK model for rifampicin was modified using data from adult TB patients, and then the DDI between LPV/RTV with rifampicin was evaluated in adults.[32] Using the optimized rifampicin model, we simulated standard dosing (400/100 mg), double dosing (800/200 mg), and boosted dosing (400/400 mg) of LPV/RTV PO BID with 600 mg PO daily rifampicin, and compared these results with observed values reported in healthy and HIV infected adults. The simulated LPV $AUC_{0-\tau,ss}$ for standard dosing was decreased by 79% with rifampicin, compared to 75% reported in healthy adults and 68% reported in HIV infected adults.[5,19] However, the simulated LPV $C_{min,ss}$ geometric mean fold ratio for standard dosing with rifampicin was 9-fold higher than reported in healthy adults. The actual timing of the trough measurements may differ since the study details were not well described in the package insert.[5] Additionally, a diurnal pattern for RTV has been reported clinically with lower exposures and

higher troughs following the evening dose which was not accounted for in the PBPK model.[26] Consistent with clinical studies in HIV-infected and healthy adults, the simulations for double and boosted dosing of LPV/RTV overcame rifampicin induction and resulted in similar exposures as the standard dosing without rifampicin (Table 3.7 and Figure 3.8).

In the adult and pediatric DDI simulations, rifampicin resulted in lower induction of LPV/RTV oral clearance in children relative to adults, probably due to lower expression of P-glycoprotein and CYP3A4 in pediatric patients (Figure 3.8). A PopPK model developed for LPV/RTV with rifampicin in adults and children reported that rifampicin induced the clearance of LPV and RTV to lesser extent in children than adults, but rifampicin co-administration significantly diminished the bioavailability of LPV and especially RTV in children relative to adults.[20] Furthermore, observed data in children suggest that there is a critical RTV concentration ($\leq$ approximately 0.1 mg/L) around which RTV can no longer adequately boost LPV concentrations. The PBPK model underestimates the boosted effect of RTV on LPV bioavailability at low RTV concentrations, which may occur in children receiving LPV/RTV with rifampicin.[20,56] The Kaletra® liquid also has a poor taste, so it is also possible that the entire dose is not swallowed or absorbed when given in large volumes with double LPV/ RTV dosing with rifampicin in children. The bioavailability of LPV/RTV is also lower in infants and young children due, in part, to dietary and formulation issues. We accounted for these differences in the PBPK model by assuming that infants < 6 months of age received LPV/RTV in the fasted state and that the bioavailability of the liquid formulation was a fraction of that of the soft-gel capsule based on a bioequivalence study performed in adults with and without food.[3] However, the bioavailability of liquid Kaletra® may be much different in infants receiving breast-milk or formula relative to the adult bioequivalence study data.

Despite the lack of confidence for the PBPK model predicted double dosing of LPV/RTV with rifampicin, we were able to capture the DDI between boosted LPV/RTV with rifampicin (Table 3.4). Therefore, we simulated weight-based dosing for boosted LPV/RTV with rifampicin in virtual pediatric subjects from 2 months to 8 years of age between 3.0-24.9 kg body weights. A prospective study in 96 HIV-infected children with TB (median age of 18.2 months) found that there was a non-inferior difference, measured by LPV troughs > 1 mg/L, of -1.1% (95% confidence interval of -6.9 to 3.2) in children receiving boosted LPV/RTV with 10 mg/kg rifampicin relative to standard LPV/RTV without rifampicin.[62] However, studies have not yet evaluated boosted dosing of LPV/RTV in combination with the WHO revised rifampicin dosing of 15 mg/kg in the fixed-dose combination. The clinical endpoint was to achieve LPV troughs > 1 mg/L based on the concentration of half maximum inhibition of 0.1 µM for wild-type HIV in 50% serum.[3] Based on our simulations, 16 mg/kg of boosted PO BID with 15 mg/kg PO daily rifampicin in children weighing between 3.0 kg to 24.9 kg resulted in >90% of virtual subjects with LPV $C_{min,ss}$ > 1 mg/L. In contrast, the WHO recommends standard LPV/RTV (4:1) weight-based without rifampicin of approximately 20-40 mg/kg, 12-20 mg/kg, 12-16 mg/kg, 10-14 mg/kg, and 10-12 mg/kg for the 3-5.9 kg, 6-9.9 kg, 10-13.9 kg, 14-19.9 kg, and 20-24.9 kg weight-bands. We are predicting a less-pronounced age effect on LPV/RTV disposition than the WHO dosing.[63] We identified minor differences in our simulated dosing recommendations for virtual infants and children receiving 10 mg/kg or 15 mg/kg of PO daily rifampicin. This is likely because the mean rifampicin average concentration during the dosing interval in children receiving the 10 mg/kg daily dose was 0.67 mg/L, which exceeds the CYP3A4 and P-glycoprotein EC_{50} value (0.28 mg/L) thus induction is already functioning close to the E_{max}.

We leveraged PBPK modeling to optimize dosing for HIV/TB co-infected pediatric patients receiving LPV/RTV plus rifampicin. Due to the complexity of this three-way interaction, there are some notable limitations and key assumptions that require further discussion. First, we performed the DDI simulations assuming that LPV/RTV had negligible impact on rifampicin exposures. Both LPV and RTV potently inhibited OATP1B1, however, we did not observe significant differences in rifampicin exposure with and without inclusion of these *in-vitro* parameters. Second, we overestimated the DDI magnitude for double dosing in children relative to observed data suggesting that the boosted effect of RTV is not adequately captured at low RTV concentrations. Therefore, this model should not be extrapolated to optimize dosing for fixed-dose (4:1 ratio) LPV/RTV in combination with rifampicin in HIV/TB co-infected pediatric patients. Finally, there may be physiological differences in HIV and TB co-infected children, such as malnourishment as well as differences between the White or Black American virtual population and South Africans, which are not incorporated in the pediatric virtual population.

In conclusion, adult and pediatric PBPK models for LPV/RTV with rifampicin were developed and evaluated in order to optimize boosted dosing for LPV/RTV with rifampicin in pediatric patients co-infected with HIV and TB. Based on our simulations, 16 mg/kg of boosted PO BID with 15 mg/kg PO daily rifampicin achieved LPV $C_{min,ss}$ values >1 mg/L in >90% of virtual pediatric subjects (2 months to 8 years of age) weighing between 3.0 kg to 24.9 kg body-weight.

3.5 Tables

Table 3.1: Clinical data available for model development and evaluation.

Drug of Interest	Sample Size	Population	Dosing and PK Sampling
RTV	24	Healthy adults	RTV (20, 50, 100, 200 mg) PO once daily with elvitegravir for 10 days with PK collected on day 10[25]
RTV	16	HIV-infected adults	RTV (200, 300, 400, 500 mg) PO every 12 hours for 17 days with PK collected on day 17[26]
LPV/RTV	N/A	Healthy male volunteers	LPV (100, 200, 400, 800 mg) plus 100 mg RTV single dose; LPV (400, 600, 800 mg PO) plus 200 mg PO RTV single dose[3]
LPV/RTV	22	Healthy adults	400/100, 200/150, 200/50 mg LPV/RTV PO BID for 7 days with PK data collected on day 7[34]
LPV/RTV	8	Healthy males	400/100 mg LPV/RTV PO single dose[35]
LPV/RTV	16	Healthy adults	400/100 mg LPV/RTV PO BID for 16 days with PK data collected on day 16[36]
LPV/RTV	12	Healthy adult volunteers	400/100 mg LPV/RTV PO BID for 10 days; PK data collected on day 11[37]
LPV/RTV	9	HIV-infected adults	400/100 mg LPV/RTV PO BID; PK data collected during the week 2 study visit (14-28 days after starting treatment)[38,39]
LPV/RTV	229	HIV-infected children from 0.2-18 years	300/75 mg/m^2 LPV/RTV PO BID; PK data collected $\geq$ 2 weeks[45]
Rifampicin	12	Healthy adult males	300 mg or 600 mg IV (30 minute infusion) rifampicin (single)[64]
Rifampicin	11	Healthy adults	300, 450, 600 mg IV (3 hour infusion) rifampicin (single dose) [41]
Rifampicin	12	Healthy adults	300 mg PO capsules (single dose)[65]
Rifampicin	8	Healthy adults	450 mg PO tablet (single dose)[32]
Rifampicin	12	Healthy males	600 mg PO capsule (single dose) and 600 mg PO capsule daily for 7 days[66]
Rifampicin	38	Healthy adults	600 mg PO capsule (single dose)[67]
Rifampicin	24	Healthy males	600 mg PO capsule (single dose)[68]

Rifampicin	12	Healthy adults	600 mg PO daily for 7 days[69]
Rifampicin	174	Adult TB patients with and without HIV	450 mg (<50 kg) or 600 mg (≥50 kg); PK data collected on day 1 and day 28[40]
Rifampicin	76	TB infected children from 0.17-11.3 years	Median (interquartile range) of 10.3 (6.37-15.9) mg/kg PO once daily; PK data collected ≥ 2 weeks[49]
LPV/RTV plus Rifampicin	21	HIV-infected adults	LPV/RTV: 400/100 mg (standard dose) with PK data collected at baseline and one week after starting 600 mg PO daily rifampicin; PK data collected one week after initiating 600 mg PO daily rifampicin plus 600/150 mg LPV/RTV (1.5 times) and 800/200 mg LPV/RTV (double dose)[19]
LPV/RTV plus Rifampicin	74	HIV-infected infants ± TB from 0.5-4.5 years	230/57.5 mg/m^2 LPV/RTV; 230/230 mg/m^2 LPV/RTV +10 mg/kg rifampicin; 430/115 mg/m^2 LPV/RTV +10 mg/kg rifampicin; PK data collected after ≥ 2 weeks of therapy[19,20,23,56]

Abbreviations: N/A: not available; TB: tuberculosis; HIV: human immunodeficiency virus; LPV: lopinavir; RTV: ritonavir; PO: oral; BID: twice daily; PK: pharmacokinetic

Table 3.2: Final physiologically-based pharmacokinetic (PBPK) model parameters for lopinavir, ritonavir, and rifampicin.

Parameter	Lopinavir	Ritonavir	Rifampicin
Physiochemical Properties			
Lipophilicity	3.32[a]	3.83[a]	2.91[a]
Molecular Weight	629 g/mol [70]	721 g/mol [70]	822.94 g/mol [70]
Fraction Unbound	0.01 [70]	0.01 [70]	0.11 [70]
Protein Binding	AAG	AAG	Albumin
Solubility	0.00192 mg/mL [70]	100 µg/mL*	2.8 mg/mL [32]
pKa (Acid or Base)	Neutral [70]	2.84 (Base) [70]	7.90 (Base)/ 1.70 (Acid) [32]
Transcellular Intestinal Permeability	$9.91 \cdot 10^{-4}$ cm/min[a]	$2.33 * 10^{-5}$ cm/min (<200 mg)[a] $8.91 * 10^{-5}$ cm/min (≥ 200 mg)[a]	$3.00 * 10^{-5}$ cm/min (adults)[a] $7.50 * 10^{-6}$ cm/min (pediatric)[a]
Metabolism and Transport			
CYP3A4 K_M	6.8 µM [3]	0.068 µM [6]	-
CYP3A4 V_{max}	9.4 nmol/mg/min [3]	1.37 pmol/min/mg [6]	-
CYP3A5 K_M	-	0.047 µM [6]	-
CYP3A5 V_{max}	-	1.00 pmol/min/mg [6]	-
CYP2D6 K_M	-	1.0 µM [6]	-
CYP2D6 V_{max}	-	0.93 pmol/min/mg [6]	-
P-glycoprotein K_M	0.13 µM [9]	0.13 µM [9]	-
P-glycoprotein V_{max}	1.28 pmol/min/pmol[a]	1.68 pmol/min/pmol[a]	-
P-glycoprotein K_{cat}	-	-	0.61 1/min [32]
AADAC K_M	-	-	162.9 µM [71]
AADAC V_{max}	-	-	47.4 pmol/min/pmol[a]
GFR fraction[b]	1.00	1.00	1.80[a]
OATP1B1 V_{max}	-	-	$8.37*10^{-4}$ pmol/min/pmol [72]
OATP1B1 K_M	-	-	1.50 µM [72]
Interactions			
CYP3A4 $K_{inact,half}$	0.41 µM [13]	0.10 µM [13]	-

CYP3A4 K_{inact}	0.10 1/min [13]	0.32 1/min [13]	-
CYP3A4 K_I	-	0.03 µM [14]	18.5 µM [18]
CYP3A4 EC_{50}	-	1.0 µM [73]	0.34 µM [15]
CYP3A4 E_{max}	-	68.5 [73]	9.0 [15]
CYP3A5 $K_{inact,half}$	1.00 µM [13]	0.12 µM [13]	-
CYP3A5 K_{inact}	0.05 1/min [13]	0.08 1/min [13]	-
CYP3A5 K_I	-	0.03 µM [14]	-
P-glycoprotein K_I	-	0.2 µM [60]	169 µM [17]
P-glycoprotein EC_{50}	-	-	0.34 µM [15,32]
P-glycoprotein E_{max}	-	-	2.5 [16]
OATP1B1 EC_{50}	-	-	10 µM [43]
OATP1B1 E_{max}	-	-	5.0 [43]
AADAC EC_{50}	-	-	0.9 µM [40]
AADAC E_{max}	-	-	5.0[a]

[a]Optimized value. [b]Adult renal clearance via the GFR fraction was predicted using a GFR fraction to account for tubular reabsorption or secretion as the empiric renal clearance (literature renal clearance value in adults) divided by the expected renal clearance as a result of GFR if there was no tubular reabsorption (fraction unbound x normal GFR). Abbreviations: pKa: negative base-10 logarithm of the acid dissociation constant; CYP3A4: cytochrome P450 3A4; CYP3A5: cytochrome P450 3A5; CYP2D6: cytochrome P450 2D6; K_M: concentration of half-maximum metabolism or transport; V_{max}: maximum rate of metabolism or transport; AADAC: human arylacetamide deacetylase; OATP1B1: organic-anion-transporting polypeptide (OATP) 1B1; EC_{50}: concentration of the drug that gives half-maximum induction; E_{max}: maximum induction; $K_{inact,half}$: concentration of half-maximum inactivation; K_{inact}: maximum rate of inactivation; K_I: concentration of half-maximum inhibition; AAG: α1-acid glycoprotein; glomerular filtration rate.

Table 3.3: Comparison between the observed and simulated lopinavir and ritonavir area under the concentration vs. time curve and maximum concentration following the Kaletra® fixed-dose combination (400/100 mg lopinavir/ritonavir) in healthy and HIV-infected adults.

	Lopinavir $AUC_{0-\tau,ss}$ (µg·h/mL)	**Ritonavir $AUC_{0-\tau,ss}$ (µg·h/mL)**	**Lopinavir $C_{max,ss}$ (µg/mL)**	**Ritonavir $C_{max,ss}$ (µg/mL)**
Virtual adults				
Simulated[a]	93.7	4.5	8.9	0.53
Healthy adults				
Observed[b]	96.8 ± 21.8	4.4 ± 1.8	11.2 ± 2.9	0.85 ± 0.45
Ratio[b]	**1.0**	**1.0**	**0.8**	**0.6**
Observed[c]	70.9 ± 37.0	3.08 ± 2.79	7.67 ± 2.93	0.42 ± 0.36
Ratio[c]	**1.3**	**1.5**	**1.2**	**1.3**
HIV-infected adults				
Observed[d]	92.6 ± 36.7	N/A	9.8 ± 3.7	N/A
Ratio[d]	**1.0**	**N/A**	**0.9**	**N/A**
Observed[e]	95.3 (60.3-119.3)	4.97 (2.82-8.74)	N/A	N/A
Ratio[e]	**1.0**	**0.9**	**N/A**	**N/A**

[a]Simulated data presented as the geometric mean ± standard deviation in a virtual population of 100 white Americans (50% female) from 25 to 47 years of age. Ratio calculated as the ratio of the simulated to observed mean value.

[b]Observed data presented as the mean ± standard deviation for 16 healthy volunteers receiving Kaletra (400 mg lopinavir with 100 mg ritonavir) PO (PO) BID for 16 days administered as the fixed-dose melt extrusion tablet formulation (Kaletra®).[36]

[c]Observed data presented as the mean ± standard deviation for 24 healthy adults receiving Kaletra (400 mg lopinavir with 100 mg ritonavir) PO BID for 11 days.[37]

[d]Observed data presented as the steady-state mean ± standard deviation for 19 HIV-infected subjects receiving Kaletra (400 mg lopinavir with 100 mg ritonavir) PO BID as the fixed-dose melt extrusion tablet formulation.[5] [e]Observed data presented as the mean (min-max) obtained from 8 HIV-infected adults receiving Kaletra 400 mg lopinavir with 100 mg ritonavir) PO BID with tenofovir with or or two other nucleotide reverse transcriptase inhibitor drugs for two weeks.[39]

Abbreviations: HIV: human immunodeficiency virus; $AUC_{0\text{-}\tau,ss}$: area under the concentration vs. time curve from 0 to tau (0 to 12 hours) at steady-state; $C_{max,ss}$: maximum concentration at steady-state, N/A: not-available.

Table 3.4: Comparison between the observed and simulated area under the concentration vs. time curve and maximum concentration of ritonavir in healthy adults.

Ritonavir Dose	**Observed $AUC_{0\text{-}\tau,ss}$ (µg*hr/mL)**	**Simulated $AUC_{0\text{-}\tau,ss}$ (µg*hr/mL)**	**Ratio**	**Observed $C_{max,ss}$ (µg/mL)**	**Simulated $C_{max,ss}$ (µg/mL)**	**Ratio**
20 mg PO daily	0.134	0.130	1.0	0.0195	0.0171	0.9
50 mg PO daily	1.12	0.766	0.7	0.130	0.089	0.7
100 mg PO daily	6.53	5.29	0.8	0.807	0.550	0.7
200 mg PO daily	16.0	28.9	1.8	2.46	3.92	1.6

Observed data presented as the arithmetic mean based on 21 healthy subjects whom received ritonavir (20, 50, 100, and 200 mg) orally (PO) once daily in combination with 125 mg elvitegravir for 10 days to achieve steady-state.[25] Simulated data based on a mean 29 year old individual receiving ritonavir (20, 50, 100, and 200 mg) PO once daily for 10 days.

Abbreviations: $AUC_{0\text{-}\tau,ss}$: area under the concentration vs. time curve from 0 to tau (0 to 24 hours) at steady-state; $C_{max,ss}$: maximum concentration at steady-state; Oral: PO administration.

Table 3.5: Comparison between the observed and simulated area under the concentration vs. time curve and maximum concentration of ritonavir in HIV-infected adults.

Ritonavir Dose	**Observed[a] $AUC_{0\text{-}24,ss}$ (µg*hr/mL)**	**Simulated[b] $AUC_{0\text{-}24,ss}$ (µg*hr/mL)**	**Ratio**	**Observed[a] $C_{max,ss}$ (µg/mL)**	**Simulated[b] $C_{max,ss}$ (µg/mL)**	**Ratio**
200 mg PO twice daily	43.8	68.1	1.6	4.5	4.8	1.1
300 mg PO twice daily	60.7	120.8	2.0	6.5	8.0	1.2
400 mg PO twice daily	114.2	184.0	1.6	11.7	11.4	1.0
500 mg PO twice daily	170.3	252	1.5	14.2	14.7	1.0

[a]Observed data presented as the arithmetic mean based on 16 HIV-infected adults from 21 to 42 years of age whom received ritonavir (200, 300, 400, 500 mg) PO twice once daily for 16 days.[25]

[b]Simulated data based on the arithmetic mean ± the standard deviation in 100 virtual adults from 21 to 42 years of age.

Abbreviations: HIV: human immunodeficiency virus; $AUC_{0\text{-}24,ss}$: area under the concentration vs. time curve from 0 to 24 hours at steady-state; $C_{max,ss}$: maximum concentration at steady-state; Oral: PO administration.

Table 3.6: Comparison between the lopinavir and ritonavir observed and simulated area under the concentration vs. time curve and maximum concentration in healthy adults.

	Lopinavir (400 mg) + Ritonavir (100 mg)		**Lopinavir (200 mg) + Ritonavir (150 mg)**		**Lopinavir (200 mg) + Ritonavir (50 mg)**	
	Lopinavir	**Ritonavir**	**Lopinavir**	**Ritonavir**	**Lopinavir**	**Ritonavir**
Observed[a] $AUC_{0-\tau,ss}$ (µg*hr/mL)	99.6	4.64	73.6	10.5	45.1	1.63
Simulated[b] $AUC_{0-\tau,ss}$ (µg*hr/mL)	88.9	7.24	76.6	13.3	31.7	1.55
$AUC_{0-\tau,ss}$ Ratio	**0.9**	**1.6**	**1.0**	**1.3**	**0.7**	**1.0**
Observed[a] C_{max} (µg/mL)	12.0	0.887	8.94	1.96	6.40	0.273
Simulated[b] C_{max} (µg/mL)	13.0	0.839	12.0	1.48	6.34	0.199
C_{max} Ratio	**1.1**	**0.9**	**1.3**	**0.8**	**1.0**	**0.7**

[a]Observed data presented as the geometric mean of 22 healthy adults (8 females) whom received PO (PO) lopinavir/ritonavir (LPV/RTV) administered PO BID for 7 days with PK data described on day 7.[34]

[b]Simulated data based on a 29 year-old European male receiving 400/100, 200/150, or 200/50 mg LPV/RTV PO BID for 7 days.

Abbreviations: $AUC_{0-\tau,ss}$: area under the concentration vs. time curve from 0 to tau (0 to 12 hours) at steady-state; $C_{max,ss}$: maximum concentration at steady-state.

Table 3.7: Comparison of observed and simulated lopinavir area under the concentration vs. time curve, maximum concentration, and minimum concentration at steady-state following co-administration with ritonavir and rifampicin in healthy and HIV/TB co-infected adults.

LPV/RTV Dose (mg) + Rifampicin	Data Source	Lopinavir $C_{max,ss}$	Lopinavir $AUC_{0-\tau,ss}$	Lopinavir $C_{min,ss}$
400/100 mg LPV/RTV	Observed[a]	0.45 (0.40, 0.51)	0.25 (0.21, 0.29)	0.01 (0.01, 0.02)
	Simulated[b]	0.29 (0.28, 0.31)	0.21 (0.21, 0.22)	0.09 (0.09, 0.10)
	Observed[c]	0.46 (0.42-0.50)	0.32 (0.28-0.36)	0.05 (0.03, 0.06)
400/400 mg LPV/RTV	Observed[d]	0.93 (0.81, 1.07)	0.98 (0.81, 1.17)	1.03 (0.68, 1.56)
	Simulated[b]	0.96 (0.94, 0.99)	0.94 (0.94, 0.99)	0.85 (0.80, 0.90)
800/200 mg LPV/RTV	Observed[d]	1.02 (0.85, 1.23)	0.84 (0.64, 1.10)	0.43 (0.19, 0.96)
	Simulated[b]	0.82 (0.79, 0.85)	0.86 (0.83, 0.89)	0.73 (0.59, 0.91)
	Observed[c]	1.13 (0.97, 1.31)	1.02 (0.90, 1.15)	N/A

Data are presented as the geometric mean ratio and the associated 90% confidence interval interval, except for the observed lopinavir $C_{min,ss}$ which is presented as the ratio of the median (inter-quartile range).

[a]Observed data are presented as the geometric mean (90% confidence interval (CI)) ratio at steady-state based on 22 healthy adults receiving 400 mg lopinavir with 100 mg ritonavir soft-gel capsules BID in combination with 600 mg PO (PO) once daily rifampicin relative to 400 mg lopinavir with 100 mg ritonavir soft-gel capsules BID for 10 days.[5]

[b]Simulated data based on 100 virtual white American adults (60% female) from 22 to 70 years of age.

[c]Observed data presented as the geometric mean ratio (90% CI) in 21 (86% female) HIV-infected adults receiving LPV/RTV with dual nucleoside reverse transcriptase inhibitors at 400/100 mg PO BID, with 600 mg PO daily rifampicin, and at 800/200 mg PO BID with 600 mg PO daily rifampicin.[19]

[d]Observed data presented as the geometric mean ratio (90% CI) in healthy adults receiving 800 mg lopinavir with 200 mg ritonavir or 400 mg lopinavir with 400 mg ritonavir soft-gel capsules BID in combination with 600 mg PO daily rifampicin for 7 days relative to receiving 400 mg lopinavir with 100 mg ritonavir soft-gel capsules BID for 10 days.[21]

Abbreviations: HIV: human immunodeficiency virus; TB: tuberculosis; N/A: not available; LPV/RTV: lopinavir/ritonavir; CI: confidence interval; $C_{max,ss}$: maximum concentration at steady-state; $C_{min,ss}$: minimum concentration at steady-state; $AUC_{0-\tau,ss}$: area under the concentration vs. time curve from 0 to tau (0 to 12 hours) at steady-state.

Table 3.8: Comparison of observed and simulated lopinavir area under the concentration vs. time curve, maximum concentration, and minimum concentration at steady-state in infants and children from 0.5 to 4.5 years of age.

Dosing Regimen	230/57.5 mg/m^2 LPV/RTV PO BID alone		230/230 mg/m^2 PO BID LPV/RTV + 10 mg/kg PO Daily Rifampicin		460/115 mg/m^2 PO BID LPV/RTV + 10 mg/kg PO Daily Rifampicin	
PK Parameter	**Observed[a,b]**	**Simulated**	**Observed[a]**	**Simulated**	**Observed[b]**	**Simulated**
$AUC_{0\text{-}12,ss}$ (mg*h/L)	117.8 (80.4, 176.1)[23]	105.9 (74.5, 148.2)	80.9 (50.9, 121.7)[23]	78.5 (57.3, 111.4)	N/A	89.6 (59.9, 125.4)
$AUC_{0\text{-}8,ss}$ (mg*h/L)	49.2 (40.7, 86.6)[22]	78.8 (55.3, 109.1)	N/A	59.5 (44.2, 83.6)	23.9 (13.8, 49.6)[22]	69.0 (46.4, 94.8)
$C_{min,ss}$ (mg/L)	4.6 (2.3, 10.4)[23]	5.5 (3.3, 9.0)	3.9 (2.3, 7.7)[23]	3.3 (2.3, 5.75)	0.7 (0.1, 2.0)[22]	3.6 (2.4, 7.1)
$C_{max,ss}$ (mg/L)	14.2 (11.9, 23.5)[23]	11.9 (9.2, 17.1)	10.5 (7.1, 14.3)[23]	9.9 (7.4, 13.6)	4.5 (2.5, 8.2)[22]	11.2 (7.1, 14.9)

Data are presented as the median (interquartile range). [a]Observed data were reported in a population of 15 children (7 months to 3.9 years) co-infected with HIV/TB receiving 230/230 mg/m^2 (boosted dose) of liquid LPV/RTV oral (PO) twice daily (BID) with 10 mg/kg PO daily rifampicin.[23] [b]Observed data presented in children (aged 0.64 to 2.43 years) receiving 460/115 mg/m^2 (double dose) BID PO solution of LPV/RTV with 10 mg/kg PO daily.[22] Simulations in a population of 100 virtual children from 6 months to 4.5 years of age. Abbreviations: LPV: lopinavir; RTV: ritonavir; $C_{min,ss}$: minimum concentration at steady-state; $C_{max,ss}$: maximum concentration at steady-state; $AUC_{0\text{-}12,ss}$: area under the concentration vs. time curve from 0 to 12 hours at steady-state; $AUC_{0\text{-}8,ss}$: area under the concentration vs. time curve from 0 to 8 hours at steady-state; PO: Oral administration.

Table 3.9: Comparison of simulated and observed AUC and C_{max} for rifampicin in TB positive pediatric patients

AUC (µg*h/mL)	C_{max} (µg/mL)	Patient Population
Observed mean (10 mg/kg PO daily rifampicin)		
14.9 (AUC_{0-6})	3.9 *(2 hour plasma level)*	21 HIV infected TB positive children with a mean age of 3.73 years[a]
7.4 (AUC_{0-5})	8.5	15 HIV uninfected TB positive children < 2 years old with a mean age of 1.09 years[b]
Simulated mean (10 mg/kg PO daily rifampicin)		
8.3 (AUC_{0-5}) 8.8 (AUC_{0-6})	3.3	100 virtual subjects (Black American population) from 2 months to 4 years of age
Observed mean (15 mg/kg PO daily rifampicin)		
26.0 (AUC_{0-8})	6.3	62 TB positive children (45.2% HIV infected) with a median age of 5.0 years[c]
12.1 (AUC_{0-8})	2.9	26 TB positive infants (13% HIV infected) with a mean age of 6.6 months[d]
Simulated mean (15 mg/kg PO daily rifampicin)		
13.6 (AUC_{0-8})	4.6	100 virtual subjects (Black American population) from 2 months to 4 years of age

[a]Mean rifampicin data for 21 HIV uninfected TB positive children with a mean age of 3.73 years receiving a mean (range) rifampicin dose of 9.61 mg/kg (6.47 to 15.58) for 1 month after commencing treatment administered as part of a fixed-dose tablet formulation designed for pediatric use.[51]

[b]Mean rifampicin data for 15 HIV uninfected TB positive children with a mean (standard deviation) age of 1.09 years (0.49 years) receiving 10 mg/kg rifampicin for ≥ 2 weeks administered as part of a fixed-dose tablet formulation that was crushed and dissolved in 2 to 5 mL of water and then PO absorbed.[74]

[c]Median rifampicin data for 62 TB positive children (45.2% HIV infected) with a median (inter-quartile range) age of 5.0 years (2.8, 6.9 years) receiving the World-Health Organization standardized rifampicin dosing (15 mg/kg daily (range of 10-20 mg/kg)) as part of the dispersible fixed-dose combination tablets with isoniazid, rifampicin, pyrazinamide, and ethambutol. Pharmacokinetic sampling was performed at or after 4 weeks of anti-tubercular treatment.[54]

[d]26 TB positive infants (13% HIV infected) with a mean (standard deviation) age of 6.6 months (3.3 months) receiving the World Health Organization standardized rifampicin dosing (15 mg/kg daily (range of 10-20 mg/kg)) as part of the dispersible fixed-dose combination tablets with isoniazid, rifampicin, pyrazinamide, and ethambutol. Pharmacokinetic sampling was performed at or after 2 weeks of anti-tubercular treatment.[75]

Abbreviations: HIV: human immunodeficiency virus; TB: tuberculosis; $AUC_{0-5:}$ area under the plasma concentration curve from 0 to 5 hours; $AUC_{0-6:}$ area under the plasma concentration curve from 0 to 6 hours; $AUC_{0-8:}$ area under the plasma concentration curve from 0 to 8 hours.

Table 3.10: Comparison of observed and simulated lopinavir area under the concentration vs. time curve, maximum concentration, and minimum concentration at steady-state following the simulated dosing recommendations for pediatric patients receiving lopinavir/ritonavir with rifampicin.

Age Range (years)	**Weight (kg)**	**Rifampicin daily dose PO (mg/kg)**	**PBPK LPV/RTV (1:1) BID dosing PO (mg/kg)**	**PopPK LPV/RTV (1:1) BID dosing PO (mg/kg)**	**LPV AUC_{τ} (mg*h/L)[a]**	**LPV $C_{max,ss}$ (mg/L)[a]**	**LPV $C_{min,ss}$ (mg/L)[a]**	**LPV $C_{min,ss}$ > 1 mg/L (%)**
0.02 - 0.5	3.0 - 5.9	10	16	22	161	16.9	9.6	100
0.5 – 1.8	6.0 - 9.9	10	16	16	142	14.9	8.2	95
0.6 – 4.7	10.0 - 13.9	10	16	14	123	8.5	5.7	95
1.5 – 6	14.0 - 19.9	10	14	12	107	11.9	5.5	94
1.5 - 7.9	20 - 24.9	10	14	N/A	96	11.1	4.6	96
0.02 - 0.5	3.0 - 5.9	15	16	N/A	139	15.0	7.9	98
0.5 – 1.8	6.0 - 9.9	15	16	N/A	130	13.9	7.3	95
0.6 – 4.7	10.0 - 13.9	15	16	N/A	113	12.7	4.9	94
1 – 7.5	14.0 - 19.9	15	16	N/A	104	11.6	5.8	94
1.5 - 7.9	20 - 24.9	15	16	N/A	94	10.9	4.5	93

[a]Simulated data presented as the geometric mean. Dosing simulations were performed to optimize dosing in infants and children (2 months to 8 years of age) receiving the boosted dose of lopinavir/ritonavir (LPV/RTV) in combination with 10 mg/kg daily rifampicin and the World Health Organization (WHO) revised rifampicin dosing recommendations of 15 mg/kg daily rifampicin.[1]

We simulated 100 virtual subjects per WHO simplified weight bands (3-5.9 kg, 6-9.9 kg, 10-13.9 kg, 14-19.9 kg, and 20-24.9 kg), and targeted weight based dosing for boosted LPV/RTV (1:1 ratio) that would achieve ≥ 85% of virtual infants and children achieving LPV trough values greater than 1 mg/L. The physiologically-based pharmacokinetic (PBPK) model simulated results were also compared with suggested dosing obtained from a population PK (PopPK) model developed using data from HIV-infected adults and children with and without tuberculosis receiving LPV/RTV with or without rifampicin.[56]

Abbreviations: LPV: lopinavir; RTV: ritonavir: BID: BID: PO: PO administration; $AUC_{0\text{-}\tau}$: area under the concentration vs. time curve from 0 to tau (0 to 12 hours) at steady-state: $C_{max,ss}$: maximum concentration at steady-state: $C_{min,ss}$: minimum concentration at steady-state; N/A: not available; PBPK: physiologically-based pharmacokinetic; PopPK: population pharmacokinetic.

3.6 Figures

Figure 3.1: Population simulations of lopinavir and ritonavir (400/100 mg) concentration vs. time profiles at steady-state following oral administration twice daily in HIV-infected and healthy adults.

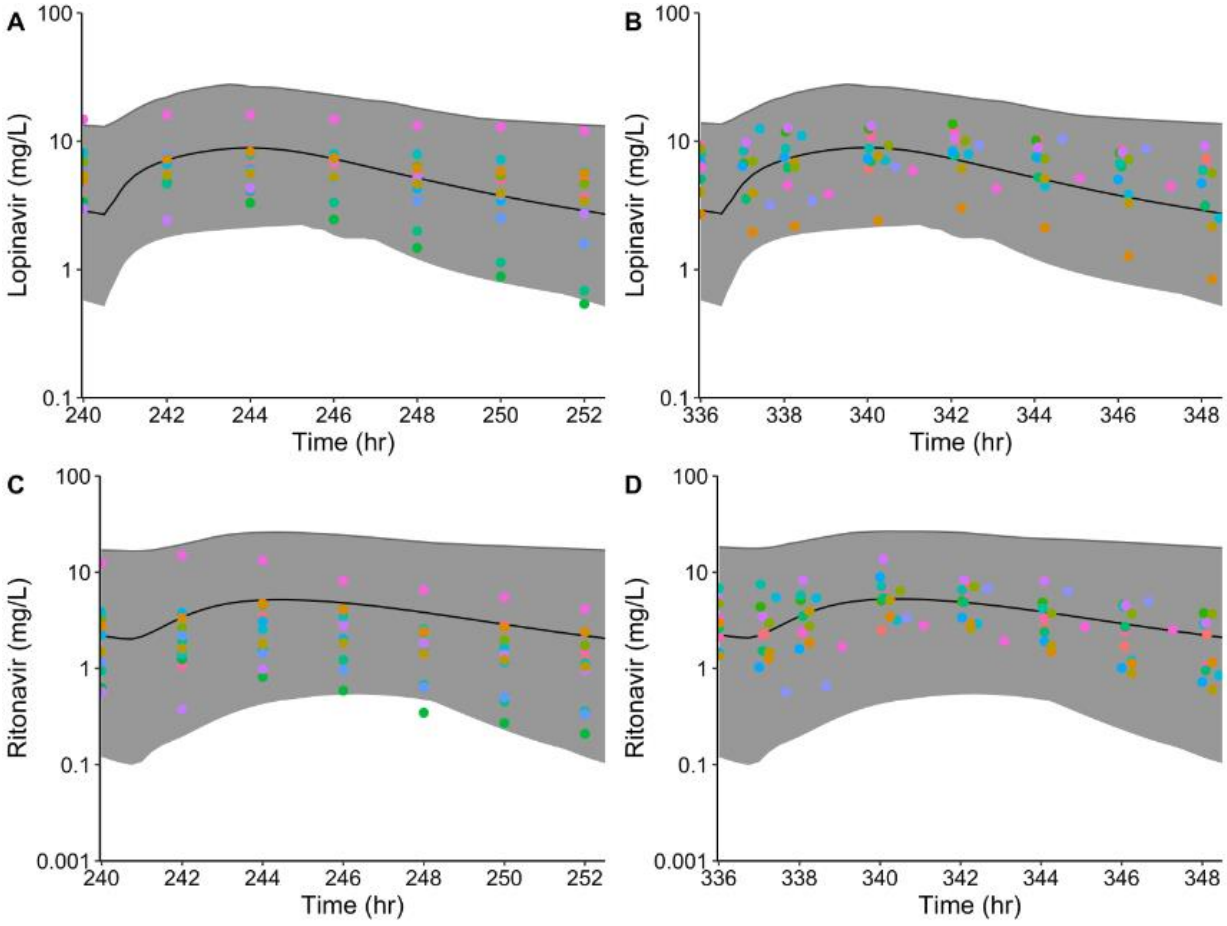

Population simulations for lopinavir (A) and (B) and ritonavir (C) and (D) based on 100 virtual white American subjects (50% female) from 25 to 47 years of age receiving 400/100 mg lopinavir/ritonavir orally BID for two weeks. The 90% prediction interval is shown as a solid grey region and the geometric mean is shown as a solid black line. Observed data for lopinavir and ritonavir in HIV infected subjects with plasma samples collected over 12 hours between study weeks 2 and 4[38,39] (B and D) and in healthy adults with plasma samples collected on day 11 [37] (A and C) are presented as dots with color stratified by individual. The average fold error,

calculated using the equation with the simulated geometric mean $10^{(1/n)\sum \log(\text{simulated/observed})}$, was 0.90 for lopinavir and 1.42 for ritonavir for both healthy and HIV infected subjects.

Figure 3.2: Population simulations of rifampicin concentration vs. time profiles following oral administration of 450 and 600 mg twice daily on day 1 (A and B) and at steady-state (C and D), respectively, in TB positive adults.

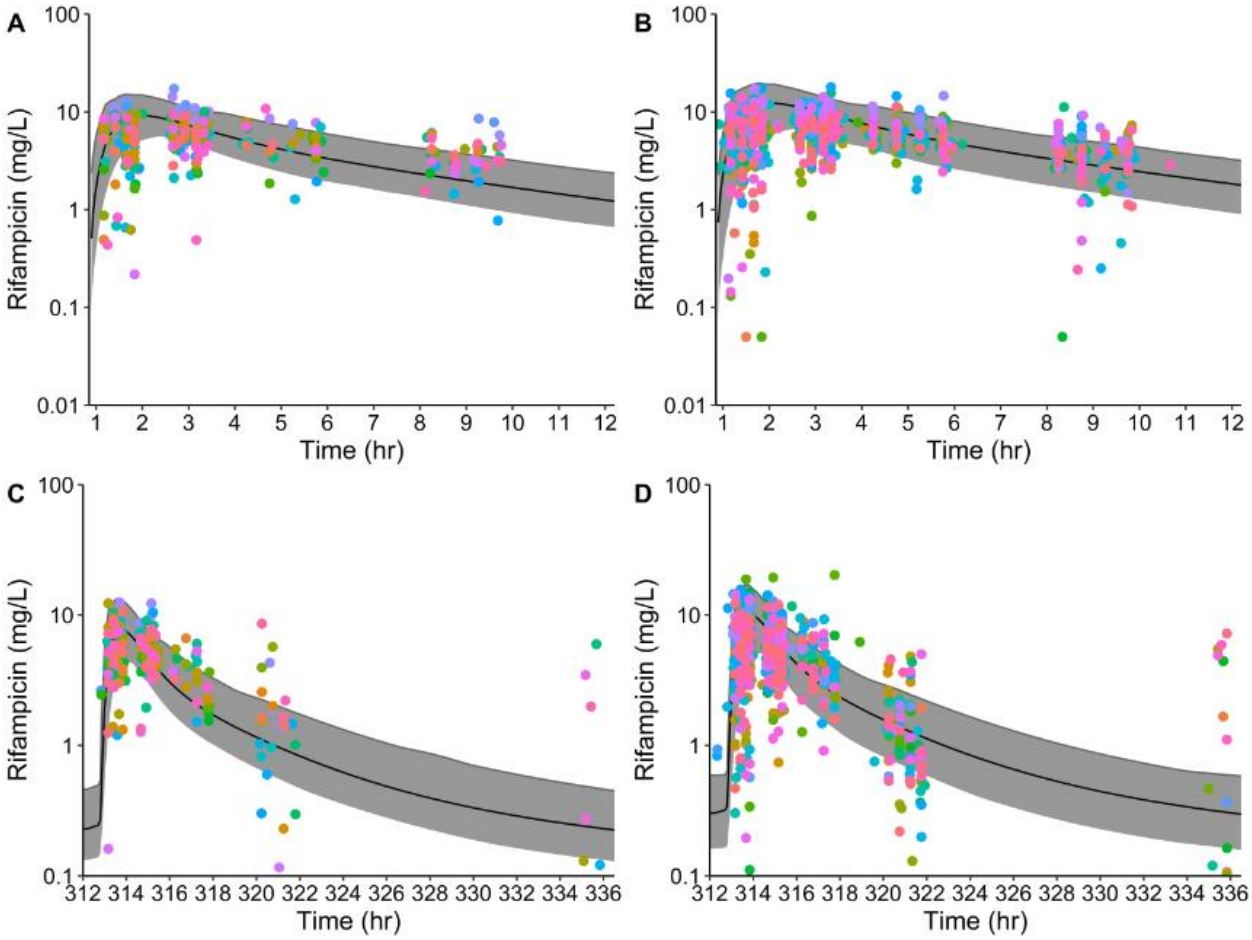

Population simulations for rifampicin in 100 Black American virtual adults (34% female) from 18 to 63 years of age receiving 450 mg (A and C) and 600 mg (B and D) oral daily rifampicin for 2 weeks. The 90% prediction interval is shown as a solid grey region and the geometric mean is shown as a solid black line on day 1 (A and B) and after two weeks of daily dosing (C and D). Observed data are presented as dots with color stratified by individual.[40] In this study, patients with newly diagnosed pulmonary tuberculosis (TB) received rifampicin at 450 mg PO BID (body weight < 50 kg) or 600 mg PO BID (body weight ≥ 50 kg) in combination with isoniazid, pyrazinamide, and ethambutol as fixed dose combination tablets.[40] Three venous blood samples

were taken per patient after the first dose (pre-induced date) and then repeated after approximately 28 days (induced state). The average fold error, calculated using the equation with the simulated geometric mean $10^{(1/n)(\sum \log(\text{simulated}/\text{observed}))}$, was 1.05 for adults receiving 450 mg daily rifampicin and was 1.44 for adults receiving 600 mg daily rifampicin.

Figure 3.3: Population simulations of lopinavir and ritonavir concentration vs. time profiles following oral liquid administration (120/30 mg lopinavir/ritonavir) twice daily in HIV-infected children <2 years of age for 2 weeks.

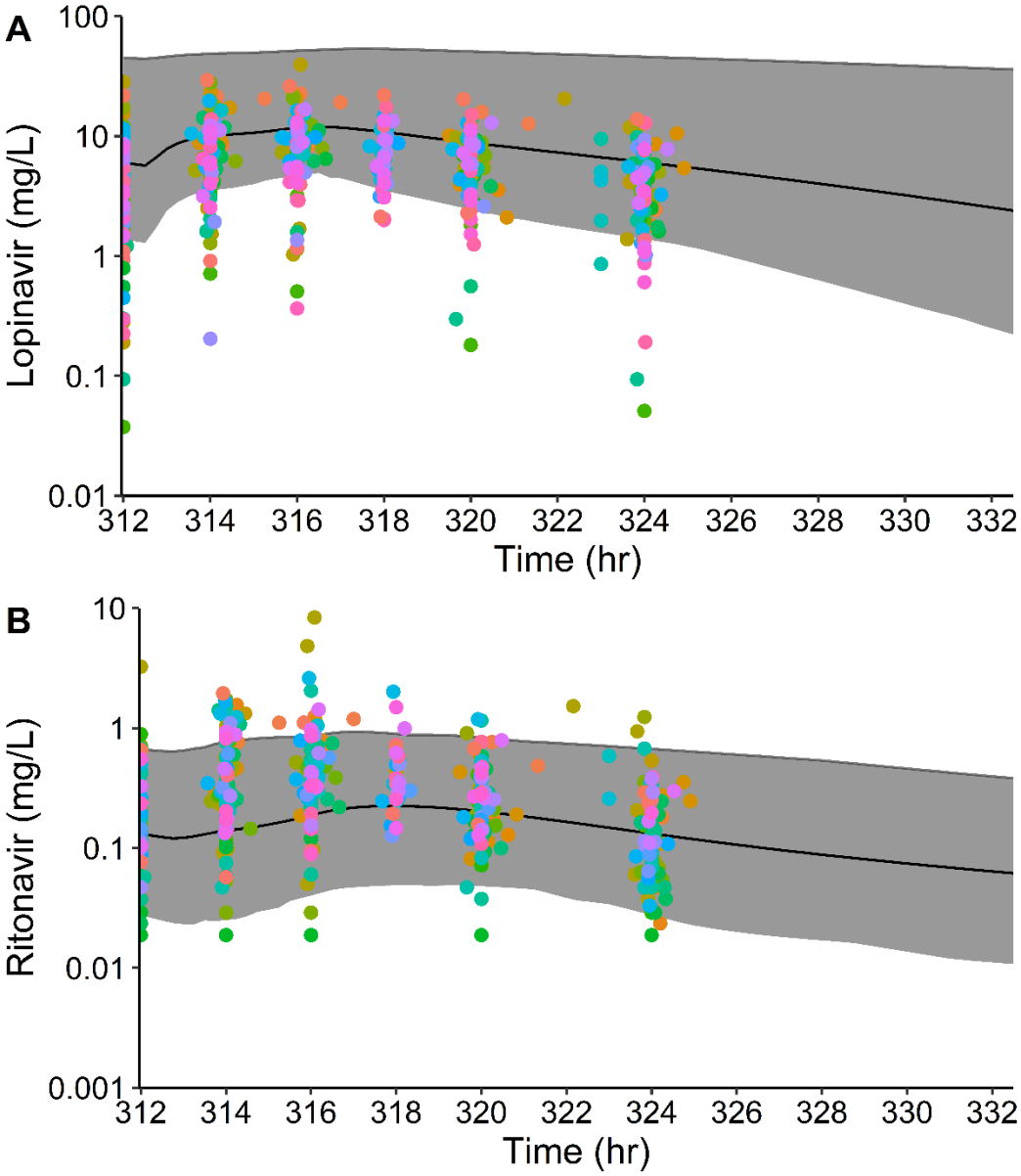

Population simulations for lopinavir (A) and ritonavir (B) based on 100 virtual white American infants and children (50% female) from 0.115 to <2 years of age receiving the liquid formation of lopinavir/ritonavir (120/30 mg) oral twice daily. The 90% prediction interval is shown as a solid grey region and the geometric mean is shown as a solid black line. Observed data (normalized to 120/30 mg for lopinavir and ritonavir) in HIV-infected children from 0.115 to <2

years of age are presented as dots with color stratified by individual.[45] The average fold error, calculated using the equation with the simulated geometric mean $10^{(1/n)\sum \log(\text{simulated/observed})}$, was 1.64 for lopinavir and 0.68 for ritonavir. Abbreviations: HIV: human immunodeficiency virus.

Figure 3.4: Population simulations of lopinavir and ritonavir concentration vs. time profiles following oral tablet administration (160/40 mg lopinavir/ritonavir) twice daily in HIV-infected children from 2 to <6 years of age for 2 weeks.

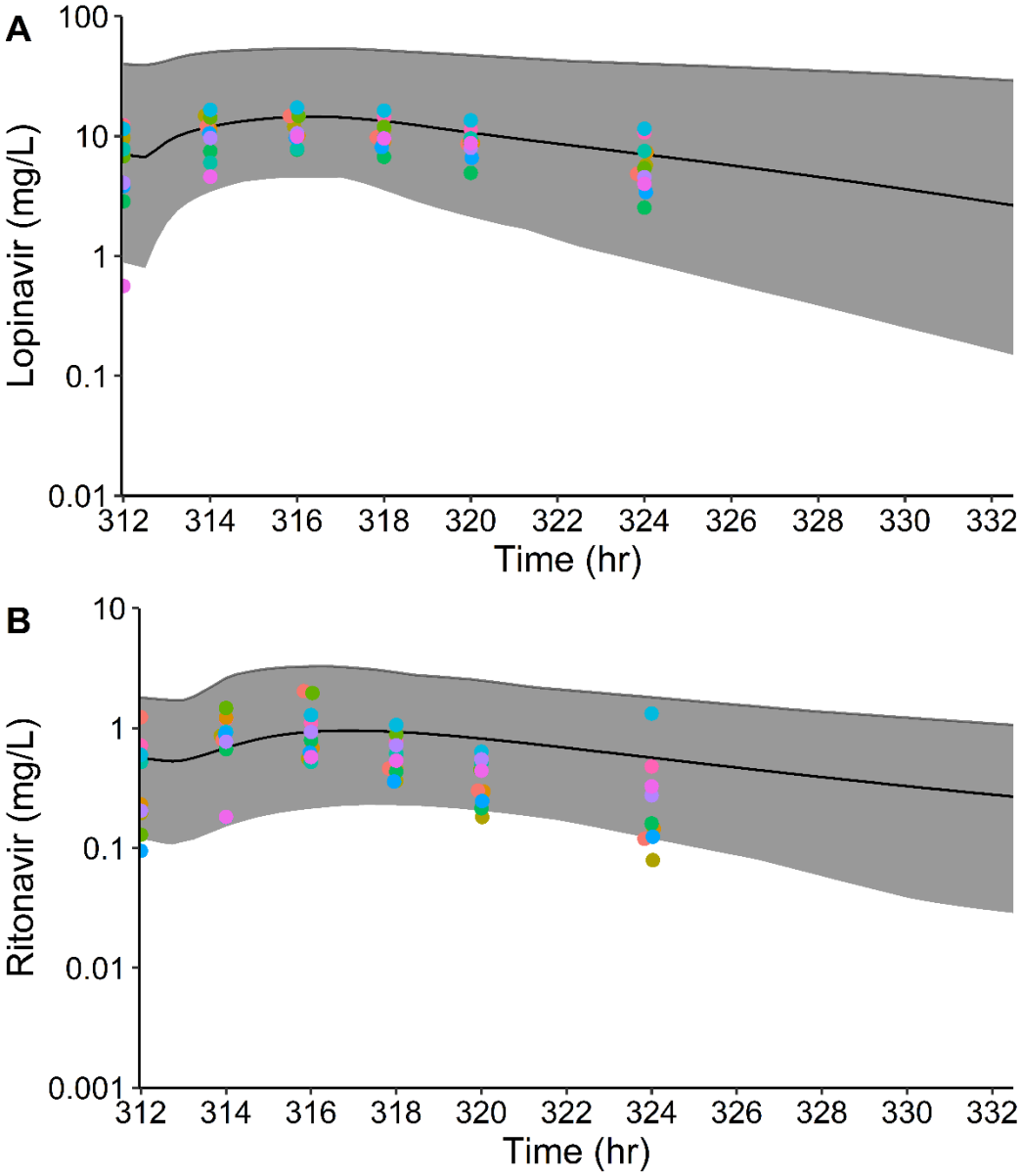

Population simulations for lopinavir (A) and ritonavir (B) based on 100 virtual white American children (50% female) from 2 to <6 years of age receiving the tablet formation of lopinavir/ritonavir (160/40 mg) orally twice daily. The 90% prediction interval is shown as a solid grey region and the geometric mean is shown as a solid black line. Observed data

(normalized to 160/40 mg dose of lopinavir/ ritonavir) in HIV-infected children from 2 to <6 years of age are presented as dots with color stratified by individual.[45] The average fold error, calculated with the simulated geometric mean using the equation $10^{(1/n)\sum \log(\text{simulated/observed})}$, was 1.25 for lopinavir and 1.58 for ritonavir. Abbreviations: HIV: human immunodeficiency virus.

Figure 3.5: Population simulations of lopinavir and ritonavir concentration vs. time profiles following oral administration (200/50 mg lopinavir/ritonavir) twice daily in HIV-infected children from 6 to <12 years of age for 2 weeks**.**

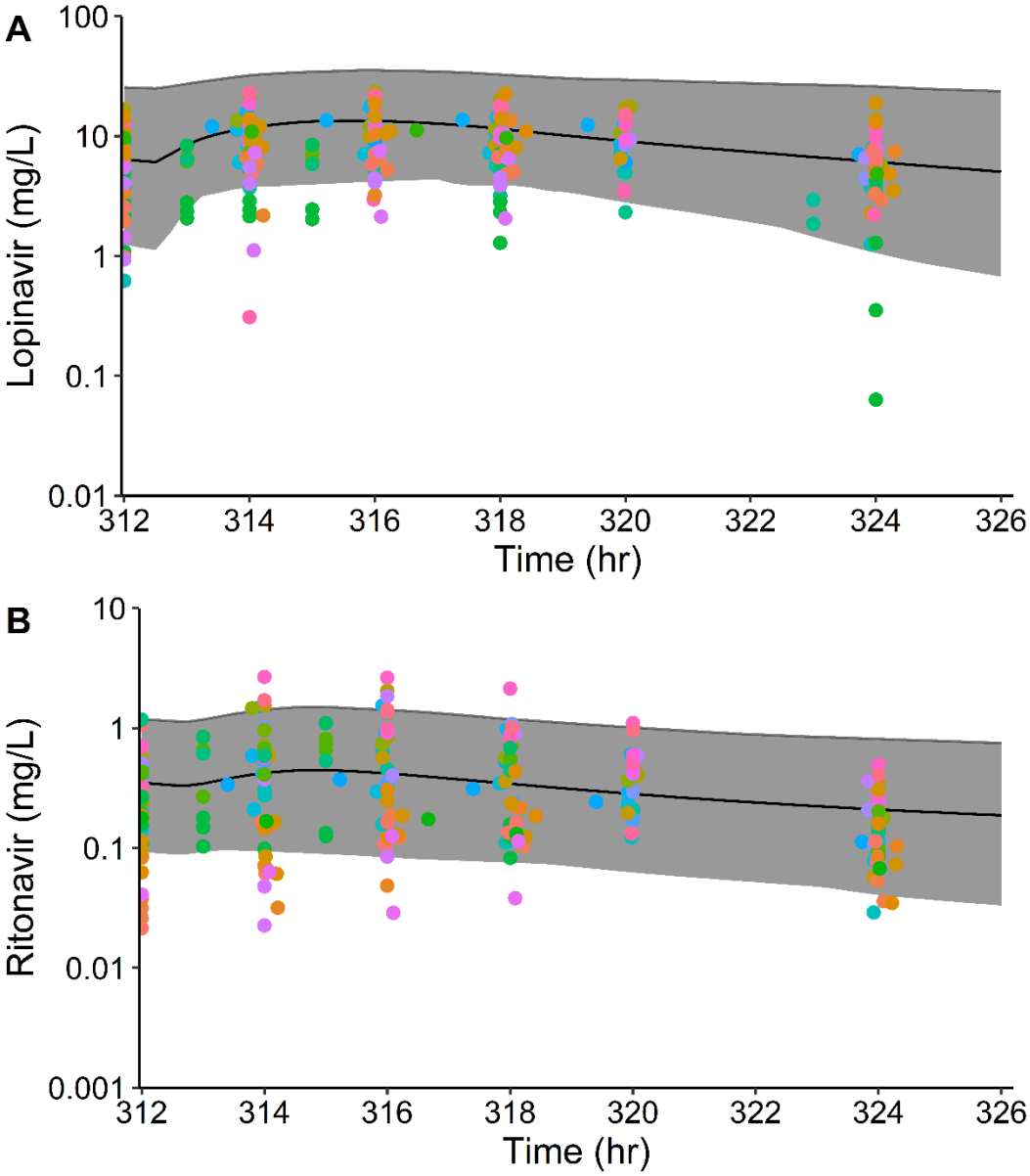

Population simulations for lopinavir (A) and ritonavir (B) based on 100 virtual white American children (50% female) from 6 to <12 years of age receiving the tablet formation of lopinavir/ritonavir (200/50 mg) orally twice daily. The 90% prediction interval is shown as a solid grey region and the geometric mean is shown as a solid black line. Observed data

(normalized to a 200/50 mg dose of lopinavir/ritonavir) in HIV infected children from 6 to <12 years of age are presented as dots with color stratified by individual.[45] The average fold error, calculated with the simulated geometric mean using the equation $10^{(1/n)(\sum \log(\text{simulated}/\text{observed}))}$, was 1.46 for lopinavir and 1.32 for ritonavir. Abbreviations: HIV: human immunodeficiency virus.

Figure 3.6: Population simulations of lopinavir and ritonavir concentration vs. time profiles following oral administration (400/100 mg) twice daily in HIV-infected adolescents from 12 to <18 years of age for 2 weeks.

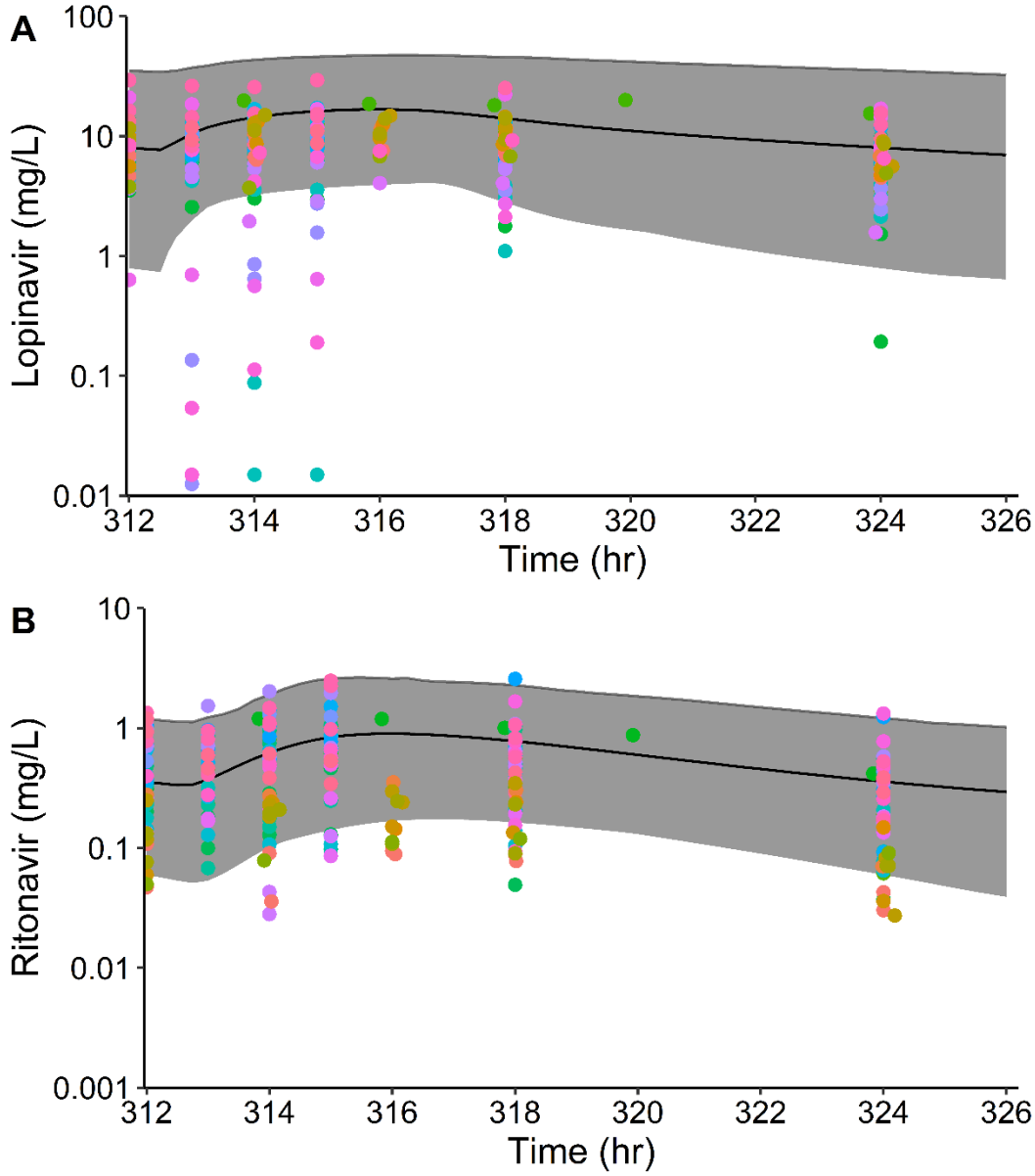

Population simulations for lopinavir (A) and ritonavir (B) based on 100 virtual white American adolescents (50% female) from 12 to <18 years of age receiving the tablet formation of lopinavir/ritonavir (400/100 mg) orally twice daily. The 90% prediction interval is shown in solid grey and the geometric mean is shown as a solid black line. Observed data for lopinavir and

ritonavir in HIV infected adolescents from 12 to <18 years of age are presented as dots with color stratified by individual.[45] The average fold error, calculated using the equation $10^{(1/n)(\sum \log(\text{simulated/observed}))}$, was 1.94 for lopinavir and 1.62 for ritonavir. Abbreviations: HIV: human immunodeficiency virus.

Figure 3.7: Population simulations of the rifampicin concentration vs. time profiles for 10 mg/kg oral daily for 2 weeks in pediatric patients from 2 months to 12 years of age.

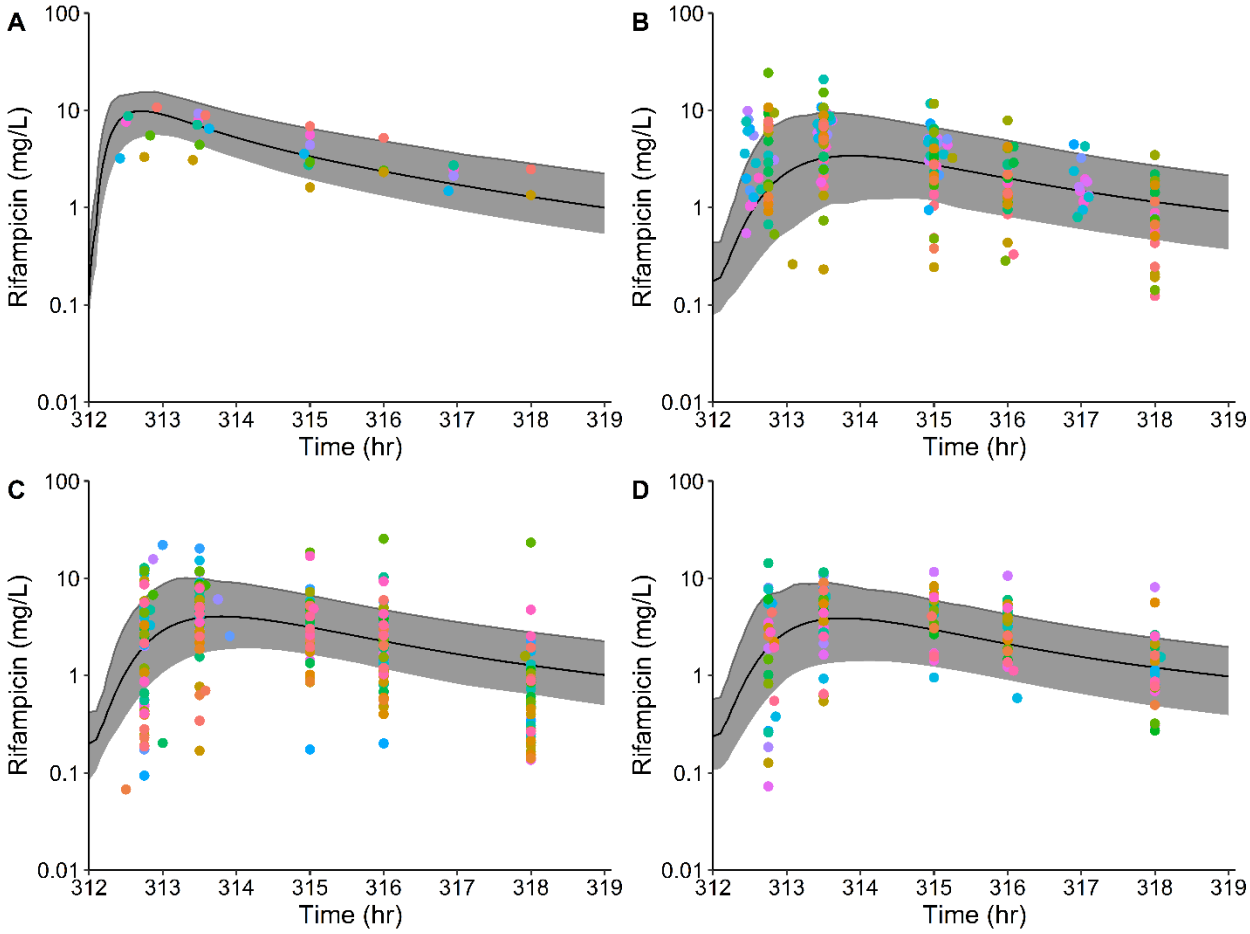

Population simulations for rifampicin in Black American virtual subjects (50% female) from 2 to < 6 months (A), 0.5 to <2 years of age (B), 2 to <6 years of age (C), and 6 to 12 years of age (D). The 90% prediction interval is shown as a solid grey region and the geometric mean is shown as a solid black line. Observed data for rifampicin was collected in children after ≥ two weeks of initiating treatment with rifampicin as part of the dispersible fixed dose combination with pyrazinamide and isoniazid.[49] Plasma concentration data for rifampicin were normalized to 10 mg/kg, and concentration data is presented as a color for each individual. The average fold error, calculated with the geometric mean using the equation $10^{(1/n)(\Sigma \log(\text{simulated/observed}))}$, was

1.02, 0.82, 1.25, and 0.96 for 2 to < 6 months, 0.5 to <2 years of age, 2 to <6 years of age, and 6 to 12 years of age, respectively.

Figure 3.8: Simulated lopinavir and ritonavir area under the concentration vs. time curve (AUC) from 0 to 12 hours at steady-state in the presence and absence of rifampicin in virtual adults, infants, and children.

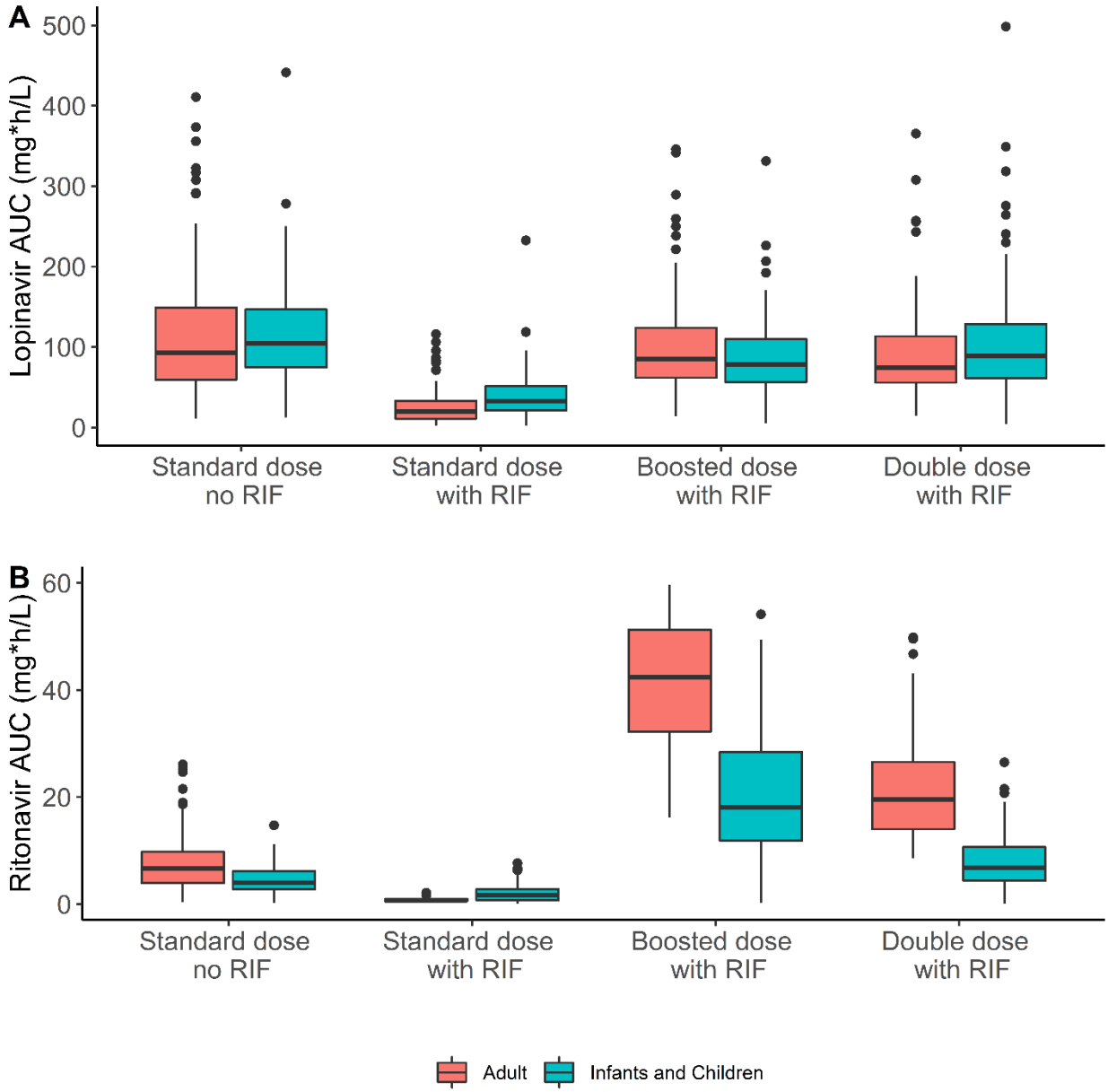

Population simulations were performed in 100 virtual infants and children (0.5 to 4.5 years of age) and 100 virtual adults (22 to 70 years of age) for lopinavir/ritonavir (LPV/RTV) with and without rifampicin. (A) Boxplots for lopinavir area under the concentration vs. time curve (AUC) from 0 to 12 hours at steady state. (B) Boxplots for ritonavir AUC at steady state from 0 to 12 hours. Data were stratified by adults (orange) and children (blue). The simulated dosing

regimens in adults were: 400/100 mg LPV/RTV orally (PO) BID (standard dose with no rifampicin (RIF)); 400/100 mg LPV/RTV PO BID with 600 mg PO daily rifampicin (standard dose with RIF); 400/400 mg LPV/RTV PO BID with 600 mg PO daily rifampicin (boosted dose with RIF); and 800/200 mg LPV/RTV PO BID with 600 mg PO daily rifampicin (double dose with RIF). The simulated dosing regimens in children were: 230/57.5 mg/m^2 LPV/RTV PO BID (standard dose no RIF); 230/57.5 mg/m^2 LPV/RTV PO BID with 10 mg/kg PO daily rifampicin (standard dose with RIF); 230/230 mg/m^2 LPV/RTV PO BID with 10 mg/kg PO daily rifampicin (boosted dose with RIF); 460/115 mg/m^2 mg LPV/RTV PO BID with 10 mg/kg PO daily rifampicin (double dose with RIF). The boxplots display the median (inter-quartile range), the upper whisker is the 75^{th} percentile to 1.5 times the inter-quartile range, the lower whisker is the 25^{th} percentile minus 1.5 times the inter-quartile range, and observations outside the whiskers are represented as black dots.

REFERENCES

1. World Health Organization. World Health Organization Global Tuberculosis Report (2018). <http://apps.who.int/medicinedocs/en/m/abstract/Js23360en/> Accessed July 11, 2020.

2. Panel on Antiretroviral Therapy and Medical Management of HIV-Infec. Guidelines for the use of antiretroviral agents in pediatric HIV infection (2020). <https://aidsinfo.nih.gov/guidelines> Accessed July 11, 2020.

3. U.S. Food and Drug Administration, Center for Drug Evaluation and Research. Lopinavir/ritonavir (Kaletra) Clinical pharmacology and biopharmaceutics review. (2000). <https://www.accessdata.fda.gov/drugsatfda_docs/nda/2000/21-226_Kaletra_biopharmr_P1.pdf.> Accessed July 11, 2020.

4. Kumar, G.N., *et al.* Metabolism and disposition of the HIV-1 protease inhibitor lopinavir (ABT-378) given in combination with ritonavir in rats, dogs, and humans. *Pharm. Res.* **21**, 1622–1630 (2004).

5. AbbVie Inc. Kaletra (lopinavir and ritonavir) prescribing information (2019). <https://www.rxabbvie.com/pdf/kaletratabpi.pdf> Accessed July 11, 2020.

6. Koudriakova, T. *et al.* Metabolism of the human immunodeficiency virus protease inhibitors indinavir and ritonavir by human intestinal microsomes and expressed cytochrome P4503A4/3A5: Mechanism-based inactivation of cytochrome P4503A by ritonavir. *Drug Metab. Dispos.* **26**, 552–561 (1998).

7. Denissen, J. F. *et al.* Metabolism and disposition of the HIV-1 protease inhibitor ritonavir (ABT-538) in rats, dogs, and humans. *Drug Metab. Dispos.* **25**, 489–501 (1997).

8. Sham, H. L. *et al.* ABT-378, a highly potent inhibitor of the human immunodeficiency virus protease. *Antimicrob. Agents Chemother.* **42**, 3218–24 (1998).

9. Woodahl, E. L., Yang, Z., Bui, T., Shen, D. D. & Ho, R. J. Y. MDR1 G1199A polymorphism alters permeability of HIV protease inhibitors across P-glycoprotein-expressing epithelial cells. *AIDS* **19**, 1617–25 (2005).

10. Vishnuvardhan, D., Moltke, L. L., Richert, C. & Greenblatt, D. J. Lopinavir: acute exposure inhibits P-glycoprotein; extended exposure induces P-glycoprotein. *AIDS* **17**, 1092–4 (2003).

11. Drewe, J. *et al.* HIV protease inhibitor ritonavir: a more potent inhibitor of P-glycoprotein than the cyclosporine analog SDZ PSC 833. *Biochem. Pharmacol.* **57**, 1147–52 (1999).

12. Perloff, M. D., Moltke, L. L. Von & Greenblatt, D. J. Ritonavir and dexamethasone induce expression of CYP3A and P-glycoprotein in rats. *Xenobiotica* **34**, 133–150 (2004).

13. Ernest, C. S., Hall, S. D. & Jones, D. R. Mechanism-based inactivation of CYP3A by HIV protease inhibitors. *J. Pharmacol. Exp. Ther.* **312**, 583–91 (2005).

14. Granfors, M. T. *et al.* Differential inhibition of cytochrome P450 3A4, 3A5 and 3A7 by five human immunodeficiency Virus (HIV) protease inhibitors in vitro. *Basic Clin. Pharmacol. Toxicol.* **98**, 79–85 (2006).

15. Templeton, I. E., Houston, J. B. & Galetin, A. Predictive utility of in-vitro rifampin induction data generated in fresh and cryopreserved human hepatocytes, Fa2N-4, and HepaRG Cells. *Drug Metab. Dispos.* **39**, 1921–1929 (2011).

16. Greiner, B. *et al.* The role of intestinal P-glycoprotein in the interaction of digoxin and rifampin. *J. Clin. Invest.* **104**, 147–153 (1999).

17. Reitman, M. L. *et al.* Rifampin's acute inhibitory and chronic inductive drug interactions: experimental and model-based approaches to drug–drug interaction trial design. *Clin. Pharmacol. Ther.* **89**, 234–242 (2011).

18. Kajosaari, L. I., Laitila, J., Neuvonen, P. J. & Backman, J. T. Metabolism of repaglinide by CYP2C8 and CYP3A4 in vitro: effect of fibrates and rifampicin. *Basic Clin. Pharmacol. Toxicol.* **97**, 249–56 (2005).

19. Decloedt, E. H. *et al.* Pharmacokinetics of lopinavir in HIV-Infected adults receiving rifampin with adjusted doses of lopinavir-ritonavir tablets. *Antimicrob. Agents Chemother.* **55**, 3195–3200 (2011).

20. Zhang, C. *et al.* Model-based evaluation of the pharmacokinetic differences between adults and children for lopinavir and ritonavir in combination with rifampicin. *Br. J. Clin. Pharmacol.* **76**, 741–51 (2013).

21. Porte, C. J. L. la *et al.* Pharmacokinetics of adjusted-dose lopinavir-ritonavir combined with rifampin in healthy volunteers. *Antimicrob. Agents Chemother.* **48**, 1553–1560 (2004).

22. McIlleron, H. *et al.* Lopinavir exposure is insufficient in children given double doses of lopinavir/ritonavir during rifampicin-based treatment for tuberculosis. *Antivir. Ther.* **16**, 417–421 (2011).

23. Ren, Y. *et al.* Effect of rifampicin on lopinavir pharmacokinetics in HIV-infected children with tuberculosis. *J. Acquir. Immune Defic. Syndr.* **47**, 566–569 (2008).

24. World Health Organization Fixed-dose combinations for the treatment of TB in children. (2018). <https://www.who.int/tb/FDC_Factsheet.pdf?ua=1> Accessed July 11, 2020.

25. Mathias, A. A., West, S., Hui, J. & Kearney, B. P. Dose-response of ritonavir on hepatic CYP3A activity and elvitegravir oral exposure. *Clin. Pharmacol. Ther.* **85**, 64–70 (2009).

26. Hsu, A. *et al.* Multiple-dose pharmacokinetics of ritonavir in human immunodeficiency virus-infected subjects. *Antimicrob. Agents Chemother.* **41**, 898–905 (1997).

27. Rodgers, T., Leahy, D. & Rowland, M. Physiologically based pharmacokinetic modeling 1: Predicting the tissue distribution of moderate-to-strong bases. *J. Pharm. Sci.* **94**, 1259–1276 (2005).

28. Open Systems Pharmacology. Open Systems Pharmacology Suite Manual, Version 7.4 (2018). <https://docs.open-systems-pharmacology.org/shared-tools-and-example-workflows/sensitivity-analysis> Accessed July 11, 2020.

29. Salerno, S. N. *et al.* Physiologically-based pharmacokinetic modeling characterizes the CYP3A-mediated drug-drug interaction between fluconazole and sildenafil in infants. *Clin. Pharmacol. Ther.* (2020). Online ahead of print.

30. Greenblatt, D. J. *et al.* Inhibition of oral midazolam clearance by boosting doses of ritonavir, and by 4,4-dimethyl-benziso-(2H)-selenazine (ALT-2074), an experimental catalytic mimic of glutathione oxidase. *Br. J. Clin. Pharmacol.* **68**, 920–927 (2009).

31. Muirhead, G. J., Wulff, M. B., Fielding, A., Kleinermans, D. & Buss, N. Pharmacokinetic interactions between sildenafil and saquinavir / ritonavir. *Clin. Pharmacol.* **50**, 99–107 (2000).

32. Hanke, N. *et al.* PBPK Models for CYP3A4 and P-gp DDI prediction: A modeling network of rifampicin, itraconazole, clarithromycin, midazolam, alfentanil, and digoxin. *CPT Pharmacometrics Syst. Pharmacol.* **7**, 647–659 (2018).

33. Penzak, S. R. *et al.* Ritonavir decreases the nonrenal clearance of digoxin in healthy volunteers with known MDR1 genotypes. *Ther. Drug Monit.* **26**, 322–330 (2004).

34. Jackson, A. *et al.* Pharmacokinetics of plasma lopinavir/ritonavir following the administration of 400/100 mg, 200/150 mg and 200/50 mg twice daily in HIV-negative volunteers. *J. Antimicrob. Chemother.* **66**, 635–40 (2011).

35. Ibarra, M. *et al.* Impact of food administration on lopinavir–ritonavir bioequivalence studies. *Eur. J. Pharm. Sci.* **46**, 516–521 (2012).

36. Schöller-Gyüre, M. *et al.* Steady-state pharmacokinetics of etravirine and lopinavir/ritonavir melt extrusion formulation, alone and in combination, in Healthy HIV-negative volunteers. *J. Clin. Pharmacol.* **53**, 202–210 (2013).

37. Lim, M. L. *et al.* Coadministration of lopinavir/ritonavir and phenytoin results in two-way drug interaction through cytochrome P-450 induction. *J. Acquir. Immune Defic. Syndr.* **36**, 1034–1040 (2004).

38. Dumond, J. B. *et al.* Significant decreases in both total and unbound lopinavir and amprenavir exposures during coadministration: ACTG protocol A5143/A5147s results. *J. Acquir. Immune Defic. Syndr.* **70**, 510–514 (2015).

39. Kashuba, A. D. M. *et al.* Combining fosamprenavir with lopinavir/ritonavir substantially reduces amprenavir and lopinavir exposure: ACTG protocol A5143 results. *Aids* **19**, 145–152 (2005).

40. Smythe, W. *et al.* A semimechanistic pharmacokinetic-enzyme turnover model for rifampin autoinduction in adult tuberculosis patients. *Antimicrob. Agents Chemother.* **56**, 2091–8 (2012).

41. Nitti, V., Virgilio, R., Patricolo, M. R. & Iuliano, A. Pharmacokinetic study of intravenous rifampicin. *Chemotherapy* **23**, 1–6 (1977).

42. Tirona, R. G., Leake, B. F., Wolkoff, A. W. & Kim, R. B. Human Organic Anion Transporting Polypeptide-C (SLC21A6) Is a Major Determinant of Rifampin-Mediated Pregnane X Receptor Activation. *J. Pharmacol. Exp. Ther.* **304**, 223–228 (2003).

43. Williamson, B., Dooley, K. E., Zhang, Y., Back, D. J. & Owen, A. Induction of influx and efflux transporters and cytochrome P450 3A4 in primary human hepatocytes by rifampin, rifabutin, and rifapentine. *Antimicrob. Agents Chemother.* **57**, 6366–6369 (2013).

44. Dixit, V. *et al.* Cytochrome P450 enzymes and transporters induced by anti-human immunodeficiency virus protease inhibitors in human hepatocytes: Implications for predicting clinical drug interactions. *Drug Metab. Dispos.* **35**, 1853–1859 (2007).

45. Yang, J. *et al.* Population pharmacokinetics of lopinavir/ritonavir: Changes across formulations and human development from infancy through adulthood. *J. Clin. Pharmacol.* **58**, 1604–1617 (2018).

46. PK-Sim. PK-Sim ® Ontogeny Database. **Version 7.**, 1–47 (2017).

47. Prasad, B. *et al.* Ontogeny of hepatic drug transporters as quantified by LC-MS/MS proteomics. *Clin. Pharmacol. Ther.* **100**, 362–370 (2016).

48. Mayer, H. *et al.* A novel approach to estimate ontogenies for PBPK applications – From literature data to simulations. *PAGE. Abstr. Annu. Meet. Popul. Approach Gr. Eur.* 27 (2018). <https://www.page-meeting.org/default.asp?abstract=8583> Accessed July 11, 2020.

49. Zvada, S. P. *et al.* Population pharmacokinetics of rifampicin, pyrazinamide and isoniazid in children with tuberculosis: In silico evaluation of currently recommended doses. *J. Antimicrob. Chemother.* **69**, 1339–1349 (2014).

50. Thee, S. *et al.* Pharmacokinetics of isoniazid, rifampin,and pyrazinamide in children younger than two years of age with tuberculosis: Evidence for implementation of revised World Health Organization recommendations. *Antimicrob. Agents Chemother.* **55**, 5560–5567 (2011).

51. Schaaf, H. S. *et al.* Rifampin pharmacokinetics in children, with and without human immunodeficiency virus infection, hospitalized for the management of severe forms of tuberculosis. *BMC Med.* **7**, (2009).

52. Hines, R. N., Simpson, P. M. & McCarver, D. G. Age-dependent human hepatic carboxylesterase 1 (CES1) and Carboxylesterase 2 (CES2) Postnatal Ontogeny. *Drug Metab. Dispos.* **44**, 959–966 (2016).

53. Groen, B. D. van *et al.* Proteomics of human liver membrane transporters: a focus on fetuses and newborn infants. *Eur. J. Pharm. Sci.* **124**, 217–227 (2018).

54. Kwara, A. *et al.* Pharmacokinetics of first-line antituberculosis drugs using WHO revised dosage in children with tuberculosis with and without HIV coinfection. *J. Pediatric Infect. Dis. Soc.* **5**, 356–365 (2016).

55. Koup, J. R., Williams-Warren, J., Viswanathan, C. T., Weber, A. & Smith, A. L. Pharmacokinetics of rifampin in children II. Oral bioavailability. *Ther. Drug Monit.* **8**, 17–22 (1986).

56. Zhang, C. *et al.* Population pharmacokinetics of lopinavir and ritonavir in combination with rifampicin-based antitubercular treatment in HIV-infected children. *Antivir. Ther.* **17**, 25–33 (2012).

57. Frigati, L., Bekker, A., Stroebele, S., Goussard, P. & Schaaf, H. S. Culture-confirmed Tuberculosis in South African Infants Younger Than 3 Months of Age. *Pediatr. Infect. Dis. J.* **38**, 351–354 (2019).

58. Klein, C. E. *et al.* The tablet formulation of lopinavir/ritonavir provides similar bioavailability to the soft-gelatin capsule formulation with less pharmacokinetic variability and diminished food effect. *J. Acquir. Immune Defic. Syndr.* **44**, 401–410 (2007).

59. Umehara, K., Huth, F., Won, C. S., Heimbach, T. & He, H. Verification of a physiologically based pharmacokinetic model of ritonavir to estimate drug-drug interaction potential of CYP3A4 substrates. *Biopharm. Drug Dispos.* **39**, 152–163 (2018).

60. Kirby, B. J. *et al.* Complex Drug Interactions of HIV Protease Inhibitors 1: Inactivation, Induction, and Inhibition of Cytochrome P450 3A by Ritonavir or Nelfinavir. *Drug Metab. Dispos.* **39**, 1070–1078 (2011).

61. Kharasch, E. D., Bedynek, P. S., Walker, A., Whittington, D. & Hoffer, C. Mechanism of ritonavir changes in methadone pharmacokinetics and pharmacodynamics: II. Ritonavir effects on CYP3A and P-glycoprotein activities. *Clin. Pharmacol. Ther.* **84**, 506–512 (2008).

62. Rabie, H. *et al.* Antiretroviral treatment in HIV-infected children who require a rifamycin-containing regimen for tuberculosis. *Expert Opin. Pharmacother.* **18**, 589–598 (2017).

63. World Health Organization. Antiretroviral therapy for HIV infection in infants and children: Towards universal access: Recommendations for a Public Health Approach: 2010 Revision. Annex E: Prescribing information and weight-based dosing of available ARV formulations for infants and. (2010). <https://www.who.int/hiv/pub/paediatric/paediatric_arv_dosing.pdf> Accessed July 11, 2020.

64. Sanofi-Aventis. RIFADIN® (rifampin capsules USP) and RIFADIN® IV (rifampin for injection USP) Prescribing Information. 1–15 (2010). <https://www.accessdata.fda.gov/drugsatfda_docs/.../050420s073,050627s012lbl.pdf%0A%0A> Accessed July 11, 2020.

65. Chouchane, N., Barre, J., Toumi, A., Tillement, J. P. & Benakis, A. Bioequivalence study of two pharmaceutical forms of rifampicin capsules in man. *Eur. J. Drug Metab. Pharmacokinet.* **20**, 315–320 (1995).

66. Acocella, G. *et al.* Kinetics of rifampicin and isoniazid administered alone and in combination to normal subjects and patients with liver disease. *Gut* **13**, 47–53 (1972).

67. U.S. Food and Drug Administration. Rifampin Review Package - FDA 064150. <https://www.accessdata.fda.gov/drugsatfda_docs/anda/97/064150review.pdf> Accessed July 11, 2020.

68. Peloquin, C. A. *et al.* Population pharmacokinetic modeling of isoniazid, rifampin, and pyrazinamide. *Antimicrob. Agents Chemother.* **41**, 2670–2679 (1997).

69. Baneyx, G., Parrott, N., Meille, C., Iliadis, A. & Lavé, T. Physiologically based pharmacokinetic modeling of CYP3A4 induction by rifampicin in human: Influence of time between substrate and inducer administration. *Eur. J. Pharm. Sci.* **56**, 1–15 (2014).

70. DrugBank. DrugBank *version 5.1.2* (2020). <https://www.drugbank.ca> Accessed July 11, 2020.

71. Nakajima, A. *et al.* Human arylacetamide deacetylase is responsible for deacetylation of rifamycins: Rifampicin, rifabutin, and rifapentine. *Biochem. Pharmacol.* **82**, 1747–1756 (2011).

72. Tirona, R. G., Leake, B. F., Wolkoff, A. W. & Kim, R. B. Human organic anion transporting polypeptide-C (SLC21A6) is a major determinant of rifampin-mediated pregnane X receptor activation. *J. Pharmacol. Exp. Ther.* **304**, 223–228 (2003).

73. Fahmi, O. A. *et al.* A Combined model for predicting CYP3A4 clinical net drug-drug interaction based on CYP3A4 inhibition, inactivation, and induction determined in-vitro. *Drug Metab. Dispos.* **36**, (2008).

74. Thee, S. *et al.* Pharmacokinetics of isoniazid, rifampin,and pyrazinamide in children younger than two years of age with tuberculosis: Evidence for implementation of revised World Health Organization recommendations. *Antimicrob. Agents Chemother.* **55**, 5560–5567 (2011).

75. Bekker, A. *et al.* Pharmacokinetics of rifampin, isoniazid, pyrazinamide, and ethambutol in infants dosed according to revised whorecommended treatment guidelines. *Antimicrob. Agents Chemother.* **60**, 2171–2179 (2016).

CHAPTER 4 : LEVERAGING PHYSIOLOGICALLY BASED PHARMACOKINETIC MODELING AND EXPERIMENTAL DATA TO GUIDE DOSING MODIFICATION OF CYP3A MEDIATED DRUG-DRUG INTERACTIONS IN PEDIATRIC PATIENTS USING SOLITHROMYCIN AS A CASE STUDY[1]

4.1 Introduction

Per the U.S. Food and Drug Administration (FDA) guidance, drug developers must perform *in vitro* studies to evaluate drug-drug interaction (DDI) potential for an investigational drug product.[1] The FDA recommends routinely evaluating cytochrome P450 (CYP) 1A2, CYP2B6, CYP2C8, CYP2C9, CYP2C19, CYP2D6, and CYP3A4/5 towards metabolism of the investigational drug, as well as the potential for inhibition of these drug-metabolizing enzymes in both a reversible and time-dependent manner. Relevant *in vitro* results can be incorporated within static and dynamic models, such as physiologically-based pharmacokinetic (PBPK), to inform the need for and to guide the design of clinical DDI studies.[1] Clinical DDI studies are typically performed in healthy adults; however, such studies are not routinely performed in pediatric patients for ethical and practical reasons. It is often assumed that DDI potential is the same in pediatric patients as in healthy adults. However, DDI potential may differ in young children relative to adults due to developmental changes in drug metabolizing enzymes and transporters. PBPK modeling can account for these developmental changes and can predict DDI potential when pediatric DDI are unavailable. The objective of this study is to develop a

[1]Part of this work has been published as an original publication by Salerno SN, Edginton A, Cohen-Wolkowiez M, Hornik CP, Watt KM, Jamieson BD, and Gonzalez D. Development of an Adult Physiologically Based Pharmacokinetic Model of Solithromycin in Plasma and Epithelial Lining Fluid. *CPT Pharmacometrics Syst. Pharmacol.* 2017; 6: 814-822

framework for leveraging PBPK modeling to predict metabolic DDI potential in pediatric patients and guide dose adjustments during drug development using solithromycin as a case study.

Solithromycin is a novel fluoroketolide antibiotic that is both a substrate and time-dependent inhibitor of cytochrome P450 (CYP) 3A4 and thus inhibits its own metabolism. Metabolism experiments using pooled human liver microsomes, CYP450 selective inhibitors, and single cDNA expressed CYP450s demonstrated that CYP3A4 is the major CYP450 enzyme responsible for the metabolism of solithromycin (sponsor data on file). Using pooled human liver microsomes with midazolam as the CYP3A substrate, solithromycin was reported to be a potent CYP3A time-dependent inhibitor with an inactivation rate constant (K_{inact}) of 0.022 min^{-1} and a concentration of half-maximal inactivation (K_I) of 0.038 µg/mL.[2] However, recombinant studies with CYP3A4, CYP3A5, and CYP3A7 were not performed. Solithromycin is also a P-glycoprotein substrate with an efflux ratio above 10 in Caco-2 cells, which reduced to unity in the presence of inhibitors (10 µM PSC833 and 60 µM verapamil) (sponsor data on file). Solithromycin undergoes biliary and urinary excretion with 76.5% and 14.1% of the dose recovered in feces and urine, respectively.[3] We previously developed a PBPK model for solithromycin in adults but it did not include CYP3A7, which may be important for predicting DDI potential in infants. Therefore, we conducted metabolism and time-dependent inhibition parameters for CYP3A4, CYP3A5, and CYP3A7 and incorporated these parameters into an adult and pediatric PBPK model for solithromycin to characterize DDI potential across the pediatric age continuum.

Solithromycin [oral (PO) regimen: 800 mg on day 1 followed by 400 mg on days 2-5 and switching from 400 mg intravenous (IV) daily to the PO regimen] was non-inferior to

moxifloxacin for patients with moderately severe community acquired bacterial pneumonia (CABP).[4,5] However, solithromycin was not approved by the FDA due to concerns of hepatotoxicity since more patients receiving IV to PO solithromycin experienced transient asymptomatic transaminitis.[6] Phase 2 studies in healthy adult volunteers have been performed to assess the DDI potential of solithromycin as a CYP3A inhibitor with midazolam, as well as to assess the impact of the strong CYP3A inhibitor, ketoconazole, on the pharmacokinetics (PK) of solithromycin. In addition, a phase 1 study was conducted in adolescents with suspected or confirmed bacterial infection receiving PO capsules of solithromycin [12-mg/kg of body weight (800 mg maximum) on day 1 and 6 mg/kg (400 mg maximum) on days 2 to 5].[7] A follow-up phase 1, open-label, multicenter PK and safety study was conducted in children (0-17 years) with suspected or confirmed bacterial infection receiving IV and PO (capsules and suspension) solithromycin as add-on therapy.[8] Using solithromycin as a case study, we will present a guideline for conducting and integrating relevant experimental studies into adult and pediatric PBPK models to predict pediatric CYP3A mediated DDI potential during drug development.

4.2 Materials and Methods

4.2.1 High Performance Liquid Chromatography-Tandem Mass Spectrometry Analysis

High performance liquid chromatography with tandem mass spectrometry (HPLC/MS/MS) assay was developed for 6β-hydroxytestosterone and the internal standard, 4-androsten-19-1al 3,17-dione [Sigma-Aldrich (St. Louis, MO)]. The lower limit of quantification for the 6β-hydroxytestosterone assay was 1 µM. The coefficients of variation (CV) for the intraday and interday precision was 11% and 7%, respectively.[9] Solithromycin was provided at no cost by Melinta Therapeutics, Inc. A Thermo TSQ Quantum Ultra triple-quadrupole mass spectrometer and Waters (Milford, MA) Acquity Ultra Performance Liquid Chromatography

CSH C18 (1.7 µm, 3 mm x 100 mm) column was used for the solithromycin assay with roxithromycin [Sigma-Aldrich (St. Louis, MO)] as the internal standard. An isocratic mobile phase consisted of 2% of 10 mM ammonium bicarbonate and 98% methanol delivered at 350 µL/min for 5 minutes. Calibration standard concentrations (1, 3.3, 10, 33, 100, 333, 1000, and 3333 nM solithromycin plus 0.5 µM roxithromycin) prepared in the same buffer as the experimental samples were used for method validation. A positive mode electrospray ionization was used. Solithromycin and roxithromycin eluted at 2.1 and 3.6 minutes, respectively. The precursor to product ions monitored with corresponding collision energies were 845.3 to 115.8 (36 V), 158.0 (35 V), 656.3 (34 V), 670.3 (29 V), and 688.3 (25 V) for solithromycin and 837.5 to 116.1 (35 V), 158.1 (32 V), and 679.6 (19 V) for roxithromycin. The lower limit of quantification for the solithromycin assay was 1 nM. The mean (range) accuracy was -5% (-15% to 11%). The mean (range) intra-day and inter-day CV was 7% (1% to 14%) and 12% (6 to 18%), respectively.

4.2.2 Time-dependent Inhibition of CYP3A Using Recombinant Enzymes

Testosterone was purchased from Sigma-Aldrich (St. Louis, MO, USA). Human CYP3A4, CYP3A5, and CYP3A7 + reductase +b5, 0.5 M phosphate buffer, pH 7.4, and NADPH Regenerating System Solutions A and B were all purchased from Corning Life Sciences (Corning, NY, USA). Experiments were first performed to determine linear 6β-hydroxytestosterone formation.[9] Time-dependent inhibition experiments for determination of K_I and K_{inact} were performed in triplicate on two different days. CYP3A4 and CYP3A5 (200 pmol/mL) were pre-incubated with solithromycin (0, 0.3, 3, 9, 15, 30, and 300 µg/mL) at 37°C for 5 minutes in 100 mM potassium phosphate pH 7.4 (200 µL reaction volume). For CYP3A7, 400 pmol/mL of CYP3A7 was pre-incubated with solithromycin (0, 30, 90, 150, 300, and 900

μg/mL). The reactions were initiated by the addition of NADPH Regenerating System Solutions A and B at a dilution of 1:20 and 1:100, respectively. After 0, 2.5, 5, 10, 15, and 30 minutes for CYP3A4 and CYP3A5 and 0, 5, 15, 30, 45, and 60 minutes for CYP3A7, 10 μL aliquots were diluted 10 fold into 90 μL of fresh buffer containing 100 mM potassium phosphate pH 7.4 and NADPH regenerating system plus 250 μM testosterone. The secondary reactions were incubated at 37°C for 5 minutes for CYP3A4 and CYP3A5 and 30 minutes for CYP3A7, and then reactions were stopped by a 1:4 dilution into ice cold acetonitrile containing 0.5 μM 4-androsten-19-1al 3,17-dione. The samples were centrifuged at 3500 rpm for 10 minutes at 4 degrees, and the supernatant was removed, and 6β-hydroxy-testosterone was measured to estimate remaining enzymatic activity.

To determine the K_I and K_{inact}, first, the percent activity remaining was calculated according to Equation 1, where $A_{inactivator}$ is the enzymatic activity of the inactivator, $A_{vehicle}$ is the enzymatic activity of the vehicle control, $T_{0,\ NADPH}$ is the 0 min pre-incubation time, and $T_{min,\ NADPH}$ is the pre-incubation measured at different time intervals.[10]

Equation 1: $$\%\ \text{activity} = 100 \times \left[\left(\frac{A_{inactivator}}{A_{vehicle}}\right) \text{ at } T_{0,\ NADPH} - \left(\frac{A_{inactivator}}{A_{vehicle}}\right) \text{ at } T_{min,\ NADPH}\right]$$

The natural log of the percent activity remaining was plotted against pre-incubation time, and the negative slope, which is the pseudo first-order rate constant of inactivation (K_{obs}), was determined using linear regression within GraphPad® Prism version 8 (GraphPad Software, San Diego, CA). Finally, the K_{obs} was determined for solithromycin by performing nonlinear regression in GraphPad® Prism version 8 according to equation 2, where I is the inactivator concentration (solithromycin).

Equation 2: $$K_{obs} = \frac{K_{inact} \times [I]}{K_I + [I]}$$

4.2.3 Solithromycin CYP3A *in vitro* Metabolism Using Recombinant Enzymes

Pilot experiments were first performed to determine the linear range of disappearance of solithromycin. CYP3A4 and CYP3A5 (60 pmol/mL) were incubated with 1 µM solithromycin in 100 mM potassium phosphate pH 7.4 plus NADPH Regenerating System Solutions A and B at a dilution of 1:20 and 1:100, respectively, for 0, 2, 5, 10, 15, 30, and 60 minutes. CYP3A7 (100 pmol/mL) was incubated with 1 µM and 10 µM of solithromycin for 0, 5, 10, 15, 20, 30, and 60 minutes. CYP3A7 (100 pmol/mL) was also incubated with 250 µM testosterone for 0, 15, 30, and 60 minutes as a positive control. The reactions were stopped by a 1:5 dilution into ice-cold methanol containing 0.5 µM roxithromycin (or acetonitrile containing 0.5 µM 4-androsten-19-1al 3,17-dione), centrifuged at 3500 rpm for 10 minutes at 4 degrees, and solithromycin and 6β-OH-testosterone were measured in the supernatant by HPLC/MS/MS.

Metabolism experiments for determination of the maximal velocity (V_{max}) and the concentration at half the maximal velocity (K_M) were performed in triplicate on three different days. CYP3A4 and CYP3A5 (60 pmol/mL) were pre-incubated with solithromycin (0.005, 0.01, 0.05, 0.1, 0.25, 0.5, 1, 2, 3, 4, 5 µM for CYP3A4 and 0.01, 0.05, 0.1, 0.25, 0.5, 1, 2, 3, 4, 5, 10, 30 µM for CYP3A5) at 37°C for 5 minutes in 100 mM potassium phosphate pH 7.4 plus NADPH Regenerating System Solutions A and B at a dilution of 1:20 and 1:100, respectively (200 µL reaction volume). The third experiment for CYP3A5 was conducted at higher concentrations (30, 50, 100, 500 1000, 3700 µM) to further characterize the V_{max}. The reactions were initiated by the addition of 12 µL (12 pmol) Corning® Supersomes™. Samples were collected at 0 minutes and 2 minutes for CYP3A4 and 15 minutes for CYP3A5. Reactions were stopped by a 1:2 to 1:1000 dilution into ice-cold methanol in order to ensure concentrations were within the assay range from 1 to 3333 nM). The samples were centrifuged at 3500 rpm for 10

minutes at 4 degrees, and the supernatant was removed, and then evaporated to remove the methanol. Samples were re-suspended in 98% methanol and 2% of 10 mM ammonium bicarbonate containing 0.5 µM roxithromycin and analyzed by HPLC/MS/MS. Solithromycin metabolite formation was calculated by subtraction of concentrations at the final time from the initial time. Finally, the K_M and V_{max} were determined by non-linear regression in GraphPad Prism 8 using the Michaelis-Menten least squares fit using Equation 3 where [S] is solithromycin concentration.[11]

Equation 3: $$\text{Velocity} = \frac{V_{max} * [S]}{K_M + [S]}$$

4.2.4 Adult Solithromycin PBPK Model Development and Evaluation

A whole body adult PBPK model was developed and evaluated in PK-Sim® (ver 9.0; Open Systems Pharmacology Suite) using plasma concentration data from 100 healthy subjects and 22 patients with CABP (1,966 plasma samples) (Table 4.1).[2] For model development based on demographics of the clinical study in healthy adults we used a 44.7-year-old black American man with a weight of 85.6 kg and a height of 180.9 cm. The model included glomerular filtration, CYP3A4 and CYP3A5 metabolism, time-dependent inhibition, P-glycoprotein transport, and enterohepatic recycling. The relative organ concentrations of P-glycoprotein and CYP3A were taken from the built-in database query, thereby allowing one set of kinetic parameters to be used in all organs.[12] Based on sponsor data, solithromycin was 78% to 84% bound in human plasma, primarily to serum albumin, and the extent of protein binding was not concentration dependent. Therefore, protein binding was mediated through albumin with an unbound fraction of 0.22. Distribution was best characterized by the Berezhkovsky algorithm.[13,14] Lipophilicity and P-glycoprotein V_{max} were manually optimized using the IV data. Transcellular intestinal permeability and the Weibull PO distribution properties (dissolution time

of 90 minutes and dissolution shape of 1.50) were manually optimized using the PO data. All other parameters were obtained from the literature or were experimentally generated (Table 4.2).

Population simulations were performed with 100 virtual Black American subjects with demographics from study CE01-102 in healthy adults: 27% female with a mean (range) age of 32.9 (20-55) years and a weight of 74.5 (61.4-90.3) kg. Population variability for P-glycoprotein was introduced using a normal distribution with a 65% coefficient of variation.[15] The PBPK model was evaluated by comparing the maximal concentration (C_{max}), area under the concentration versus time curve extrapolated to infinity ($AUC_{0-\infty}$) or during a dosing interval (AUC_{τ}), and clearance (CL) between the observed data and the PBPK model simulations on day 1 and at steady state following multiple daily dosing. The relative accuracy was calculated as a ratio of mean predicted values over mean observed values with a ratio assessed for the standard deviation (SD).[16–18]

$$\text{Equation 4: Ratio for SD} = \sqrt{\left(\frac{\text{sd (observed)}}{\text{mean (observed)}}\right)^2 + \left(\frac{\text{sd (predicted)}}{\text{mean (predicted)}}\right)^2} \times \frac{\text{mean (predicted)}}{\text{mean (observed)}}$$

The average fold error (AFE) was also calculated for each dosing regimen using the simulated geometric mean according to Equation 5 where n is the sample size:

$$\text{Equation 5: AFE} = 10^{\left(\frac{1}{n}\right) * \sum \log\left(\frac{\text{predicted}}{\text{observed}}\right)}$$

The pre-defined acceptance criteria for all PK parameters and AFE values were considered to be within 2-fold (a 0.5 to 2-fold ratio).

4.2.5 Sensitivity Analysis

Sensitivity analysis was performed for a 45 year old male receiving 800 mg PO day 1 followed by 400 mg PO days 2-5. In PK-Sim®, the input parameter (Pi) is varied around the value in the simulation by a small change and a new simulation is performed keeping all other

input values constant. The change in the PK parameter estimate (ΔPKj) is calculated as the difference between the values in the new simulation and the original simulation. The sensitivity for the PK parameter to the input parameter is calculated as the ratio of the relative change of that PK parameter (ΔPKj/PKj) and the relative variation of the input parameter (ΔPi/Pi): (ΔPKj/ΔPi)*(Pi/PKj).[14] Parameters with sensitivity values < -0.5 or > 0.5 were reported for the steady-state half-life. A sensitivity value -0.5 or 0.5 indicates that a 5% increase of the parameter leads to a 5% decrease or increase of the PK parameter value, respectively.

4.2.6 Adult Ketoconazole and Midazolam PBPK Model Development and Evaluation

PK data for ketoconazole and midazolam model development and evaluation were digitized from the literature using Plot Digitizer Version 2.6.8 (Table 4.3). Ketoconazole undergoes oxidation by CYP3A into its major metabolite (M2) along with five other minor metabolites (M3, M6, M7, M8, and M13).[19] Since parameters were not available to describe CYP3A4 CL of ketoconazole, the K_M and V_{max} were initially obtained from a study describing voriconazole CYP3A4 CL.[20] Ketoconazole also undergoes glucuronide conjugation by UDP-glucuronosyltransferase 1A4 (UGT1A4).[21] Protein binding for ketoconazole is concentration dependent (93% at 50 µg/mL and 91% at 25 µg/mL based on equilibrium dialysis), which may contribute to the non-linear kinetics for ketoconazole.[22,23] Ketoconazole also binds to blood cells resulting in ~1% free drug in plasma.[22,24] Therefore, protein binding to albumin was manually optimized based on the administered dose, and CYP3A4 V_{max} and UGT1A4 V_{max} were optimized using parameter optimization (Table 4.2). The Poulin and Theil method was used to calculate partition coefficients and the charge dependent Schmitt normalized to PK-Sim® method was used to calculate cellular permeability.[14,25] Population simulations based on 100 virtual subjects (white American population from 18 to 46 years of age) receiving 100, 200, 400, and

800 mg PO ketoconazole were performed and were evaluated by visually comparing the simulated mean and associated 90% prediction interval with the observed data from the literature. The mean simulated and observed area under the curve to 8 hours (AUC_{0-8}) or area under the curve extrapolated to infinity ($AUC_{0-\infty}$), and the maximal concentration (C_{max}) were also compared, with a two-fold ratio (0.5 to 2) considered acceptable. CYP3A4 competitive inhibition was included based on the formation of 1'-hydroxymidazolam in human liver microsomes from four human donors.[26] CYP3A5 non-competitive inhibition was included based 1'-hydroxymidazolam formation in c-DNA expressed CYP3A5 microsomal preparations.[27] P-glycoprotein inhibition was included based on a PBPK model that estimated the *in-vivo* inhibition constant (K_I) for renal P-glycoprotein to describe the clinical DDI between ketoconazole and fesoterodine in healthy adult subjects.[28]

The adult PBPK model for midazolam included key drug properties described in Table 4.2. Protein binding is approximately 97% to human plasma albumin in adults as well as pediatric patients greater than 1 year of age. Studies in human liver microsomes indicate the midazolam is primarily metabolized by CYP3A4.[29,30] Lipophilicity and transcellular intestinal permeability were optimized using both the IV and PO data with the Monte Carlo algorithm. Partition coefficients were calculated using the Rodgers and Rowland method and cellular permeability was calculated using the PK-Sim® Standard method.[14,31] Population simulations based on 100 virtual subjects (white American population from 18 to 46 years of age) receiving a 2 mg IV infusion over 30 minutes and 15 mg PO midazolam were performed and visually compared with observed data. The simulated versus observed mean $AUC_{0-\infty}$ and C_{max} were also compared, with a two-fold range considered acceptable. To validate ketoconazole as a CYP3A inhibitor, we simulated the CYP3A mediated DDI between ketoconazole and midazolam in

adults and compared with observed data obtained in the literature from clinical studies (Table 4.4).

4.2.7 Solithromycin DDI Predictions in Healthy Adult Volunteers

The solithromycin and midazolam PBPK models were co-modeled based on the previously described drug properties, which included CYP3A4 and CYP3A5 time-dependent inhibition (Table 4.2). Healthy adults (21 to 54 years of age) received PO solithromycin (400 mg on days 3-7 in one period and 800 mg day 3 followed by 400 mg on days 4-7 in another period) in combination with PO midazolam 0.075 mg/kg given on days 1, 3, and 7 of each period (sponsor data on file). Simulations were also performed and compared with observed data in healthy adults receiving solithromycin in combination with ketoconazole incorporating CYP3A4 and CYP3A5 time-dependent inhibition by solithromycin, in addition to CYP3A4 and P-glycoprotein reversible inhibition by ketoconazole (Table 4.2). Healthy adults (23 to 54 years of age) received a single PO dose of solithromycin (400 mg on day 1), a 5-day washout period, 4 days of PO ketoconazole (400 mg alone on days 7-10), and then 400 mg PO solithromycin plus ketoconazole on day 11. We calculated the geometric mean ratio for C_{max} and $AUC_{0-\infty}$ along with the associated 90% confidence interval for the drug combinations (solithromycin plus ketoconazole or solithromycin plus midazolam) relative to solithromycin or midazolam alone.

4.2.8 Pediatric PBPK Model Development and Evaluation

A virtual 32-year-old white male was scaled to a virtual 7.56 year old child based on the mean pediatric solithromycin data using anthropomorphic and ontogeny functions. Ontogeny functions were included for all relevant enzymes involved in solithromycin, midazolam, and ketoconazole drug disposition. The PK-Sim® ontogeny functions for CYP3A4 and uridine diphosphate glucuronosyltransferase family 1 member A1 (UGT1A1) in the liver were based on

post-menstrual age (PMA) in weeks (Equations 6 and 7). CYP3A5 has an ontogeny factor of 1 across all ages due to the high variability of the data and the inability to fit an ontogeny function. P-glycoprotein expression was calculated as a function of age and then normalized to mean adult expression based upon data quantified using 69 human pediatric and 41 adult livers (Equation 8).[32] Protein binding to albumin was scaled according to the default ontogeny factor within PK-Sim® (Equation 9).

Equation 6: CYP3A4 ontogeny factor = $\frac{\text{PMA}^{3.331}}{73.019^{3.331}+\text{PMA}^{3.331}}$

Equation 7: UGT1A1 ontogeny factor = $\frac{\text{PMA}^{20.67}}{50.754^{20.67}+\text{PMA}^{20.67}}$

Equation 8: P-glycoprotein expression (fmol/µg) at age (years) = $0.15 + \frac{0.41 * Age^{0.78}}{2.94^{0.78} + Age^{0.78}}$

Equation 9: Albumin ontogeny factor = $\frac{\text{PMA}^{3.24}}{21.533^{3.24}+\text{PMA}^{3.24}}$

The solithromycin pediatric PBPK model was evaluated using a total of 684 plasma samples available from 96 pediatric patients ranging from 4 days to 17.9 years after excluding 96 samples below the lower limit of quantification. These data were derived from two phase 1 studies, the first of which was conducted in adolescents with suspected or confirmed bacterial infection receiving PO capsules of solithromycin [12-mg/kg of body weight (800 mg maximum) on day 1 and 6 mg/kg (400 mg maximum) on days 2 to 5].[7] A follow-up phase 1, open-label, multicenter PK and safety study was conducted in children (0-17 years) with suspected or confirmed bacterial infection receiving IV and PO (capsules and suspension) solithromycin as add-on therapy.[8] A virtual population of 100 pediatric subjects (4 days to 17.9 years of age) was used for model evaluation. Pediatric simulations were performed for these 100 virtual pediatric subjects receiving IV, PO suspension, and PO capsules of solithromycin, and the AFE was calculated for each dosing regimen stratified by age cohort (0 to <2, 2 to <6, 6 to <12, and 12 to

<18 years) using the simulated arithmetic mean. The solithromycin PO suspension was modeled as a solution (e.g. instantaneous dissolution), while the PO capsules were modeled using the Weibull function as fit using the adult data. Solithromycin plasma concentration data were normalized by dose and time relative to the last drug administration since dose because administration differed slightly for each individual. We also compared weight normalized CL values from the PBPK simulation to the individual empirical Bayesian post-hoc parameter estimates based on a published population PK (PopPK) model developed using plasma data from these same 96 children. The PopPK model was a 2-compartment model with linear elimination and first-order absorption with a PO absorption lag time. Significant covariates included weight and a sigmoidal maturation function for PMA on CL and weight on the volume of distribution (V). Modeling time-dependent inhibition did not improve the model fits in these pediatric patients.[8]

Individual level concentration-time PK data were not available for pediatric patients receiving ketoconazole, so simulated PK parameters were compared with observed PK parameters in children receiving PO ketoconazole from the literature. Population simulations were performed for 100 virtual subjects (5 months to 14 years) receiving 9 mg/kg PO ketoconazole daily for 2 weeks, and the C_{max} and the daily steady-state AUC steady-state ($AUC_{0-24,ss}$) was compared with data from 26 children with candidiasis who received an average (range) daily dosage of PO ketoconazole of 9 (6-13) mg/kg.[33,34] Population simulations were also performed for 100 virtual subjects from 2 to 12.5 years of age receiving a single 5 mg/kg suspension, and the C_{max} and $AUC_{0-\infty}$ was compared with 12 children with PO candidiasis and superficial dermatophytoses whom received 5 mg/kg ketoconazole suspension.[35] The

transcellular intestinal permeability for ketoconazole was decreased to $2*10^{-4}$ cm/min (fraction absorbed of 0.80) in order to capture the observed AUC and C_{max} in pediatric patients.

Population simulations for midazolam were performed for 100 virtual subjects with similar ages, doses, and formulations as described in the study population reported in the literature (Table 4.3). The midazolam pediatric PBPK model was evaluated by comparing the CL and V to values reported in pediatric patients from 2 days to 16.2 years receiving IV midazolam.[36–38] We also compared the $AUC_{0-\infty}$ and C_{max} to values reported in pediatric patients from 0.5 to <16 years receiving a single PO dose (0.25 mg/kg, 0.5 mg/kg, and 1.0 mg/kg) of midazolam.[37] Acceptance criteria was for the simulated CL, V, $AUC_{0-\infty}$ and C_{max} to be within 0.5 to 2-fold of the observed PK parameters.

4.2.9 Solithromycin Plus Midazolam Pediatric Simulations

Since the inhibitor concentration influences the magnitude of the DDI, we simulated IV doses (60 minute infusion) for solithromycin from ages from 1 month to 17 years of age that achieved similar $AUC_{0-24,ss}$ as the simulated healthy adult population receiving 400 mg IV daily (400 mg maximum). Since there were only two neonates who received solithromycin, we decided to focus on term infants > 1 month of age. Dosing simulations were performed for 500 virtual subjects in each age group (1 month to < 6 months, 6 months to < 2 years, 2 years to < 6 years, 6 years to < 12 years, 12 to 17 years of age, and 18 to 65 years of age. Midazolam dosing was based upon the recommended IV starting dose in the package insert for sedation, anxiolysis, and amnesia prior to procedure in pediatric patients > 6 months and healthy adults < 60 years of age, as well as the loading dose for sedation/anxiolysis/amnesia in critical care settings for non-neonatal infants between 1 and 6 months.[29,39] We simulated a single dose of midazolam administered alone (day 1) and on the last day of solithromycin daily dosing for 5 days (day 6).

The geometric mean ratio and associated 90% confidence interval for midazolam $AUC_{0-\infty}$ and C_{max} were calculated for midazolam plus solithromycin relative to midazolam alone.

4.2.10 Solithromycin Plus Ketoconazole Pediatric Simulations

Ketoconazole PO dosing in pediatric patients ≥ 2 years and adults was based upon recommendations in the package insert: 3.3 mg/kg once daily (200 mg maximum) and 200 mg PO once daily, respectively.[39,40] Given the lack of information in children < 2 years of age, we simulated ketoconazole dosing in this population that would result in similar $AUC_{0-24,ss}$ as the simulated children and adults receiving 3.3 mg/kg or 200 mg PO daily, respectively. Solithromycin IV dosing in pediatric patients (60 minute infusion) were used that achieved similar AUC_{24ss} as in observed and simulated healthy adults receiving 400 mg IV daily (400 mg maximum). We simulated solithromycin administered IV alone for 5 days and after 5 days of dosing in combination with PO ketoconazole. The geometric mean ratio and associated 90% confidence interval for solithromycin $AUC_{0-24,ss}$ and C_{max} at steady-state ($C_{max,ss}$) were calculated for solithromycin plus ketoconazole administered concurrently for 5 days relative to solithromycin administered alone for 5 days.

4.3 Results

4.3.1 Time-Dependent Inhibition of CYP3A Using Recombinant Enzymes

The time-dependent inhibition parameters (K_{inact} and K_I) for CYP3A4 and CYP3A5 are presented in Table 4.5 and in Figure 4.1 and Figure 4.2. CYP3A7 was not a significant time-dependent inhibitor at concentrations up to 150 µg/mL for pre-incubation times up to 60 minutes (Figure 4.3). Reversible inhibition of CYP3A7 was observed at solithromycin concentrations concentrations >300 µg/mL, but time-dependent inhibition was not observed (Figure 4.3).

Pre-incubation times beyond 60 minutes could not be explored because of the loss of recombinant enzyme activity associated with longer incubation times. Additionally, greater dilutions could not be implemented since the maximum quantity of CYP3A7 was added in the pre-incubation reaction and the remaining velocity was approaching the lower limit of detection for 6β-hydroxy-testosterone. Therefore, CYP3A7 time-dependent inhibition parameters could not be generated and was deemed clinically insignificant, for solithromycin.

4.3.2 Solithromycin CYP3A *in vitro* Metabolism Using Recombinant Enzymes

Pilot experiments demonstrated that CYP3A4 and CYP3A5 solithromycin metabolite formation, assessed by disappearance of solithromycin, was in the linear stage up to 10 and 60 minutes, respectively. Kinetic parameters could not be determined for CYP3A7, since no disappearance of solithromycin was detected up to 60 minutes for 1 µM and 10 µM solithromycin (Figure 4.4). Michaelis-Menten kinetic parameters for CYP3A4 and CYP3A5 are presented in Table 4.5, Figure 4.5 and Figure 4.6. For CYP3A5, the V_{max} could not adequately be assessed because of the high K_M and the influence of time-dependent inhibition at concentrations > 30 µM (Figure 4.6 and Table 4.5).

4.3.3 Adult PBPK Model Evaluation

The final model parameters for solithromycin, ketoconazole, and midazolam are shown in Table 4.2. The solithromycin PBPK model was evaluated using concentration-time data from 100 healthy subjects and 22 patients with CABP (1,966 plasma samples) from phase 1 and phase 2 studies (Figure 4.7 and Figure 4.8)[2]. The simulated PK parameters (C_{max} and AUC_{τ} were all within two-fold of the observed values except for the 200 mg PO day 1 C_{max} and the 600 mg PO day 7 AUC_{τ} (Table 4.6). Similarly, the day 1 and day 7 CL and CL divided by bioavailability (CL/F) were all within two-fold of observed values except for the 200 mg PO day 1 CL/F (Table

4.7). Furthermore, the AFE values were all within 2-fold of observed values for all dosing regimens administered (Table 4.8).

Ketoconazole population simulations were performed in virtual adults receiving single PO doses (100, 200, 400, and 800 mg) of ketoconazole and visually compared with digitized mean observed data in healthy adults (Figure 4.9). Ketoconazole population simulations were also performed in virtual adults receiving 200 mg PO daily and 400 mg PO daily multiple dosing administration and resulted in reasonable agreement with the digitized mean data observed in healthy adults (Figure 4.10). Furthermore, the simulated versus observed AUC_{0-8} and C_{max} in 10 adult patients with fungal disease receiving a single 100 mg dose of ketoconazole were 5.30 versus 5.73 µg*h/mL and 1.70 versus 1.60 µg/mL, respectively.[41] The simulated versus observed $AUC_{0-\infty}$ reported in healthy volunteers receiving a single dose of 200 mg and 400 mg ketoconazole were 23.84 versus 17.55 µg*h/mL and 47.8 versus 40.9 µg*h/mL, respectively.[42] The simulated versus observed C_{max} in healthy volunteers receiving a single dose of 200 mg ketoconazole was 5.04 versus 3.60 µg/mL and for a single 400 mg dose of ketoconazole was 10.1 versus 6.5 µg/mL, respectively.[42] Midazolam population simulations were performed for a single dose of 15 mg PO and a single 2 mg IV (30 minute infusion) and resulted in reasonable agreement with the digitized mean data observed in healthy adults (Figure 4.11). Furthermore, the simulated versus observed mean $AUC_{0-\infty}$ and C_{max} for 15 mg PO midazolam (one hour post meal) were 184 versus 184 ng*hr/mL and 41 versus 48 ng/mL, respectively, based on a study conducted in 18 healthy volunteers.[43] Additionally, the simulated versus observed mean $AUC_{0-\infty}$ and C_{max} for 2 mg IV midazolam were 69.61 versus 84.76 ng*hr/mL and 48.40 versus 45.68 ng/mL, respectively, based on a study in 27 healthy adult volunteers.[44]

4.3.4 Adult Solithromycin DDI Predictions in Healthy Volunteers

The geometric mean ratio (90% confidence interval) for C_{max} and $AUC_{0-\infty}$ for PO midazolam (0.075 mg/kg) plus PO solithromycin (400 mg daily for 5 days or 800 mg day 1 followed by 400 mg daily for 4 days) relative to PO midazolam alone were similar between the simulations and the observed data collected from phase 1 studies in healthy adult volunteers (Table 4.9). Furthermore, the geometric mean ratio (90% confidence interval) for C_{max} and $AUC_{0-\infty}$ following a single dose of 400 mg PO solithromycin with 5 days of PO ketoconazole dosing relative to a single dose of 400 mg PO solithromycin alone were comparable between the simulations and the observed data (Table 4.9). The mean simulated versus observed fold ratios for C_{max} and $AUC_{0-\infty}$ were all within 0.75 to 1.25-fold (Table 4.9).

4.3.5 Sensitivity Analysis

The most sensitive parameters for the steady-state half-life in an adult receiving the PO regimen of solithromycin were the liver volume, the relative expression of CYP3A4 in liver, lipophilicity, CYP3A4 time-dependent inhibition and metabolism parameters (K_M, V_{max}, K_{inact}, K_I), the CYP3A4 ontogeny factor, and the CYP3A4 half-life in the liver.

4.3.6 Pediatric PBPK Model Evaluation

The AFE comparing simulated and observed plasma concentrations in pediatric patients receiving IV solithromycin was 0.7 overall and was 0.6, 0.5, 1.3, and 0.7 for age groups 0 to <2 years, 2 to <6 years, 6 to <12 years, and 12 to <18 years, respectively Figure 4.12 and Table 4.8). The AFE for pediatric patients receiving the PO suspension of solithromycin was 0.8 overall and was 0.8, 0.9, and 0.8 for age groups 0 to < 2 years, 2 to <6 years, and 6 to <12 years, respectively. The AFE was 0.7 for pediatric patients from 6 to 17 years of age receiving the solithromycin PO capsule (Figure 4.13 and Table 4.8). The day 1 weight normalized CL from

the PBPK simulation were similar to the individual empirical Bayesian post-hoc parameter estimates from the published PopPK model for all ages except 2 to <6 year old children Table 4.10).[8]

After scaling the adult PO ketoconazole PBPK model to pediatric patients from 0.42 to 14 years of age, the AUC and C_{max} was over-predicted by two- to three-fold. For example, the simulated versus observed mean $AUC_{0\text{-}24,ss}$ and C_{max} for the 9 mg/kg PO daily ketoconazole dose in 5 month to 14 year olds was 69.1 versus 32.7 µg*h/mL and 14.6 versus 4.9 µg/mL, respectively. Likewise, the simulated versus observed $AUC_{0\text{-}\infty}$ and C_{max} for the 5 mg/kg PO single dose in 2 to 12 year olds was 38.7 versus 15.3 µg*h/mL and 7.9 versus 4.4 µg/mL, respectively. Reducing the transcellular intestinal permeability approximately 10-fold from the adult permeability value resulted in similar AUC and C_{max} values as reported in 26 children (0.42 to 14 years) with candidiasis [33,34] and 12 children with PO candidiasis and superficial dermatophytoses [35] (Table 4.11).

The adult IV and PO midazolam PBPK model was scaled to pediatric patients ranging from 2 days to 16 years of age. The mean CL and volume of distribution at steady-state (V_{ss}) for the pediatric midazolam PBPK model were within 0.67- to 1.27-fold to values reported in pediatric patients from 2 days to 16.2 years receiving IV midazolam except for the V_{ss} in children from 12 to <16 years (Table 4.12).[36–38] The $AUC_{0\text{-}\infty}$ and C_{max} were generally within 0.5 to 2-fold of values reported in pediatric patients from 0.5 to <16 years receiving a single PO dose of midazolam (Table 4.13).[37]

4.3.7 Solithromycin Plus Midazolam DDI Simulations

The simulated age and weight based solithromycin IV doses (60 minute infusion) resulted in comparable solithromycin exposure but higher variability when compared to the mean ±

standard deviation $AUC_{0\text{-}24,ss}$ value (13 ± 4.38 mg*h/L) reported in healthy adults receiving 400 mg IV daily for 7 days (Figure 4.14 and Table 4.6). The simulated solithromycin $AUC_{0\text{-}24,ss}$ was generally the same across age groups, albeit slightly higher in pediatric patients to adults overall and highest and most variable in infants from 1 to <6 months of age (Figure 4.14). The geometric mean $AUC_{0\text{-}\infty}$ ratio and associated 90% confidence interval for midazolam with solithromycin relative to midazolam alone were slightly higher in simulated pediatric patients relative to simulated adults and highest in infants from 1 to <6 months of age. Therefore, the proposed dose adjustment for midazolam when given in combination with solithromycin is approximately 6-fold lower in infants <6 months of age and 4 to 5-fold lower in ages ≥ 6 months (Table 4.14 and Figure 4.15).

4.3.8 Solithromycin Plus Ketoconazole DDI Simulations

The simulated median ketoconazole $AUC_{0\text{-}24,ss}$ was generally the same across age groups using the recommended dosing, but the mean was higher in simulated infants from 1 to <6 months of age due to higher variability (Figure 4.14). The geometric mean $AUC_{0\text{-}\infty}$ ratio and associated 90% confidence interval for solithromycin with ketoconazole relative to solithromycin alone was similar between virtual pediatric patients ≥ 6 months of age and adults but higher in infants from 1 to <6 months of age. Therefore, the proposed dose adjustment for solithromycin when given in combination with ketoconazole is approximately 2-fold lower in infants <6 months of age and approximately 1.4-fold lower in ages ≥ 6 months (Table 4.14 and Figure 4.15).

4.4 Discussion

Although phenotyping studies for CYP3A4 are routinely performed for new investigational drugs, the role of CYP3A7 is rarely investigated since CYP3A7 is minimally

expressed in adults.[1] However, CYP3A7 is the predominantly expressed CYP3A isoenzyme in fetal tissue and newborns, and CYP3A7 played a critical role in the CYP3A mediated DDI between sildenafil plus fluconazole in preterm and term neonates.[9] Therefore, the objective of this study was to leverage solithromycin as a case study to suggest a framework for investigating and incorporating CYP3A into adult and pediatric PBPK models to predict pediatric CYP3A mediated DDI potential during drug development. As demonstrated in this study, adult and pediatric PBPK models can be developed incorporating relevant CYP3A parameters, evaluated using adult and pediatric PK and adult DDI data, and then dosing can be simulated in pediatric patients receiving CYP3A drug combinations (Figure 4.16). This approach can be applied to guide DDI assessment throughout drug development for other CYP3A drug combinations that are likely to be administered to infants.

We evaluated CYP3A4, CYP3A5, and CYP3A7 metabolism and time-dependent inhibition, and incorporated these parameters into a previously published adult PBPK model for solithromycin.[2] Using recombinant enzymes, we reported a higher K_{inact} and K_I for CYP3A4 than studies identified using human liver microsomes (0.084 min^{-1} versus 0.022 min^{-1} and 1.49 µg/mL versus 0.038 µg/mL).[2] There may be altered activity and expression between recombinant enzymes and human liver microsomes. In addition, we investigated solithromycin concentrations ≤ 300 µg/mL and used the NADPH regenerating system and testosterone as the probe substrate, whereas, the sponsor investigated solithromycin ≤ 0.3 µg/mL and used NADPH and midazolam as the probe substrate (sponsor data on file). Solithromycin was not a substrate or time-dependent inhibitor for CYP3A7 at the concentrations (≤900 µg/mL) and times (60 minutes) investigated in this study. In contrast, CYP3A7 metabolizes other CYP3A substrates, such as

midazolam, tacrolimus, clarithromycin, and alprazolam.[45–49] Although substrate specificity can overlap for the CYP3A family, CYP3A7 generally has lower catalytic activity than CYP3A4.[47]

The final solithromycin PBPK model included CYP3A4 and CYP3A5 metabolism and time-dependent inhibition, glomerular filtration, and P-glycoprotein transport and enterohepatic recirculation. The AFE and simulated PK parameters were all within 2-fold of observed values in healthy subjects and CABP patients, except for the 200 mg PO day 1 C_{max} and the 600 mg PO daily day 7 AUC_{τ} (Table 4.6-Table 4.8). The model overpredicted exposures for the 200 mg and 600 mg dosing regimens particularly on day 1 (Figure 4.8). However, solithromycin regimens that demonstrated efficacy for CABP [800 mg on day 1 followed by 400 mg on days 2-5 PO and 400 mg IV daily] were well characterized.[4,5] In addition, simulated geometric mean ratios for midazolam with and without solithromycin and solithromycin with and without ketoconazole for C_{max} and $AUC_{0-\infty}$ were within 0.75 to 1.25-fold of values reported in healthy adults from phase II DDI studies (Table 4.9).

The adult solithromycin PBPK model was scaled to pediatric patients from 4 days to 17.9 years of age. The AFE values comparing the simulated and observed plasma concentrations were within 0.5- to 2.0-fold (Table 4.8). However, the model was underpredicting variability in the pediatric population, which is likely due to differences in the pediatric patients with bacterial infection receiving solithromycin as add-on therapy from the virtual pediatric population in PK-Sim® (Figure 4.12 and Figure 4.13). Additionally, the weight-normalized day 1 CL for the PBPK simulations were similar to the individual empirical Bayesian post-hoc parameter estimates from a published PopPK model developed using PK data from these 96 children (Table 4.10).[8] However, our steady-state CL and simulated age and weight based dosing for IV solithromycin were lower than the PopPK model recommendation of 8 mg/kg IV daily across all

pediatric ages (Table 4.14).[8] The final PopPK model included weight and a sigmoidal maturation function for PMA on CL, but time-dependent inhibition was not included because model fits were not improved.[8] Therefore, differences in steady-state CL and dosing between the PopPK and PBPK models can be explained by the influence of time-dependent inhibition along with different maturation functions incorporated for CYP3A4. For example, the maturation function for the PopPK model and PBPK model achieved 50% of the adult CYP3A4 activity at approximately 52.6 weeks and 73.0 weeks PMA, respectively.[8,50] The PBPK model also included an ontogeny function for P-glycoprotein with a mean ± standard deviation age at which 50% of adult expression is reached at 2.94 ± 1.33 years, which may explain why the PBPK model dosing recommendations were particularly lower in infants <6 months of age. [32]

In order to evaluate CYP3A mediated DDI potential for solithromycin, adult and pediatric PBPK models were developed for the CYP3A probe substrate, midazolam, as well as the strong CYP3A inhibitor, ketoconazole. After scaling the adult PO ketoconazole PBPK model to pediatric patients, the plasma concentrations were over-predicted. The hypothesis was that children with candidiasis had impaired absorption of ketoconazole. Oral absorption of ketoconazole is highly affected by the presence of food in the gastrointestinal tract and by gastric acidity, which may differ in sick pediatric patients relative to healthy adults.[22] For example, the intragastric pH is relatively elevated in neonates and a study in neonates reported that gastric pH above 2.5 and continuous PO feeding resulted in insufficient ketoconazole absorption in preterm infants during the first week of life.[51,52] There are also formulation considerations and pediatric patients (2 to 12.5 years of age) receiving ketoconazole suspension had mean plasma concentrations 1.6 to 4 times higher than children receiving crushed tablets in applesauce.[35] After reducing the transcellular intestinal permeability to reflect this hypothesized lower bioavailability

in children, simulated exposures were similar to observed data in children with candidiasis. Of note, the optimized transcellular intestinal permeability for ketoconazole is significantly greater than the predicted value ($2.39 * 10^{-6}$ cm/min) in PK-Sim® based on its physiochemical properties. The aqueous solubility of ketoconazole can be greater when formulated with the excipients in the tablet formulations, which might in part explain this discrepancy. In addition, as a base, the solubility and absorption of ketoconazole is likely enhanced in the acidic environment of the gastrointestinal tract. Ketoconazole has not been systematically studied in children under 2 years of age, so dosing was simulated to achieve similar AUC_{τ} relative to adults receiving 200 mg tablets PO daily as well as children ≥ 2 years of age receiving 3.3 mg/kg/day ketoconazole (Table 4.14 and Figure 4.14).

The differences in DDI potential simulated across age cohorts for midazolam plus solithromycin and solithromycin plus ketoconazole reflect minor differences in inhibitor concentrations (Table 4.14 and Figure 4.15). For example, due to the high variability in solithromycin and ketoconazole concentrations between 1 to <6 months of age, exposures were highest and resulted in the highest AUC ratios with and without inhibition in this age group. Therefore, as long as the inhibitor concentrations are appropriately matched to adult concentrations, CYP3A mediated DDI potential should be similar between pediatric subjects > 1 month of age and adults. However, the exposure-response relationship and drug concentrations can differ between pediatric and adult patients due to differences in disease progression and treatment response, such as for drugs involved in the treatment of gastroesophageal reflux disorder in infancy, neonatal bacterial conjunctivitis, type 2 diabetes, oncology products, major depression disorder, as well as attention-deficit hyperactivity disorder.[53] Additionally, DDI potential may differ in neonates for other CYP3A substrates metabolized by CYP3A7 since

CYP3A7 has greater expression in neonates and generally has lower catalytic activity than CYP3A4. The simulated adult AUC ratio following IV solithromycin plus IV midazolam was lower than the simulated adult AUC ratio following the phase II study dosing (PO solithromycin plus PO midazolam) because of the lack of intestinal involvement. In addition, the simulated adult AUC ratio following multiple PO dosing of solithromycin with ketoconazole was slightly lower than the simulated adult AUC ratio following the the phase II study dosing (a single dose of PO solithromycin after multiple PO ketoconazole dosing) presumably due to the time-dependent inactivation of CYP3A by solithromycin (Table 4.9 and Table 4.14).

In conclusion, we present a framework for investigating and incorporating CYP3A *in vitro* data into adult and pediatric PBPK models to predict pediatric CYP3A mediated DDI potential during drug development. However, there are some notable limitations that warrant further discussion. First, we were unable to determine the "true" V_{max} for CYP3A5 because of the high K_M and the influence of time-dependent inhibition at higher solithromycin concentrations. However, CYP3A5 played a minor role in the metabolism of solithromycin as indicated by the lack of sensitivity for CYP3A5 on the solithromycin steady-state half-life. Second, the lack of significant metabolism of solithromycin by CYP3A7 made it difficult to evaluate the role of CYP3A7 in CYP3A mediated DDI potential in neonates. Since we cannot predict in advance if a drug will be a CYP3A7 substrate, CYP3A7 metabolism should still be explored if the investigational drug is likely to be given to infants. Finally, the simulated solithromycin age and weight based dosing differed from the recommended dosing of 8 mg IV daily that was investigated for safety in pediatric studies, likely due to different ontogeny functions implemented and the lack of time-dependent inhibition included in the PopPK model.

Additionally, there are likely disease-state differences in the pediatric population that are not accounted for in the virtual pediatric population.

4.5 Tables

Table 4.1: Clinical data used for physiologically-based pharmacokinetic (PBPK) model development.

Study	**CE01-102 [57]**	**CE01-121 [**Sponsor data on file]	**CE01-110** [Sponsor data on file]	**CE01-114 [58]**	**CE01-200 [59]**
Trial phase	1	1	1	1	2
Number of Adult Subjects	25	30	14	31	65[2]
Regimen	200, 400, and 600 mg daily for 7 days	400 mg daily x 7 days; 800mg single-dose	800 mg on day 1, 400 mg daily x 4 days	400 mg daily x 5 days	800 mg on day 1, 400 mg daily x 4 days
Formulation[a]	PO	IV	PO	PO	PO
% Female	27%	23%	54%	19%	57%
Age (years)	32.9 (20-55)	44.6 (23-59)	34.2 (21-43)	33.6 (19-46)	56.0 (25-87)
Weight (kg)	74.5 (61.4-90.3)	82.75 (66-102)	76.2 (61.5-95.6)	82.2 (58.1-97)	N/A
Plasma Samples	676	801	356	31	102

[a]Formulation: capsule (PO) or Intravenous suspension (IV).[2] Pharmacokinetic (PK) data was available for 22 of these subjects. Data presented as the average (range).

Table 4.2: Final physiologically-based pharmacokinetic (PBPK) model parameters for solithromycin, ketoconazole, and midazolam.

Parameter	Solithromycin	Source	Ketoconazole	Source	Midazolam	Source
Molecular Weight (g/mol)	845.01	a	531.44	[24]	325.77	[24]
LogP	4.04	a	2.44	b	2.76	b
Compound type	Base	a	Base	[24]	Base	[24]
pKa	9.44	a	2.90, 6.50	[24]	6.57	[24]
Solubility (mg/mL)		a	$9.31 * 10^{-3}$	[24]	0.01	[24]
Fraction unbound	0.22	a	2% (100 mg) 1% (200, 400 mg) 0.75% (800 mg)	b [24] b	3%	[24]
UGT1A1 K_M (µM)	N/A	N/A	22.3	[21]	N/A	N/A
UGT1A1 V_{max} (mg/protein/min)	N/A	N/A	9366	b	N/A	N/A
CYP3A4 K_M (µM)	0.60	c	235	[20]	1.88	[30]
CYP3A4 V_{max} (pmol/min/pmol)	3.44	c	0.90	b	6.12	[30]
CYP3A5 K_M (µM)	57.8	c	N/A	N/A	N/A	N/A
CYP3A5 V_{max} (pmol/min/pmol)	23.4	c	N/A	N/A	N/A	N/A
CYP3A4 K_{inact} (1/min)	0.08	c	N/A	N/A	N/A	N/A
CYP3A4 K_I (µM)	1.76 (TDI)	c	0.0038 (Competitive)	[26]	N/A	N/A
CYP3A5 K_{inact} (1/min)	0.03	c	N/A	N/A	N/A	N/A
CYP3A5 K_I (µM)	3.08 (TDI)	c	0.109 (Non-Competitive)	[27]	N/A	N/A

P-glycoprotein K_M (µM)	45	[60]	N/A	N/A	N/A	N/A
P-glycoprotein V_{max} (µmol/L/min)	1.24	b	N/A	N/A	N/A	N/A
P-glycoprotein K_I (ng/mL)	N/A	N/A	2.27	[28]	N/A	N/A
Transcellular Intestinal permeability (cm/min)	$8 * 10^{-5}$	b	$3.14 * 10^{-3}$ (adult) $2 * 10^{-4}$ (pediatric)	b b	$1.25 * 10^{-5}$	b

[a]Sponsor data on file.

[b]Optimized Value.

[c]Exerimentally derived.

Abbreviations: Log P: logarithmic of drug permeability; P-gp: P-glycoprotein; pKa: negative logarithmic of the acid dissociation constant; N/A: not applicable; V_{max}: maximal rate of metabolism; K_M: Michaelis-Menten constant; K_I: inhibition constant; K_{inact}: maximal inactivation rate constant. K_{cat}: catalytic activity; TDI: time-dependent inhibition; UGT1A1: uridine diphosphate glucuronosyltransferase 1A1; CYP: cytochrome P450; CYP3A4: cytochrome P450 3A4; CYP3A5: cytochrome P450 3A5.

Table 4.3: Clinical data for ketoconazole and midazolam physiologically-based pharmacokinetic (PBPK) model development and evaluation.

N, Population[a]	Study Drug	Dose and Administration	Reference
23 healthy males 20 (18-25) years	Ketoconazole	200 mg PO tablet, suspension, and solution, fasted; 400 mg PO solution, 800 mg PO solution; single dose	23
6 healthy males 28-44 years	Ketoconazole	200 mg and 400 mg PO tablet, single, administered with standard breakfast	42
Healthy adults	Ketoconazole	100 mg, 200 mg, 400 mg tablet, 200 mg solution, single dose	22
8 Healthy males 25 (21-46) years	Ketoconazole	200 mg tablets PO twice daily for 5 days, fasted on day 1, breakfast allowed on day 5	61
10 healthy adults 24 (22-26) years	Ketoconazole	200 mg tablet, fasting, orange juice, standard breakfast, single dose	62
21 healthy adults 31.2 (20-45) years	Ketoconazole	200 mg PO tablets daily for 7 days, fasted	54
26 children with candidiasis (0.42-14 years)	Ketoconazole	daily doses ranged from 3-13 mg/kg (suspension or tablet) for 7 days to 18 months	33,34
12 children 6 (2-12.5) years	Ketoconazole	5 mg/kg crushed tablets or suspension, fasted, single dose	35
27 healthy adults 27.6 (18-51) years	Midazolam	2 mg IV over 30 minutes, single 6 mg PO, single dose	44
9 healthy adults 34.1 (25-55) years	Midazolam	2.5 mg IV bolus, single dose	63
5 males 22.4 ± 6.4 years[b]	Midazolam	5, 15 and 30 µg/kg IV bolus, single 15, 50 and 100 µg/kg PO, single dose	64
18 healthy adults 32 (19-46) years	Midazolam	15 mg PO, single dose	43
18 healthy males 27 (20-44) years[c]	Midazolam	7.5 mg PO, single dose	65
14 healthy adults 27.2 (19-46) years	Midazolam	2 mg PO syrup, single dose	66
18 healthy adults 31 (21-49) years[c]	Midazolam	0.075 mg/kg PO, single dose	67

9 healthy adults 26 (19-41) years	Midazolam	2 mg IV, single dose 6 mg PO, single dose	[56]
87 children from 6 months to < 16 years of age	Midazolam	0.25, 0.5, or 1 mg/kg (40 mg maximum) oral syrup and 0.15 mg/kg single IV bolus dose	[37]
10 critically ill neonates 2-10 post-natal days and 37 34-41 weeks gestational age	Midazolam	0.2 mg/kg single IV bolus dose	[36]
23 critically ill children 3.6 years (8 days-16.2 years)	Midazolam	49-385 µg/kg/hr IV continuous infusion for 0.3-10.9 hours	[38]

[a]Age presented as mean (range), mean ± standard deviation[b], or median (range)[c] as presented in the original publication. Abbreviations: N: number of subjects; IV: intravenous; PO: oral

Table 4.4: Adult drug-drug interaction (DDI) predictions for midazolam plus ketoconazole.

	Observed		Simulated		
Dosing Regimen	**$AUC_{0-\infty}$ Fold**	**C_{max} Fold**	**$AUC_{0-\infty}$ Fold**	**C_{max} Fold**	**Reference**
midazolam 7.5 mg PO ± 400 mg PO daily ketoconazole x 4 days[a]	15.9	4.1	7.8	3.8	[55]
2 mg IV midazolam bolus ± 200 mg ketoconazole x 3 days[b]	5.0	N/A	3.2	N/A	[56]
6 mg PO midazolam ± 200 mg ketoconazole x 3 days[b]	13.6	4.2	8.6	4.0	[56]
10 mg PO midazolam ± 200 mg PO ketoconazole daily x 12 days[c]	6.6	3.0	5.6	3.4	[68]
0.075 mg/kg midazolam ± 400 mg ketoconazole x 10 days[d]	9.5	2.4	9.1	4.0	[69]

[a]Nine healthy adult volunteers received oral ketoconazole (400 mg daily) or placebo for 4 days, and then a single dose of 7.5 mg oral midazolam was administered on day 4.[55]

[b]Nine healthy individuals received single doses of 2 mg intravenous or 6 mg oral midazolam alone and then single doses of 2 mg intravenous or 6 mg oral midazolam after 3 daily doses of 200 mg oral ketoconazole.[56]

[c]Forty healthy subjects received single 10 mg oral midazolam solutions before and after 12 daily doses of 200 mg ketoconazole.[68]

[d]Nineteen subjects received single oral doses of 0.075 mg/kg midazolam before and after 10 daily doses of 400 mg oral ketoconazole.[69]

Data are presented as the mean fold change for midazolam plus ketoconazole relative to midazolam alone based on simulations using a mean individual (32 year-old white American male, weight of 81 kg, height of 178 cm, body mass index of 25.48 kg/m^2).

Abbreviations: $AUC_{0-\infty}$: area under the curve from zero to infinity; C_{max}: maximal concentration; PO: oral; IV: intravenous.

Table 4.5: Time-dependent inhibition and Michaelis-Menten kinetic parameters.

Enzyme	K_{inact} (1/min)	K_I (µg/mL)	K_M (µM)	V_{max} (pmol/min/pmol CYP3A)
CYP3A4	0.084 (0.078, 0.092)	1.49 (0.96, 2.26)	0.60 (462, 781)	3.44 (3.21, 3.71)
CYP3A5	0.029 (0.026, 0.032)	2.61 (1.52, 4.15)	57.8 (41.8, 87.8)	23.4 (18.7, 32.0)

Data are presented as the mean (95% confidence interval) fitted using GraphPad Prism version 8.0 based on triplicates from two different dates for time-dependent inhibition parameters and from three different dates for Michaelis-Mentin parameters. Abbreviations: K_{inact}: inactivation rate constant; K_I: concentration of half-maximal inactivation; V_{max}: maximal velocity; K_M: concentration at half-maximal velocity; CYP3A4: cytochrome P450 3A4; CYP3A5: cytochrome P450 3A5.

Table 4.6: Comparison of maximal concentration (C_{max}) and area under the concentration versus time curve within a dosing interval (AUC_{τ}) in adults for solithromycin between observed data and physiologically-based pharmacokinetic (PBPK) model simulations.

		C_{max} (µg/mL)			**AUC_{τ} or $AUC_{0-\infty}$ (µg*h/mL)**		
Dosing Regimen	**Day**	**Observed**	**Simulated**	**Ratio**	**Observed**	**Simulated**	**Ratio**
400 mg IV, 60 minute infusion, daily for 7 days	7	2.2 ± 0.44	2.6 ± 0.68	1.2 ± 0.4	13 ± 4.38	13 ± 12	1.1 ± 1.0
800 mg IV, 40 minute infusion, single dose	1	2.9 ± 0.54	5.5 ± 0.51	1.9 ± 0.4	19 ± 4.79	14 ± 4.81	0.8 ± 0.3
200 mg PO daily for 7 days	1	0.11 ± 0.05	0.26 ± 0.03	2.4 ± 1.1	0.84 ± 0.41	1.7 ± 0.27	2.0 ± 1.0
	7	0.25 ± 0.08	0.31 ± 0.08	1.2 ± 0.5	2.3 ± 0.77	2.3 ± 1.1	1.0 ± 0.6
400 mg PO daily for 7 days	1	0.58 ± 0.37	0.53 ± 0.06	0.9 ± 0.6	4.8 ± 3.1	3.9 ± 0.8	0.7 ± 0.5
	7	1.1 ± 0.52	1.1 ± 0.69	1.0 ± 0.8	13 ± 7.4	12 ± 12	0.9 ± 1.1
600 mg PO daily for 7 days	1	0.86 ± 0.53	0.80 ± 0.10	0.9 ± 0.6	7.7 ± 4.6	5.6 ± 1.3	0.7 ± 0.5
	7	1.5 ± 0.40	3.0 ± 1.5	2.0 ± 1.1	18 ± 5.6	42 ± 29	2.4 ± 1.8
800 mg PO day 1, 400 mg PO day 2-5	1	1.5 ± 0.55	1.2 ± 1.1	0.8 ± 0.8	21 ± 9.4[a]	10 ± 6.3[a]	0.5 ± 0.4
	5	1.2 ± 0.36	1.1 ± 0.68	0.9 ± 0.7	17 ± 7.2	11 ± 12	0.69 ± 0.8

Data are presented as the mean ± standard deviation. [a]Data are reported as the area under the concentration versus time curve from 0 to infinity ($AUC_{0-\infty}$). The ratio was calculated as the ratio of mean predicted values over mean observed values ± the ratio for the standard deviation as described previously.[16–18]

Abbreviations: IV: intravenous administration; PO: oral administration; AUC_{τ}, area under the concentration versus time curve within a dosing interval.

Table 4.7: Comparison of adult clearance values for solithromycin between the observed data and the simulated PBPK model.

	CL/F or CL on Day 1 (L/h)						CL/F or CL after multiple doses (L/h					
	Observed data		PBPK model				Observed data		PBPK model			
Dosing Regimen	**Mean**	**SD**	**Mean**	**SD**	**Ratio**	**SD**	**Mean**	**SD**	**Mean**	**SD**	**Ratio**	**SD**
200 mg PO daily	267	140	112	19	0.42	0.23	102	60	95	23	0.94	0.60
400 mg PO daily	103	141	106	20	1.03	1.43	96	198	63	34	0.66	1.40
600 mg PO daily	131	178	101	22	0.77	1.06	35	11	27	25	0.77	0.76
800 mg PO day 1, 400 mg PO day 2-5	61	54	93	26	1.53	1.42	32	13	63	34	1.96	1.33
400 mg IV daily	70	17	65	10	0.92	0.26	34	13	45	20	1.31	0.78
800 mg IV day 1	42	8	59	12	1.40	0.39	N/A	N/A	N/A	N/A	N/A	N/A

The ratio was calculated as the ratio of mean predicted values over mean observed values with a ratio for the standard deviation as described previously.[16–18].

Abbreviations: CL/F: clearance following oral administration; CL: clearance; PBPK: physiologically-based pharmacokinetic model; SD: standard deviation; PO: oral

Table 4.8: Average fold errors for the adult and pediatric solithromycin physiologically-based pharmacokinetic (PBPK) model.

Population	Dosing and Administration	Average Fold Error
Adults	200 mg PO daily	1.7
Adults	400 mg PO daily	1.1
Adults	600 mg PO daily	2.0
Adults	800 mg PO day 1, 400 mg PO day 2-5	0.8
Adults	400 mg IV daily	1.0
Adults	800 mg IV day 1	0.7
Pediatric Patients	**IV Formulation**	**0.7[a]**
12 to 17 years	6 mg/kg daily	0.7
6 to <12 years	7 mg/kg daily	1.3
2 to < 6 years	8 mg/kg daily	0.5
0 to < 2 years	7 (≤1 months) or 8 mg/kg daily (> 1 month)	0.6
Pediatric Patients	**Oral Suspension**	**0.8[a]**
6 to < 12 years	15 mg/kg daily	0.8
2 to < 6 years	15 mg/kg daily	0.9
0 to < 2 years	15 mg/kg daily	0.8
Pediatric Patients	**Oral Capsules**	**0.7[a]**
12 to 17 years	6 mg/kg daily	0.7
6 to < 12 years	15 mg/kg daily	0.7

[a]Overall values for pediatric patients for each formulation and dosing administration. The adult model was evaluated using plasma concentration data from 100 healthy subjects and 22 patients with community acquired bacterial pneumonia (CABP) (1,966 plasma samples) as described previously (Table 1) [2]. The solithromycin pediatric PBPK model was evaluated using 684 plasma concentration data available from 96 pediatric patients ranging from 4 days to 17.9 years. The pediatric concentration data was normalized to a 1 mg/kg dose. The average fold error was calculated for each dosing regimen according to the equation where predicted is the simulated geometric mean value for adults and the arithmetic mean value for pediatric subjects:

$10^{\left(\frac{1}{n}\right)*\sum \log\left(\frac{\text{predicted}}{\text{observed}}\right)}$.

Table 4.9: Comparison of adult drug-drug interaction (DDI) simulations and observed data for solithromycin plus midazolam or ketoconazole.

Treatment Group	**Geometric Mean [90% CI] C_{max} Ratio**		**Geometric Mean [90% CI] $AUC_{0-\infty}$ Ratio**	
	Observed	**Simulated**	**Observed**	**Simulated**
Solithromycin (400 mg daily x 5 days) plus midazolam[a]	2.45 [2.16-2.77]	2.71 [2.62-2.81]	8.96 [7.82-10.3]	6.89 [5.87-8.08]
Solithromycin (800 mg x 1, 400 mg daily x 4 days) plus midazolam[b]	2.45 [2.16-2.77]	2.94 [2.83-3.05]	9.09 [7.92-10.4]	8.96 [7.49-10.7]
Solithromycin (400 mg) plus Ketoconazole (400 mg)[c]	1.56 [1.39-1.76]	1.91 [1.88, 1.95]	2.55 [2.24-2.91]	2.30 [2.25-2.36]

[a]Midazolam 0.075 mg/kg PO on days 1, 3, and 7 and solithromycin 400 mg once daily PO on days 3 to 7. The ratio was calculated for midazolam on day 7 compared to day 1.

[b]Midazolam 0.075 mg/kg PO on days 1, 3, and 7 and solithromycin 800 mg PO on day 3 followed by 400 mg once daily PO on days 4 to 7. The ratio was calculated for midazolam on day 7 compared to day 1.

[c]Solithromycin 400 mg PO on Day 1 followed by a 5-day washout period, and then 4 days of ketoconazole 400 mg PO (days 7-10), with solithromycin and ketoconazole PO (400 mg each) on day 11. The ratio was calculated for solithromycin on day 11 compared to day 1.

Abbreviations: confidence interval (CI); maximal concentration (C_{max}), area under the curve from 0 to infinity ($AUC_{0-\infty}$); PO, oral administration; IV: intravenous administration.

Table 4.10: Comparison of the population pharmacokinetic (PopPK) and physiologically-based pharmacokinetic (PBPK) model weight-normalized clearance estimates.

Cohort	PopPK estimates[a] CL (L/h/kg)	PBPK Simulated CL day 1 (L/h/kg)	PBPK Simulated CL day 5 (L/h/kg)
12 to 17 years (IV)	0.78 (0.19-2.00)	0.88 (0.20-1.63)	0.62 (0.08-1.55)
6 to <12 years (IV)	1.20 (0.43-2.50)	1.14 (0.14, 2.07)	0.85 (0.07, 1.93)
2 to <6 years (IV)	0.53 (0.18-2.40)	1.37 (0.43-2.26)	0.96 (0.08-2.11)
0 to <2 years (IV)	0.87 (0.28-1.40)	1-6 months: 1.05 (0.07-1.90) 0.5-2 years: 1.25 (0.19-2.06)	1-6 months: 0.46 (0.06-1.83) 0.5-2 years: 0.96 (0.08-1.85)

Clearance values are reported as the median (range). [a]Individual empirical Bayesian post-hoc parameter estimates were obtained based on a published population based pharmacokinetic (PopPK) model developed using plasma data from these 96 children (780 plasma samples). The structural model was a 2-compartment model with linear elimination and first-order absorption with an oral absorption lag time. Significant covariates included weight and a sigmoidal maturation function for post-menstrual age on clearance and weight on the volume of distribution. Modeling time-dependent inhibition did not improve the model fits in these pediatric patients so only one individual clearance value was reported per subject.[8] Abbreviations: IV: intravenous; CL: clearance.

Table 4.11: Ketoconazole pediatric physiologically-based pharmacokinetic (PBPK) model evaluation.

Dosing Regimen	**Age Range**	**AUC (µg*h/mL)**		**C_{max} (µg/mL)**	
		Simulated	Observed	Simulated	Observed
9 mg/kg PO daily, tablets or suspension[33,34]	0.42 - 14 years	33.5 (5.9-85.3)	32.7 (5.9-82.0)	5.7 (0.93-14.1)	4.9 (1.2-14.0)
5 mg/kg PO single, suspension[35]	2 - 12.5 years	23.6 (4.1-70.3)	15.3 (2.6-36.4)	4.1 (0.8-9.3)	4.4 (0.3-8.8)

Data presented as the mean (range). AUC: area under the concentration versus time curve from 0 to 24 hours at steady-state for multiple dosing or 0 to infinity for single dose administration, C_{max}, maximal concentration.

Abbreviations: GA: gestational age; PNA: post-natal age.

Table 4.12: Midazolam pediatric PK parameters for children receiving intravenous midazolam

Reference	Age Range	CL (L/h/kg)		V (L/kg)	
		Simulated	Observed	Simulated	Observed
[36]	2-5 days PNA 37 (34-41) weeks GA	0.08 ± 0.02	0.12 ± 0.07	0.7 ± 0.1	0.9 ± 0.4
[37]	0.5 to < 2 years	0.57 ± 0.20	0.68 ± 0.38	2.8 ± 1.0	2.2 ± 0.5
[37]	2 to < 12 years	0.65 ± 0.20	0.60 ± 0.23	2.6 ± 1.1	2.5 ± 1.4
[37]	12 to < 16 years	0.48 ± 0.14	0.56 ± 0.23	1.3 ± 0.4	3.6 ± 1.5
[38]	8 days – 16.2 years	0.08 to 1.12	0.1 to 3.1	0.6 to 5.1	0.2 to 3.5

Data are presented as the mean (±standard deviation) for all studies except for [38], where the data were presented as the range.

Abbreviations: CL: clearance; V: volume of distribution; L: liters; h: hour; kg: kilogram; PNA: post-natal age; GA: gestational age.

Table 4.13: Midazolam pediatric PBPK model predictions for children receiving oral midazolam

Dosing Regimen	Reference	Age Range	$AUC_{0-\infty}$ (ng*h/mL)		C_{max} (ng/mL)	
			Simulated	Observed	Simulated	Observed
0.25 mg/kg PO single	[37]	0.5 to < 16 years	278 ± 160	137 ± 86	64 ± 41	56 ± 30
0.5 mg/kg PO single	[37]	0.5 to < 16 years	388 ± 275	356 ± 320	77 ± 54	123 ± 76
1.0 mg/kg PO single	[37]	0.5 to < 16 years	563 ± 375	684 ± 581	87 ± 63	186 ± 99

Data arepresented as the mean ± standard deviation.

Abbreviations: $AUC_{0-\infty}$: area under the concentration versus time curve from 0 to infinity; C_{max}: maximal concentration: PO: oral.

Table 4.14: Simulated dosing and drug-drug interaction (DDI) potential stratified by age group for solithromycin in combination with midazolam and ketoconazole.

Age Group	Solithromycin Simulated Dose[a]	Midazolam Simulated Dose	Ketoconazole Simulated Dose[b]	Midazolam plus Solithromycin $AUC_{0-\infty}$ Fold Change[c]	Solithromycin plus Ketoconazole $AUC_{0-24,ss}$ Fold Change[d]
1 to <6 months	3.25 mg/kg IV	0.05 mg/kg IV	3.3 mg/kg PO daily	5.9 (5.5, 6.4)	1.8 (1.8, 1.9)
0.5 to <2 years	6 mg/kg IV	0.05 mg/kg IV	4 mg/kg PO daily	4.1 (3.8, 4.4)	1.2 (1.2, 1.3)
2 to <6 years	7 mg/kg IV	0.05 mg/kg IV	3.3 mg/kg PO daily	4.9 (4.5, 5.3)	1.5 (1.4, 1.5)
6 to <12 years	6 mg/kg IV	0.025 mg/kg IV	3.3 mg/kg PO daily	5.2 (4.8, 5.6)	1.5 (1.4, 1.6)
12 to <18 years	5.5 mg/kg IV	0.5 mg IV	3.3 mg/kg PO daily	4.9 (4.6, 5.3)	1.2 (1.2, 1.2)
18 to 65 years	400 mg IV	0.5 mg IV	200 mg PO daily	4.1 (3.8, 4.4)	1.4 (1.4, 1.4)

[a]The maximum simulated solithromycin dose was 400 mg. [b]The maximum simulated ketoconazole dose was 200 mg. [c]The fold-change values are presented as the geometric mean (90% confidence interval) for midazolam based on 500 simulations in each age group receiving midazolam plus solithromycin for 5 days relative to midazolam alone for 5 days. [d]The fold-change values are presented as the geometric mean (90% confidence interval) for solithromycin based on 500 simulations in each age group receiving solithromycin plus ketoconazole for 5 days relative to solithromycin alone for 5 days. Abbreviations: IV: intravenous; $AUC_{0-\infty}$: area under the concentration versus time curve from 0 to infinity; $AUC_{0-24,ss}$: area under the concentration versus time curve from 0 to 24 hours at steady-state.

4.6 Figures

Figure 4.1: Cytochrome P450 3A4 (CYP3A4) time-dependent inhibition.

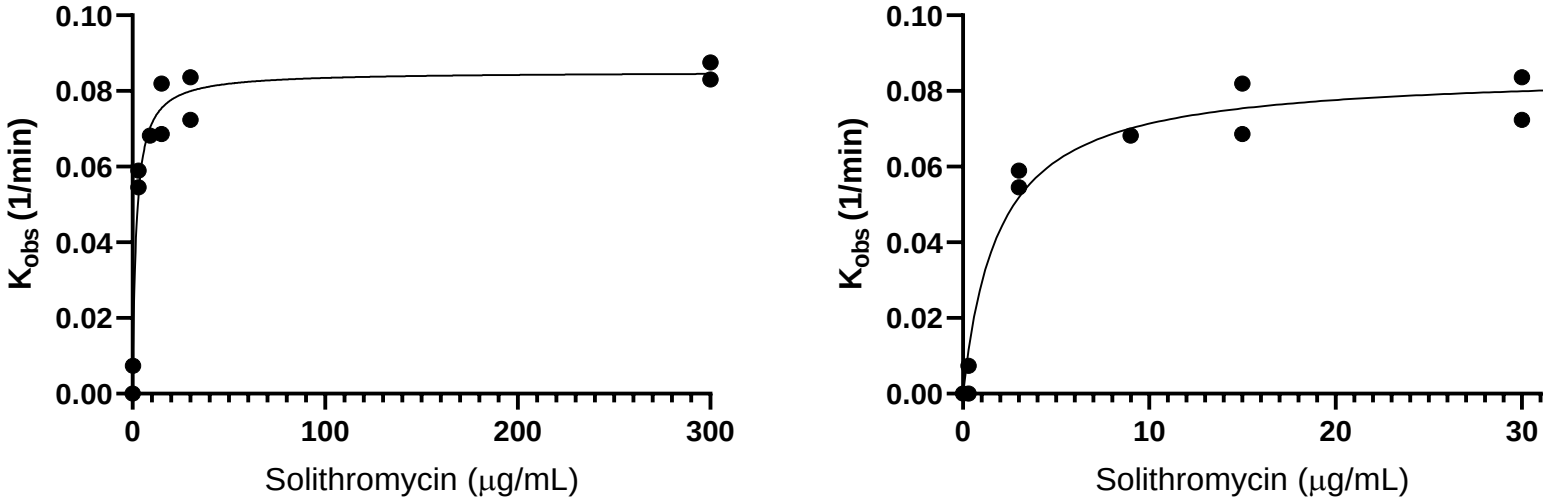

CYP3A4 (200 pmol/mL) was pre-incubated at 37 degrees Celsius with solithromycin (0, 0.3, 3, 9, 15, 30, and 300 μg/mL) for 0, 2.5, 5, 10, 15, and 30 minutes, and then diluted 10-fold into fresh buffer containing 250 μM testosterone and incubated at 37 degrees Celsius for five minutes. Remaining enzymatic activity was measured by the formation of 6β-hydroxy-testosterone using a validated high-performance liquid chromatography-tandem mass spectrometry (HPLC/MS/MS) assay. Each data point represents the mean of duplicates and data from two independent experiments are shown. The negative slope of the natural log of the percent activity remaining at each pre-incubation time, the pseudo first-order rate constant of inactivation (K_{obs}), was plotted against solithromycin concentration.

Figure 4.2: Cytochrome P450 3A5 (CYP3A5) time-dependent inhibition.

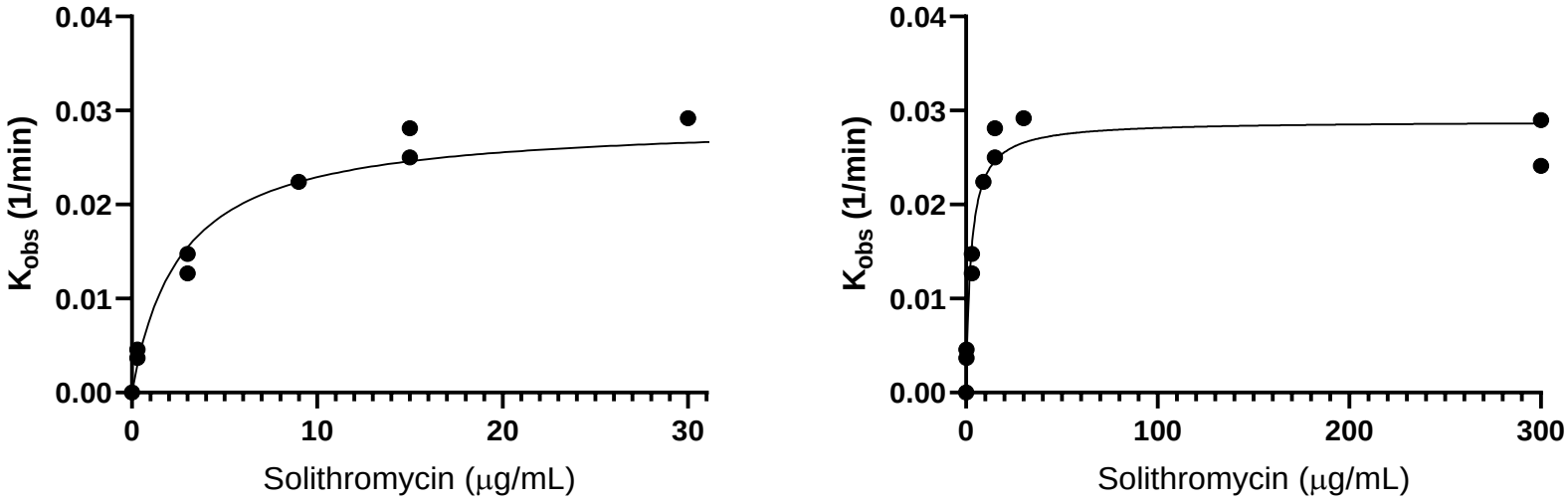

CYP3A5 (200 pmol/mL) was pre-incubated at 37 degrees Celsius with solithromycin (0, 0.3, 3, 9, 15, 30, and 300 μg/mL) for 0, 2.5, 5, 10, 15, and 30 minutes, and then diluted 10-fold into fresh buffer containing 250 μM testosterone and incubated at 37 degrees Celsius for five minutes. Remaining enzymatic activity was measured by the formation of 6β-hydroxy-testosterone using a validated high-performance liquid chromatography-tandem mass spectrometry (HPLC/MS/MS) assay. Each data point represents the mean of duplicates and data from two independent experiments are shown. The negative slope of the natural log of the percent activity remaining at each pre-incubation time, the pseudo first-order rate constant of inactivation (K_{obs}), was plotted against solithromycin concentration.

Figure 4.3: Cytochrome P450 3A7 (CYP3A7) time-dependent inhibition.

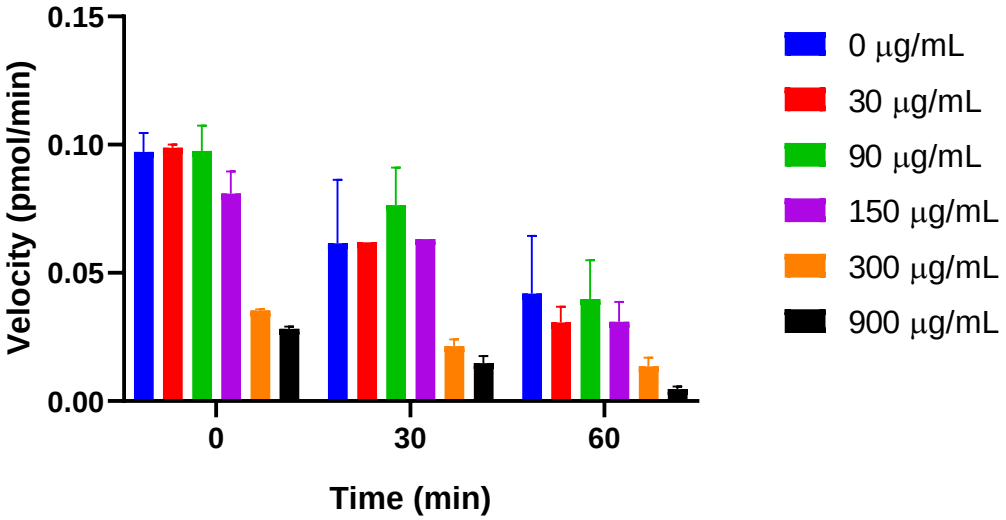

CYP3A7 (400 pmol/mL) was pre-incubated at 37 degrees Celsius with solithromycin (0, 30, 90, 150, 300, and 900 µg/mL). After 0, 5, 15, 30, 45, and 60 minutes, the pre-incubations were diluted 10-fold into fresh buffer containing 250 µM testosterone and incubated at 37 degrees Celsius for 30 minutes. Remaining enzymatic activity was measured by the formation of 6β-hydroxy-testosterone using a validated high-performance liquid chromatography-tandem mass spectrometry (HPLC/MS/MS) assay. Velocity for formation of 6β-hydroxy-testosterone versus time are shown with the mean and standard error of triplicates from a single experiment.

Figure 4.4: Linearity with time for Cytochrome P450 CYP3A-mediated metabolism of solithromycin.

A)

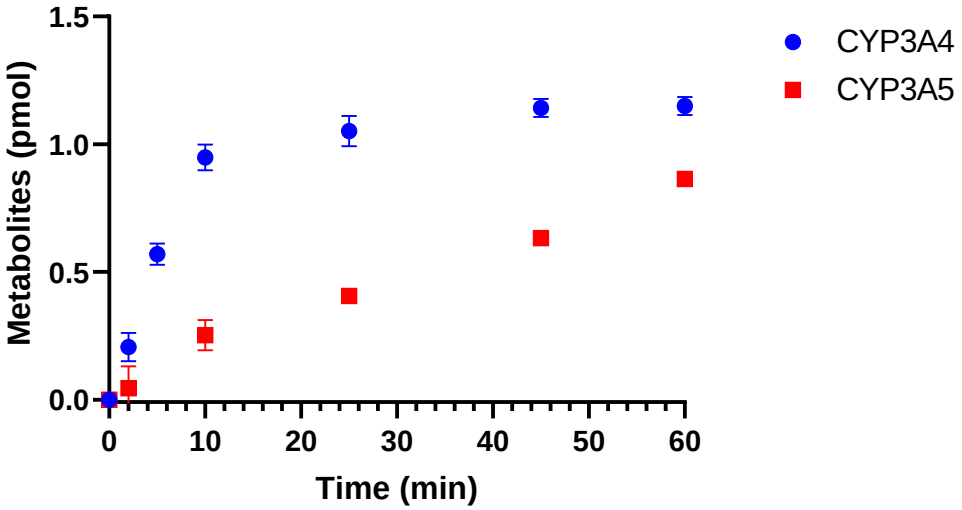

B)

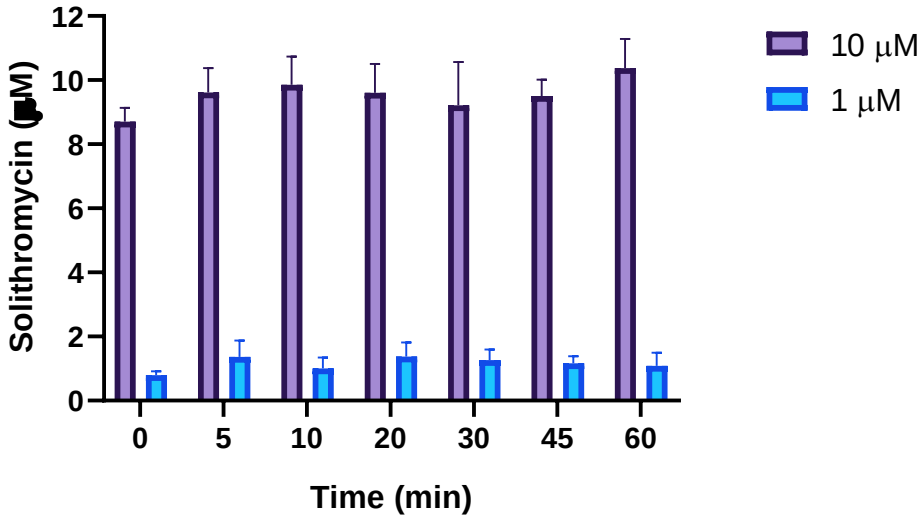

C)

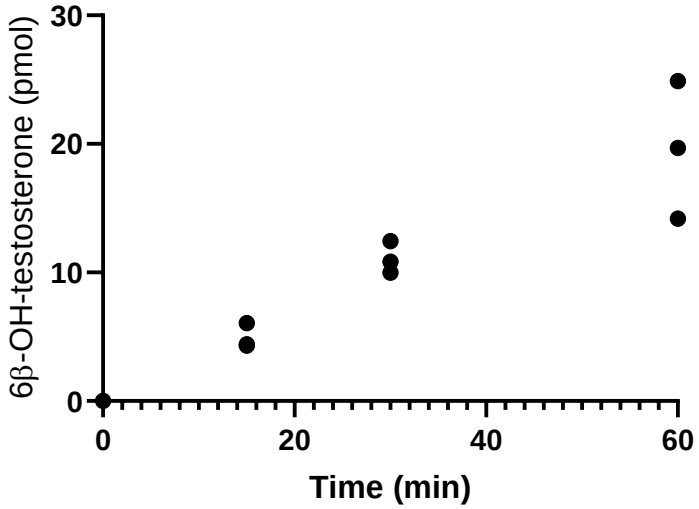

Pilot experiments were first performed to determine the linear range of disappearance of solithromycin. (A) 60 pmol/mL of cytochrome P450 (CYP) 3A4 and CYP3A5 were incubated with 1 µM solithromycin in 100 mM potassium phosphate pH 7.4 plus NADPH Regenerating System Solutions A and B at a dilution of 1:20 and 1:100, respectively, for 0, 2, 5, 10, 15, 30, and 60 minutes. Data are presented as the mean and standard deviation from a single experiment. (B) For CYP3A7, 100 pmol/mL were incubated with 1 µM and 10 µM solithromycin for 0, 5, 10, 15, 20, 30, and 60 minutes. Data are presented as the mean and standard deviation from a single experiment. (C) CYP3A7 was also incubated with 250 µM testosterone for 0, 15, 30, and 60 minutes as a positive control. Data are presented as triplicate samples. The reactions were stopped by a 1:5 dilution into ice-cold methanol containing 0.5 µM roxithromycin (or 1:4 dilution into acetonitrile containing 0.5 µM 4-androsten-19-1al 3,17-dione), centrifuged at 3500 rpm for 10 minutes at 4 degrees, and solithromycin and 6β-OH-testosterone were measured in the supernatant by high-performance liquid chromatography-tandem mass spectrometry (HPLC/MS/MS).

Figure 4.5: Rate of Cytochrome P450 3A4 (CYP3A4) mediated metabolism (velocity) of solithromycin as a function of concentration.

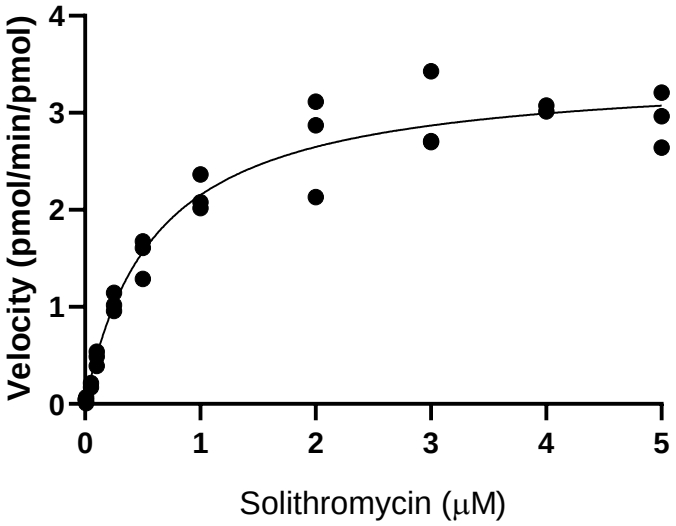

CYP3A4 (60 pmol/mL) was incubated with solithromycin (0.005, 0.01, 0.05, 0.1, 0.25, 0.5, 1, 2, 3, 4, 5 μM) for 2 minutes in order to determine the concentration at half-maximal velocity (K_M)/maximal velocity (V_{max}). Data is presented as the mean of triplicates from three individual experiments.

Figure 4.6: Rate of Cytochrome P450 3A5 (CYP3A5)-mediated metabolism (velocity) of solithromycin as a function of concentration.

A)

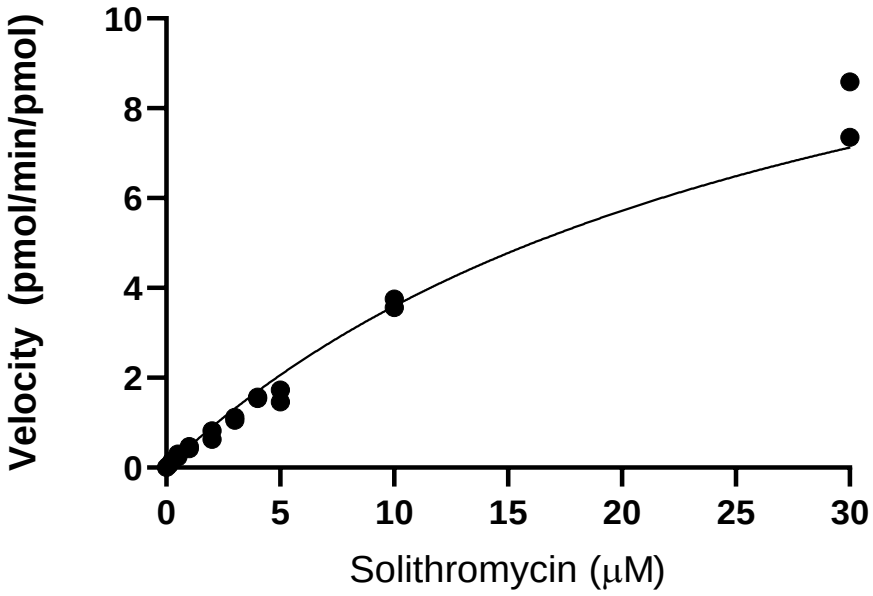

B)

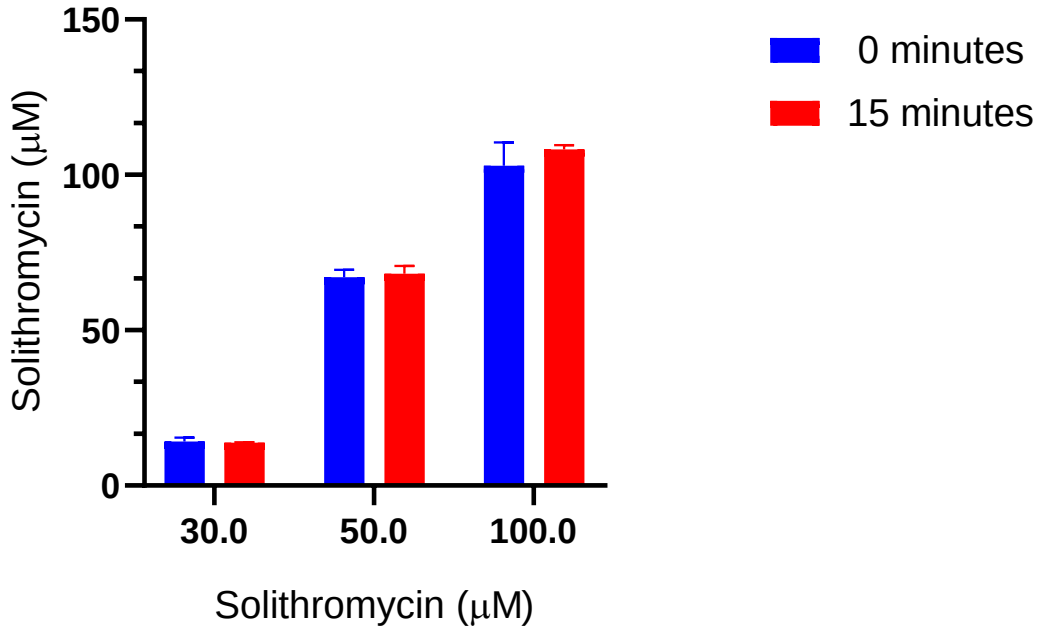

(A) CYP3A5 (60 pmol/mL) was incubated with solithromycin (0.01, 0.05, 0.1, 0.25, 0.5, 1, 2, 3, 4, 5, 10, 30 µM) at 37 degrees Celsius for 15 minutes. Data are presented as the mean of triplicates from two individual experiments.

(B) The third experiment for CYP3A5 was conducted at higher concentrations (50 to 3700 µM) to further characterize the maximal velocity (V_{max}). However, activity starts to decrease >30 µM due to time-dependent inhibition so values beyond 30 µM were not included in determination of concentration at half-maximal velocity (K_M)/V_{max}.

Figure 4.7: Population simulations depicting concentration versus time after first dose following solithromycin intravenous (IV) administration in healthy adults.

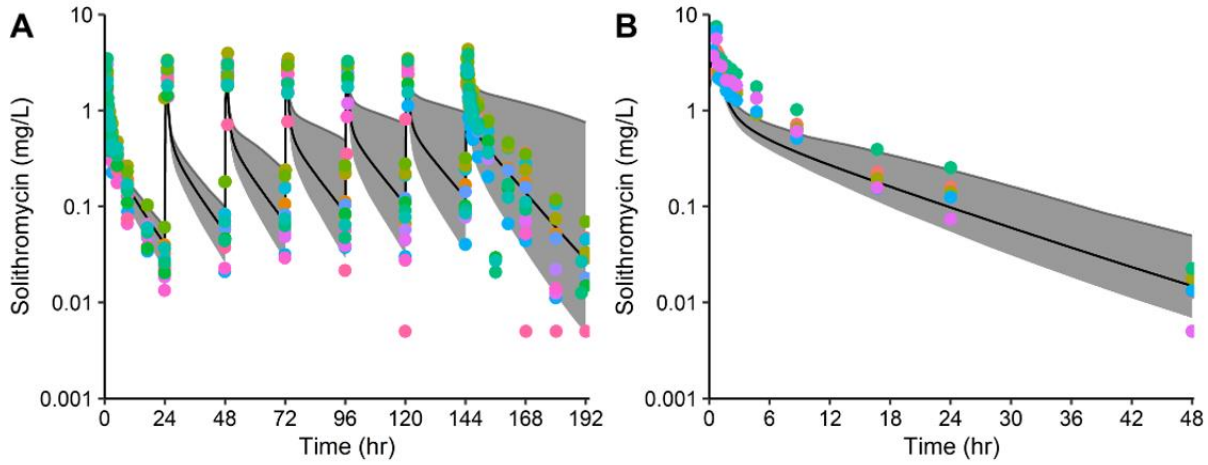

Population simulations were performed for 100 virtual subjects using a Black American population with demographics from study CE01-102 for healthy subjects: 27% female with a mean (range) age of 32.9 (20-55) years and a weight of 74.5 (61.4-90.3) kg. A: 400 mg IV daily x 7 days administered over a 60-minute infusion; B: 800 mg IV single dose administered over a 40 minute infusion. The solid grey region is the 90% prediction interval, the solid black line is the geometric mean, and colored dots are observations stratified by individual. The average fold error (AFE) was calculated as $10^{\left(\frac{1}{n}\right)*\sum \log\left(\frac{\text{predicted}}{\text{observed}}\right)}$, where the predicted values were the simulated geometric mean values and n was the sample size. The AFE was 1.0 and 0.7 for the 400 mg IV and 800 mg IV plots, respectively.

Figure 4.8: Population simulations for oral solithromycin in healthy adults.

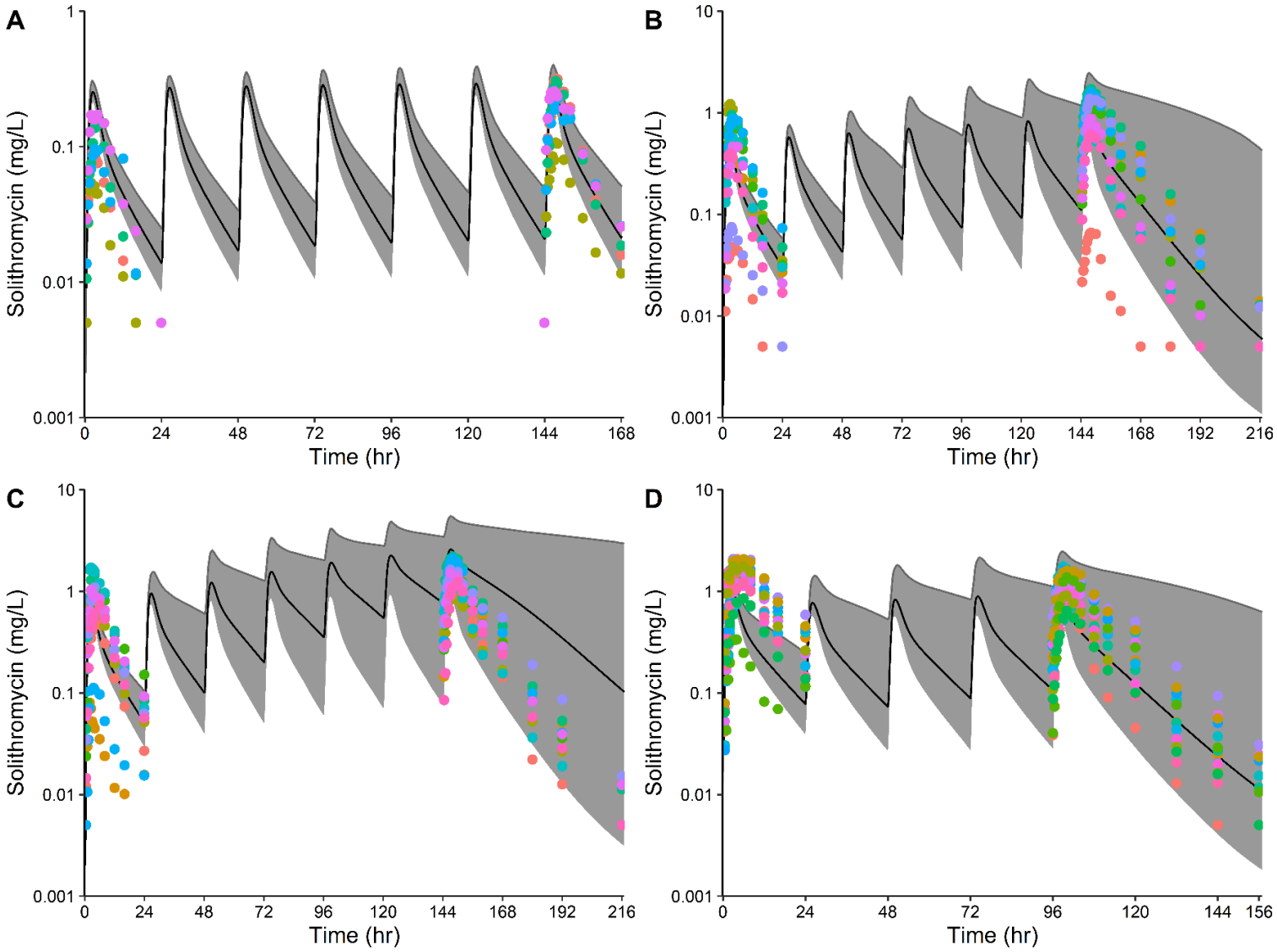

Population simulations were performed for 100 virtual subjects using a Black American population with demographics from study CE01-102 for healthy subjects: 27% female with a mean (range) age of 32.9 (20-55) years and a weight of 74.5 (61.4-90.3) kg. A: 200 mg oral (PO) daily x 7 days; B: 400 mg PO daily x 7 days; C: 600 mg PO daily x 7 days; D: 800 mg PO on day 1,400 mg PO daily on days 2-5. The solid grey region is the 90% prediction interval, the solid black line is the geometric mean, and the colored dots are observations stratified by individual. The average fold error (AFE) was calculated as $10^{\left(\frac{1}{n}\right)*\sum \log\left(\frac{\text{predicted}}{\text{observed}}\right)}$, where the predicted values were the simulated geometric mean values and n was the sample size. The AFE was 1.7, 1.1, 2.0 and 0.8 for the 200 mg, 400 mg, 600 mg PO daily and 800 mg followed by 400 mg PO plots, respectively.

Figure 4.9: Population simulations for 100 mg, 200 mg, 400 mg, 800 mg oral single dose ketoconazole in adults.

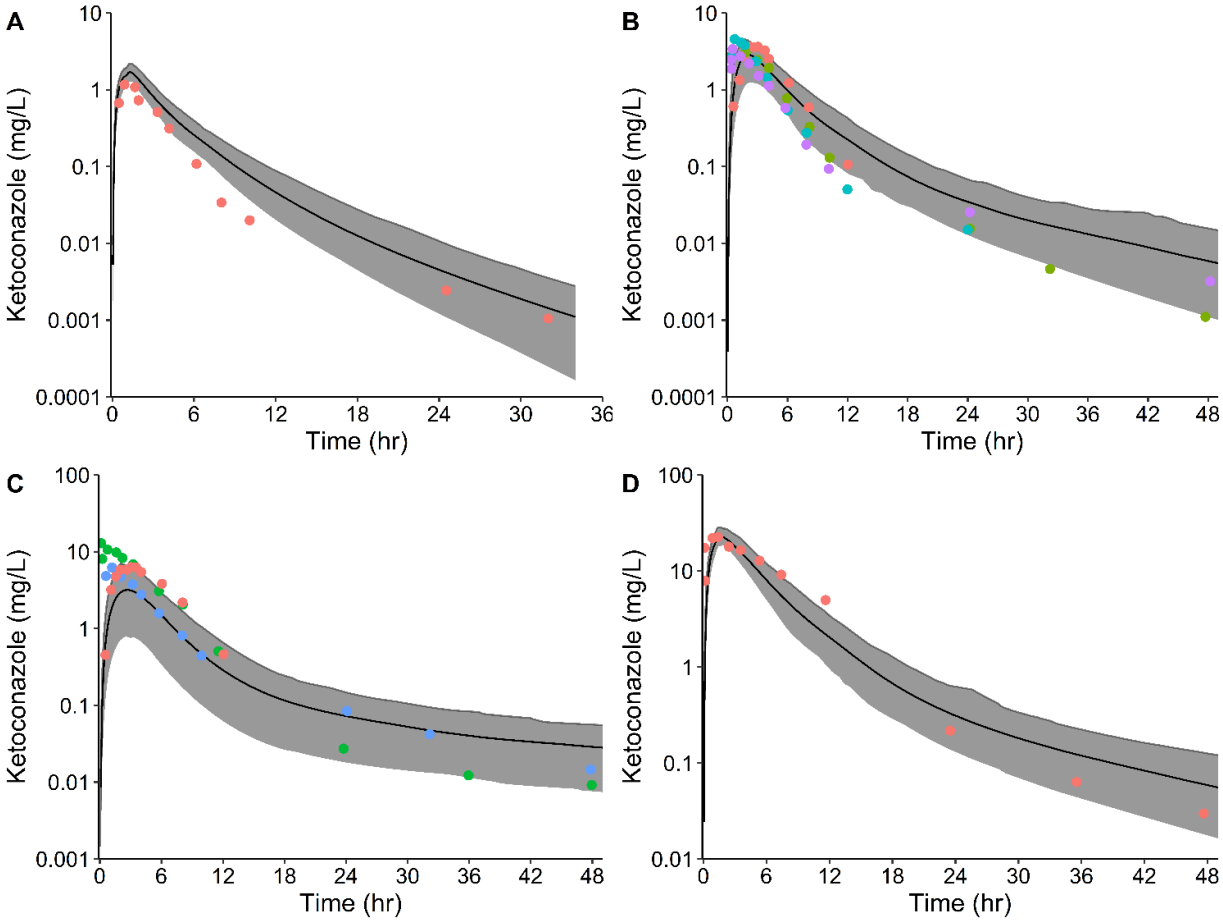

Population simulations based on 100 virtual subjects (white American population from 18 to 46 years of age) receiving 100, 200, 400, and 800 mg PO ketoconazole were performed. Single dose (A=100 mg PO, B=200 mg PO, C=400 mg PO, D=800 mg PO) administration. The solid grey region is the 90% prediction interval, the solid black line is the mean, and the colored dots are the mean observations stratified by study. Observed data in orange are from healthy adults receiving a single dose of the oral solution of ketoconazole.[22] For the 200 mg PO simulation, the observed data in blue are from adults receiving the suspension, purple from adults receiving the tablet, and green is adults receiving the solution formulation of ketoconazole. [23] For the 400 mg PO simulation, the observed data in green are from adults receiving the solution [23] and the observed data in blue are from adults receiving the tablet formulation of ketoconazole.[42]

Figure 4.10: Population simulations for 200 mg and 400 mg oral multiple dose ketoconazole in adults.

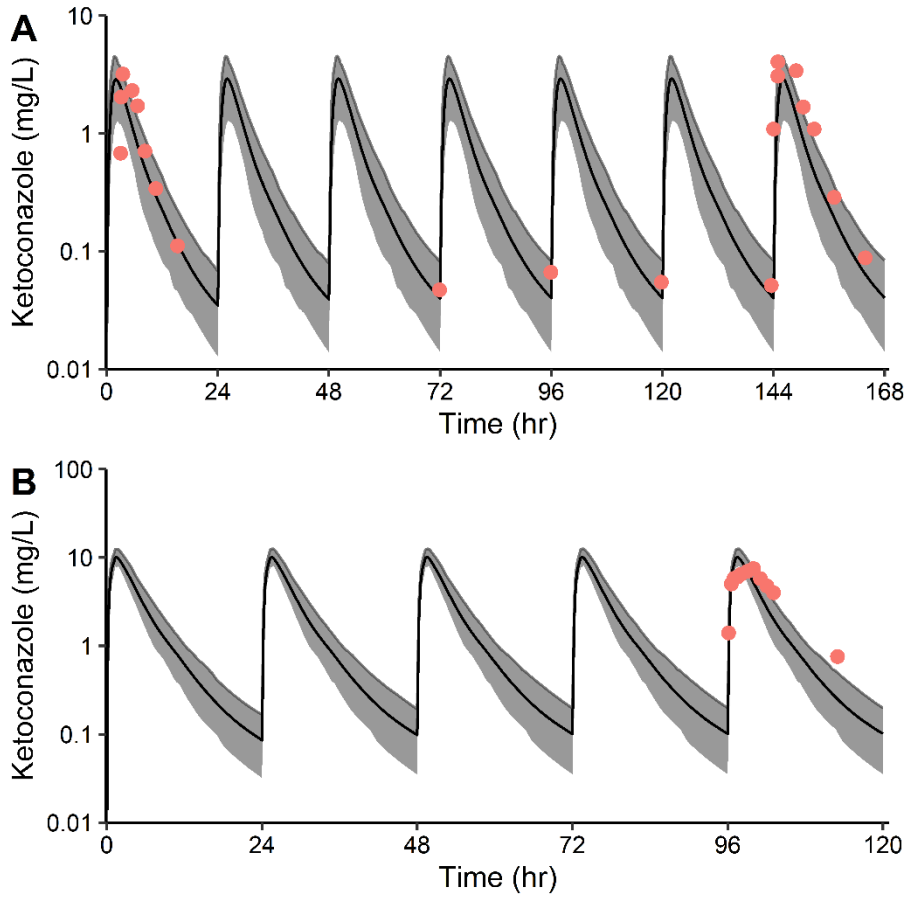

Population simulations based on 100 virtual subjects (white American population from 18 to 46 years of age) receiving 100, 200, 400, and 800 mg PO ketoconazole were performed. Multiple dose (A=200 mg daily x 7 days=A; B=400 mg daily x 5 days) administration. The solid grey region is the 90% prediction interval, the solid black line is the mean, and the colored dots are the mean observations from clinical studies: 200 mg tablets once daily fasted for 7 days [54] and 400 mg once daily for 5 days.[55]

Figure 4.11: Population simulations for midazolam in adults.

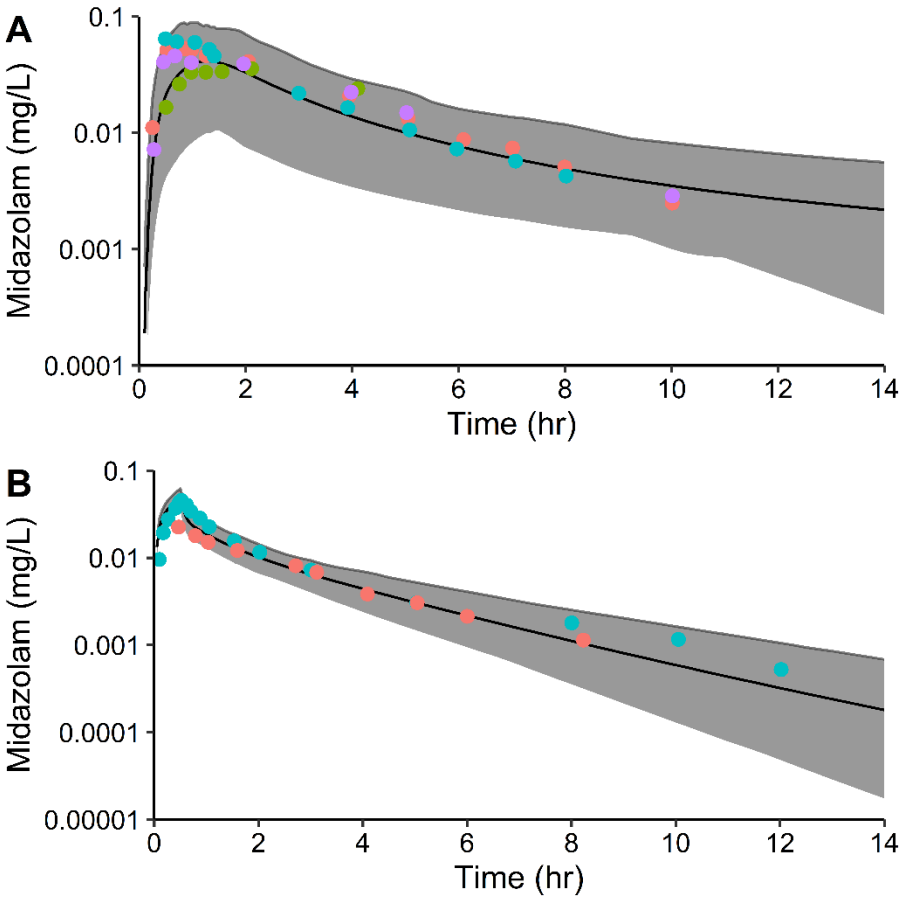

Population simulations based on 100 virtual subjects (white American population from 18 to 46 years of age) were performed. A: 15 mg oral (PO) midazolam single dose; B: 2 mg intravenous (IV) intravenous single dose. The solid grey region is the 90% prediction interval, the solid black line is the mean, and the colored dots are the mean observations from clinical studies. A: observed data in healthy adults following a 15 mg oral tablet dose under fasting conditions (orange), one hour before a meal (blue), with a meal (purple), and one-hour after a meal (green).[43]. B: observed data from healthy adults receiving 2 mg IV midazolam over a 30 minute infusion, blue [44] and orange.[56]

Figure 4.12: Population simulations depicting concentration versus time after first dose following solithromycin intravenous (IV) administration in pediatric patients.

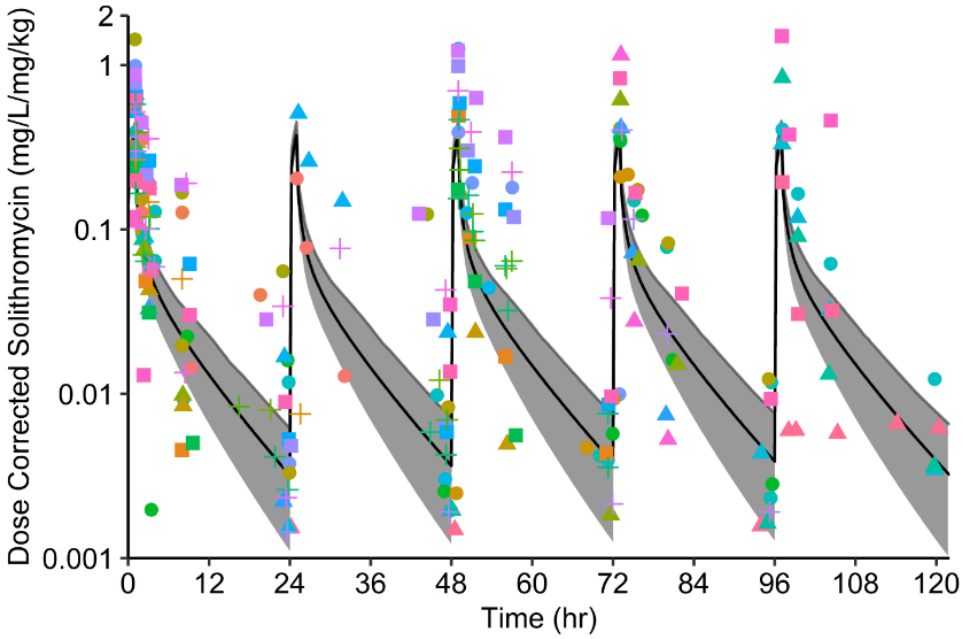

Pediatric population simulations for 100 virtual White American subjects from 4 days to 17.9 years of age receiving 1 mg/kg intravenous (IV) solithromycin. The solid grey region is the 90% prediction interval, the solid black line is the arithmetic mean line, the colors are stratified by individuals, and shapes are stratified by age group (circles: 12 to 17 years; triangle: 6 to <12 years; squares: 2 to <6 years; cross: 0 to < 2 years). Solithromycin plasma concentration data were normalized by dose and time relative to the last drug administration since dose and administration differed slightly for each individual.

Figure 4.13: Population simulations depicting concentration versus time after first dose following solithromycin oral administration (capsules or suspension) in pediatric patients.

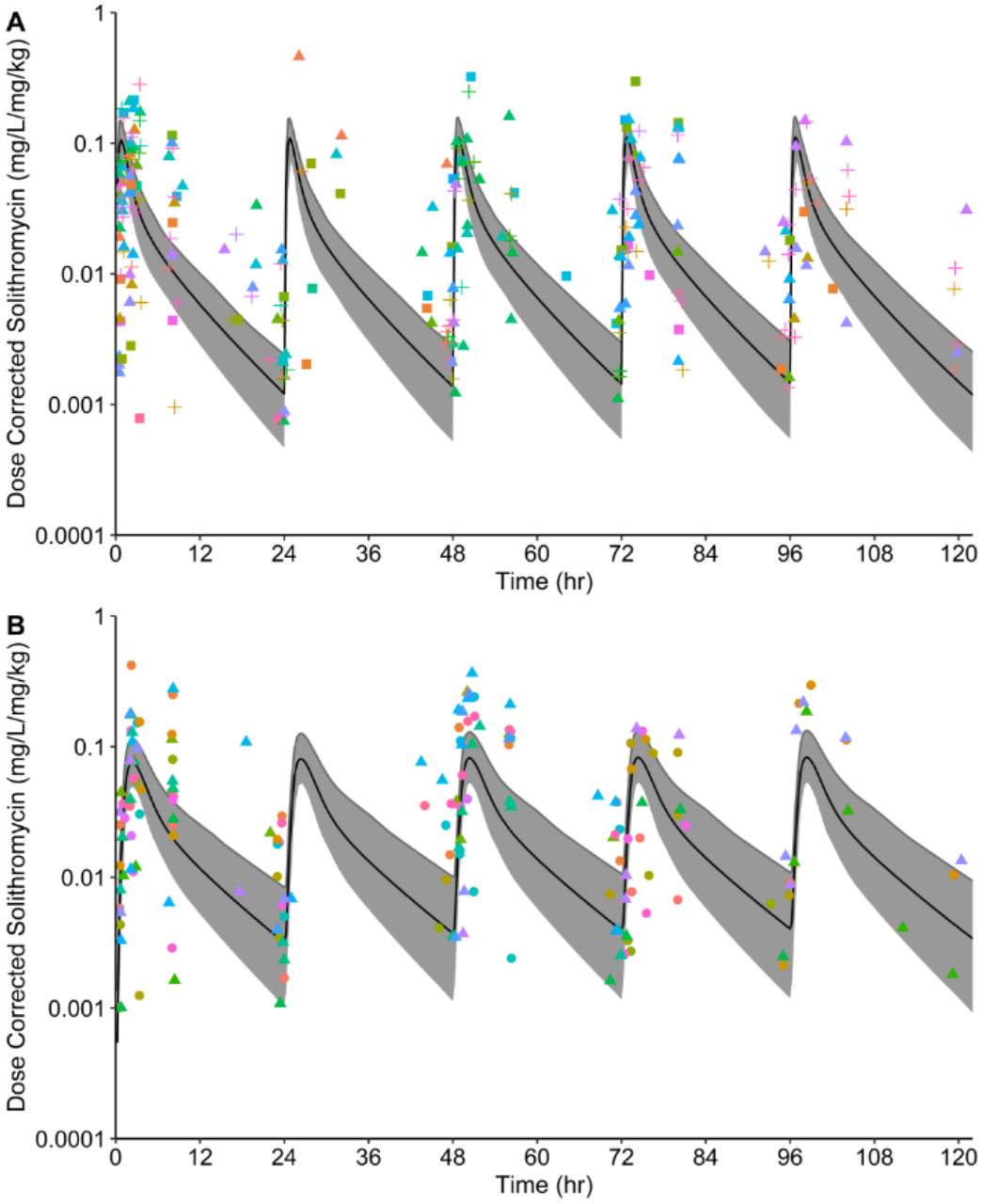

(A) Population simulations for 100 White American virtual infants and children from 4 days to 12 years of age receiving 1 mg/kg PO solithromycin as a suspension.

(B) Population simulations for 100 white American virtual children and adolescents from 6 to 17 years of age receiving 1 mg/kg oral (PO) solithromycin as a capsule. The solid grey region is the 90% prediction interval, the solid black line is the arithmetic mean, the colors are stratified by individuals, and shapes are stratified by age group (circles: 12 to 17 years; triangle: 6 to <12 years; squares: 2 to <6 years; cross: 0 to < 2 years). Solithromycin plasma concentration data were normalized by dose and time relative to the last drug administration since dose and administration differed for each individual.

Figure 4.14: Simulated solithromycin and ketoconazole daily steady-state area under the concentration versus time curve ($AUC_{0\text{-}24,ss}$) stratified by age group.

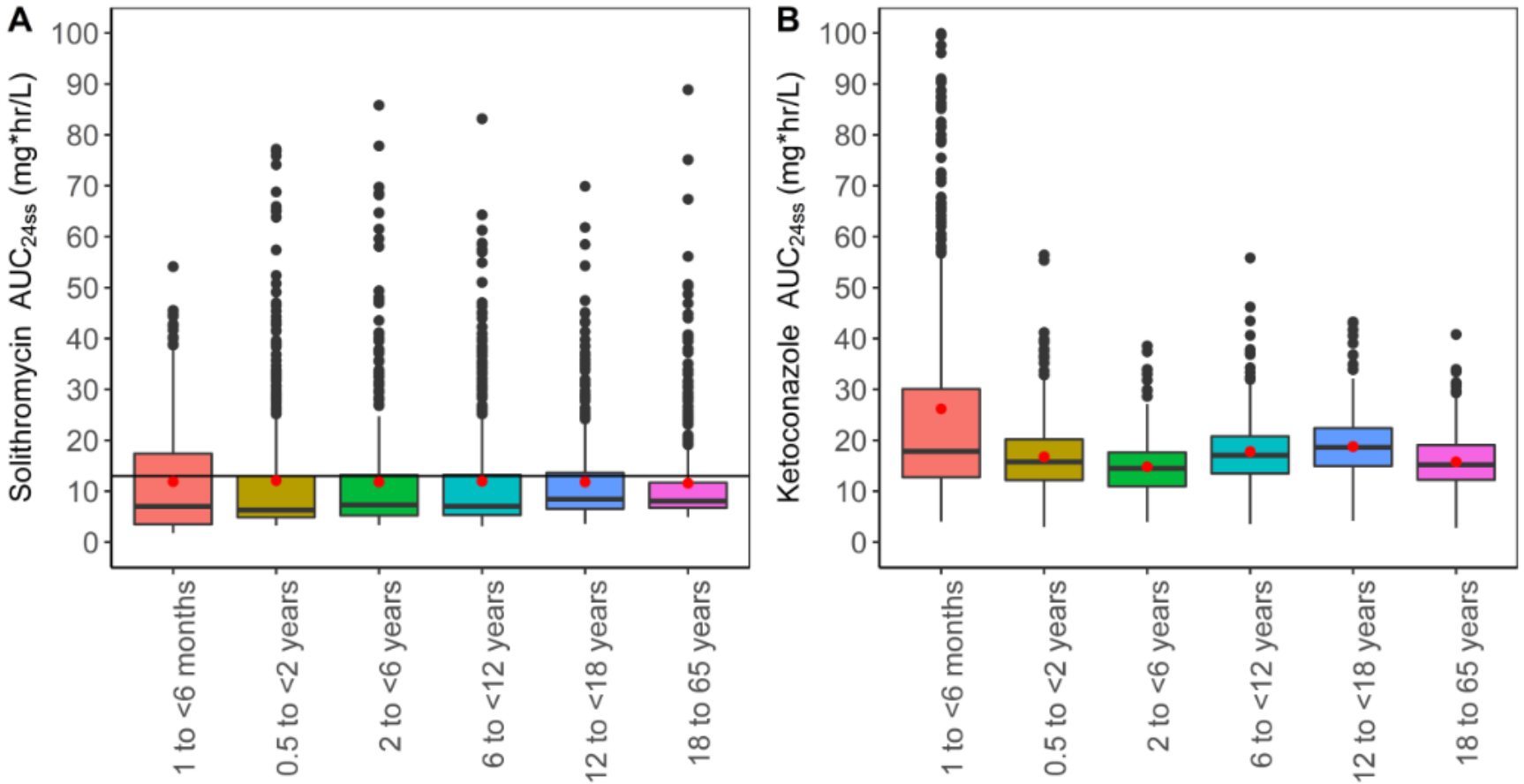

Dosing was simulated in 500 virtual individuals between the ages of 1 to <6 months, 0.5 to <2 years, 2 to <6 years, 6 to <12 years, 12 to <18 years, and 18 to 65 years. The boxplots displays the median (inter-quartile range), the upper whiskers is the 75th percentile to 1.5 times the inter-quartile range, the lower whisker is the 25th percentile subtract 1.5 times the inter-quartile range, and observations outside the whiskers are represented as black dots.

(A) The simulated solithromycin daily steady-state area under the concentration versus time curve ($AUC_{0\text{-}24,ss}$) based on the age and weight based IV solithromycin dosing for 5 days as presented in Table 5. The red dot is the arithmetic mean for each age group. The black horizontal line refers to the mean daily $AUC_{0\text{-}24,ss}$ value observed in healthy adults whom received 400 mg intravenously for 7 days, in which the reported mean ± standard deviation was 13 ± 4.38 mg*hr/L (Sponsor data on file).

(B) The simulated ketoconazole daily $AUC_{0\text{-}24,ss}$ based on the age and weight based PO ketoconazole dosing for 5 days as presented in Table 14.

Figure 4.15: Forest plots of the geometric mean fold ratios for the simulated area under the concentration versus time curve (AUC) of midazolam with and without solithromycin and of solithromycin with and without ketoconazole, stratified by age groups.

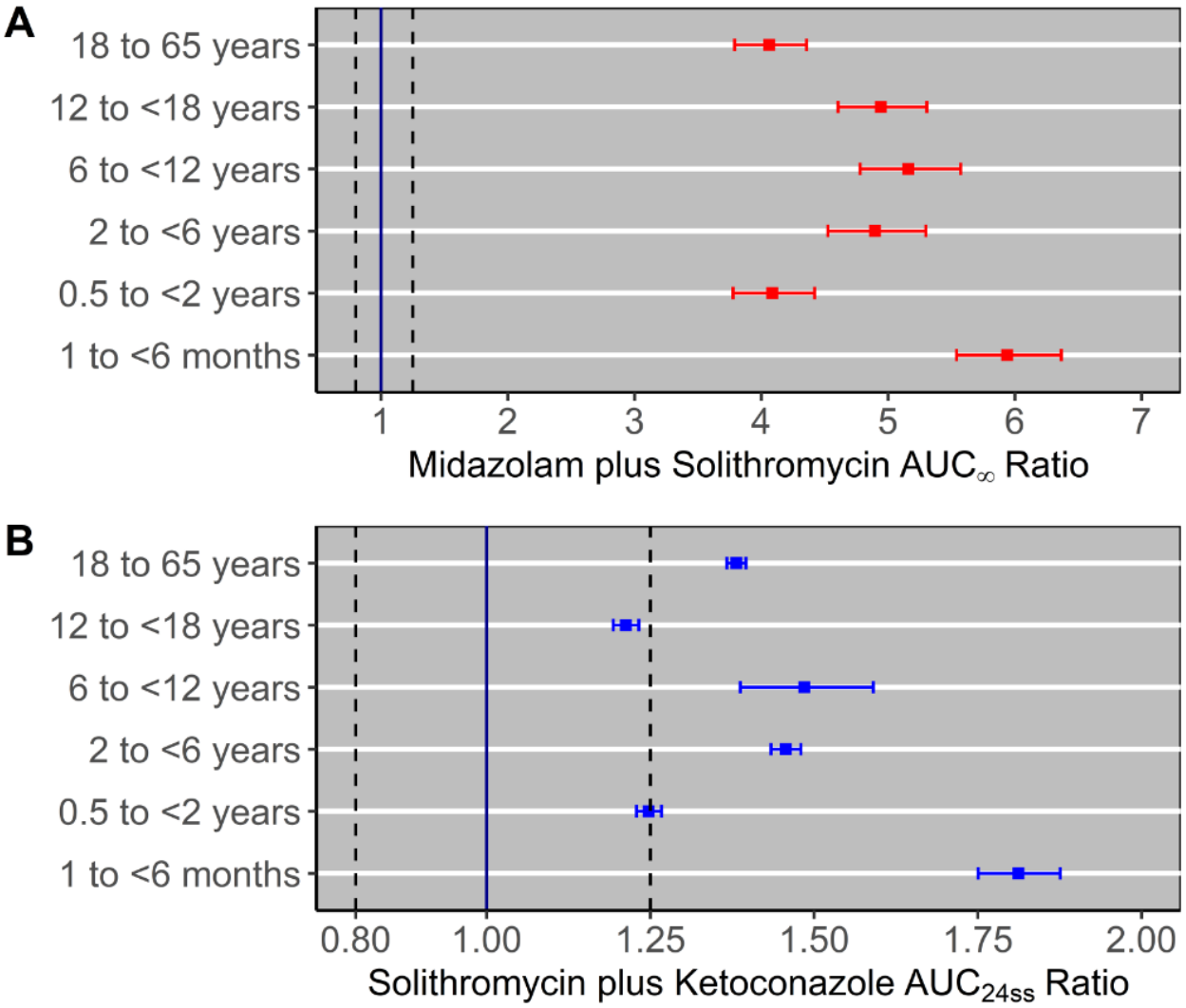

Dosing was simulated in 500 virtual individuals in each age category (1 to <6 months, 0.5 to <2 years, 2 to <6 years, 6 to <12 years, 12 to <18 years, and 18 to 65 years) according to the age and weight based dosing presented in Table 14. The vertical blue line corresponds to a ratio of 1.00 and the dotted vertical lines refer to the equivalence range of 0.80 to 1.25. (A) Virtual individuals received a single intravenous (IV) dose of midazolam alone and on the last date after 5 days of daily solithromycin IV dosing. The geometric mean ratio and 90% confidence interval of the

area under the midazolam concentration versus time curve from 0 to infinity ($AUC_{0-\infty}$) was calculated for a group of virtual individuals receiving midazolam plus solithromycin relative to a group of virtual individuals receiving midazolam alone. (B) Virtual individuals received 5 days of solithromycin IV dosing alone as well as in combination with 5 days of oral ketoconazole dosing. The geometric mean ratio and 90% confidence interval of the area under the solithromycin concentration versus time curve from 0 to 24 hours at steady-state ($AUC_{0-24,ss}$) was calculated for the group of patients solithromycin plus ketoconazole relative to a group receiving of virtual individuals solithromycin alone.

Figure 4.16: Approach for leveraging experimental data and physiologically-based pharmacokinetic (PBPK) modeling to predict drug-drug interactions (DDIs) mediated via cytochrome P450 3A (CYP3A) inhibition in adults and pediatric patients during drug development.

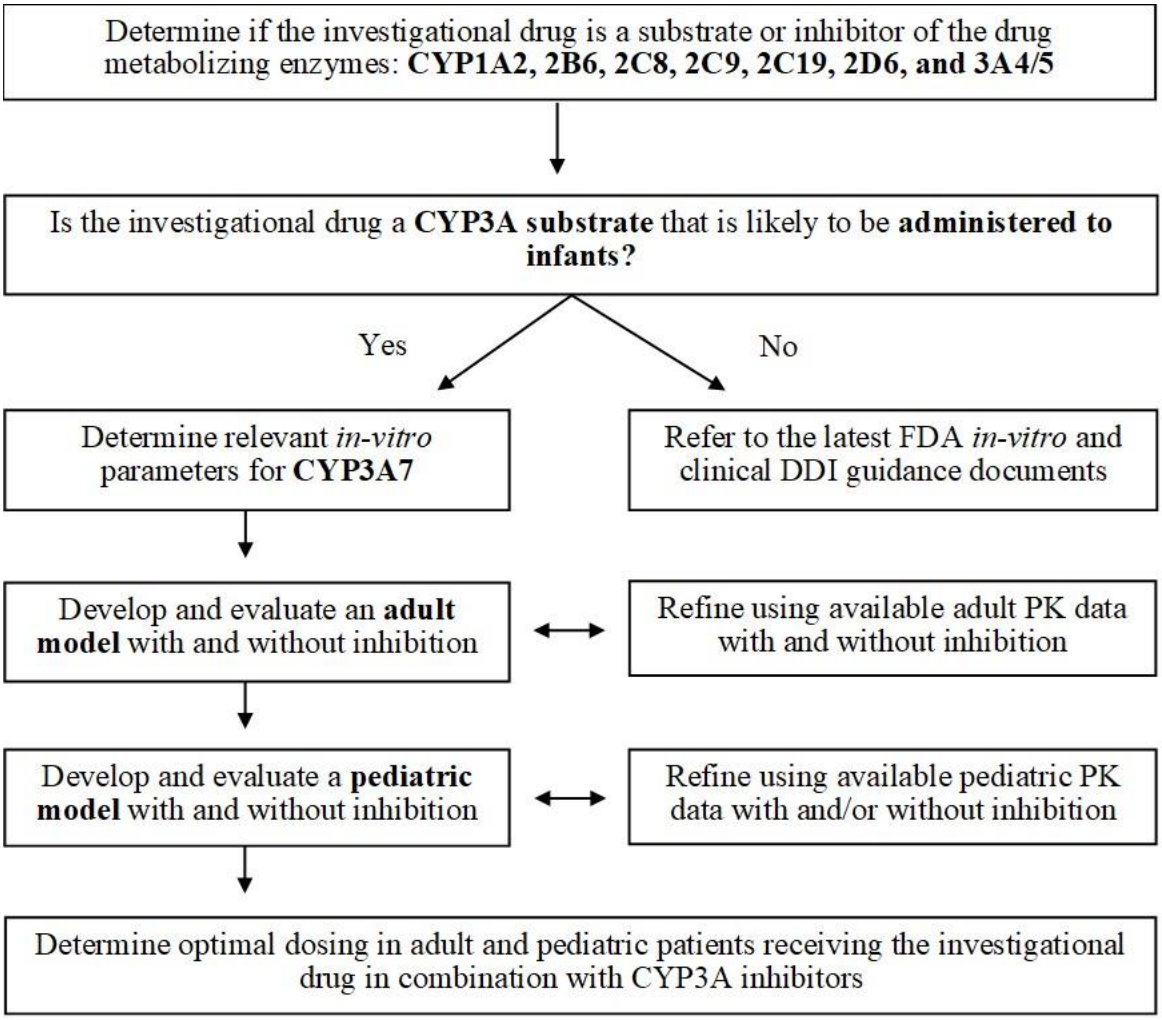

We have proposed a framework for conducting and integrating relevant experimental studies into adult and pediatric PBPK models to predict pediatric CYP3A mediated DDI potential during drug development. Although *in vitro* studies for CYP3A4 and CYP3A5 are routinely performed to evaluate metabolism and drug interaction potential for new investigational drugs, *in vitro* studies for CYP3A7 are rarely performed since CYP3A7 is minimally expressed in adults [1]. However, CYP3A7 is the predominantly expressed CYP3A isoenzyme in fetal tissue and

newborns, and we have previously demonstrated that CYP3A7 was integral for evaluating CYP3A mediated DDIs in infants ≤ 2 months of age using the CYP3A substrate, sildenafil, as an example [9]. Therefore, we recommend determining whether a drug is a substrate and/or inhibitor of CYP3A7 if this drug is likely to be administered concurrently to infants with other CYP3A inhibitors/inducers or CYP3A7 substrates, respectively. These *in vitro* parameters can be incorporated into an adult PBPK model developed and evaluated using clinical PK data and DDI data collected in healthy adults. The adult DDI PBPK model can be scaled to pediatric patients and evaluated using available pediatric PK data with and/or without drug inhibition. We recommend extensively evaluating the victim and perpetrator pediatric PBPK models using pediatric PK data for the drugs administered separately prior to co-modeling and simulated the DDI in pediatric patients. Finally, dosing recommendations with and without drug inhibitors can be simulated across the pediatric age continuum and provided within the product labeling. The advantage of this approach is that it does not require pediatric clinical DDI data since such studies are rarely performed unless children receive the drug combinations per standard of care. However, as clinical data becomes available in pediatric patients receiving the drug combinations per standard of care, the dosing recommendations can be further refined using opportunistic PK data.

REFERENCES

1. U.S. Food and Drug Administraiton. In vitro metabolism- and transporter-mediated drug-drug interaction studies guidance for industry. (2017) <http://www.raps.org/Regulatory-Focus/News/2017/10/25/28747/FDA-Offers-Two-Draft-Guidances-on-Drug-Drug-Interactions/> Accessed July 11, 2020.

2. Salerno, S. N. *et al.* Development of an adult physiologically based pharmacokinetic model of solithromycin in plasma and epithelial lining fluid. *CPT Pharmacometrics Syst. Pharmacol.* 2017; 6: 814-822.

3. MacLauchlin, C., Schneider, S. E., Keedy, K., Fernandes, P. & Jamieson, B. D. Metabolism, excretion, and mass balance of solithromycin in Humans. *Antimicrob. Agents Chemother.* **62**, (2018).

4. File, T. M. *et al.* SOLITAIRE-IV: A randomized, double-blind, multicenter study comparing the efficacy and safety of intravenous-to-oral solithromycin to intravenous-to-oral moxifloxacin for treatment of community-acquired bacterial pneumonia. *Clin. Infect. Dis.* **63**, 1007–16 (2016).

5. Barrera, C. M. *et al.* Efficacy and safety of oral solithromycin versus oral moxifloxacin for treatment of community-acquired bacterial pneumonia: a global, double-blind, multicentre, randomised, active-controlled, non-inferiority trial (SOLITAIRE-ORAL). *Lancet. Infect. Dis.* **16**, 421–30 (2016).

6. Buege, M. J., Brown, J. E. & Aitken, S. L. Solithromycin: A novel ketolide antibiotic. *Am. J. Heal. Pharm.* **74**, 875–887 (2017).

7. Gonzalez, D. *et al.* Solithromycin pharmacokinetics in plasma and dried blood spots and safety in adolescents. *Antimicrob. Agents Chemother.* **60**, 2572–6 (2016).

8. Gonzalez, D. *et al.* Population pharmacokinetics and safety of solithromycin following intravenous and oral administration in infants, children, and adolescents. *Antimicrob. Agents Chemother.* **62**, (2018).

9. Salerno, S. N. *et al.* Physiologically-based pharmacokinetic modeling characterizes the CYP3A-mediated drug-drug interaction between fluconazole and sildenafil in infants. *Clin. Pharmacol. Ther.* (2020).

10. Grimm, S. W. *et al.* The conduct of in vitro studies to address time-dependent inhibition of drug-metabolizing enzymes: A Perspective of the pharmaceutical research and manufacturers of America. *Drug Metab. Dispos.* **37**, 1355–1370 (2009).

11. Motulsky, H. J. *GraphPad Curve Fitting Guide.* (2020). <http://www.graphpad.com/guides/prism/7/curve-fitting/index.htm> Accessed July 11, 2020.

12. Meyer, M., Schneckener, S., Ludewig, B., Kuepfer, L. & Lippert, J. Using expression data for quantification of active processes in physiologically based pharmacokinetic modeling. *Drug Metab. Dispos.* **40**, 892–901 (2012).

13. Berezhkovskiy, L. M. Determination of Volume of Distribution at Steady State with Complete Consideration of the Kinetics of Protein and Tissue Binding in Linear Pharmacokinetics. *J. Pharm. Sci.* **93**, 364–374 (2004).

14. Open Systems Pharmacology Suite Community. Open Systems Pharmacology Suite Manual, Version 7.4. (2018). < https://docs.open-systems-pharmacology.org/copyright > Accessed July 2020.

15. Harwood, M. D., Neuhoff, S., Carlson, G. L., Warhurst, G. & Rostami-Hodjegan, A. Absolute abundance and function of intestinal drug transporters: a prerequisite for fully mechanistic in vitro-in vivo extrapolation of oral drug absorption. *Biopharm. Drug Dispos.* **34**, 2–28 (2013).

16. Jiang, X.-L., Zhao, P., Barrett, J. S., Lesko, L. J. & Schmidt, S. Application of physiologically based pharmacokinetic modeling to predict acetaminophen metabolism and pharmacokinetics in children. *CPT pharmacometrics Syst. Pharmacol.* **2**, e80 (2013).

17. Johnson, T. N., Zhou, D. & Bui, K. H. Development of physiologically based pharmacokinetic model to evaluate the relative systemic exposure to quetiapine after administration of IR and XR formulations to adults, children and adolescents. *Biopharm. Drug Dispos.* **35**, 341–52 (2014).

18. Zhou, W. *et al.* Predictive performance of physiologically based pharmacokinetic and population pharmacokinetic modeling of renally cleared drugs in children. *CPT pharmacometrics Syst. Pharmacol.* **5**, 475–83 (2016).

19. Fitch, W., Tran, T., Young, M., Liu, L. & Chen, Y. Revisiting the metabolism of ketoconazole using accurate mass. *Drug Metab. Lett.* **3**, 191–198 (2009).

20. Hyland, R., Jones, B. C. & Smith, D. A. Identification of the cytochrome P450 enzymes involved in the N-oxidation of voriconazole. In *Drug Metab. Dispos.* **31**, 540–547

21. Bourcier, K. *et al.* Investigation into UDP-glucuronosyltransferase (UGT) enzyme kinetics of imidazole- and triazole-containing antifungal drugs in human liver microsomes and recombinant UGT enzymes. *Drug Metab. Dispos.* **38**, 923–929 (2010).

22. Tyle, J. H. Van Van Ketoconazole mechanism of action, spectrum of activity, drug interactions, adverse reactions and therapeutic use. *Pharmacotherapy* **4**, 343–373 (1984).

23. Huang, Y. -C, Colaizzi, J. L., Bierman, R. H., Woestenborghs, R. & Heykants, J. J. P. Pharmacokinetics and dose proportionality of ketoconazole in normal volunteers. *Antimicrob. Agents Chemother.* **30**, 206–210 (1986).

24. DrugBank. DrugBank *version 5.1.2* (2019) <https://www.drugbank.ca> Accessed July 11, 2020.

25. Poulin, P. & Theil, F. P. A priori prediction of tissue: Plasma partition coefficients of drugs to facilitate the use of physiologically-based pharmacokinetic models in drug discovery. *J. Pharm. Sci.* **89**, 16–35 (2000).

26. Moltke, L. L. Von *et al.* Midazolam hydroxylation by human liver microsomes in vitro: Inhibition by fluoxetine, norfluoxetine, and by azole antifungal agents. *J. Clin. Pharmacol.* **36**, 783–791 (1996).

27. Gibbs, M. A., Thummel, K. E., Shen, D. D. & Kunze, K. L. Inhibition of cytochrome P-450 3A (CYP3A) in human intestinal and liver microsomes: Comparison of Ki values and impact of CYP3A5 expression. *Drug Metab. Dispos.* **27**, 180–187 (1999).

28. Oishi, M., Takano, Y., Torita, Y., Malhotra, B. & Chiba, K. Physiological based pharmacokinetic modeling to estimate in vivo Ki of ketoconazole on renal P-gp using human drug-drug interaction study result of fesoterodine and ketoconazole. *Drug Metab. Pharmacokinet.* **33**, 90–95 (2018).

29. U.S. Food and Drug Administraiton. *Midazolam Injection, USP*. **March**, (2017). Accessed July 11, 2020.

30. Xiao, K. *et al.* CYP3A4/5 Activity Probed with Testosterone and Midazolam: Correlation between two substrates at the microsomal and enzyme levels. *Mol. Pharm.* **16**, 382–392 (2019).

31. Rodgers, T. & Rowland, M. Physiologically based pharmacokinetic modelling 2: Predicting the tissue distribution of acids, very weak bases, neutrals and zwitterions. *J. Pharm. Sci.* **95**, 1238–1257 (2006).

32. Prasad, B. *et al.* Ontogeny of hepatic drug transporters as quantified by LC-MS/MS proteomics. *Clin. Pharmacol. Ther.* **100**, 362–370 (2016).

33. Pietrogrande, M. C., Tortorano, A. M., Viviani, M. A., Cohen, E. & Bardare, M. Ketoconazole treatment of candidiasis in children: clinico-pharmacokinetic study. *Pediatr. Med. Chir.* **5**, 91–4 (1983).

34. Bardare, M., Tortorano, A. M., Pietrogrande, M. C. & Viviani, M. A. Pharmacokinetics of ketoconazole and treatment evaluation in candidal infections. *Arch. Dis. Child.* **59**, 1068–1071 (1984).

35. Ginsburg, C. M., McCracken, G. H. & Olsen, K. Pharmacology of ketoconazole suspension in infants and children. *Antimicrob. Agents Chemother.* **23**, 787–789 (1983).

36. Jacqz-Aigrain, E., Wood, C. & Robieux, I. Pharmacokinetics of midazolam in critically ill neonates. *Eur. J. Clin. Pharmacol.* **39**, 191–2 (1990).

37. Reed, M. D. *et al.* The single-dose pharmacokinetics of midazolam and its primary metabolite in pediatric patients after oral and intravenous administration. *J. Clin. Pharmacol.* **41**, 1359–1369 (2001).

38. Nahara, M. C., McMorrow, J., Jones, P. R., Anglin, D. & Rosenberg, R. Pharmacokinetics of midazolam in critically ill pediatric patients. *Eur. J. Drug Metab. Pharmacokinet.* **25**, 219–221 (2000).

39. Lexicomp. Lexicomp Drug Information. (2020). Accessed July 11, 2020.

40. Teva Ketoconazole Tablets USP, 200 mg Product Monograph. (2020) <www.tevacanada.com> Accessed July 11, 2020.

41. Brass, C. *et al.* Disposition of ketoconazole, an oral antifungal, in humans. *Antimicrob. Agents Chemother.* **21**, 151–158 (1982).

42. Daneshmend, T. K., Warnock, D. W., Turner, A. & Roberts, C. J. C. Pharmacokinetics of ketoconazole in normal subjects. *J. Antimicrob. Chemother.* **8**, 299–304 (1981).

43. Bornemann, L. D., Crews, T., Chen, S. S., Twardak, S. & Patel, I. H. Influence of food on midazolam absorption. *J. Clin. Pharmacol.* **26**, 55–9 (1986).

44. Pentikis, H. S., Connolly, M., Trapnell, C. B., Forbes, W. P. & Bettenhausen, D. K. The effect of multiple-dose, oral rifaximin on the pharmacokinetics of intravenous and oral midazolam in healthy volunteers. *Pharmacotherapy* **27**, 1361–1369 (2007).

45. Li, H. & Lampe, J. N. Neonatal cytochrome P450 CYP3A7: A comprehensive review of its role in development, disease, and xenobiotic metabolism. *Arch. Biochem. Biophys.* **673**, (2019).

46. Lacroix, D., Sonnier, M., Moncion, A., Cheron, G. & Cresteil, T. Expression of CYP3A in the human liver - Evidence that the shift between CYP3A7 and CYP3A4 occurs immediately after birth. *Eur. J. Biochem.* **247**, 625–634 (1997).

47. Williams, J. A. *et al.* Comparative metabolic capabilities of CYP3A4, CYP3A5, and CYP3A7. *Drug Metab. Dispos.* **30**, 883–91 (2002).

48. Takahiro, R. *et al.* Contribution of CYP3A isoforms to dealkylation of PDE5 inhibitors: a comparison between sildenafil N-demethylation and tadalafil demethylenation. *Biol. Pharm. Bull.* **38**, 58–65 (2015).

49. Kamdem, L. K. *et al.* Contribution of CYP3A5 to the in vitro hepatic clearance of tacrolimus. *Clin. Chem.* **51**, 1374–1381 (2005).

50. PK-Sim. PK-Sim ® Ontogeny Database. **Version 7.**, 1–47 (2017).

51. Kearns, G. L. *et al.* Developmental pharmacology — Drug disposition, action, and therapy in infants and children. *N. Engl. J. Med.* **349**, 1157–1167 (2003).

52. Anker, J. N. Van Der, Ussel-Dijk, A. Van, Woestenborghs, R., Koster, M. & Sauer, P. J. J. The effect of gastric pH on the absorption of ketoconazole by very-low-birth-weight infants. *Pediatr. Res.* **36**, (1994).

53. Sun, H. *et al.* Extrapolation of efficacy in pediatric drug development and evidence-based medicine: Progress and lessons learned. *Ther. Innov. Regul. Sci.* **52**, 199–205 (2018).

54. Tiseo, P. J., Perdomo, C. A. & Friedhoff, L. T. Concurrent administration of donepezil HCl and ketoconazole: Assessment of pharmacokinetic changes following single and multiple doses. *Br. J. Clin. Pharmacol.* **46**, 30–34 (1998).

55. Olkkola, K. T., Backman, J. T. & Neuvonen, P. J. Midazolarn should be avoided in patients receiving the systemic antimycotics ketoconazole or itraconazole. *Clin. Pharmacol. Ther.* **55**, 481–485 (1994).

56. Tsunoda, S. M., Velez, R. L., Moltke, L. L. von & Greenblatt, D. J. Differentiation of intestinal and hepatic cytochrome P450 3A activity with use of midazolam as an in vivo probe: Effect of ketoconazole. *Clin. Pharmacol. Ther.* **66**, 461–471 (1999).

57. Still, J. G. *et al.* Pharmacokinetics of solithromycin (CEM-101) after single or multiple oral doses and effects of food on single-dose bioavailability in healthy adult subjects. *Antimicrob. Agents Chemother.* **55**, 1997–2003 (2011).

58. Rodvold, K. A., Gotfried, M. H., Still, J. G., Clark, K. & Fernandes, P. Comparison of plasma, epithelial lining fluid, and alveolar macrophage concentrations of solithromycin (CEM-101) in healthy adult subjects. *Antimicrob. Agents Chemother.* **56**, 5076–81 (2012).

59. Oldach, D. *et al.* Randomized, double-blind, multicenter phase 2 study comparing the efficacy and safety of oral solithromycin (CEM-101) to those of oral levofloxacin in the treatment of patients with community-acquired bacterial pneumonia. *Antimicrob. Agents Chemother.* **57**, 2526–34 (2013).

60. Pachot, J. I., Botham, R. P., Haegele, K. D. & Hwang, K. Experimental estimation of the role of P-Glycoprotein in the pharmacokinetic behaviour of telithromycin, a novel ketolide, in comparison with roxithromycin and other macrolides using the Caco-2 cell model. *J. Pharm. Pharm. Sci.* **6**, 1–12 (2003).

61. Daneshmend, T. K. *et al.* Multiple dose pharmacokinetics of ketoconazole and their effects on antipyrine kinetics in man. *J. Antimicrob. Chemother.* **12**, 185–188 (1983).

62. Mannisto, P. T., Mantyla, R., Nykanen, S., Lamminsivu, U. & Ottoila, P. Impairing effect of food on ketoconazole absorption. *Antimicrob. Agents Chemother.* **21**, 730–733 (1982).

63. Veldhorst-Janssen, N. M. L. *et al.* Pharmacokinetics and tolerability of nasal versus intravenous midazolam in healthy dutch volunteers: A single-dose, randomized-sequence, open-label, 2-period crossover pilot study. *Clin. Ther.* **33**, 2022–2028 (2011).

64. Misaka, S. *et al.* Pharmacokinetics and pharmacodynamics of low doses of midazolam administered intravenously and orally to healthy volunteers. *Clin. Exp. Pharmacol. Physiol.* **37**, 290–295 (2010).

65. Juif, P.-E., Boehler, M., Donazzolo, Y., Bruderer, S. & Dingemanse, J. A pharmacokinetic drug–drug interaction study between selexipag and midazolam, a CYP3A4 substrate, in healthy male subjects. *Eur. J. Clin. Pharmacol.* **73**, 1121–1128 (2017).

66. Winter, H. *et al.* Evaluation of Pharmacokinetic Interaction between PA-824 and Midazolam in Healthy Adult Subjects. *Antimicrob. Agents Chemother.* **57**, 3699–3703 (2013).

67. Ma, J. D., Nafziger, A. N., Rhodes, G., Liu, S. & Bertino, J. S. Duration of pleconaril effect on cytochrome P450 3A activity in healthy adults using the oral biomarker midazolam. *Drug Metab. Dispos.* **34**, 783–785 (2006).

68. Lam, Y. W. F., Alfaro, C. L., Ereshefsky, L. & Miller, M. Pharmacokinetic and pharmacodynamic interactions of oral midazolam with ketoconazole, fluoxetine, fluvoxamine, and nefazodone. *J. Clin. Pharmacol.* **43**, 1274–1282 (2003).

69. Chung, E., Nafziger, A. N., Kazierad, D. J. & Bertino, J. S. Comparison of midazolam and simvastatin as cytochrome P450 3A probes. *Clin. Pharmacol. Ther.* **79**, 350–361 (2006).

CHAPTER 5 : SUMMARY AND CONCLUSION

5.1 Introduction

It is important to understand and clinically manage drug-drug interactions (DDIs) because they can lead to therapeutic failure or life-threatening adverse events. Children are at risk for experiencing DDIs because they often receive multiple medications throughout hospitalization. In fact, one retrospective study reported that children hospitalized in the pediatric intensive care unit were exposed on average to 10 distinct medications daily and to 20 medications cumulatively during hospitalization.[1] Another retrospective study reported that approximately half of 498,956 pediatric hospitalizations were associated with a potential DDI.[2]

Although DDIs frequently occur in pediatric patients, DDIs are rarely evaluated in infants and children for ethical and practical reasons. As a vulnerable population, it is unethical to conduct DDI studies in pediatric patients unless they receive the medications per standard of care. Pediatric studies are also logistically challenging to perform due to a small number of children to enroll with the disease of interest, difficulties recruiting and consenting subjects, and less blood volume available that can be collected for pharmacokinetic (PK) sampling.

The U.S. Food and Drug Administration (FDA) requires that DDI studies be performed in healthy adult volunteers during drug development if an investigational drug is suspected to interact with concomitant medications. Since pediatric DDI studies are rarely conducted, we typically rely on adult DDI studies to guide clinical management in children who must receive unavoidable drug combinations. However, changes in metabolic pathways during development

may lead to differences in DDI potential between adults and children. For example, cytochrome P450 (CYP) 3A7 is the predominant CYP3A isoform expressed in neonates and it has lower catalytic activity compared to CYP3A4, the predominant CYP3A isoform expressed in older children and adults.[3–6]

Physiologically-based pharmacokinetic (PBPK) modeling can potentially overcome these challenges by conducting prospective pediatric DDI studies and predicting pediatric DDI potential when pediatric data are sparse or unavailable. The workflow first involves developing an adult PBPK model incorporating drug, system, and formulation properties, and then evaluating and further refining the model using adult clinical data. Second, DDI potential can be evaluated in adults by incorporating *in vitro* induction or inhibition parameters and then assessing and refining the model using robust adult DDI data. Third, adult PBPK models can be scaled to pediatric patients including anthropomorphic and ontogeny functions. The pediatric PBPK model can then be evaluated using available PK data, and DDI potential can be simulated in pediatric patients of various age groups who are likely to receive the drug combination. Finally, the simulated dosing recommendations can be prospectively evaluated using opportunistic PK data in children receiving the drug combination per standard of care or through an adaptive trial design where safety is monitored at pre-determined interim analysis (Figure 5.1).

In this dissertation, we deployed PBPK modeling to develop a systematic approach to provide dosing recommendations in pediatric patients experiencing CYP3A mediated DDIs spanning a variety of interaction mechanisms across the pediatric age continuum.

First, we evaluated the DDI interaction between the reversible CYP3A inhibitor, fluconazole, and the CYP3A substrate, sildenafil, administered to neonates for the co-treatment of invasive candidiasis and pulmonary hypertension. Second, we evaluated the complex DDI between lopinavir/ritonavir (LPV/RTV) plus rifampicin involving mixed CYP3A time-dependent and competitive inhibition plus induction in pediatric patients co-infected with human immunodeficiency virus (HIV) and tuberculosis (TB). Finally, this systematic approach was applied to predict DDI potential and to optimize dosing in pediatric patients receiving a novel antibiotic and time-dependent CYP3A inhibitor (solithromycin) in combination with the CYP3A substrate midazolam and the strong CYP3A inhibitor ketoconazole (Figure 5.2). This final chapter will briefly summarize the findings from each of these simulated DDI scenarios and will describe how this framework can be applied to predict other metabolic and transporter mediated DDIs relevant in the pediatric population.

5.2 PBPK Modeling Characterizes the CYP3A-Mediated DDI between Fluconazole and Sildenafil in Infants (Aim 1)

In infants for whom treatment of pulmonary hypertension and prevention or treatment of invasive candidiasis are indicated, sildenafil with fluconazole may be given concurrently. To account for developmental changes in CYP3A, we determined and incorporated fluconazole inhibition constants (K_I) for CYP3A4, CYP3A5, and CYP3A7 into a PBPK model developed for sildenafil and its active metabolite, N-desmethylsildenafil. Fluconazole was a weaker mixed competitive inhibitor for CYP3A5 and CYP3A7 relative to CYP3A4. PK data in preterm infants receiving sildenafil with and without fluconazole were used for model development and evaluation. The simulated PK parameters were comparable to observed values for sildenafil, however, there was some model misspecification for the active metabolite, N-desmethyl-

sildenafil, particularly at early concentrations. Following fluconazole co-administration, fold increase in simulated steady-state area under the sildenafil plasma concentration versus time curve from 0 to 24 hours ($AUC_{0\text{-}24,ss}$) was greater in virtual infants than in virtual adults (2.11- versus 2.82-fold change). When given in combination with treatment doses of fluconazole (12 mg/kg IV daily), reducing the sildenafil dose to virtual infants by 64% relative to the sildenafil alone dose resulted in a geometric mean ratio of 1.01 for simulated $AUC_{0\text{-}24,ss}$. Sensitivity analysis for sildenafil across age found that the sildenafil AUC extrapolated to infinity ($AUC_{0\text{-}\infty}$) was more sensitive to the reference concentration of CYP3A7 compared to CYP3A4 in infants ≤ 2 months of age. This study highlights the feasibility of using PBPK modeling to predict DDIs in infants and the need to include CYP3A7 parameters in neonates. However, we often do not have CYP3A7 parameters readily available and instead only scale CYP3A4 activity, which may lead to poor prediction by the model in infants ≤ 2 months of age. Finally, this study demonstrated that DDI potential can differ between infants and adults and should be evaluated further for other CYP3A mediated DDIs that occur for commonly administered medicines to infants.

5.3 PBPK Modeling Characterizes CYP3A and P-glycoprotein Inhibition and Induction between Lopinavir/Ritonavir plus Rifampicin in Infants and Children (Aim 2)

HIV and TB co-infection is a serious problem worldwide and particularly in sub-Saharan Africa. LPV/RTV and rifampicin are key medications used for HIV and TB treatment, which result in a clinically significant DDI. The objective of this study was to use PBPK modeling to optimize dosing of LPV/RTV plus rifampicin in pediatric patients (≥ 2 months of age) using the World Health Organization (WHO) revised dosing of rifampicin (15 mg/kg) stratified by WHO weight-bands. Adult LPV/RTV plus rifampicin PBPK models were first developed and evaluated in adults prior to scaling to pediatric patients. The RTV PBPK model included CYP3A4,

CYP3A5, and CYP2D6 metabolism; P-glycoprotein transport; glomerular filtration; CYP3A4 and CYP3A5 time-dependent and competitive inhibition; CYP3A4 induction and P-glycoprotein inhibition. The LPV PBPK model included CYP3A4 metabolism and P-glycoprotein transport, glomerular filtration, and CYP3A4 and CYP3A5 time-dependent inhibition. The rifampicin PBPK model included metabolism and auto-induction by AADAC, P-glycoprotein and OATP1B1 transport, glomerular filtration, P-glycoprotein and CYP3A4 competitive inhibition and induction. The average fold error (AFE) and PK parameters were all within two-fold for LPV, RTV, and rifampicin in adults and pediatric patients (2 weeks to 17 years of age). In the adult simulations, rifampicin decreased the steady-state area under the concentration vs. time curve under the dosing interval of LPV ($AUC_{0\text{-}\tau,ss}$) by 79% compared to 75% reported in healthy adults receiving standard dosing of LPV/RTV. In the pediatric simulations, PK parameters were comparable for standard dosing alone (230/57.5 mg/m^2) and boosted-dosing (230/230 mg/m^2) of LPV/RTV administered orally twice daily with 10 mg/kg daily rifampicin. This approach can be applied to other complex transporter and metabolic DDI scenarios relevant in the pediatric population in order to optimize dosing.

5.4 Use of PBPK Modeling and Experimental Data to Guide Dosing Modification of CYP3A Mediated DDIs in Pediatric Patients during Drug Development (Aim 3)

Solithromycin is a novel fluoroketolide antibiotic that is both a substrate and time-dependent inhibitor of CYP3A. Solithromycin demonstrated efficacy in adults with community-acquired bacterial pneumonia (CABP) and has been investigated in pediatric patients. Using solithromycin as a case study, we developed an approach for incorporating CYP3A4, CYP3A5, and CYP3A7 *in vitro* data into adult and pediatric PBPK models to predict CYP3A mediated DDI potential across all age groups during drug development. This represented the typical

situation where there was robust adult DDI data but pediatric DDI data were lacking. To account for age, we performed substrate depletion studies to evaluate metabolism as well as time-dependent inhibition studies of CYP3A4, CYP3A5, and CYP3A7 by solithromycin. Solithromycin was not a substrate or time-dependent inhibitor for CYP3A7 in the incubation times and concentrations assessed in this study. The final PBPK model included CYP3A4- and CYP3A5-mediated metabolism of solithromycin and time-dependent inhibition by this drug of the two CYP3A enzymes, glomerular filtration, and P-glycoprotein transport and enterohepatic recirculation. The AFE for adult and pediatric simulations were all within the 0.5- to 2.0-fold acceptance criteria based on 122 adults (1966 plasma samples) and 96 pediatric patients from 4 days to 17.9 years (684 plasma samples). The DDI between solithromycin with midazolam and ketoconazole was simulated and compared to observed data in adults. The simulated geometric mean ratios for the $AUC_{0-\infty}$ were within 0.75- to 1.25-fold of observed values in healthy adults receiving solithromycin in combination with midazolam or ketoconazole. DDI potential was simulated in pediatric patients from 1 month to 17 years of age and compared with virtual adults. Solithromycin increased the AUC of midazolam from 4 to 6 fold, and ketoconazole increased the AUC of solithromycin from 1 to 2 fold in virtual subjects ranging from 1 month to 65 years of age. In this study, differences in the magnitude of the DDI as a function of age were driven primarily by minor differences in inhibition concentrations. For example, infants <6 months of age had the highest and most variable inhibitor concentrations and thus the greatest magnitude of CYP3A mediated inhibition. Therefore, age-related differences in DDI potential can be minimized by closely matching adult and pediatric inhibitor concentrations for drugs with similar exposure response relationships between adults and pediatric patients.

5.5 Conclusion and Future Directions

We have suggested a framework for conducting and integrating relevant experimental studies into adult and pediatric PBPK models to predict pediatric CYP3A mediated DDI potential during drug development (Figure 5.3). Although *in vitro* studies for CYP3A4 and CYP3A5 are routinely performed to evaluate metabolism and drug interaction potential for new investigational drugs, *in vitro* studies for CYP3A7 are rarely performed since CYP3A7 is minimally expressed in adults.[7] However, CYP3A7 is the predominantly expressed CYP3A isoenzyme in fetal tissue and newborns, and we have demonstrated that CYP3A7 was integral for evaluating CYP3A mediated DDIs in infants ≤ 2 months of age using the CYP3A substrate, sildenafil, as an example. Therefore, we recommend determining CYP3A7 parameters for CYP3A drug combinations that are likely to be co-administered to infants. However, as demonstrated with solithromycin, not all CYP3A4 substrates will be catalytically active for CYP3A7. Since we cannot predict *a priori* whether a compound will be metabolized by CYP3A7, CYP3A7 mediated metabolism and inhibition should be performed for any CYP3A substrate or inhibitor that is anticipated to be administered to infants.

We have also demonstrated that this systematic approach can be applied to complex DDI scenarios involving reversible and irreversible inhibition, induction, as well as transporter mediated interactions. For example, the DDI between LPV/RTV plus rifampicin included P-glycoprotein inhibition, CYP3A time-dependent inhibition, CYP3A competitive inhibition, as well as CYP3A induction. The dynamic changes in perpetrator and victim concentrations can be modeled as a function of time with PBPK modeling since some drugs (such as rifampicin) can act as both reversible inhibitors and inducers, which can lead to net inhibition on the first few days of therapy and net induction at steady-state. It is possible; therefore, that the magnitude of

the DDI for drugs acting as both inhibitors and inducers may differ between infants and adults based on the ontogeny pattern of relevant metabolizing enzymes and transporters.

Another important finding is that the perpetrator concentration profoundly impacts the extent of the DDI for the victim drug, at least for drugs primarily metabolized by CYP3A4 such as solithromycin. Using solithromycin as an example, we found that small differences in inhibitor concentrations between infants and adults resulted in significant differences in the magnitude of the DDI. Although we generally dose drugs in pediatric patients to result in similar exposures observed in adults, subtle differences in exposure may result in clinically significant differences in DDI potential between adults and pediatric patients. Furthermore, we may target different drug exposures in children relative to adults if safety and efficacy differ in children.

This systematic approach can be applied to other metabolic and transporter mediated DDIs in pediatric patients. A major advantage of this approach is that it does not require intensive PK data in pediatric patients receiving the drug combinations. Some important limitations are that (1) it does require pediatric PK data for the victim and perpetrator drugs administered alone to evaluate PBPK model performance prior to co-modeling the drug combination, (2) CYP3A7 data are rarely available and must therefore be experimentally generated, and (3) it requires an extensive understanding of developmental physiology such as the ontogeny of enzymes and transporters. Future studies that characterize the expression and ontogeny of transporters throughout different organs of the body can bolster the accuracy of predicting transporter mediated DDI potential. Finally, there is extensive variability in the population simulations and we often report the geometric mean and its associated 90% confidence interval for the exposure ratio with and without the perpetrator drug. To individualize dosing for pediatric patients receiving drug combinations, future studies should be performed to

incorporate patient specific information into PBPK modeling, such as other concomitant drugs, the exact dosing and timing of drug co-administration, individual enzyme and transporter concentrations, and personalized pharmacodynamic endpoints (viral resistance, drug tolerance, and individual minimum inhibitory concentrations). It is also important to recognize that the virtual pediatric populations may differ from the actual pediatric populations, as we found that the virtual population often underpredicts the true variability in the patient population. Exploring changes in protein binding, hepatic or renal function, blood flow, organ sizes, altered gene expression of enzymes for specific disease states may improve PBPK model predictions.

Another area of research that should be explored further is how drug induction may differ between pediatric patients and adults. There is extremely limited information in the literature describing enzyme induction in the pediatric population. In order to properly characterize CYP3A-mediated drug induction in infants, induction parameters should be generated separately for CYP3A4, CYP3A5, and CYP3A7, and then these parameters can then be incorporated within PBPK models to predict DDI potential and optimize dosing in infants and young children. It is also possible that the ontogeny of nuclear receptors and associated co-repressors and co-activators may lead to differences in DDI potential between infants and adults. Finally, it is also possible that induction due to stabilization of messenger ribonucleic acid or protein stability will differ in the pediatric population, which could be explored further with additional studies.

5.6 Figures

Figure 5.1: Application of physiologically-based pharmacokinetic (PBPK) modeling and simulation to predict drug-drug interaction (DDI) potential in pediatric patients

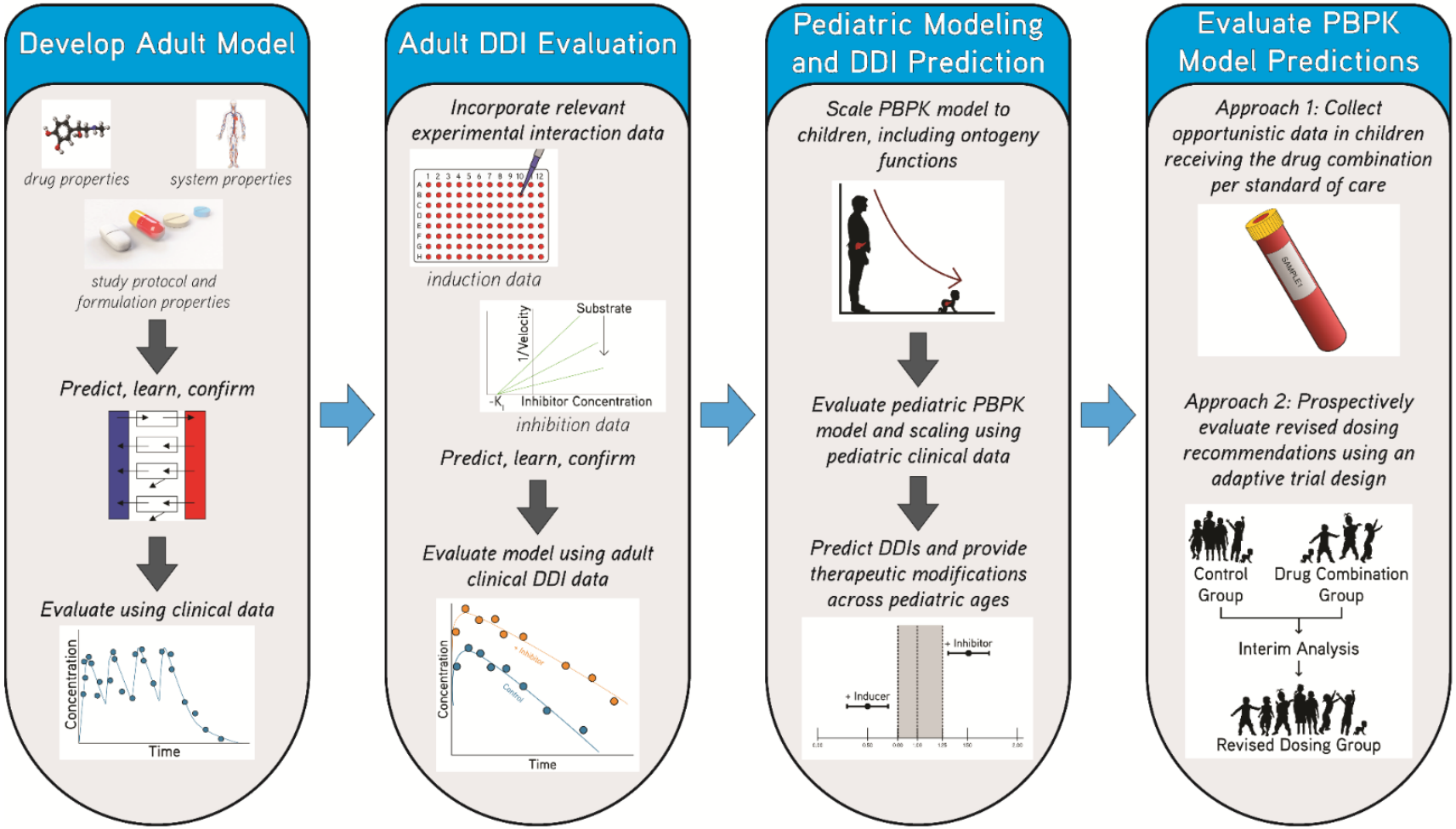

Adult physiologically-based pharmacokinetic (PBPK) models can be developed incorporating drug-specific, system-specific, and study protocol and formulation properties, and then evaluated and further refined using adult clinical data. Next, drug-drug interaction (DDI) potential can be evaluated by incorporating *in-vitro* induction or inhibition parameters and then further refined using adult DDI data. Adult PBPK models can be scaled to pediatric patients including anthropomorphic and ontogeny functions, and then model performance and scaling can be evaluated using available pediatric data. Next, DDIs can be simulated in pediatric patients in order to provide therapeutic recommendations across pediatric ages likely to receive the drug. Finally, dosing recommendations can be evaluated using opportunistic pharmacokinetic data or using prospectively captured data from an adaptive trial. During adaptive trials, efficacy and safety of the dosages and drug combinations can be monitored in pediatric patients throughout the trial at pre-specified times and the dosing regimen can be modified according to these interim study results.

Figure 5.2: Dissertation research overview

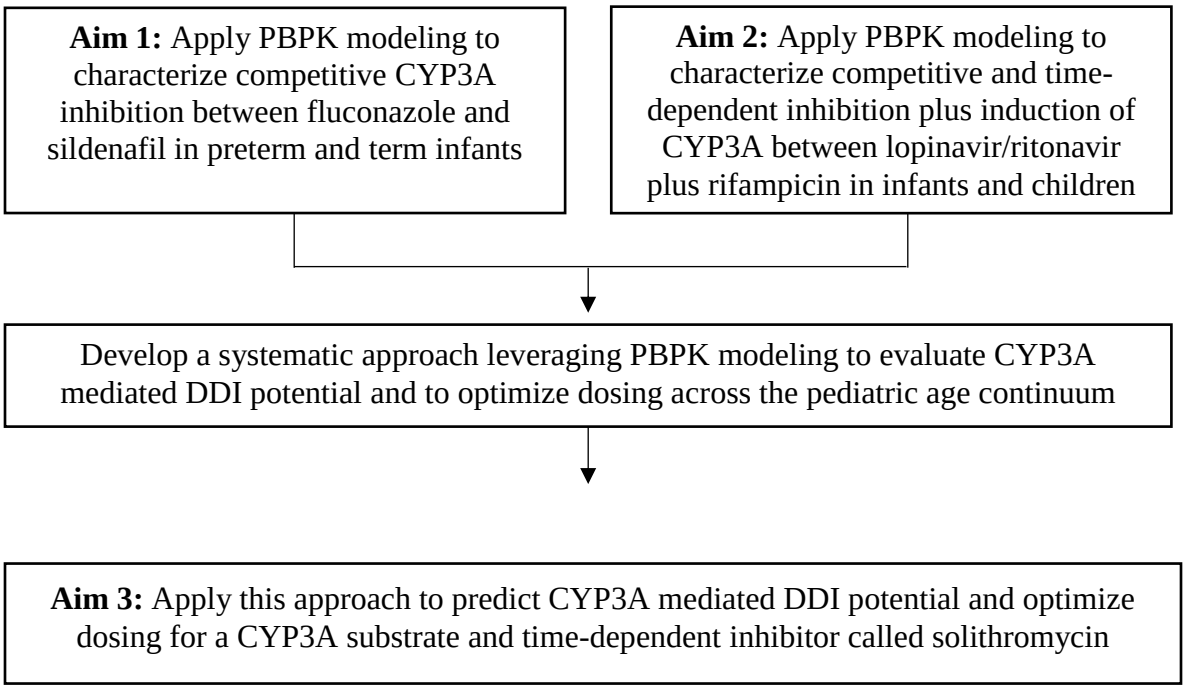

Figure 5.3: Approach for leveraging experimental data and PBPK modeling to predict CYP3A mediated DDI inhibition in adults and pediatric patients during drug development

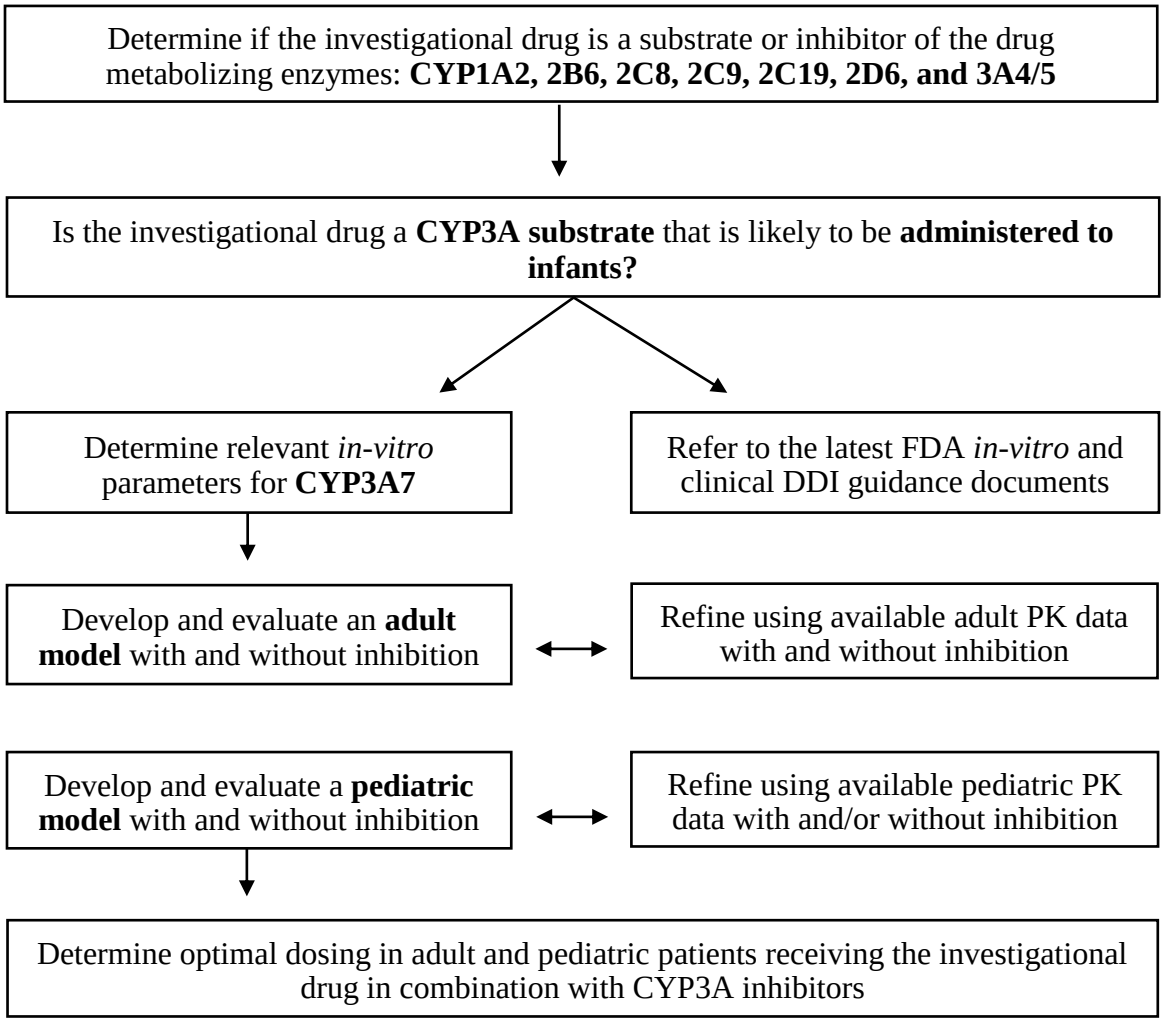

We have proposed a framework for conducting and integrating relevant experimental studies into adult and pediatric PBPK models to predict pediatric CYP3A mediated DDI potential during drug development. Although *in vitro* studies for CYP3A4 and CYP3A5 are routinely performed to evaluate metabolism and drug interaction potential for new investigational drugs, *in vitro* studies for CYP3A7 are rarely performed since CYP3A7 is minimally expressed in adults [1]. However, CYP3A7 is the predominantly expressed CYP3A isoenzyme in fetal tissue and newborns, and we have previously demonstrated that CYP3A7 was integral for evaluating

CYP3A mediated DDIs in infants ≤ 2 months of age using the CYP3A substrate, sildenafil, as an example. [9] Therefore, we recommend determining whether a drug is a substrate and/or inhibitor of CYP3A7 if this drug is likely to be administered concurrently to infants with other CYP3A inhibitors/inducers or CYP3A7 substrates, respectively. These *in vitro* parameters can be incorporated into an adult PBPK model developed and evaluated using clinical PK data and DDI data collected in healthy adults. The adult DDI PBPK model can be scaled to pediatric patients and evaluated using available pediatric PK data with and/or without drug inhibition. We recommend extensively evaluating the victim and perpetrator pediatric PBPK models using pediatric PK data for the drugs administered separately prior to co-modeling and simulated the DDI in pediatric patients. Finally, dosing recommendations with and without drug inhibitors can be simulated across the pediatric age continuum and provided within the product labeling. The advantage of this approach is that it does not require pediatric clinical DDI data since such studies are rarely performed unless children receive the drug combinations per standard of care. However, as clinical data becomes available in pediatric patients receiving the drug combinations per standard of care, the dosing recommendations can be further refined using opportunistic PK data.

REFERENCES

1. Dai, D., Feinstein, J. A., Morrison, W., Zuppa, A. F. & Feudtner, C. Epidemiology of polypharmacy and potential drug–drug interactions among pediatric patients in ICUs of U.S. children's hospitals. *Pediatr. Crit. Care Med.* **17**, e218–e228 (2016).

2. Feinstein, J., Dai, D., Zhong, W., Freedman, J. & Feudtner, C. Potential drug−drug interactions in infant, child, and adolescent patients in children's hospitals. *Pediatrics* **135**, 3–12 (2015).

3. Hines, R. N. Ontogeny of human hepatic cytochromes P450. *J. Biochem. Mol. Toxicol.* **21**, 169–75 (2007).

4. Stevens, J. C. *et al.* Developmental expression of the major human hepatic CYP3A enzymes. *J. Pharmacol. Exp. Ther.* **307**, 573–582 (2003).

5. Williams, J. A. *et al.* Comparative metabolic capabilities of CYP3A4, CYP3A5, and CYP3A7. *Drug Metab. Dispos.* **30**, 883–91 (2002).

6. Soars, M. G., Grime, K. & Riley, R. J. Comparative analysis of substrate and inhibitor interactions with CYP3A4 and CYP3A5. *Xenobiotica* **36**, 287–299 (2006).

7. Food and Drug Administraiton In Vitro Metabolism- and Transporter-Mediated Drug-Drug Interaction Studies Guidance for Industry. (2017). <http://www.raps.org/Regulatory-Focus/News/2017/10/25/28747/FDA-Offers-Two-Draft-Guidances-on-Drug-Drug-Interactions/> Accessed September 1, 2020.